UNIVERSITY OF NOTTINGHAM
SCHOOL OF MECHANICAL, MATERIALS,
MANUFACTURING ENGINEERING AND
MANAGEMENT

Forming and Consolidation of Textile Composites

by

Rafael Garcia Gil

Thesis submitted to the University of Nottingham
for the degree of Doctor of Philosophy
May 2003

Table of Contents

ABSTRACT I

ACKNOWLEDGEMENTS II

GLOSSARY III

NOMENCLATURE V

1 INTRODUCTION AND OBJECTIVES 1

1.1 INTRODUCTION TO COMPOSITES 1

1.2 PRODUCT FORMS 1

1.3 TEXTILE COMPOSITES 4

1.4 PROCESSING TECHNIQUES FOR THERMOPLASTIC TEXTILE COMPOSITES 5

1.5 THEME OF THIS WORK 9

2 LITERATURE REVIEW 11

2.1 INTRODUCTION 11

2.2 VACUUM FORMING OF TEXTILE COMPOSITES 11

2.3 VOID CONTENT ANALYSIS 12

2.4 CONSOLIDATION OF THERMOPLASTIC TEXTILE COMPOSITES 13

2.4.1 Fibre bed permeability 14

2.4.2 Fibre bed compaction 16

2.4.3 Impregnation of thermoplastic composites 18

2.4.4 Heat Transfer 23

2.5 EFFECT OF VOID CONTENT ON MECHANICAL PROPERTIES 24

2.5.1 Notched Strength of Composite Laminates 25

2.6 EFFECT OF DEFORMATION ON MECHANICAL PROPERTIES 29

2.6.1 Reinforcement Efficiency 29

2.6.2 Classical Laminate Theory 30

2.6.3 Effects of Fibre Misalignment/Waviness 30

2.7 CONCLUSIONS 33

3 EXPERIMENTAL TECHNIQUES 34

3.1 INTRODUCTION 34

3.2 MATERIALS 34

3.3 VACUUM CONSOLIDATION OF TEXTILE COMPOSITES 35

3.3.1 Thermoplastic composites 35

3.3.2 Sheared flat plaques 39

3.3.3 Three-dimensional shapes 40

3.3.4 Prepreg flat plaques 41

3.3.5 Helicopter pilot helmet 42

3.4 FLEXURAL TESTING 43
3.5 TENSILE TESTING 43
3.6 COMPACTION TESTING 44
3.7 VOID CONTENT IMAGE ANALYSIS 44
3.7.1 Preparation of specimens 44
3.7.2 Microscopy analysis 46
3.8 AUTOMATED STRAIN ANALYSIS AND MEASUREMENT ENVIRONMENT 49
3.8.1 Shear angle measurement 51
3.8.2 Thickness measurements 54
3.8.3 Extension ratio measurements 55

4 VACUUM FORMING OF TEXTILE COMPOSITES 57

4.1 INTRODUCTION 57
4.2 EFFECT OF PROCESSING PARAMETERS ON VOID CONTENT FOR GLASS/POLYPROPYLENE COMPOSITES 57
4.2.1 Effect of time at pressure on void content 57
4.2.2 Effect of processing temperature on void content 59
4.2.3 Effect of pressure on void content 60
4.3 EFFECT OF PROCESSING PARAMETERS ON MECHANICAL PROPERTIES FOR GLASS/POLYPROPYLENE COMPOSITES 61
4.3.1 Flexural properties 61
4.3.2 Tensile properties 64
4.4 SHEARED GLASS/POLYPROPYLENE FLAT PLAQUES 66
4.4.1 Effect of shear angle on consolidation 66
4.4.2 Effect of shear angle on mechanical properties 68
4.4.3 Realignment of fibres 71
4.5 PREPREG FLAT PLAQUES 73
4.5.1 Void content analysis 73
4.5.2 Effect of void content on mechanical properties 74
4.6 CONCLUSIONS 75

5 CONSOLIDATION OF TEXTILE COMPOSITES 77

5.1 INTRODUCTION 77
5.2 PROBLEM DESCRIPTION 77
5.2.1 Evolution of microstructure 79
5.2.2 Void distribution 82
5.3 CONSOLIDATION MODELLING 86
5.3.1 Compaction sub-model 87
5.3.2 Permeability sub-model 91
5.3.3 Heat transfer sub-model 92
5.3.4 Impregnation sub-model 93

5.3.5 Shear Thinning *97*
5.4 VACUUM FORMING 100
5.4.1 Isothermal case *100*
5.4.2 Non-isothermal case *104*
5.5 PRESSURE FORMING 106
5.5.1 Remaining void content *108*
5.6 EFFECT OF IN-PLANE SHEARING ON CONSOLIDATION 110
5.7 CONCLUSIONS 114

6 PREDICTION OF MECHANICAL PROPERTIES OF TEXTILE COMPOSITES 116
6.1 INTRODUCTION 116
6.2 THEORETICAL ANALYSIS OF THE EFFECT OF VOID CONTENT ON COMPOSITE STRENGTH USING STRESS FRACTURE CRITERIA 117
6.3 THEORETICAL ANALYSIS OF THE EFFECT OF DEFORMATION ON MECHANICAL PROPERTIES 120
6.3.1 Laminate theory and failure stress criterion *120*
6.3.2 Effects of fibre misalignment/waviness *130*
6.3.3 Fibre reorientation during tensile testing *131*
6.4 CONCLUSIONS 133

7 CHARACTERISATION OF FORMED MATERIALS 135
7.1 INTRODUCTION 135
7.2 DRAPE MODEL 136
7.3 HEMISPHERE 136
7.3.1 Thickness *137*
7.3.2 Shear angle *140*
7.3.3 Extension ratio *141*
7.3.4 Void content *146*
7.3.5 Comparison between ASAME and Kinematic Drape Model *148*
7.4 HELMET 151
7.4.1 Shear Angle *151*
7.4.2 Extension ratio *154*
7.4.3 Comparison between ASAME and Kinematic Drape Model *158*
7.5 CONCLUSIONS 161

8 DISCUSSION AND CONCLUSIONS 163
8.1 INTRODUCTION 163
8.2 GENERAL DISCUSSION 163
8.3 RECOMMENDATION FOR FURTHER WORK 165
8.4 MAJOR CONCLUSIONS 166

REFERENCES 168

APPEMDIX 1.1 PROJECT PUBLICATIONS **178**

APPENDIX 3.1 STEPS TO CALCULATE PERCENTAGE OF VOID CONTENT USING APHELION **180**

Abstract

Forming and Consolidation of Textile Composites

by

Rafael García Gil

Textile composite materials are of increasing interest not only in the automotive and aerospace industries, but also in other fields such as in the sporting and the marine sectors. However, textile composite materials are not always easy to form and consolidate, and defects such as voids, fibre displacements or wrinkling can inhibit the mechanical performance of the final component. Current tendencies in the textile composite industry focus on predicting such problems through the use of software packages for composite forming, such as PAM-FORM (ESI Software) and PATRAN Laminate Modeler (MSC. Software Ltd.). However, these packages are in their infancy, and so further work is needed to validate their results.

This thesis is concerned with the manufacturing of components from textile composites, and addresses the effect that process parameters and deformation have on the consolidation of the component. A simple vacuum forming process is chosen because process parameters are easily controllable and complicated components can be produced at a reasonable cost. A consolidation model is proposed, which predicts the level of void content of a component as a function of the processing parameters, based on experimental data. The validity of the model is assessed by comparison between predictions and measurements, which were correlated with mechanical property measurements to illustrate the effects of processing on subsequent performance. A combination of theoretical models is proposed to predict the effects of void content and in-plane deformation on mechanical properties. Finally, an automated strain analysis system used in the metal forming industry is adapted to analyse components formed from composite materials and parameters such as fibre angle, extension ratios along the fibre direction and change in thickness on demonstrator components are measured. These measurements are used to validate deformation simulations based on draping algorithms.

Acknowledgements

The author would like to thank his supervisors Dr. A. C. Long and Dr. M. J. Clifford for their guidance and assistance during this research.

The funding for this project was supplied by the EPSRC and their support has been gratefully received. The DEPART project partners: Ford Motor Company, BAE Systems, QinetiQ, BP Amoco, ESI Software, MSC. Software Ltd., Saint-Gobain Vetrotex, Hexcel Composites, University of Leeds and University of Cambridge are also thanked, especially Dr. S. B. Sharma and Dr. M. P. F. Sutcliffe for their input into the research.

The Head of the School, Professor Hyde, receives thanks for allowing the use of facilities. The technical assistance of Paul Johns, Geoff Tomlinson, Roger Smith, and Dave Smith was much appreciated.

Thanks are given to my fellow researchers/colleagues Dr. Phil Harrison, Dr. Francois Robitaille, Jon Crookston, Brendon Weager, Jo Wiggers, Peter Schubel, Nuno Correia, Agnes Ragondet and Graham Aitchison who have not only provided technical assistance but have created a relaxed friendly working environment over the last few years.

Finally, special thanks goes to my family who have shown interest and support during the time of this research project.

Glossary

Anisotropic:	Material exhibiting properties that vary with orientation within the material.
Composite:	Material created by the synthetic assembly of reinforcing elements and compatible matrix binder to maximise specific characteristics and properties.
Commingled:	The result of intimately mixing two separate fibres into a strand.
Cure:	Change of a thermosetting resin state from liquid to solid by polymerisation.
Delamination:	Split occurring in a laminated composite material along the plane of its layers
Drape:	The ability to conform to an irregular shape.
Drape Model:	Model used to predict the deformation of reinforcement after forming over the surface of a component.
Fabric:	Material formed of interlaced yarns.
Fibre:	A single homogeneous strand of material, which can be spun into a yarn or roving.
Generator path:	A path required by a kinematic drape model to perform a drape simulation over a component.
Fibre Angle:	The acute angle between warp and weft tows.
In-plane shear:	Fabric deformation via rotation at yarn intersections.
In-plane slip:	Fabric deformation via the increase or decrease in yarn spacing.
Isotropic:	A material with uniform properties in all directions. The measured properties of an isotropic material are independent of the axis of testing.
Locking angle:	Maximum shear angle before wrinkling occurs
Matrix:	Resinous phase of a composite in which the fibre system is embedded.
Melt temperature:	The temperature at which the resin changes from a solid phase to a liquid phase.

Permeability:	The property of a porous material that characterise the ease of fluid impregnation.
Prepreg:	Thermoset composite supplied in sheet form ready for moulding. The resin is partly cured.
Pitch:	The spacing between yarns.
Reinforcement:	Assembly of high modulus flexible fibres usually bonded into a matrix to improve its mechanical properties.
Roving:	A number of yarns or tows collected into a parallel bundle with little or no twist.
Shear Angle:	The reduction in angle between warp and weft tows from their original configuration to their sheared configuration.
Tex:	A unit for expressing linear density equal to the mass in grams of 1000 metres of yarn.
Thermoplastic:	Material that is melted and formed into a plastic article.
Thermoset:	Material that undergoes a chemical transformation to become a permanent plastic article.
Tow:	An untwisted bundle of continuous filaments.
Void:	Pockets of entrapped gas or air in a laminate.
Viscosity:	The resistance to flow existing between two liquid layers when they are moved relative to each other
Warp:	The direction along the roll of a commercial reinforcement.
Weft:	The direction across the roll of a commercial reinforcement.
Weave:	A method of interlacing tows or yarns to form a fabric.
Yarn:	An assembly of twisted fibres used to weave textile composites.

Nomenclature

Symbol	Definition	
∇P	Pressure gradient	Pam^{-1}
ΔH	Flow activation energy	kJ/mol
Θ	Temperature difference	K
ψ	Distance characteristic of the material in stress fracture criteria	m
ς	Amplitude in fibre waviness equation	m
α	Thermal diffusivity	m^2s^{-1}
β_{lv}	Surface tension of the wetting liquid	Jm^{-2}
δ	Angular deviation of fibre from the principal direction	°
ε	Strain	
ϕ	Average void content	
γ	Shear strain	
η	Load bearing efficiency	
σ	Stress	Pa
τ	Shear stress	Pa
φ	Fibre angle	°
λ	Wavelength of tow	m
λ_{cy}	Fitting parameter used in Carreau-Yasuda model	
μ	Matrix viscosity	Pas
ρ	Density	kgm^{-3}
θ	Shear angle	°
ν	Poisson's ratio	
ω	Contact angle between the solid and the liquid	°
ζ	Constant in stress fracture criteria	
ξ	Constant in Halpin-Tsai equations	
a	Length parallel to major axis of a tow cross-section	m
a_T	Shift factor used in Carreau-Yasuda model	
A	Area	m^2
A_s	Fibre bed elastic constant	m^2

A_t	Area of a fully consolidated yarn	m^2
b	Length parallel to minor axis of a tow cross section	m
B	Compaction pressure exponent	
c	Heat capacity	$Jkg^{-1}K^{-1}$
C	Gebart constant	
d	Diameter	m
D	Compaction pressure constant	
e	Ply surface geometric parameter (height)	m
E	Young's modulus	GPa
f	Ply surface geometric parameter (width)	m
g	Power law index	
G	Shear modulus	GPa
h	Laminate thickness	M
H_C	Composite fracture toughness	$MNm^{-3/2}$
i	Fitting parameter used in Carreau-Yasuda model	
k	Thermal conductivity	$Wm^{-1}K^{-1}$
k'	Modified Kozeny constant	
K	Permeability	m^2
K'	Kozeny constant	
l	Side length	m
L	Length of the fibre over the wavelength	m
m	Fitting parameter used in Carreau-Yasuda model	
n	Tow shape equation exponent	
n_l	Number of layers	
N_a	Number of agglomerations	
N_t	Number of reinforcing fibres	
p	Population	
P	Pressure	Pa
q	Flow velocity	ms^{-1}
r	Radius	m
r_{eq}	Hydraulic equivalence factor	
R	Boltzmann gas constant	$kJ/mol^{-1}K^{-1}$
R_f	Effective fibre radius	m

SD	Standard deviation	
t	Elapsed time	seconds
T	Temperature	K
u	Velocity	ms^{-1}
v_a	Fibre volume fraction at zero permeability	
v_f	Fibre volume fraction within the tow	
V	Velocity	ms^{-1}
V_a	Available fibre volume fraction	
V_c	Void content	
V_f	Laminate fibre volume fraction	
w	Ply surface geometrical parameter (gap)	m
x	Space between fibres	
z	Standardised normal variable	

Subscripts

0	Property before initial consolidation
1	Principal axis of unidirectional lamina
2	Transverse axis of unidirectional lamina
3	Through thickness axis of unidirectional lamina
∞	Property at full consilidation
a	Property applied
atm	Property of the atmosphere
b	Property of fibre bundle
e	Property of encroached matrix
f	Property of fibre
g	Property of gas or void
i, j	Matrix element indices
Inter-Tow	Property of inter-tow
k	Property of k^{th} lamina
l	Property of whole laminate
m	Property of matrix
r	Property of resin (when molten)

ref	Reference property value
S	Tow-pitch
t	Matrix after transformation
Tow	Property of tow
True	Logarithmic definition
u	Ultimate
x	Axis of loading

Superscript

*	Estimated value
θ	Property of laminate sheared by an angle θ

1 Introduction and objectives

1.1 Introduction to Composites

Composites materials have existed since ancient times as simple structures that used natural fibres such as cotton, silk or wool as reinforcement. However, the development of new materials has boosted the creation of industries dedicated to produce novel raw materials and manufacture goods ranging from aerospace vehicles to household appliances. In the production of composites, cost reduction in terms of energy consumption is a major factor to consider, with reduction in weight and increased specific modulus being the main criteria. The US Office of Technology Assessment has identified toughness improvement and reduction of fabrication cost as two of the major requirements for composite materials used in aerospace and military applications **[1]**, which affect directly the choice of composite components.

Thermoplastic matrix composites offer many advantages compared with thermosetting composites. These include increased toughness, impact resistance, environmental stability and considerable reduction in the initial and in-service cost of components **[2]**. The main disadvantages of thermoplastic composites include difficulty of impregnation **[3]** due to increased matrix viscosities, lack of a class A surface finish, poor solvent resistance for amorphous polymers and susceptibility to environmental stress cracking. In contrast, thermoset polymers have relatively low viscosities during the impregnation stage and can be readily impregnated into the reinforcing fibres using a variety of techniques.

1.2 Product Forms

In order not only to achieve full structural performance but also an adequate fibre-matrix interface, proper impregnation of the matrix into the reinforcement is required. During recent years, several impregnation techniques have been developed resulting in different product forms that affect the handling, processing and properties of the composite. The techniques may be divided into those that give a

pre-impregnated material, such as melt impregnation and solvent aided impregnation, and those that give a post-impregnated form **[2]**. The main feature of the pre-impregnated materials is full wetting and impregnation of the reinforcement fibres before final forming. Melt impregnation is in principle the simplest method of impregnation, involving pulling the reinforcement fibres through the molten matrix without requiring any solvents that must be removed at a later stage. In contrast, post-impregnation techniques achieve physical mixing of the matrix and the reinforcement, with full impregnation achieved by subsequent processing. Four main methods have been identified consisting of:

a) ***Film stacking***

Layers of polymer film are placed between layers of reinforcing fibres. Impregnation is achieved by the application of pressure at elevated temperature. Figure 1.1 shows this technique.

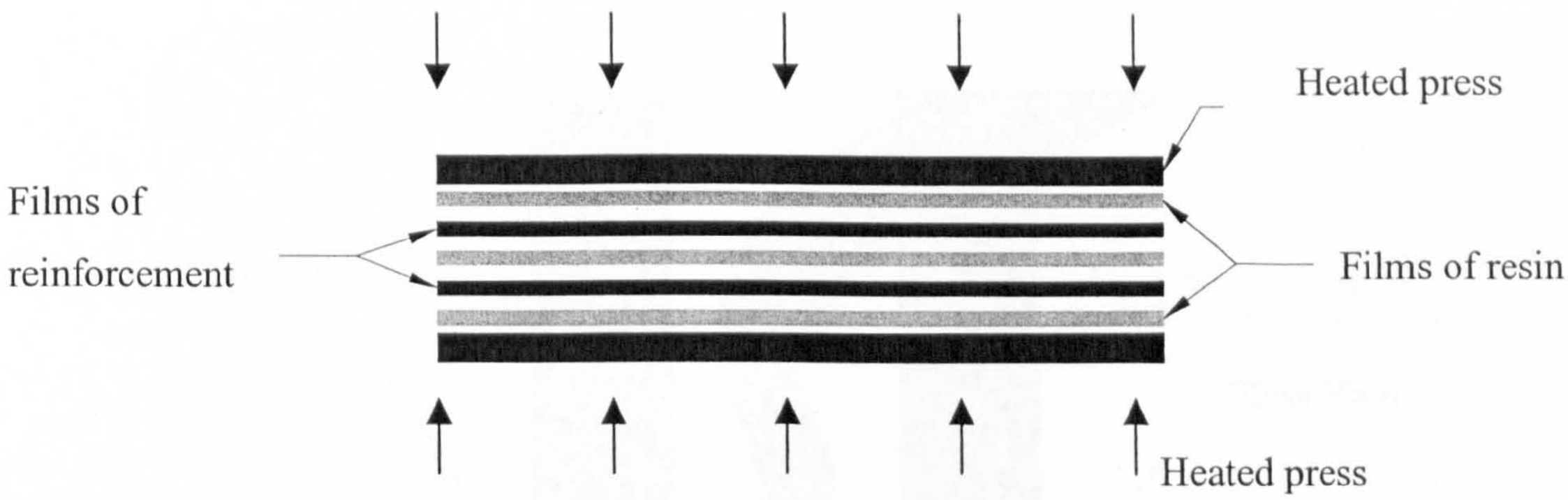

Figure 1.1 Film stacking.

b) ***Powder coating***

Fine polymer particles are uniformly distributed within the reinforcing fibre bundle. Powder coating is shown in Figure 1.2.

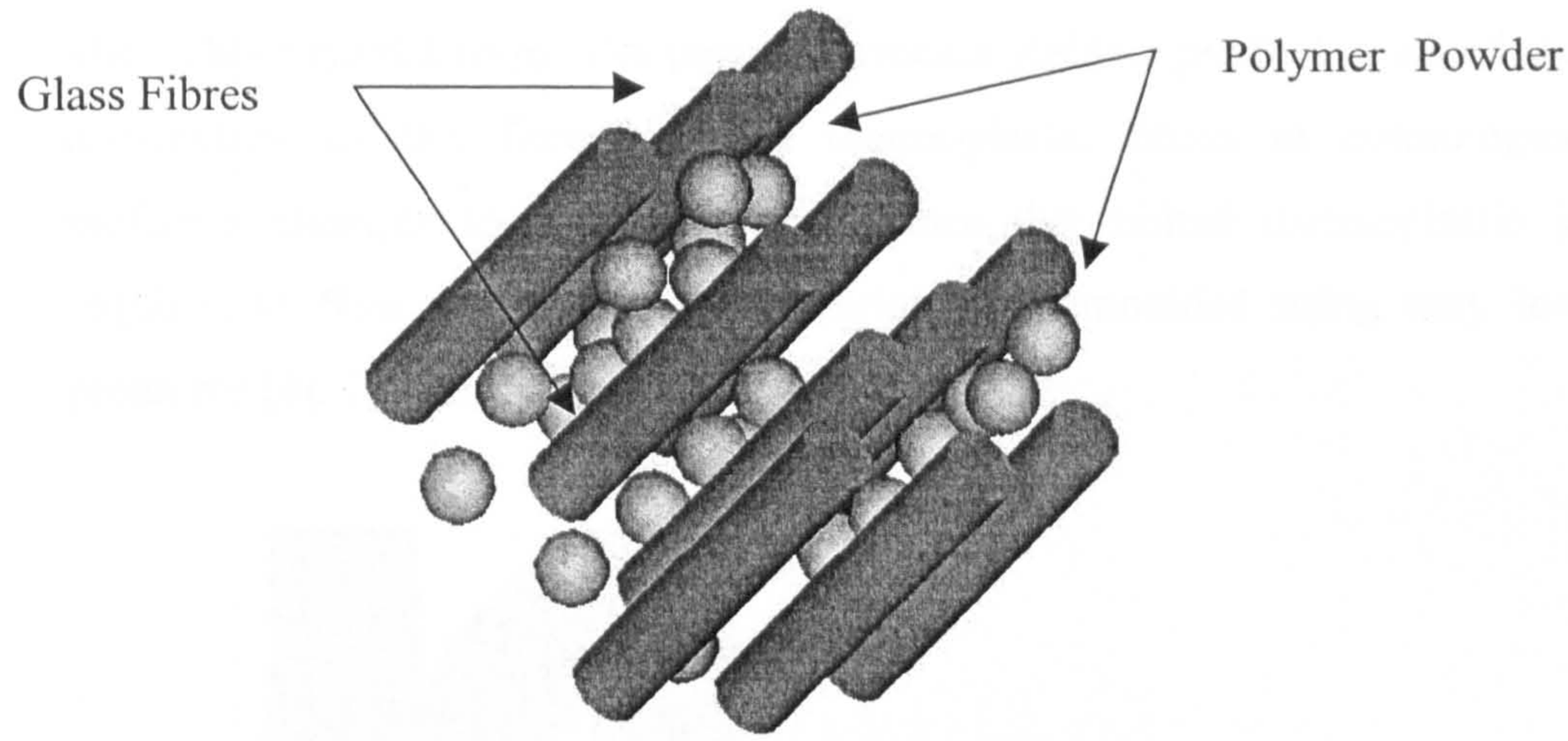

Figure 1.2 Powder coating.

c) Co-weaving

Co-weaving consists of weaving tows of the reinforcing fibre and polymer fibre together. Co-weaving is shown in Figure 1.3.

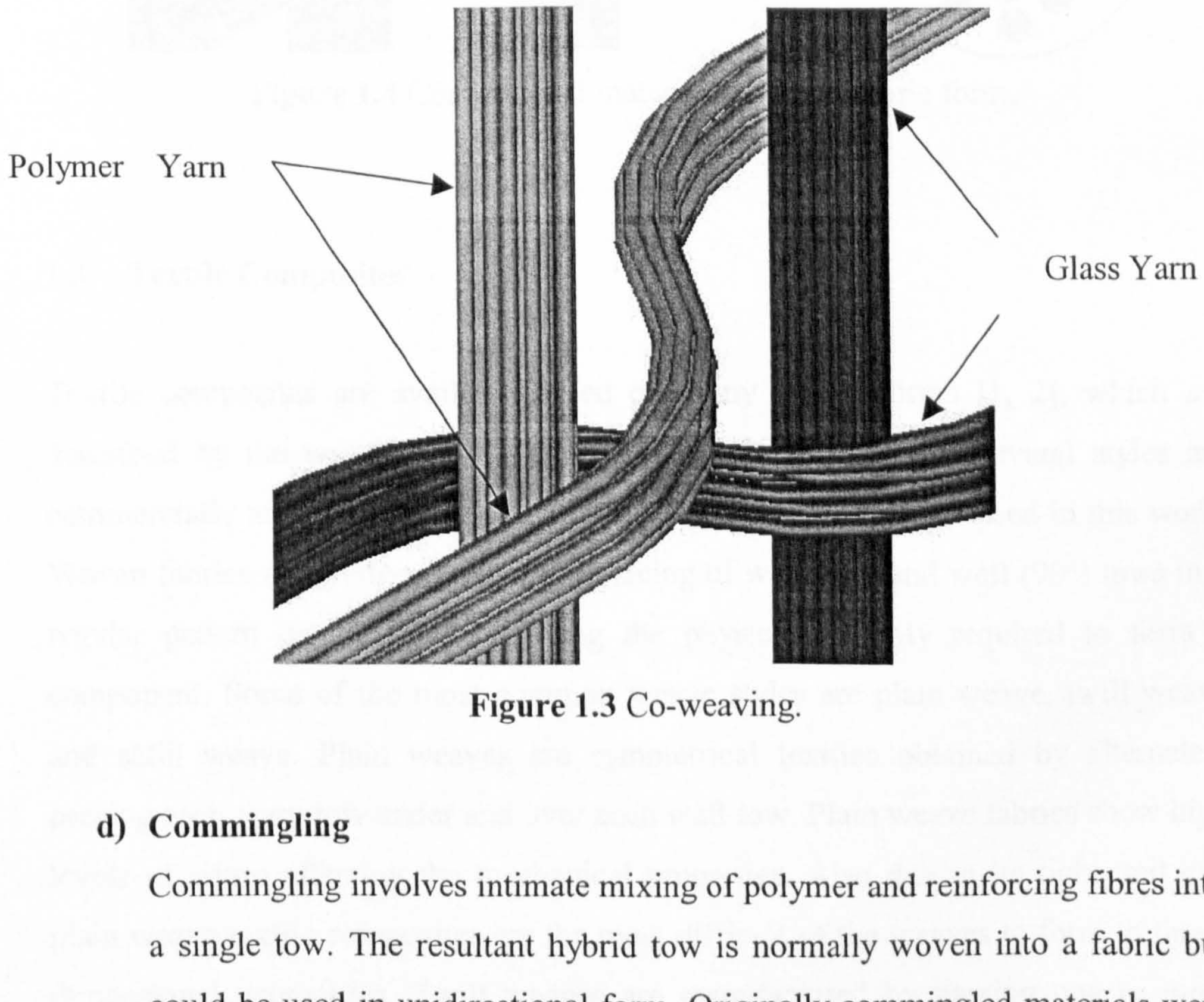

Figure 1.3 Co-weaving.

d) Commingling

Commingling involves intimate mixing of polymer and reinforcing fibres into a single tow. The resultant hybrid tow is normally woven into a fabric but could be used in unidirectional form. Originally commingled materials were

expensive, but the introduction of Twintex® by Vetrotex has made this an affordable material form. The patented process yields a product in which the distribution of the fibreglass and thermoplastic fibres in commingled preforms attempts to minimise the distance the molten thermoplastic is required to flow and allows the material to be moulded using very low pressures **[4]**. Commingling is shown in Figure 1.4.

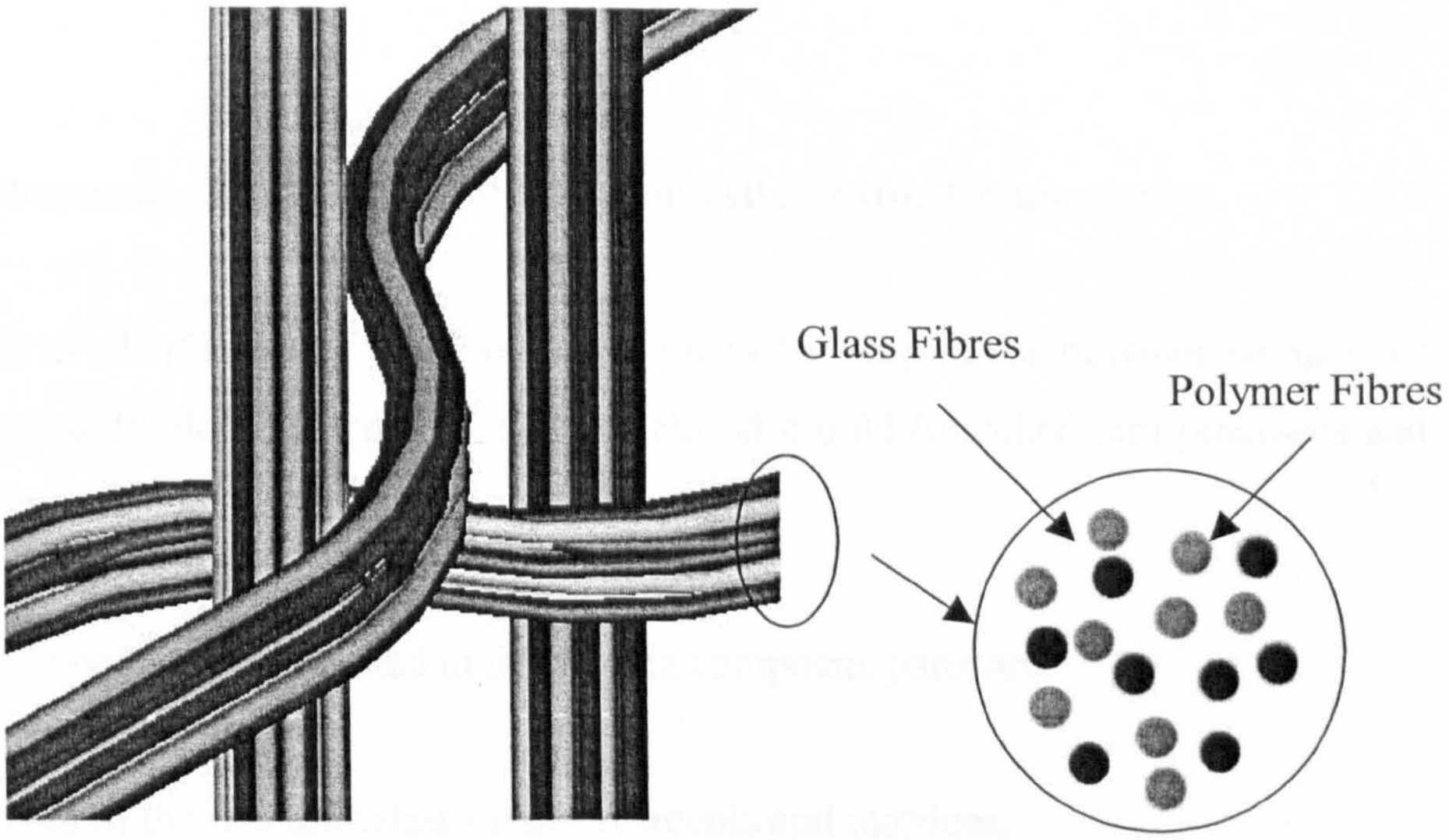

Figure 1.4 Commingled material in woven fabric form.

1.3 Textile Composites

Textile composites are available based on many textile forms **[1, 2]**, which are described by the unit cell (or representative volume element). Several styles are commercially available at present. However, only 2D weaves are used in this work. Woven fabrics are produced by the interlacing of warp (0°) and weft (90°) tows in a regular pattern or weave style giving the physical integrity required to form a component. Some of the most common weave styles are plain weave, twill weave and satin weave. Plain weaves are symmetrical textiles obtained by alternately passing each warp tow under and over each weft tow. Plain weave fabrics show high levels of crimp affecting the mechanical properties. Also due to its tight unit cell plain weave textile composites are the most difficult of the weaves to form to three-dimensional geometries. Twill weaves are manufactured by passing one or more

warp tow over and under two or more weft tows. Superior wet out and drape is seen in the twill weave over the plain weave with only a small reduction in stability. Due to its lower crimp the twill weave provides slightly higher in-plane mechanical properties. Satin weaves are basically twill weaves modified to produce fewer intersections of warp and weft. The harness number used in the designation represents the total number of tows crossed and passed under, before the weave is repeated.

1.4 Processing Techniques for Thermoplastic Textile Composites

Akovali et al. **[5]** discussed several processing techniques for polymer composites that can be divided into open mould and closed mould (matched die) processes and pultrusion.

The basic operations involved in fabricating composite parts are:

- Lay-up of the raw materials - reinforcements and matrices.
- Application of heat and pressure, and cooling and consolidation into the final desired form.
- Assembly and joining of separate components.

In open mould process only one mould surface is used, which can be a male or a female tool. The main matrix materials used are thermosetting resins such as epoxy and polyester, while E-glass fibres are the most widely used reinforcement material. Different fibre reinforcement such as mats, woven roving or yarns can be used. One of the advantages of open mould techniques is the ability to produce very large and complex structures. However, open mould has disadvantages such as heating of large structures, surface finishing, required amount of labour, processing times and exposure of operators to potentially harmful emissions.

Currently, most of the open mould processes applied to thermoplastic composites are bag moulding processes. The purpose of the bag moulding process is to compact the laminate on the open mould surface and to evacuate volatiles by applying usually

vacuum pressure to the textile composite. The simplest technique is vacuum bagging in which only atmospheric pressure is used for consolidation and forming. Complex shapes, including double contours and relatively large parts, can be handled without difficulty. The required number of plies for a lay-up are pre-cut to size and positioned in the mould one ply at a time. The complete lay-up is covered with a porous, non-adhering material, which provides easy release and vacuum access to the lay-up. A simple classification is as follows:

a) Vacuum bag moulding

In vacuum bag moulding, the laminate is laid-up by hand. In order to achieve even distribution of pressure a breather film and an extensible polymeric sheet must be used. After sealing the edges of the vacuum bag, a vacuum pressure is applied during processing. Vacuum consolidation is shown in Figure 1.5

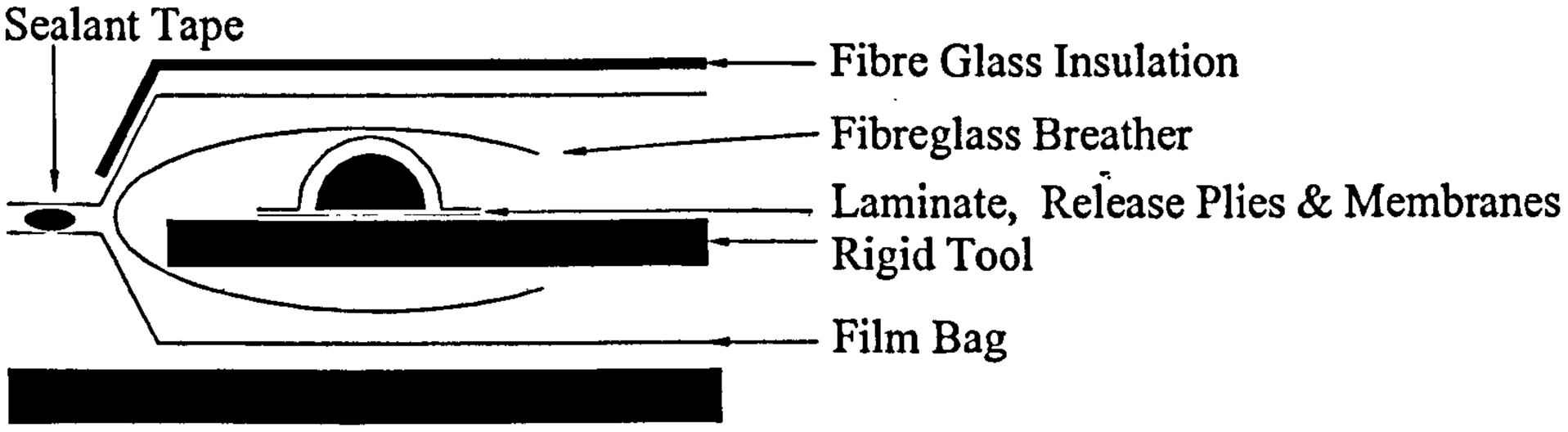

Figure 1.5 Vacuum consolidation.

b) Pressure bag moulding

In this method positive pressure is applied by blowing air to inflate a bag covering the laminate on the open mould surface. Pressure bag moulding is especially suitable for complex hollow components.

c) Diaphragm forming

In diaphragm forming the laminate is placed between two deformable diaphragms. The diaphragms are sealed and the space between the diaphragms is evacuated. This arrangement is then heated and the upper

diaphragm is loaded with the forming pressure, which forces the material into the vented mould. The main disadvantages of this process are that the geometry of the component is limited by the deformation of the diaphragm and long cycle times are required due to the thermal inertia in heating and cooling of the whole system.

d) Autoclave systems

The autoclave moulding process is used mainly in industries where production rate is not important. Although autoclaves have traditionally been used for thermoset composite curing, they are increasingly used for thermoplastic **[6]**. The principles of autoclave forming are similar to those for diaphragm forming, although higher pressures can be applied in order to form and consolidate laminates in shorter cycle times. Figure 1.6 shows this technique.

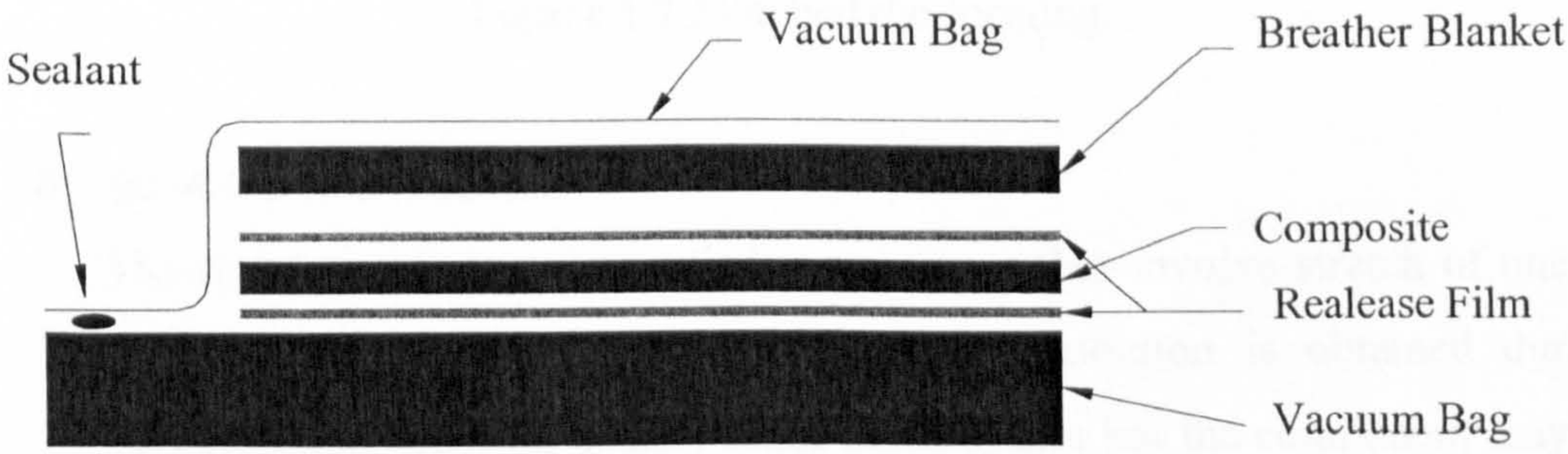

Figure 1.6 Autoclave processing of thermoplastic composites.

Closed mould processes are used widely in the composite industry for the fabrication and manufacturing of three-dimensional components and products. Closed mould processes can be divided into matched–mould techniques and stretch-draw processes.

e) Matched-Mould Techniques

In these techniques the material being formed is heated above the melting point of the resin and then transferred and shaped between two matched dies, which must be properly machined and aligned. The simplest technique is to mould a flat panel using a single platen press, where the material must have a uniform thickness. To produce more complex shapes, matched male-female

tools must be used. The main disadvantages of this technique are that it requires a high temperature press and the size of the parts is limited by the temperature distribution and clamping force required. Additionally, variations in thickness caused by forming may lead to an uneven pressure distribution and consequently poor consolidation. Matched die forming is shown in Figure 1.7.

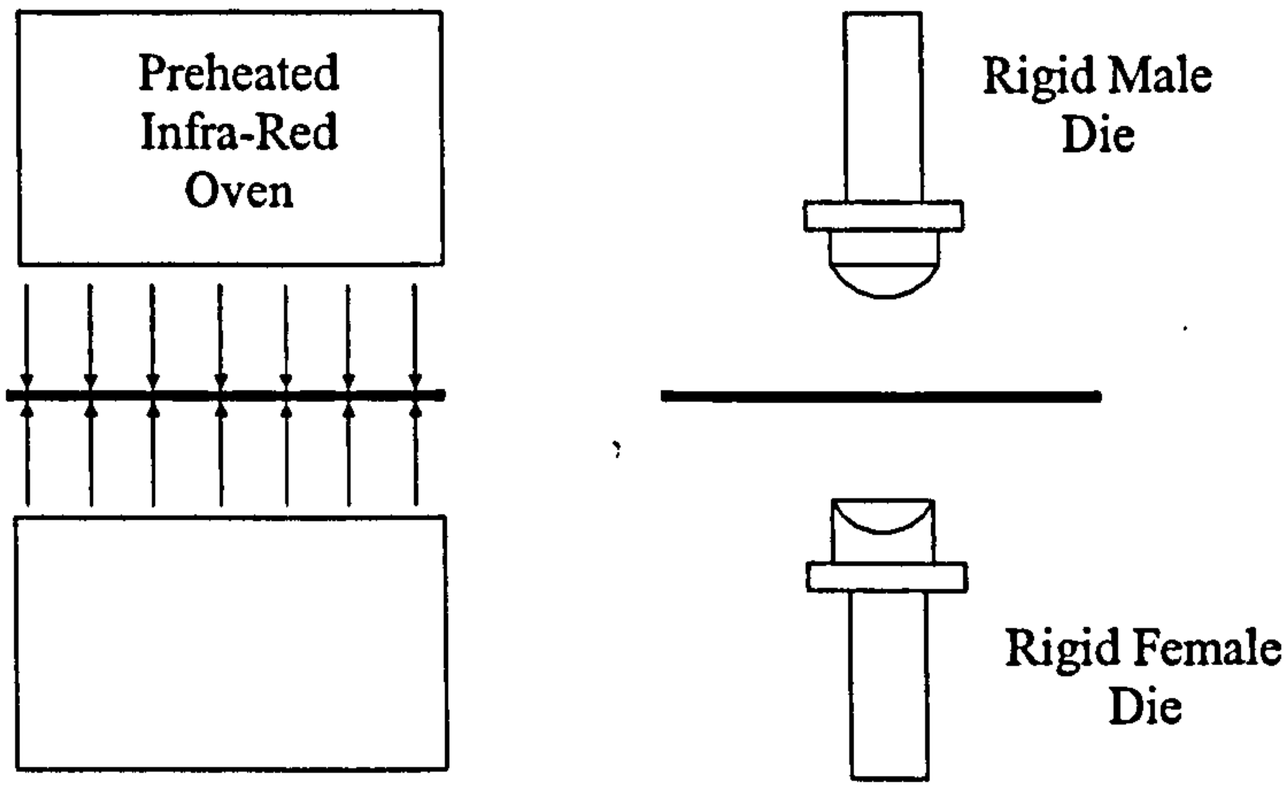

Figure 1.7 Matched die forming.

f) ***Stretch-Draw Processes***

The term stretch-draw is applied to processes that involve stretch of one of the dies. As a result, an even pressure distribution is obtained during consolidation. Cooling usually takes place in-situ but the component may be removed from the forming station for cooling. Hydroforming, Figure 1.8, uses hydrostatic pressure provided by an oil reservoir to form the part over the mould. The blanks are usually preheated and then quickly transferred to a male or female mould for forming. A similar process to hydroforming is rubber block forming where a rubber block is substituted for the oil reservoir.

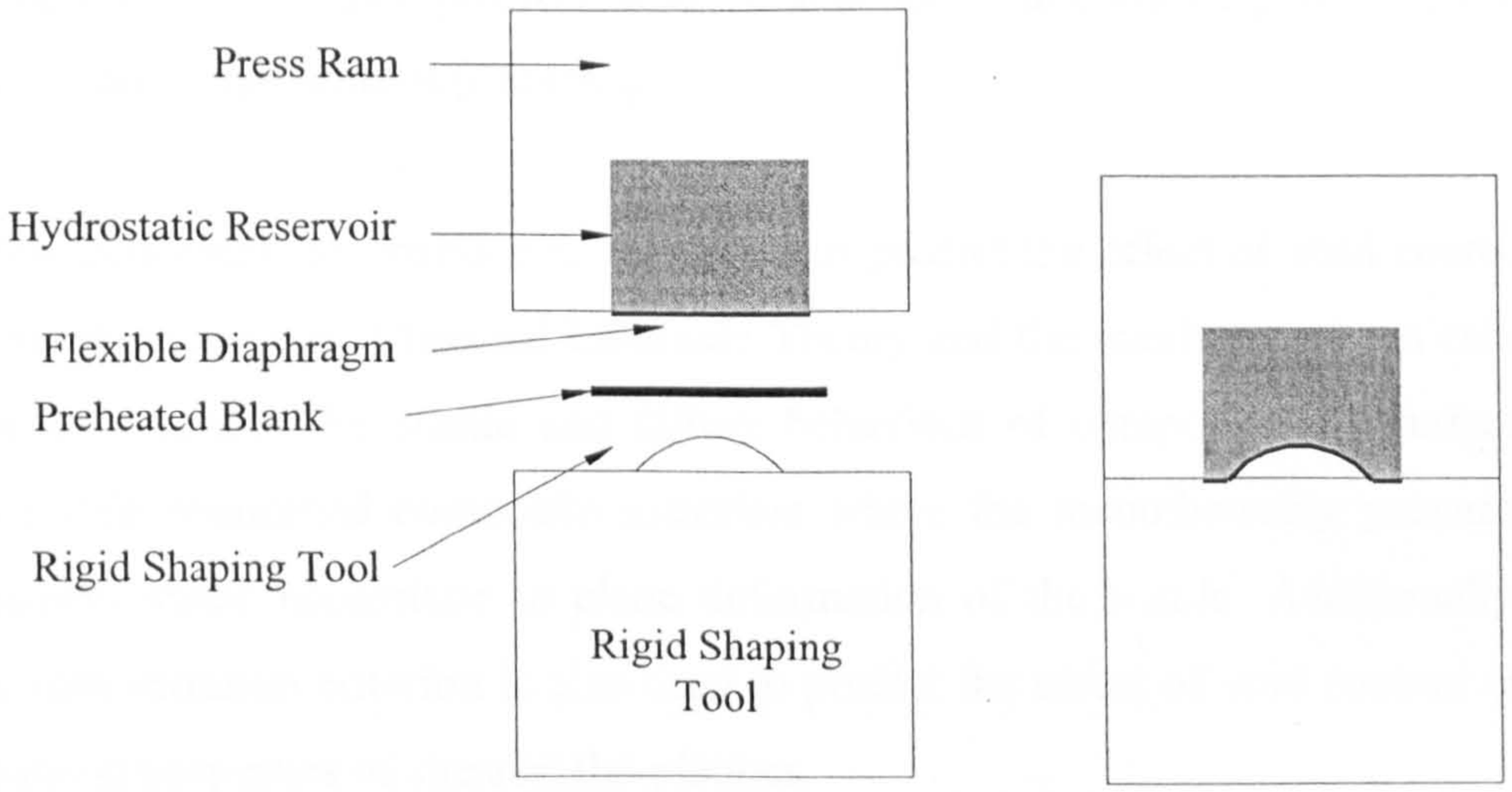

Figure 1.8 Hydroforming.

1.5 Theme of this Work

This thesis is concerned with the study and prediction of defects that may appear during forming and consolidation of textile composites, which may inhibit the mechanical performance of the final component. Special attention is dedicated to the presence of voids and fibre displacements, which are a direct result of the forming and consolidation process. A list of publications resulting from this research is presented in Appendix 1.1.

This research examines the use of commingled polypropylene matrix composites and carbon fibre prepreg for a wide range of applications. The work is concerned with how the vacuum forming process affects the mechanical properties of continuous glass reinforced polypropylene composites and carbon fibre / epoxy matrix prepregs.

A vacuum forming process is used to consolidate flat plaques with a range of void contents due to the ability to control the processing parameters. A limited number of components (flat plaques and demonstrator components) are produced to assess the effect of void content and deformation on mechanical properties. Once the effect of processing parameters and deformation on mechanical properties is assessed, a

consolidation model that predicts void content as a function of pressure, time at pressure and temperature is presented. .

A stress concentration criterion is then used to predict the effect of void content on mechanical properties. Classical Laminate Theory and the maximum stress criterion are used to model the elastic and failure behaviour of components manufactured from textile reinforced composite materials where the manufacturing process and component shape necessitate in plane deformation of the textile. Additionally, the stress concentration criterion is also used to predict the effect of void content on the mechanical properties of sheared flat plaques.

Finally, complicated demonstrator components are manufactured using a non-isothermal vacuum forming process. A strain analysis system that calculates thickness, shear angle and inter-tow slippage is developed with the aim of characterising formed materials and comparing fibre patterns with simulations produced using available software packages. Different mechanisms of deformation depending on the material characteristics are identified and the effects of these on the final fibre pattern are assessed.

2 Literature Review

2.1 Introduction

This chapter contains a review of current literature relating to low pressure forming and consolidation of textile composites. A brief description of the vacuum forming process and its applications is given. Special emphasis is given to the measurement and prediction of void content and the effect of voids on the mechanical properties of components. A review of different consolidation models suitable for thermoplastic textile composites is presented. A number of existing models that explain the effect of in-plane shear on the mechanical properties are also summarised and analysed.

2.2 Vacuum forming of textile composites

Vacuum bagging is used to consolidate composites used in automotive, aerospace parts and other applications **[5]**. Materials that are pre-impregnated with resin are typically consolidated using vacuum bagging techniques. The components include a film or fabric, breather medium and plastic film that is applied in sequence on top of a laminate stack in an airtight mould. Air between the mould and film is extracted with a vacuum pump, resulting in a positive-pressure force. This compression forces air and excess resin from a composite laminate or components. The main disadvantages of vacuum forming processes include: impracticality of the process when higher pressures are needed in order to form the component, consolidation timescales, high labour costs and cost of disposable bagging materials **[6]**. However, the vacuum forming process is still suitable for the production of components such as golf cars, wind turbine blades, army assault crafts, powerboats, sailboats or rigid inflatable boats **[5]**.

2.3 Void content analysis

Voids are among the most common manufacturing induced defects in polymer matrix composites. Void formation can be due to a number of reasons, including air entrapment during the formulation of the resin system, moisture absorption during material storage or processing and incorrect tow placement during moulding **[7]**. The detrimental effect of void content on mechanical properties of composite laminates is well known for thermosetting composites **[8, 9]**. In thermoplastic composites, recent studies have clarified the link between the application of optimised moulding parameters, the reduction in void content and the improvement in some properties of the laminate, such as interlaminar shear strength and Charpy impact strengths **[10, 11]**. Techniques most commonly identified so far for the determination of void content in composites can be divided into three large groups: methods based on density measurements, non-destructive methods and microscopy based methods.

As reported in ASTM D1505-98, void content accurate to ±2.5% by volume can be determined by comparison of the theoretical density based upon constituent proportions and densities. On a similar principle, burn-off is probably the most widely used technique for void content measurement in composite materials and is standardised in ASTM D2734-94. Burn-off results are accurate at levels of ± 1% void content **[2]**, if the effect of ignition on the materials is known and assuming that the density of the resin is the same in the composite as it is in a large cast mass. However, differences in curing, heat and pressure, and molecular forces from the reinforcement surface change the composite resin density from the bulk resin density. Problems related with void content measurement in thermoplastic laminates were address by Wakeman **[2]**. He stated that composite resin density was difficult to measure due to air trapped on a sample affecting the void content measurement.

Other methods for void measurement in composites have also been proposed, which involve pore filling, for example, by measuring the limiting moisture content **[12]** and acid digestion techniques **[13]**. These methods are only suitable in the case that the volume of closed porosity, which does not allow moisture to enter the material, is negligible compared to the total void content. This is often the case with natural fibre composites, but it is not necessarily the case for all polymeric matrix composites.

Among methods based on non-destructive techniques **[14]**, void content measurement is possible using ultrasound, since a high void content (exceeding 10%) gives appreciable variations of ultrasound attenuation coefficient **[15, 16]**. Nuclear magnetic resonance imaging (NMRI) has also been used to detect voids with diameters of more than 100 μm, assuming that water collects at defects and an image is acquired of water absorbed by the composite **[17]**.

From the above considerations, a number of limitations are apparent, which leave a considerable scope for alternative techniques, such as those based on microstructural image analysis. A review of such techniques for composites has been provided by Guild et al. **[18]**. Accurate void content measurements at low levels of porosity (less than 1%) can be carried out using a statistical point-counting technique from optical or electron microscopy images **[19, 20]**. The morphology of voids has been analysed under a microscope, mainly for carbon fibre reinforced composites **[21 - 24]**. In some cases, the complex geometric profile of the microvoids in composites was resolved from micrographs with the support of fractal geometry **[25, 26]**.

Due to the facilities required for some of the techniques and lack of accuracy for others, this work concentrates on the use of microscopy and image analysis to determine void content. This requires that a representative number of photomicrographs must be analysed. To measure the void content quantitatively using image analysis techniques, the voids must appear different from the fibres and matrix. The percentage of the image corresponding to the voids can then be calculated. In order to address these issues, an extensive analysis of this technique, which includes the determination of a representative number of micrographs required to obtain an accurate measurement of the void content, is presented in Section 3.7.

2.4 Consolidation of thermoplastic textile composites

In this section, a review of the different sub-models required to predict the through thickness fibre deformation and matrix flow during compaction for commingled thermoplastic textile composites is presented. From this review four main

components of a consolidation model are identified: deformation of the reinforcement, fibre bundle permeability, heat transfer and matrix flow.

2.4.1 Fibre bed permeability

Flow of the matrix through the porous medium formed by the fibres is usually modelled using Darcy's law, derived from experiments on macroscopically isotropic particle beds consisting of sphere like particles. Darcy's law (Eqn. 2.1) relates the flow velocity to the driving pressure gradient, the Newtonian viscosity of the fluid, and a constant permeability *K*.

$$q = -\frac{K}{\mu}\nabla P \qquad (2.1)$$

Numerous researchers extended the relationship to conditions encountered in the production of fibre reinforced composites, where the changing permeability and viscosity is required. Permeability is affected mainly by changes in the fibre volume fraction. One theory, which accounts for such effect, is the Kozeny-Carman equation (Eqn. 2.2) **[27]**.

$$K = \frac{r_f^2}{4K'}\frac{(1-v_f)^3}{v_f^2} \qquad (2.2)$$

Here r_f is the fibre radius, K' is the Kozeny constant and v_f is the fibre volume fraction. Gutowski et al. **[28]** proposed an alternative expression for transverse permeability to overcome the limitations in Kozeny-Carman equation. When the fibre volume fraction approaches a limit v_a, the transverse flow of matrix can be blocked as the fibres are forced into contact with one another along their entire lengths **[29]**.

$$K = \frac{r_f^2}{4k'} \frac{\left(\sqrt{\frac{v_a}{v_f}} - 1\right)^3}{\frac{v_a}{v_f} + 1} \qquad (2.3)$$

The Kozeny-Carman theory was initially developed for granular beds consisting of ellipsoids, and is the basis for most of the research concerned with impregnation of a fibrous bed.

In connection with Darcy's law, the Kozeny-Carman definition has been modified to model the flow in the direction transverse to the fibres **[30 - 34]**, the flow in the axial direction **[35 - 37]** and finally as a combined flow in both transverse and axial direction **[38, 39]**.

Gebart **[40]** studied the permeability of unidirectional reinforcement consisting of regular ordered parallel fibres. Gebart's model does not involve a permeability parameter that needs to be determined experimentally and is only based on fibre arrangement parameters. Eqn. 2.4 represents Gebart's model.

$$K = C\left(\sqrt{\frac{v_a}{v_f} - 1}\right)^{2.5} R_f^2 \qquad (2.4)$$

where C is a constant, v_a is the fibre volume fraction at zero permeability, v_f is the fibre volume fraction and R_f is the effective fibre radius. The values of these parameters depending on the fibre arrangement are:

Quadratic arrangement: $$C = \frac{16}{9\pi\sqrt{2}};\ v_a = \frac{\pi}{4} \qquad (2.5)$$

Hexagonal arrangement: $$C = \frac{16}{9\pi\sqrt{6}};\ v_a = \frac{\pi}{2\sqrt{3}} \qquad (2.6)$$

Although excellent agreement was stated between the theoretical model and the experimental data in Gebart's work, the effective fibre radius was used as a fitting parameter whose value was four times larger than the real fibre radius.

2.4.2 Fibre bed compaction

Gutowski et al. **[28]** developed a mathematical expression for the applied pressure based on compaction experiments carried out on aligned carbon fibres impregnated with constant viscosity oils.

$$P_a = P_r + P_f \tag{2.7}$$

where P_f is a function of the initial fibre volume fraction V_0, the available fibre volume fraction V_a and a fibre bed elastic constant A_s.

$$P_f = A_s \frac{\left(\frac{V_f}{V_0} - 1\right)}{\left(\frac{1}{V_f} - \frac{1}{V_a}\right)^4} \tag{2.8}$$

Gutowski et al. suggested that when the consolidation pressure P_a is first applied and the volume fraction is low, the fibres carry no load (P_f=0) and the pressure in the fluid P_r (they used constant viscosity oil) is equal to the applied pressure. When resin squeezes out and the fibre volume fraction increases uncountable contacts between fibres, which carry a portion of the load, are produced.

Van West **[33, 34]** used a fibre compaction model of similar form to that presented by Gutowski and based on work by Hou **[41]**:

$$P_f = A_s \frac{h_o - h}{\left(1 - \frac{h_o - h}{h_o - h_\infty}\right)^n} \tag{2.9}$$

Where P_{fb} is the fibre bed pressure, A_s is a fibre bed elastic constant, h_o is the initial laminate thickness, h_∞ is the minimum laminate thickness and h is the instantaneous laminate thickness. This expression relies on experimental compaction data to determinate suitable values for A_s and n. Cain et al. **[42, 43]** carried out experiments for the same commingled fabric as used in the present study to evaluate the compaction characteristics of the glass fibres within the commingled fabric in isolation. Samples were heated to 400°C for 300 seconds to burn off the polypropylene. The fabric was then soaked in mineral oil as the fibre bed would be lubricated by the molten matrix material during the moulding process. The samples were compacted between flat platens using an Instron model 1195 testing machine at 1 mm/minute. A simple power law model was used to model the compaction behaviour:

$$P_f = C\left(\frac{h_o}{h}\right)^B \qquad \textbf{(2. 10)}$$

The constants C and B were determined to be 0.035495 Pa and 10.1 respectively.

A different expression was developed by Bernet **[44, 45]**, who took into account the contribution of capillary pressure and pressure within entrapped voids. The applied pressure is then rearranged as:

$$P_0 = P_f + P_r + P_g - P_c \qquad \textbf{(2. 11)}$$

where P_c is the capillary pressure counted here as positive when it enhances resin flow. Following Bernet's model, the capillary pressure can be estimated theoretically using the Young-Laplace equation:

$$P_c = \frac{4\beta_{lv}\cos\omega}{d_e} \qquad \textbf{(2. 12)}$$

Where β_{lv} is the surface tension of the resin, ω is the contact angle and Eqn. 2.13 expresses d_e as a function of the fibre diameter d_f and fibre volume fraction v_f.

$$d_e = 2d_f \frac{1-v_f}{v_f} \tag{2.13}$$

Substituting Eqn. 2.13 in Eqn. 2.12, the capillary pressure can be expressed as a function of fibre volume fraction.

$$P_c = \frac{4\beta_{lv}\cos\omega}{d_f}\frac{v_f}{1-v_f} \tag{2.14}$$

Gibson et al. **[30]** noted that in systems characterised by a good wetting between the fibres and the matrix the capillary pressure is usually positive and in the range 4-40 kPa. This suggests that for high applied pressures, capillary pressure may be neglected. However for vacuum forming where the maximum pressure is 100 kPa, capillary pressure may be important.

2.4.3 Impregnation of thermoplastic composites

The consolidation of commingled yarns has been addressed by several researchers **[2, 33, 34]**, **[42 – 44]**, **[48 – 51]** and has been reviewed by Svensson et al. **[7]**. In all cases, it has been shown that reinforcing fibres are generally not distributed homogeneously within a yarn, and that the problem could be reduced to that of impregnation of dry fibre bundles surrounded by molten matrix pools.

Lee and Springer **[46]** proposed a model simulating the steps involved in the manufacturing process of semi-crystalline thermoplastic matrix composites. These steps were impregnation, consolidation and crystallisation. The results of the models were verified by test performed with PEEK 150P polymer powder with graphite fibres and APC-2 graphite/PEEK composite. They described the radial and longitudinal impregnation process in the absence of pressure where surface tension is a dominant driving force for impregnation. The matrix moves along the fibres until the next contact point between fibres is reached. Their results can be applied mostly

to the impregnation process for resins with low viscosity or to processes with a very long impregnation time **[47]**. They also proposed a model to predict the evolution of gaps located in the inter-ply region. They represented the ply surface as rectangles of identical size and proposed a flow model to represent the deformation of these rectangles as a function of processing parameters. This model is presented and analysed in more detail in Section 5.2.2. Tests were carried out with PEEK 150P polymer and APC-2 graphite/PEEK composite to validate the different sub-models. Reasonable agreement was found between the measured and calculated degrees of impregnation and intimate contact.

Yun et al. **[32]** proposed a model based on experiments carried out with fibre tow surrounded by PEEK resin powder, which extended the approach of Lee and Springer **[46]** for impregnation in the absence of pressure. To establish a relationship between the degree of impregnation (ratio between the total number of fibres and the number of impregnated fibres) and processing parameters, Yun developed a model where permeability was constant, although it is well known the permeability of the fibre bundle decreases as fibre volume fraction increases.

To consider the effects of the shear strain rate dependency of the resin viscosity on matrix flow into a single fibre bundle Seo et al. **[47]** developed a model describing the impregnation of a thermoplastic resin into a continuous fibre bundle. Seo assumed a power law fluid model and that Darcy's law governed impregnation. Isothermal compaction trials with carbon and PEEK were also performed. However, poor agreement between the predicted and the measured degree of impregnation was found.

Van West et al. **[33, 34]** examined the draping and consolidation of commingled fabrics to predict fibre orientations on the draped surfaces and the thickness of laminates consisting of initially separate fibre bundles. The impregnation model was based on the analysis of micrographs obtained at different stages of consolidation. These micrographs were also used to measure the distance that the resin must flow to impregnate the fibres. This distance was then used to calculate an effective bundle radius, which was defined as the radius of a circle with the same fill time as the elliptical fibre bundle. Van West observed that fibre moved within the fibre bundle

during flow of the matrix. However, a constant permeability was used. The material resistance to compaction was assumed to be the sum of the fibre bed resistance and the matrix pressure. No validation was presented.

Figure 2.1a shows an idealised single bundle in section and illustrates the parameters required to determinate the flow front radius. Given the area of fibre remaining in the bundle, the flow front radius r_i can be calculated using Van West's hydraulic equivalence factor **[33, 34]**, which relates an elliptical bundle to a circular bundle with an equal fill time, see Figure 2.1b. This hydraulic equivalence factor is expressed as:

$$r_{eq} = \frac{\sqrt{2}}{2}\frac{a_0 b_0}{\sqrt{a_0^2 + b_0^2}} \qquad \textbf{(2. 15)}$$

where a_0 and b_0 are the ellipse major and minor axis lengths. The flow front radius r_i can be calculated using Eqn. 2.16:

$$r_i = \sqrt{\left(\frac{2\frac{a_0}{b_0}}{\pi\left(\frac{a_0^2}{b_0^2}+1\right)}(A_b - A_e)\right)} \qquad \textbf{(2. 16)}$$

where A_b is the area of the fibre bundle including an internal void and A_e is the area of the encroached matrix.

In several papers **[48 - 51]**, Friedrich et al. modelled the fibre bed impregnation mechanism by matrix flowing in one direction, orthogonal to the fibre axis, for a range of commingled yarn based thermoplastic composites. They assumed that part of the yarn was impregnated quickly by well-distributed polymer fibres or during melting of the polymer. A commingling parameter was defined corresponding to an adjusted thickness of the dry bundle. In addition, the fibre volume fraction was set to a chosen value that may depend on the applied pressure. However, agreement with experimental void contents was not very satisfactory.

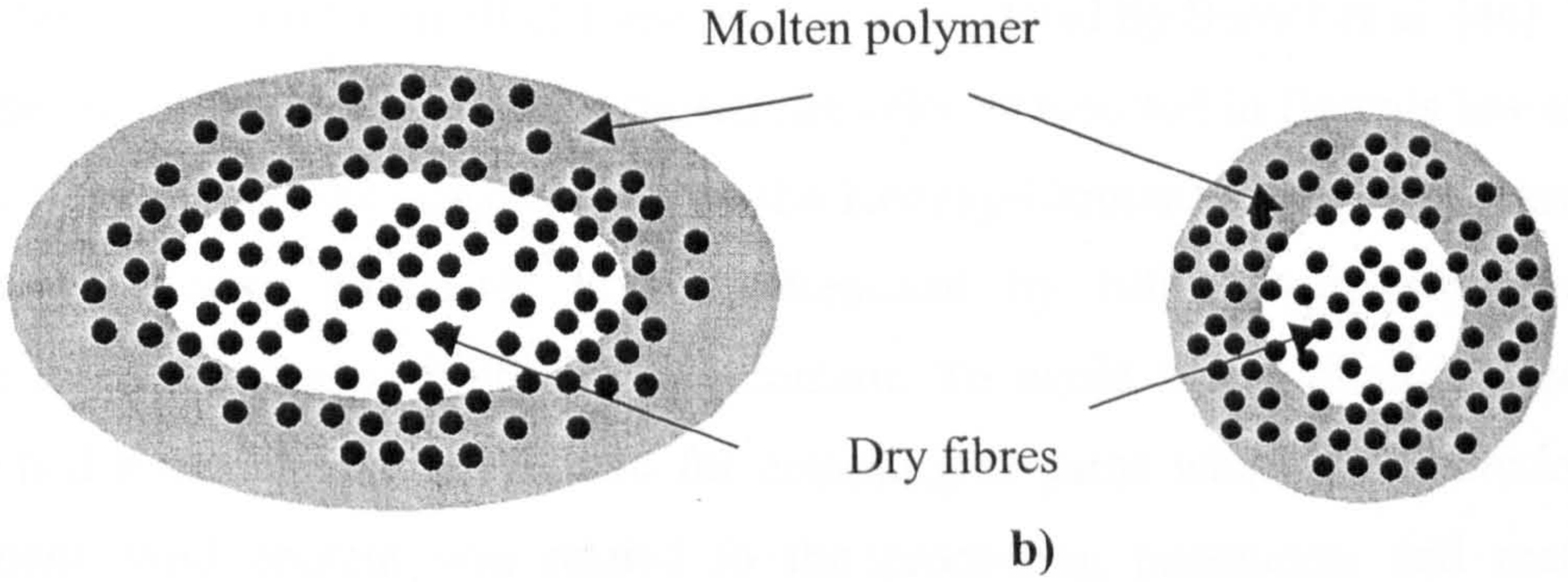

Figure 2.1 a) Cross-section of an idealised fibre bundle **b)** Equivalent circular fibre bundle using Van West's hydraulic equivalence factor.

Ye et al. **[50, 51]** presented a consolidation model to predict variations of void content during consolidation as a function of processing parameters in commingled yarn based thermoplastic composites. Low shear rate gave a Newtonian flow. Darcy's law was used to model the impregnation into fibre tows and fibre tow permeability was defined by the Kozeny-Carman equation. Ye assumed transverse laminar flow. The applied pressure and laminate length and width were constant in the plane of the laminate. Thus, fibre volume fraction was assumed constant and independent of the degree of compaction during impregnation. Capillary effects and gravitational forces were considerable negligible. Poor correlation was found between the measured and predicted void content.

Cain et al. **[42 - 43]** extended the model developed by Van West to study the effect of in-plane shear to represent fibre movement during component forming for commingled glass/PP composite. As shear angle increased, the required compaction pressure increased. Cain's model assumed a constant rate of compaction was applied to the material, the matrix material was non-Newtonian, and the viscosity of the matrix material was temperature dependent. Cain et al. considered the effects of compaction rate and in-plane shear on fabric compaction. Cain also developed his model from the observation of micrographs at different stages of consolidation. The model used four sub-models examining fibre compaction, permeability, impregnation and matrix shear thinning. Poor agreement was observed between the measured and predicted developed moulding pressure at a specific laminate thickness, possibly due to the difficulties in acquiring reliable permeability data.

Limitations encountered in all of these models were stated by Bernet et al. **[44]**. Two of these are the assimilation of the superficial velocity reported in Darcy's law to the matrix velocity and the consideration of the Kozeny-Carman permeability equation that adds another parameter to be determined by fitting with experimental measurements of permeability or void content. To avoid such limitations Bernet developed a model of impregnation for commingled yarns where the evolution of composite void content was related to the processing parameters and material properties. The analysis of the laws governing fibre bundle impregnation took into account a distribution in dry fibre bundle sizes. Residual porosity was considered to result from pore closing at a given stage during fibre bundle impregnation. Bernet's model used a different variation of permeability with fibre bundle volume fraction, which was proposed by Gebart **[40]**. Although Bernet's model showed reasonable agreement between measured and predicted void content for unidirectional commingled fabric made of polyamide 12 resin and carbon fibres, Bernet relied on the assumption that only voids within fibre bundles contribute to the final void content without considering the contribution of voids located in the inter-tow regions. However inter-tow voids reduce the fibre volume fraction of the laminate and consequently compaction pressure and permeability are also affected. Micrographs shown by Wilks et al. **[2, 52]** showed that a large amount of voids are located in the inter-tow region during the consolidation of commingled glass/PP composites. Wilks also suggested that voids attain a constant size when a large pressure is reached. In the case of vacuum forming process this pressure is never reached. Leterrier and G'Sell studied the formation and consolidation of glass/PP composites **[53]** and found that as temperature increases to 175°C from the melting range of 160°C - 165°C, large void reductions were observed, whereas a further temperature increase did not have any major influence on the void content. However, they also stated that high final pressures lead to the dissolution of the trapped gas into the resin. Klinkmuller et al. **[48, 49]** found a similar temperature effect in the consolidation of commingled glass/PP composites, and also observed that pressures greater than 1 or 2 MPa only slightly reduced the void content.

2.4.4 Heat Transfer

Cunningham et al. **[54]** developed a model to simulate the pre-heating of thermoplastic composites panels prior to press forming. The time required during the pre-heating cycle depends directly on the form of pre-heating used, therefore Cunningham et al. modelled the three main mechanisms of composite pre-heating: infrared, contact and convection heating. Time and temperature predictions were compared to experimental data showing good agreement.

Transverse thermal conductivity

Tavman et al. **[55]** studied the transverse thermal conductivity of high density polyethylene reinforced with chopped strand glass fibre mat. Several models were summarised and compared with each other and with experimental results. The series model and geometric mean model are two of the simplest models that predicted transverse thermal conductivity within 5%. However, the use of the series model is more extensive between composites reinforced with continues fibres.

For the series model the alignment of the composite is perpendicular to the direction of the thermal flux:

$$k_l = \frac{1}{\frac{V_f}{k_f} + \frac{1-V_f}{k_m}} \qquad (2.17)$$

The geometric mean model is suitable for composites where the fibre alignment with respect to the thermal flux is unclear:

$$k_l = k_f^{V_f} \cdot k_m^{1-V_f} \qquad (2.18)$$

In the above k_l, k_f and k_m are the thermal conductivity of the laminate, fibres and resin respectively and V_f is the fibre volume fraction.

2.5 Effect of void content on mechanical properties

It is difficult to predict theoretically the effect that voids have on the strength of composite laminates because of their irregular shape and distribution. Ye et al. **[52, 53]** studied the consolidation of commingled yarn based thermoplastic composites and correlated void content between 0% and 10% with flexural properties. They found that void content of 10% decreased flexural properties over 50%. Almeida et al. **[56]** studied the effect of void content on the static strength and fatigue life of carbon/epoxy laminates through the analysis of the ultrasonic absorption coefficient due to different levels of void content. Although Almeida et al. found that 6% void content decreased the four point bending flexural strength by 20%, no correlation was stated for higher levels of voidage. Similar findings were presented by Costa et al. **[57]**, who studied the effect of voids on the interlaminar shear strength of carbon/epoxy and carbon/bismaleimide fabric laminates Wakeman et al. **[58]** studied the effect of time at pressure on the mechanical properties for compression moulded glass mat thermoplastic (GMT). They found that levels of voids up to 25% reduced tensile strength of the laminates by 50%. Nilson et al. **[59]** focused on the effect of void content under 5% on the tensile properties of compression moulded GMT. Nilson suggested that at this level void content has no clear effect on the tensile strength and modulus. Lee et al. **[60]** analysed the effect of vacuum pressure, mould temperature and cooling rate on mechanical properties of glass fibre/PET laminates manufactured by a rapid press consolidation techniques. The use of vacuum during an initial pre-heating section decreased void content from 1.9% to 0.3%, increasing tensile strength accordingly. Henninger et al. **[61]** discussed the effect of processing parameters on the mechanical properties of GF/PP tubular components formed by a filament winding process. They found that 9% void content decreased tensile strength by 20% and interlaminar shear strength by 40% as a result of a reduction in the effective shear area.

2.5.1 Notched Strength of Composite Laminates

This section is concerned with the prediction of the effect of void content on mechanical properties. Several studies have been reviewed, though none of them is focused on the stress concentration around voids. However, linear elastic fracture mechanics and stress concentration criteria for notched composites provides an insight into the field given that voids are cracks enclosed into the laminate.

Fracture behaviour and toughness of composite systems containing induced holes or cracks has been the focus of many studies. Awerbuch et al. **[62]** and more recently Ng et al. **[63]** reviewed several fracture models for predicting the notched strength of composite laminates, most of which were applied to tensile loading. The experimental results presented by Awerbuch showed that for unidirectional glass reinforced composite laminates with centrally located cracks in the directions of the fibres, fracture mechanics is adaptable to orthotropic materials.

It is well established that the fracture behaviour of composite laminates depends on a variety of intrinsic and extrinsic variables. Among the former are laminate configuration, stacking sequence, constituent properties, fibre volume fraction, fibre matrix interface characteristics or fabrication procedure. The most important extrinsic parameters are specimen geometry, test temperature, moisture content, loading function and loading rate. Awerbuch **[62]** stated that only when very specific conditions are satisfied may the techniques of isotropic fracture mechanics be directly applied to anisotropic plates. The stated conditions are:

- The orientation of the defect with respect to the principal axis of symmetry must be fixed.
- The stress intensity factors defined for anisotropic cases must be consistent with the isotropic case in stress distribution and in crack displacements modes.
- The critical orientation coincides with one of the principal directions of elastic symmetry.

Whitney et al. **[64]** stated that single cracks of the types observed in metals do not form in resin matrix composites under repeated loads. Waddoups et al. **[65]** applied

linear elastic fracture mechanics (LEFM) to composites on a macroscopic scale, extending LEFM from metals to composites. Acceptable correlation was observed between the predicted and the measured fracture stress of $[0/90]_S$ carbon/epoxy laminate containing holes of different radii. Waddoups et al. also stated that the details of the crack-tip damage zone are complex and vary among the different laminate configurations and materials systems. While Waddoups criteria is based on an effective crack length, Mar et al. **[66]** proposed that the fracture of the composite is governed by the composite fracture toughness H_c (analogous to the critical stress intensity factor) and an exponent n that represents the order of the singularity of a crack with its tip at the interface of yarn and matrix material. This exponent is laminate lay-up dependant and like the composite fracture toughness requires additional experiments to be performed. Eqn. 2.19 represents Mar's model.

$$\sigma = H_c(2r)^{-n} \tag{2.19}$$

A similar approach was used by Soriano et al. **[67]** to analyse the notch sensitivity of carbon/epoxy fabric laminates with circular holes. Soriano's approach is based on the assumption that fibre failure in the principal load bearing plies precipitates the failure of notched laminates.

Mar's approach was further developed by Almeida et al. **[56]**, who assessed the effect of void content on the static strength and fatigue life of carbon/epoxy laminates under flexural loading. Almeida et al. modified Mar's approach by substituting the circular notch diameter by the absorption coefficient used in ultrasonic inspection. Although reasonable correlation with experimental results of interlaminar shear and flexural strength was obtained, the two already mentioned parameters have to be obtained by additional experiments. In addition, limitations of ultrasound inspections have already been mentioned in Section 2.3.

Whitney et al. **[64]** proposed the first stress failure models for predicting the notched strength of composite laminates containing circular holes without applying the principles of LEFM. The two criteria formulated are the point stress and the average stress criteria, which predict the uniaxial tensile strength of laminated composites

containing through thickness discontinuities of a general shape. These are illustrated in Figure 2.2.

Both criteria assume that fracture occurs when the stress at some characteristic distance ψ_i away from the discontinuity reaches the un-notched strength.

$$\frac{\sigma}{\sigma_\infty}=\frac{2}{2+\zeta_1^2+3\zeta_1^4};\ \frac{\sigma}{\sigma_\infty}=\frac{2(1-\zeta_2)}{2-\zeta_2^2-\zeta_2^4} \qquad (2.20)$$

where σ_∞ is the strength of an un-notched laminate, σ is the predicted laminate strength for a specific void content and

$$\zeta_i=\frac{r}{r+\psi_i} \qquad (2.21)$$

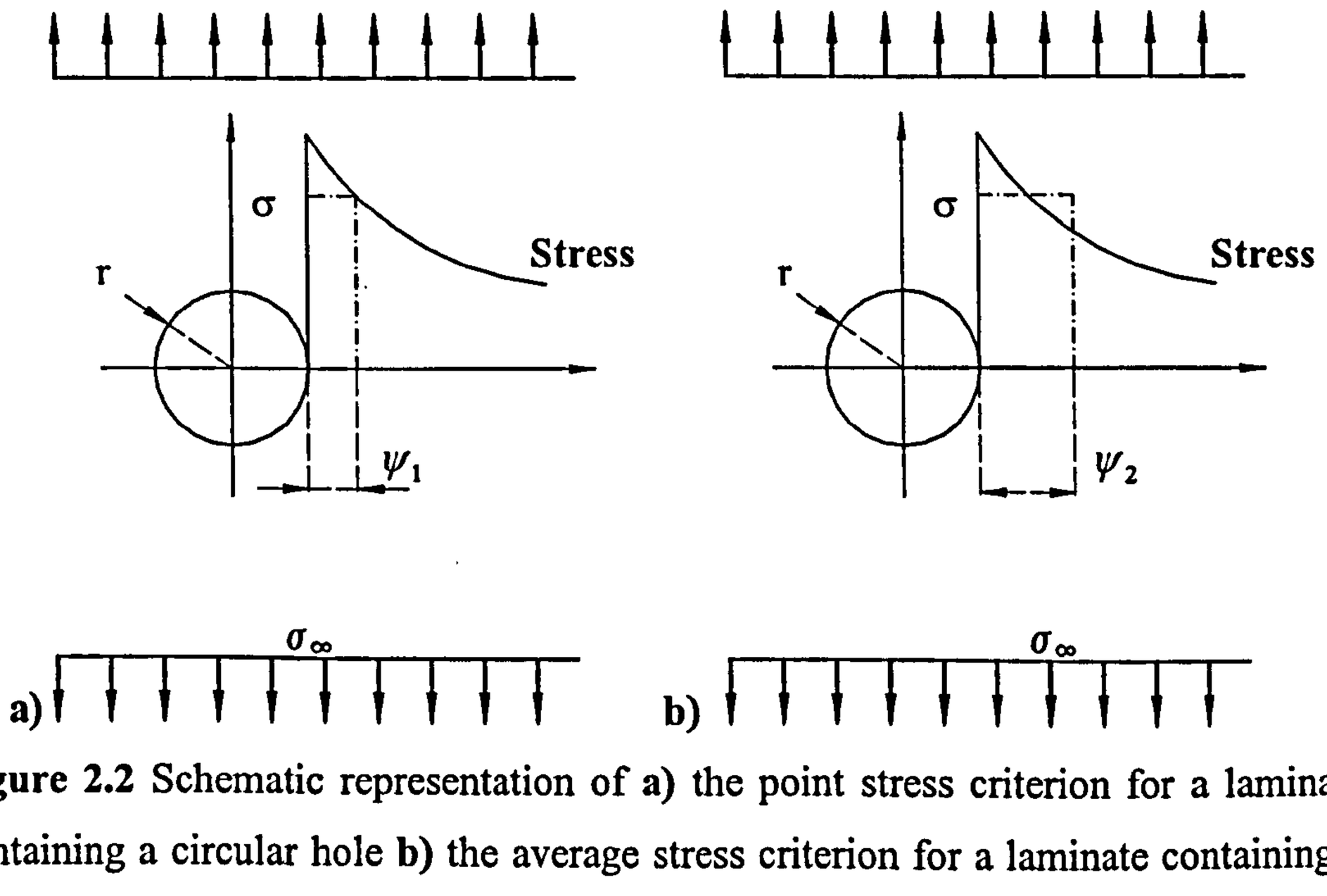

Figure 2.2 Schematic representation of **a)** the point stress criterion for a laminate containing a circular hole **b)** the average stress criterion for a laminate containing a circular hole.

Experimental measurements on glass/epoxy laminates were compared with the theory showing excellent correlation. The same degree of agreement was found by Awerbuch et al. **[62]**, who compared measured and predicted tensile strength for graphite/epoxy laminate and boron/aluminium laminates.

Critics of these models stated that the characteristic distances depend on the laminate and they must be determined *a priori* for each material system and laminate configuration independently. However, once the characteristic distances are known the simplicity of the models makes them extremely attractive to designers. Soriano et al. **[67]** presented a comparison between the average stress criterion, Mar's approach and a modified Mar's approach. Although good agreement between experimental data and the three theories was presented for carbon/epoxy fabric laminates, supplementary experiments were required to calculate additional parameters in both of Mar's approaches.

Karlak **[68]** modified the Whitney stress criteria by incorporating a relationship between the notch radius and the characteristic length. Karlak concluded that the Whitney point stress criterion length is related to the square root of the hole radius. Although good agreement was found between measured and predicted tensile strength of graphite/epoxy laminates, an additional parameter that has to be determined experimentally was introduced. Pipes el al. **[69]** extended Karlak's model considering the assumption that the characteristic dimension is a material constant to be invalid. However, in this model a more general exponential relationship between the characteristic dimension and the size of the discontinuity was assumed. As in Karlak's model an additional parameter that may vary with laminate configuration was determined experimentally.

Recently Srivasta **[70]** presented a modified point stress criterion for predicting the notched strength of glass and carbon fibre laminated composites containing through thickness centrally located circular or elliptical hole or a central crack. The results showed that for the point stress criterion, the characteristic length depends on the hole size as well as width of the plate for each particular material. Reasonable agreement was obtained between the predicted and measured notched strength of glass/epoxy and carbon/epoxy laminates.

Chen et al. **[71]** as Soriano et al. **[67]** proposed a lay-up independent failure criterion, the load-bearing ply-failure criterion (LBPF). They showed that the strength of a notched fibre-dominated laminate can be evaluated from the failure prediction for 0°

plies in the laminate and the concept of characteristic length. This criterion relates the laminate strength to the failure of the principal load-bearing ply once the characteristic length is estimated from experiments. Reasonable consistency was observed between measurement and predictions.

2.6 Effect of deformation on mechanical properties

This section is concerned with the effect of different mechanisms of deformation – i.e. fibre movement during forming - on mechanical properties. In sectors such as the aerospace and automotive industries, where high specific structural performance is required, the ability to tailor mechanical properties by placing reinforcing fibres along lines of maximum stress is vital. In-plane shear is assumed to be the primary mechanism of deformation when the textile is draped over the component, therefore special attention is given to models that predict the effect of in-plane shear on mechanical properties.

2.6.1 Reinforcement Efficiency

Krenchel **[72]** presented a modified rule of mixtures to predict the laminate modulus (Eqn. 2.22) by introducing the load bearing efficiency, η, of the reinforcement. This efficiency factor accounts for the effect of fibre orientation with respect to the loading direction.

$$E_1 = \eta E_f V_f + E_m(1 - V_f) \qquad \textbf{(2.22)}$$

This efficiency factor ranges from one to zero when the fibres of a unidirectional laminate and the loading direction are parallel or perpendicular respectively. Smith et al. **[73]** studied the effect of shear on mechanical properties of engineered and woven glass fabrics. They showed reasonable agreement between measured and predicted composite stiffness of laminates, which were previously sheared by using a four-bar frame that allowed the isolation of in-plane shear from other mechanism of

deformation. However, Turner **[74]** stated that the reinforcement efficiency approach neglects the effects of transverse deformation (Poisson effects). As the fibres become transverse to the load, especially for angles above ±45° with respect to the loading direction, Poisson effects become increasingly important.

2.6.2 Classical Laminate Theory

Authors such as Tsai **[75]**, Morley **[76]** and Jones **[77]** have applied classical laminate theory to predict stiffness for the design of composite structures. This approach accounts for the effects of shear modulus and Poisson's ratio in the calculation of laminate stiffness. A full explanation of this approach is given in Chapter 6.

Although Smith et al. **[73]** showed that the classical laminate model gives a better approximation of the off-axis laminate stiffness than the modified rule of mixtures, their study did not address failure prediction. Hofstee et al. **[78 - 80]** have published studies incorporating experimental and predicted elastic properties of sheared plain-weave thermoplastic composites. Good agreement was found between the measured and predicted laminate stiffness. Crookston et al. **[81, 82]** have published similar data for components manufactured by draping of dry non-crimp fabrics before resin transfer moulding (RTM). Simple failure criteria were considered and results compared with experimental data from tensile tests on angle ply laminates manufactured at a range of ply angles. Reasonable agreement was found, though compressive and shear behaviour was not considered.

2.6.3 Effects of Fibre Misalignment/Waviness

Several mechanisms of deformation affect the processing and performance of textile composites. Fibre misalignment, especially in the form of fibre waviness, affects tensile and compressive behaviour of composites **[83 - 86]**. Although fibre waviness is found mostly in woven fabrics due to the crimp between the warp and weft yarns, fibre and ply misalignments are induced in a variety of manufacturing processes.

The effects of fibre waviness on the mechanical properties of composites have been investigated by several researchers and summarised by Turner **[74]**. Bolotin **[85]** developed expressions to account for the reduction in the modulus of composites with random initial irregularities (presented as sine waves) and predicted a linear relationship between compliance and the square of the angular deviation:

$$E_x = \frac{E_1 G_{12}}{G_{12} + \delta^2 E_1} \qquad \textbf{(2. 23)}$$

where G_{12} is the shear modulus and δ^2 is the mean square angular deviation of the fibre from the principal direction, which can be calculated from:

$$\delta^2 = 2\pi^2 \frac{\varsigma^2}{\lambda^2} \qquad \textbf{(2. 24)}$$

where ς is the amplitude and λ is the wavelength for an assumed sinusoidal fibre path:

$$y = \varsigma \sin\left(2\pi \frac{x}{\lambda}\right) \qquad \textbf{(2. 25)}$$

Mrse et al. **[86]** used Bolotin's analysis to report a reduction of 8% for δ^2=30 in compressive modulus due to fibre waviness of unidirectional carbon prepreg samples which had been crimped to various degrees to vary the fibre waviness. Good correlation was observed.

Bogetti et al. **[87]** and Ishikawa et al. **[88]** used classical laminate theory to predict the behaviour of thermoplastic composites and woven fabric composites associated with layer waviness. Bogetti et al. found that stiffness reduction due to ply waviness was most significant in the direction of ply undulation. However, other in-plane mechanical properties, such as transverse stiffness, Poisson's ratio and in-plane shear modulus, were relatively insensitive to undulation amplitude. Their analysis

predicted individual ply stress and strain distributions as well as ply failure in local regions.

Other researchers such as Chan et al. **[89]**, Rai et al. **[90]** and Hsaio et al **[91, 92]** used the classical laminate method and modelled waviness by a sine wave. They modelled the effect of fibre waviness on stiffness by assuming the effective modulus of a composite to be obtained using an average strain approach:

$$E_x = \frac{\overline{\sigma_x}}{\overline{\varepsilon_x}} = \frac{\lambda}{\int_0^{\lambda} \overline{S_{11}}\, dx} \qquad (2.26)$$

where λ is the wavelength, $\overline{S_{11}}$ is the reduced compliance for a ply oriented at an angle, θ, with respect to material axis system. As θ varies along the axis of the sine wave, the effective stiffness was calculated by numerical integration. Hsaio et al. **[91, 92]** found that a uniform 4.3% waviness (determined as the ratio of fibre amplitude to wavelength) reduced compressive modulus by 42% for carbon composites. Good correlation was observed between experimental data and the classical laminate approach.

Turner **[74]** studied tensile properties of E-glass/epoxy and carbon/epoxy with an in-plane sinusoidal fibre distribution and compared experimental data with predictions using Bolotin's model, the modified rule of mixtures and classical laminate theory. Classical laminate theory and modified rule of mixtures correlated well with experimental data. However, the model presented by Bolotin **[85]** gave poor results. Turner also studied the effect of waviness due to crimp in woven material on tensile properties of woven E-glass and carbon fibre fabrics. Both the modified rule of mixtures and modified classical laminate theory showed good agreement between the measured and predicted woven composite modulus.

2.7 Conclusions

Processing of textile composites involves the forming or draping of the reinforcement over the mould surface followed by consolidation and curing or cooling depending on the resin used. Therefore a wide understanding of the problems that may arise during in-service life is required.

Much research has been published on consolidation modelling of textile composites. Most of the compaction models presented here were based on high levels of pressure possibly limiting their use in modelling of vacuum consolidation. Although modelling of the impregnation phase has been the focus of many studies, none of these is fully representative of vacuum forming of textile composites. A consolidation model that links and extends existing sub-models is presented in Chapter 5 to predict the void content for commingled laminates consolidated by vacuum forming.

It is clear that void content has a significant effect on the mechanical behaviour of textile composites. Several authors have studied and tried to predict the effect of processing parameters on the mechanical behaviour of textile composites, and a few have shown the effect of remaining void content on mechanical properties. None of the reviewed papers has shown a clear trend relating void content to mechanical properties. Several fracture models that predict mechanical properties of notched laminates have been presented. Although the models from Karlak et al. [68] and Pipes et al. [69] showed good agreement between theory and experimental measurements, the introduction of additional empirical parameters makes the Whitney stress criteria more attractive.

A substantial body of work has addressed compaction of textile composites. The effects of fabric drape on consolidation and subsequent mechanical properties of the resulting component are not fully understood, and in particular appropriate failure criteria for draped fabrics have yet to be defined. This is complicated by the fact that fabric deformation may lead to areas of poor consolidation and hence relatively high voidage.

3 Experimental Techniques

3.1 Introduction

This chapter describes the equipment and methodologies used to characterise the processing and performance of textile composite materials using a vacuum forming process. The standard test methods to measure moduli and strength and an image analysis technique developed to measure levels of void content are then presented. To gain understanding of textile composite deformation and to validate some of the models developed to simulate textile composite manufacturing, an automated strain analysis system is presented.

3.2 Materials

Three textile composite materials are considered in this thesis; a thermoplastic and two thermosetting materials. This thesis is focused on the behaviour of commingled glass/PP and carbon/epoxy prepreg woven materials.

The thermoplastic composite material used for this work was commingled glass/PP woven material, supplied by Saint-Gobain Vetrotex under the trade name Twintex® and denoted as material B. This was a balanced 2x2 twill weave fabric of density 1.5 g/cm^3 consisting of a yarn of 60% by mass commingled E-glass with polypropylene.

The prepreg composite materials were used mainly to study the effect of deformation on consolidation. The first prepreg used (material C) was a five-harness satin woven prepreg of density 1.301 g/cm^3 consisting of a tow of 55% by volume carbon fibre with epoxy matrix supplied by Hexcel Composites and known as AS4/8552. A second prepreg (material D) used to form and consolidate demonstrator components was Fibredux 6376 a five-harness satin woven carbon/epoxy prepreg also supplied by Hexcel Composites. The material is similar in weave style and composition to the AS4/8552 woven prepreg, but the tow width is smaller.

3.3 Vacuum consolidation of textile composites

A vacuum process was used to form materials B, C and D. This is a low pressure processing method, which reduces the requirements of the processing equipment and hence the cost of composite parts.

3.3.1 Thermoplastic composites

A normal processing cycle for vacuum forming components from composite laminates made with thermoplastic commingled yarns consists of three main stages.

1. Heat the material while applying a constant pressure.
2. Once a specific temperature is reached, continue to apply pressure for a specified period of time to consolidate the laminate.
3. Cool the material while maintaining pressure.

A 12 kW Warlow-Whitney model 999B hot air oven was used to preheat fabric samples whilst the vacuum was applied. A thin flexible nylon membrane (WN1500) was used to cover the composite lay-up. A nylon breather fabric (Ultraweave® 606) was used to achieve even extraction of vacuum throughout the vacuum bag. A vacuum bag sealant tape made of synthetic rubber and suitable for high temperatures (GS213/3) was used to form a seal around the vacuum bag. The fabric samples were placed over the preheated (50°C) aluminium tool and a type K thermocouple, with a digital thermometer to monitor heating, was placed within the material. A Eurotherm type 812 proportional-integral-derivate temperature controller was used to control the oven air temperature to 215°C. Tygavac Advance Materials Ltd supplied all the disposable materials.

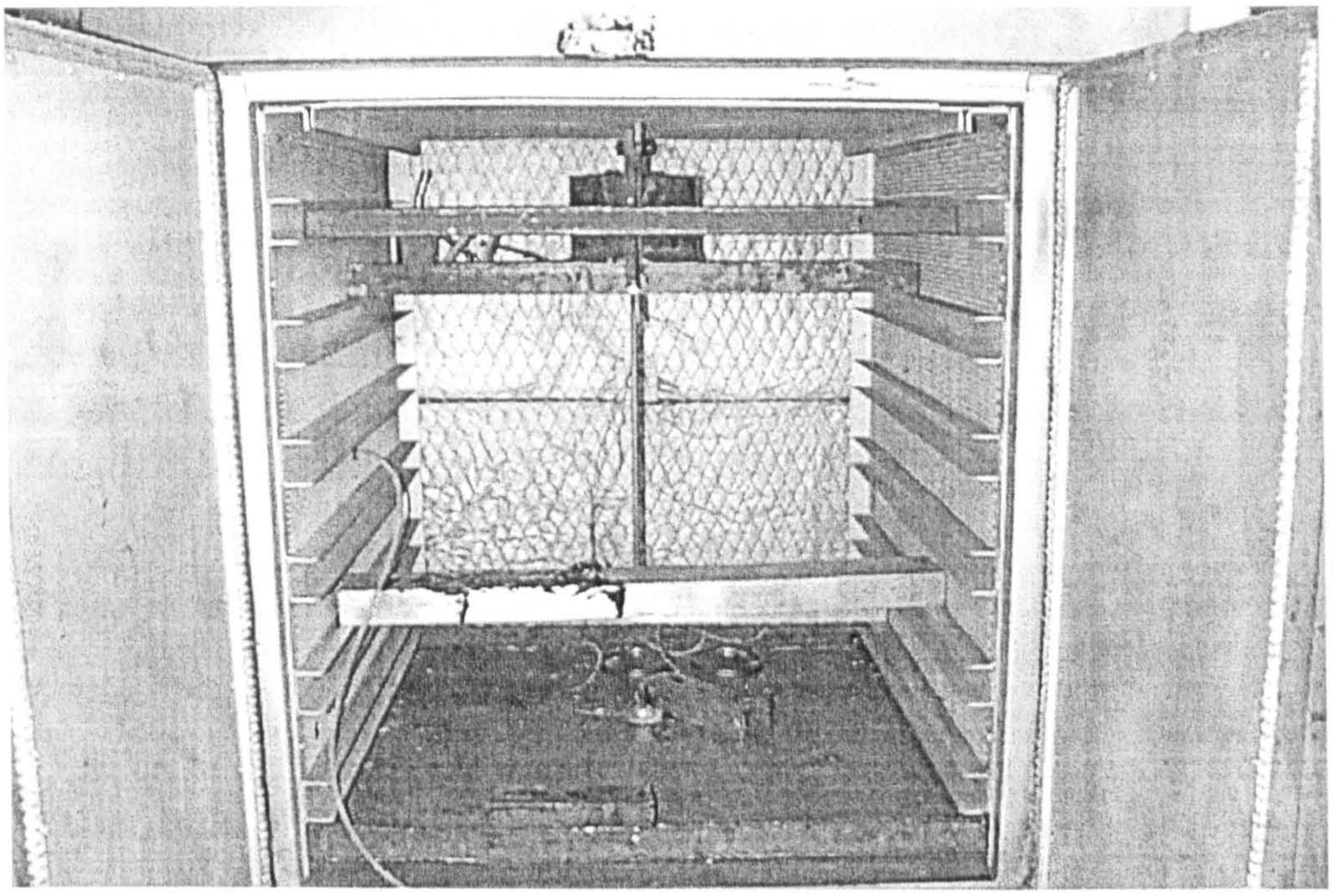

Figure 3.1 Hot air oven.

In order to apply the vacuum to a sample inside the oven (Figure 3.1), the use of an oven with a hole in the sidewall was necessary. The moulding arrangement used is shown in Figure 3.2.

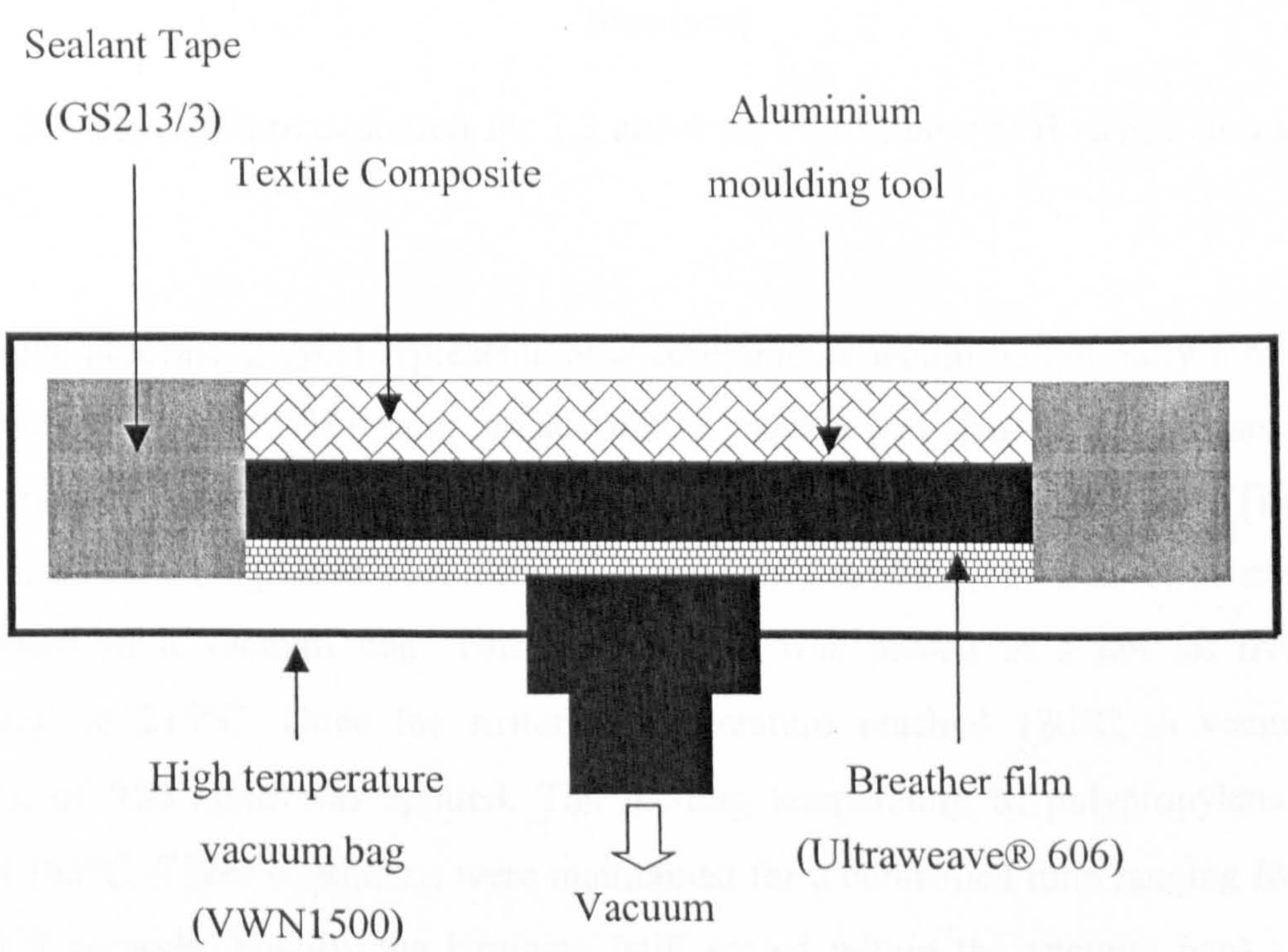

Figure 3.2 Vacuum forming of thermoplastic textile composites.

Figure 3.3 shows the temperature history during the process for three samples, corresponding to 2, 3 and 4 layers of material B formed at 180°C. Experimental work on material temperature showed that the temperature measured in the centre of the laminates was similar to that at the surface.

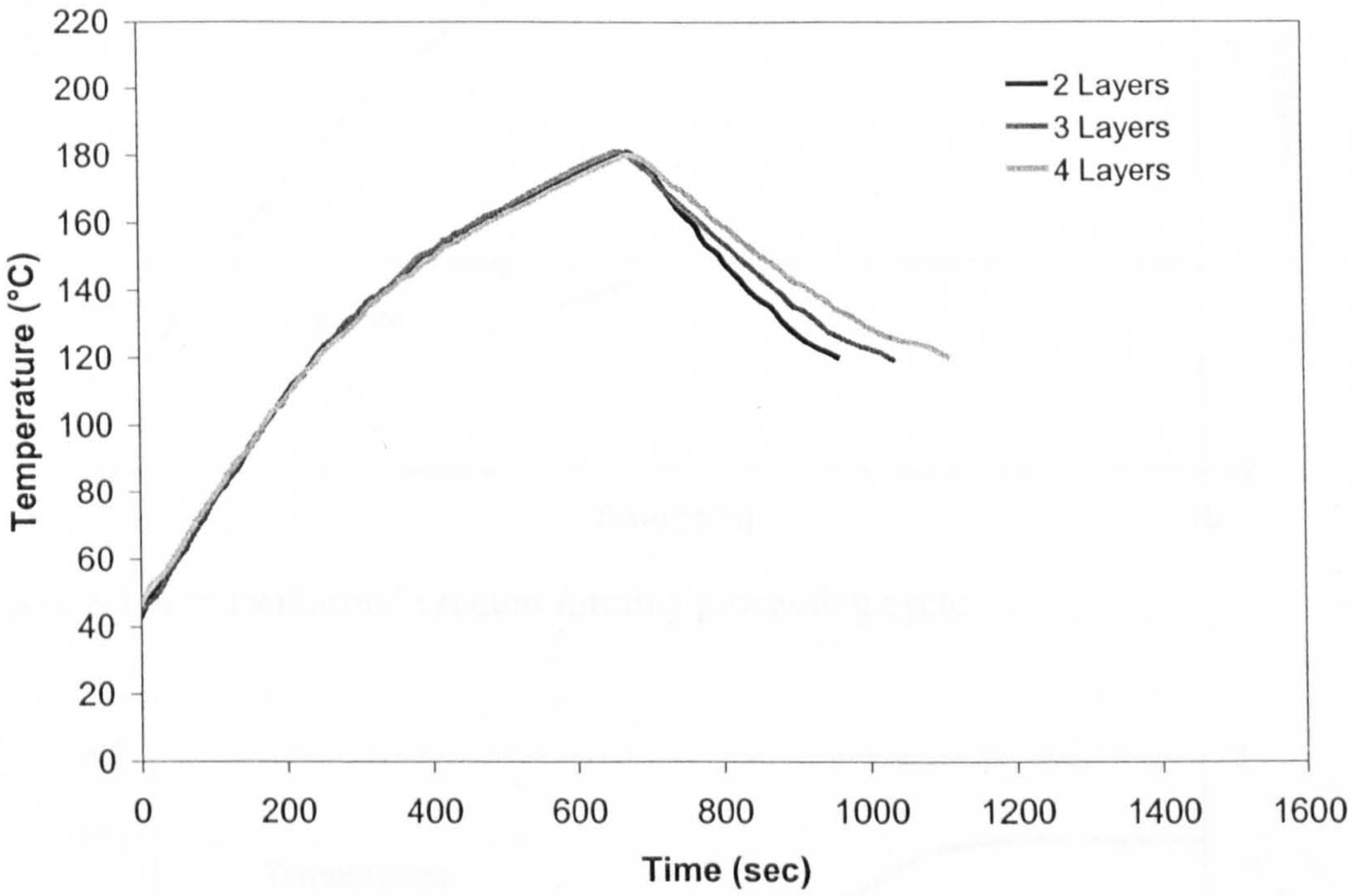

Figure 3.3 Temperature evolution for 2,3 and 4 layers of material B sample formed at 180°C.

The above processing cycle represents how components would be normally formed in an industrial context. However, an alternative process was also used in this study, which ensured that the consolidation process occurred at constant temperature. Three layers of fabric were placed over a single aluminium flat plate (150 mm x 250 mm), and sealed in a vacuum bag. This arrangement was placed in a hot air oven, preheated to 215°C. Once the material temperature reached 180°C, a vacuum pressure of 950 mbar was applied. The melting temperature of polypropylene is around 165°C. These conditions were maintained for a controlled time ranging from 0 to 300 seconds. Finally, the laminate (still sealed within the vacuum bag) was quenched in a cold-water bath until the temperature fell below 120°C.

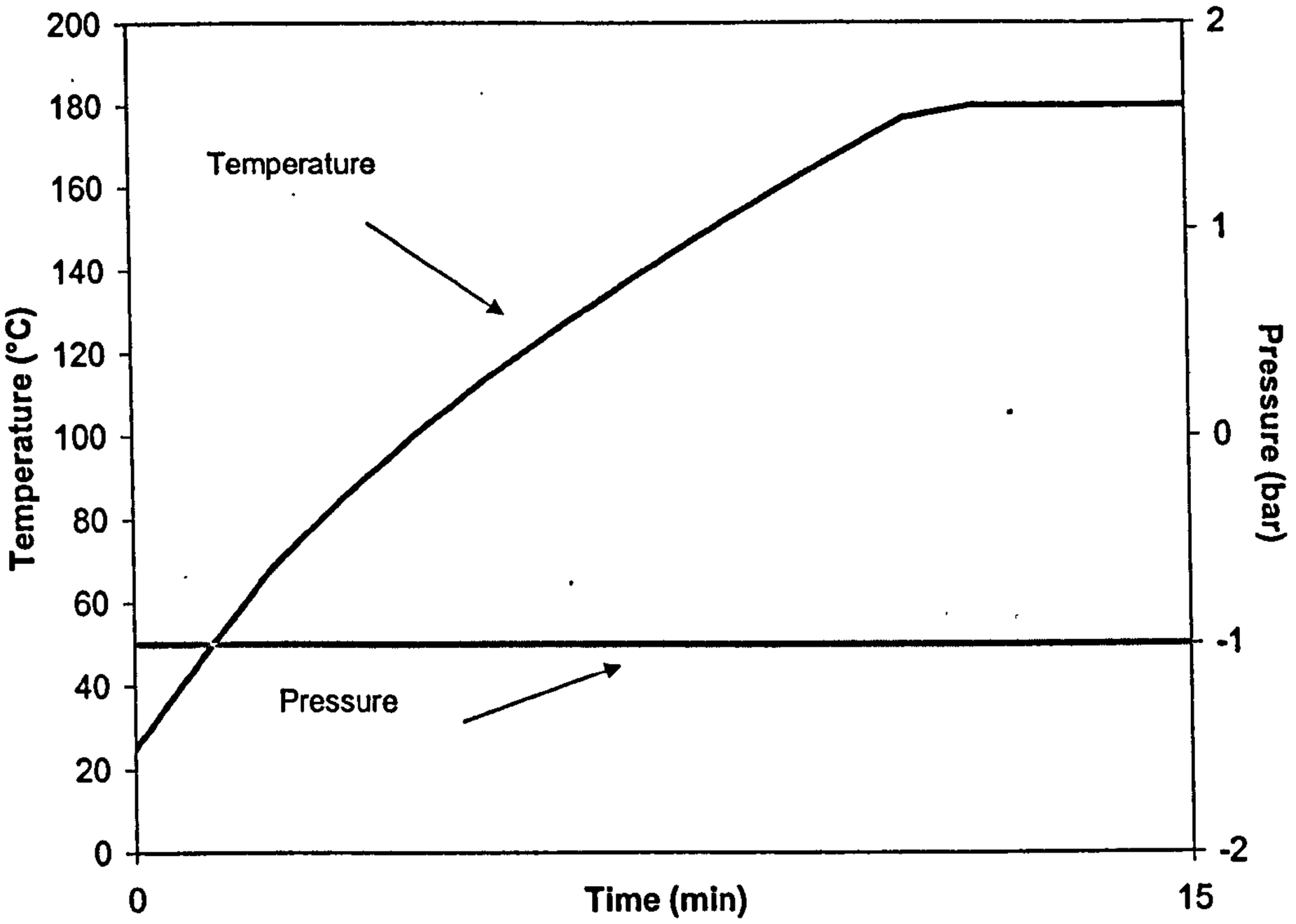

Figure 3.4 Non-isothermal vacuum forming processing cycle.

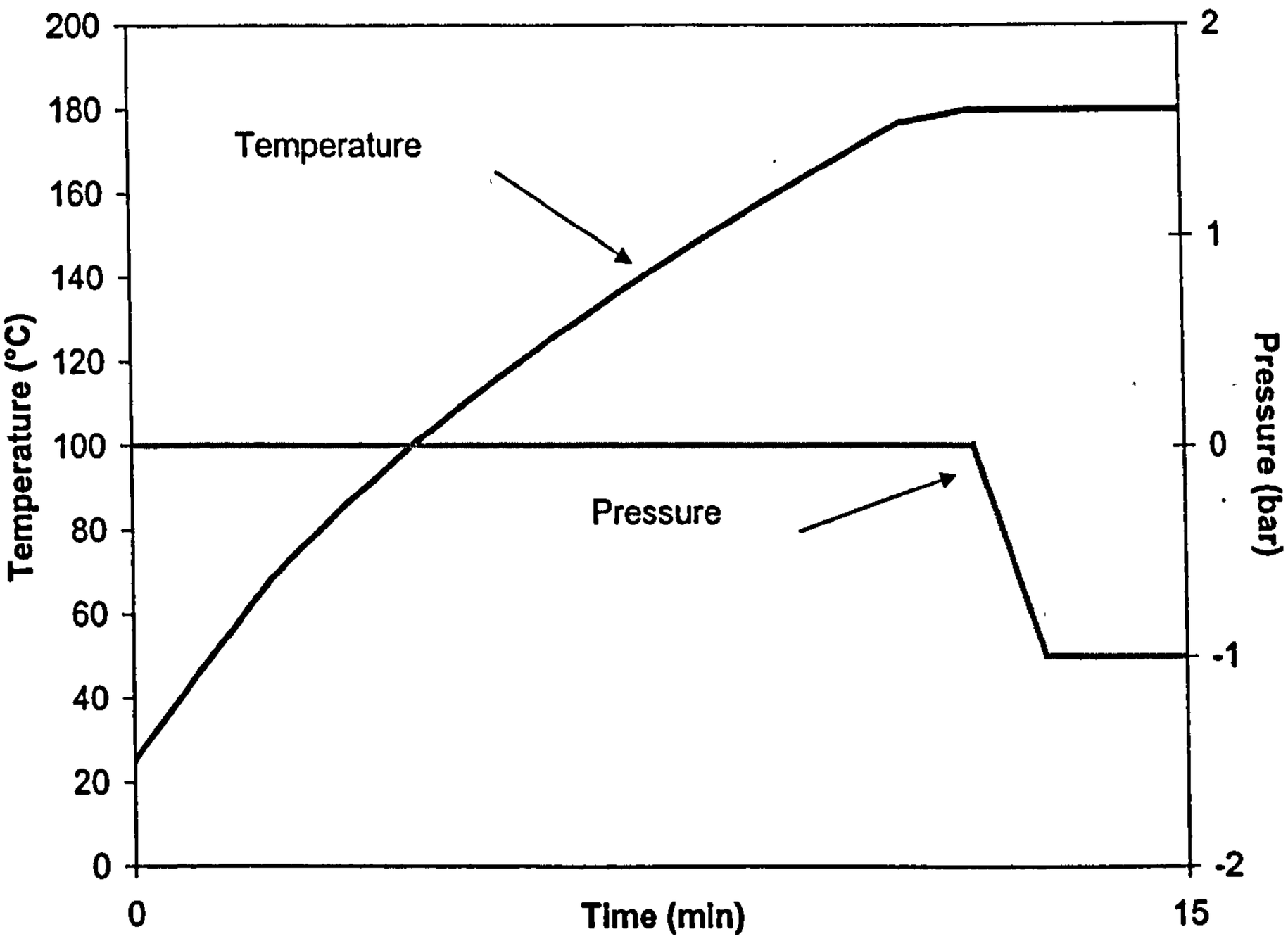

Figure 3.5 Isothermal vacuum forming processing cycle.

This process was developed to provide validation data for the consolidation model presented in Chapter 5, which predicts void content as a function of pressure, time at

pressure and temperature. Figures 3.4 and 3.5 show schematic diagrams of the non-isothermal and isothermal processing cycles used to consolidate commingled glass/PP woven materials.

3.3.2 Sheared flat plaques

In-plane shear is the primary deformation mechanism during forming for composites based on biaxial fabrics. Therefore sheared flat plaques were formed and consolidated not only to study the effect of deformation on consolidation but also to validate the consolidation model presented in Chapter 5; thus the consolidation model could be related to void content measurements carried out on formed material.

Three layers of material B were sheared to a range of angles and then consolidated by the non-isothermal vacuum forming process using different pressures at a material temperature of 180°C. Pressure was varied from 100 mbar to 500 mbar. Figure 3.6 shows the metal frame used to shear the textile composite by an angle θ. Once the 1300 mm x 1000 mm fabric was sheared using the metal frame, the layers were cut and placed on an aluminium tool. These layers were placed inside a 270 mm x 170 mm metal frame to minimise further deformation.

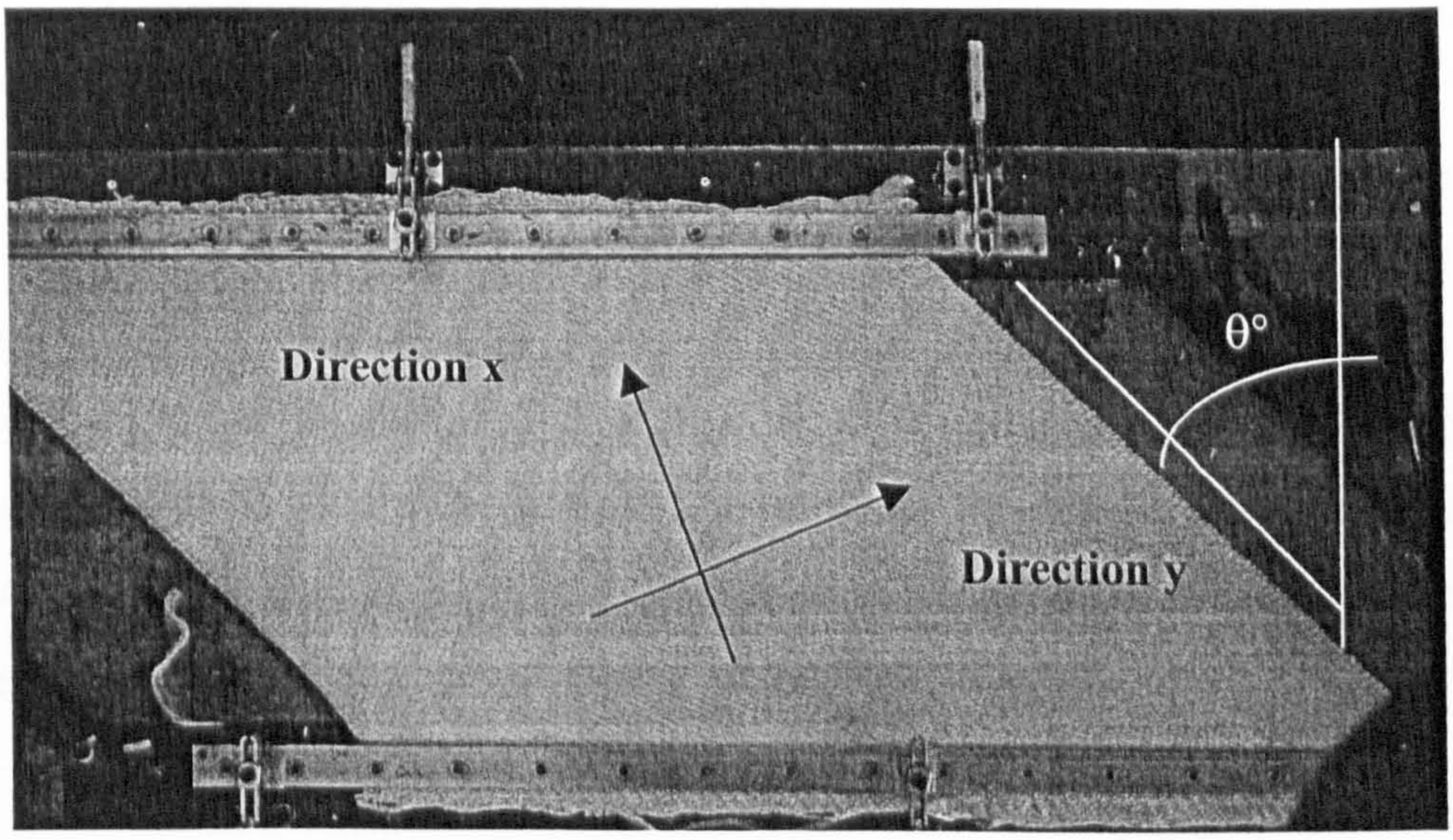

Figure 3.6 Facility used to shear material B by an angle θ°, where *x* and *y* correspond to the bias directions.

3.3.3 Three-dimensional shapes

This section is concerned with consolidation of 3D components using the non-isothermal vacuum forming process. Figure 3.7 shows a schematic of the apparatus used for a hemispherical moulding. The principal objective of this work is to study the effect of deformation on consolidation. Ultimately, the consolidation model could incorporate these effects by linking it to draping/forming simulations.

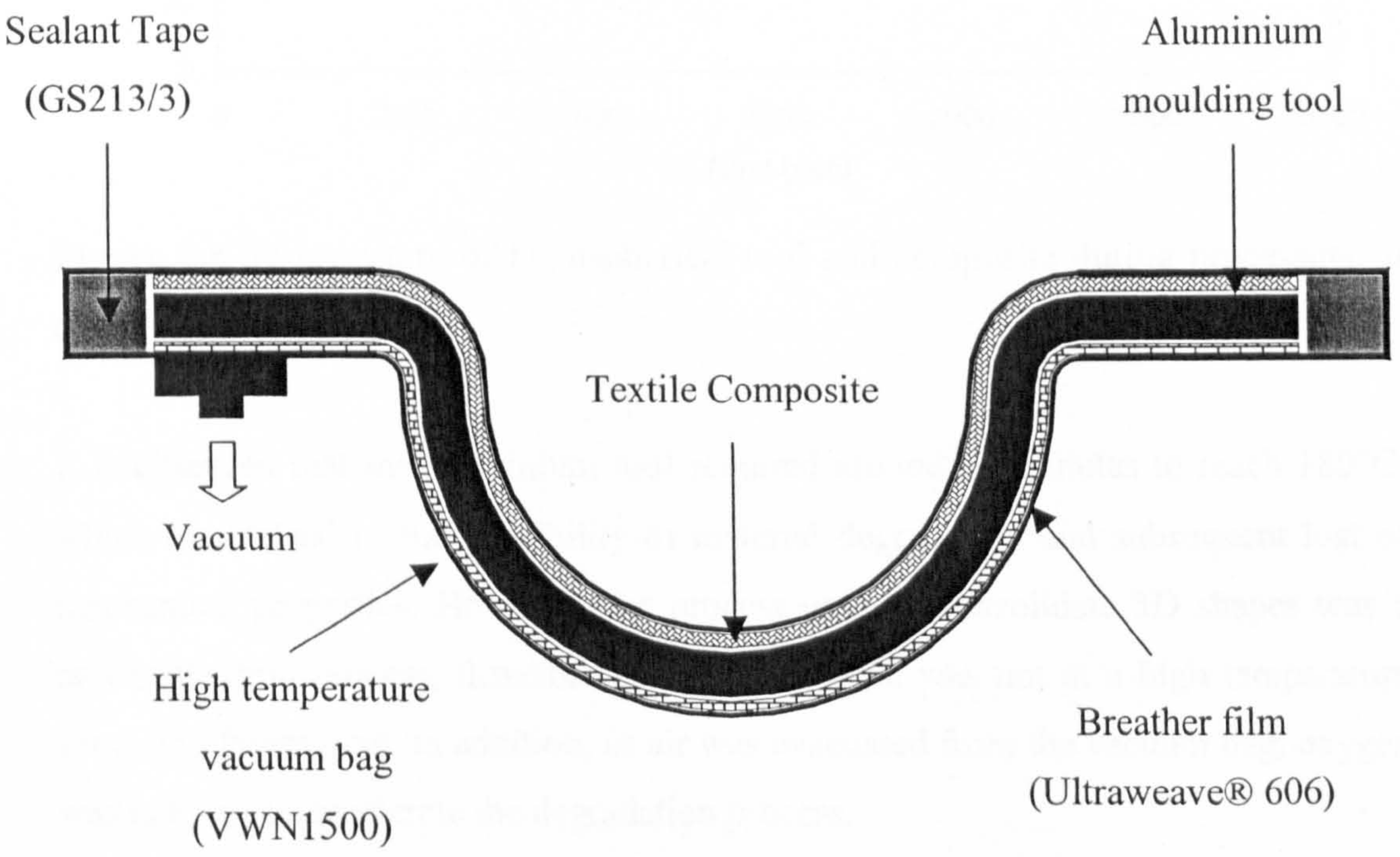

Figure 3.7 Apparatus to produce 3D samples by non-isothermal vacuum forming.

In this process, vacuum pressure is applied before the material was placed in the pre-heated oven. Once the material reaches the desired temperature, it is cooled to room temperature outside of the hot air oven. Initial trials were carried out using 2 layers of material B. The maximum material temperature was 180°C. The hot air oven has preheated at 215°C. Figure 3.8 shows the processing cycle.

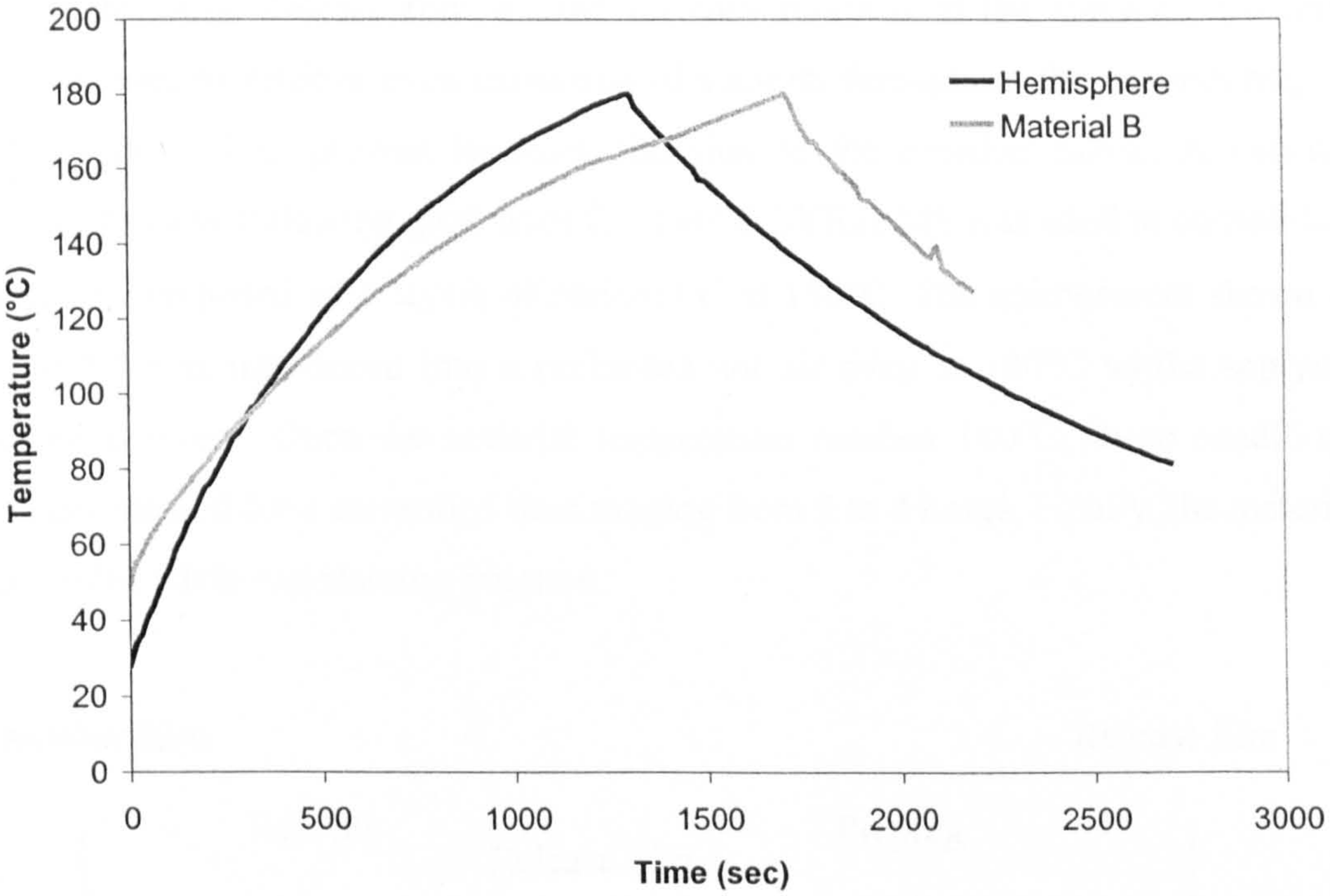

Figure 3.8 Temperature of hemispherical tool and composite during processing of commingled material.

It is observed that the aluminium tool required around 25 minutes to reach 180°C, which could lead to the possibility of material degradation and subsequent lost of mechanical properties. However, the process used to consolidate 3D shapes was a non-isothermal process, therefore the polypropylene was not at a high temperature for a significant time. In addition, as air was evacuated from the vacuum bag, oxygen was not able to accelerate the degradation process.

3.3.4 Prepreg flat plaques

This section is concerned with the effects of process parameter during forming on the mechanical properties of continuous carbon fibre reinforced epoxy composites (material C). The aim was to characterise a low pressure forming process to determine the resulting void content and mechanical properties.

The technique is similar to that used to consolidate commingled materials presented in Section 3.3.1. Figure 3.9 shows the arrangement used to consolidate prepregs by

vacuum forming. Release film is used for easy removal of the laminate. Breather fabric is used to achieve even extraction of vacuum throughout the vacuum bag. A peel ply is used to prevent laminate adhesion to the breather fabric. A vacuum forming process following guidelines from BAE SYSTEMS was used to consolidate laminates composed of 4 layers of material C at 180°C. The arrangement shown in Figure 3.9 was introduced into a preheated hot air oven at 180°C whilst applying vacuum pressure. Once the material temperature reached 180°C, these conditions were maintained for a controlled time ranging from 2 to 4 hours. Finally, the material was cooled while maintaining pressure.

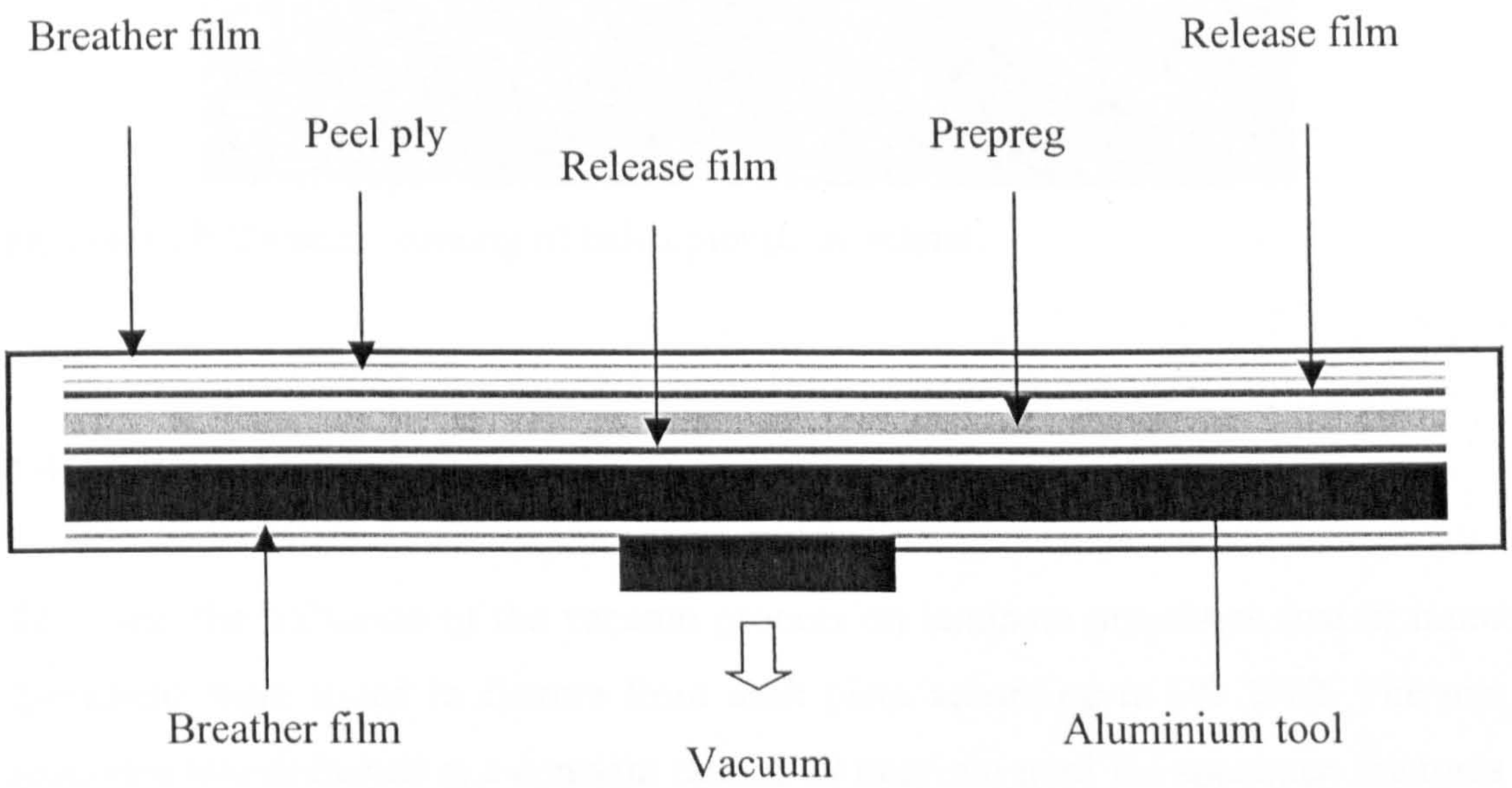

Figure 3.9 Arrangement used to consolidate prepregs by vacuum forming.

3.3.5 Helicopter pilot helmet

Helmet components were produced at the University of Cambridge using material D. In this process, both helmet tool and prepreg material were preheated up to 60°C. The preheated material was transferred onto the helmet and laid up by hand. Once the rest of the layers of the arrangement were assembled, vacuum pressure was applied to consolidate the material (see Figure 3.10). This arrangement was placed into a preheated hot air oven. The preheat temperature inside the oven was 210°C. Once the material reached 180°C, the arrangement was kept inside the oven at 180°C

for approximately 3 hours. After the specified dwell time, the arrangement was quenched in a water tank until the material temperature reached 80°C.

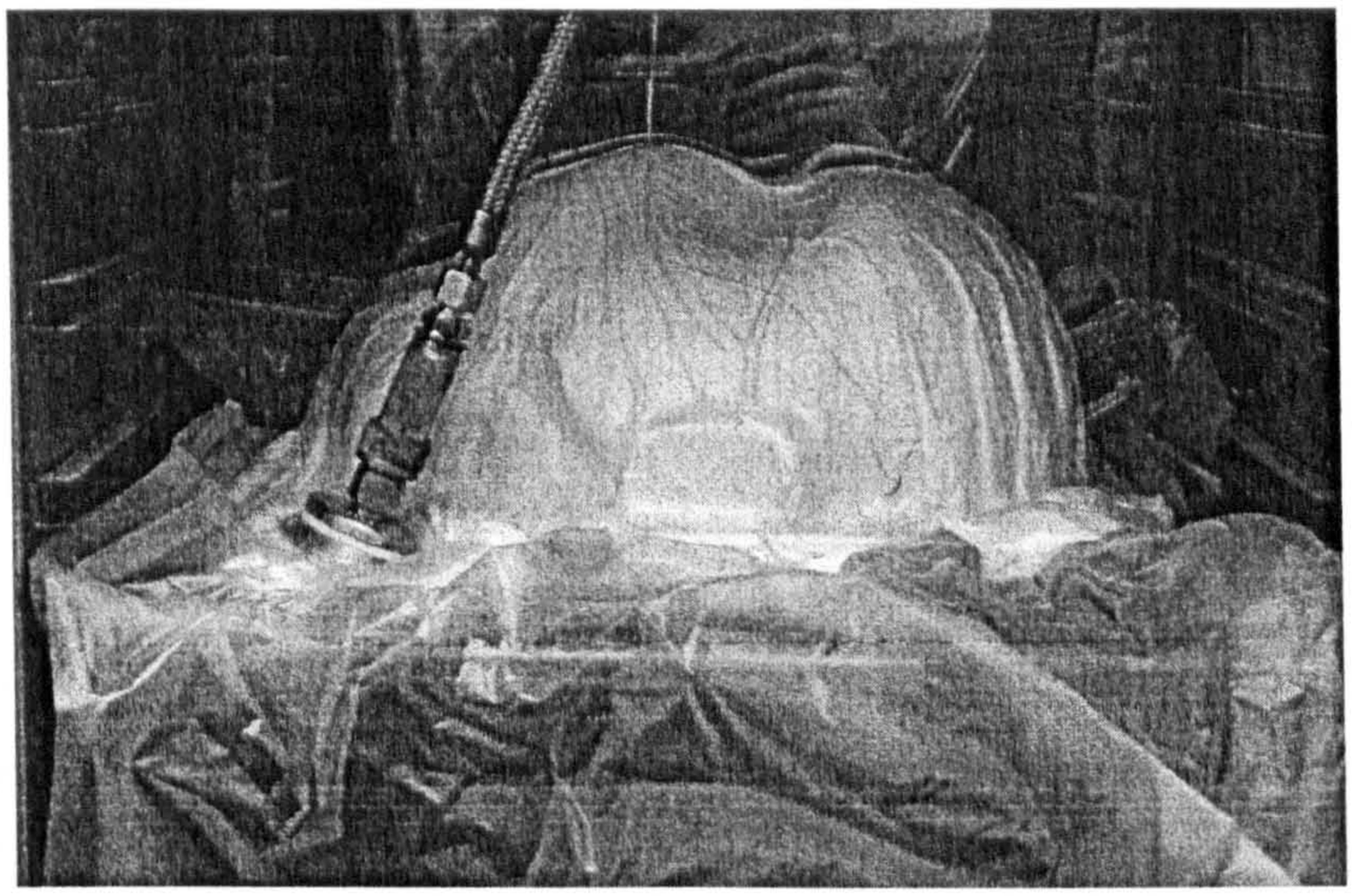

Figure 3.10 Vacuum forming of helicopter pilot helmet.

3.4 Flexural testing

To assess the influence of the vacuum process on laminate properties five or more specimens were tested in flexure from each plate according to BS 2782. The test specimen was deflected at a constant rate of 10 mm/min until the specimen fractures or until the deformation reaches some pre-determined value. The tests were performed using a Hounsfield Universal Testing machine. The dimensions of specimens were 15 mm wide and 80 mm long. The three point loading system had a load span of 60 mm. Flexural modulus was calculated from the force-deflection curve using the deflections that correspond to strain values between 0.0005 and 0.0025.

3.5 Tensile testing

Tensile tests were performed using an Instron Universal Testing machine. Samples were tested following BS EN ISO 527 –4:1997. The test specimen was loaded to tension at a constant rate of 2 mm/min until the specimen fractures. The dimensions

of specimens were 25 mm wide and 250 mm long. An extensometer was attached to the test specimen and the change in gauge length monitored. Initial gauge length was 50mm. At least 5 specimens were taken from each sample. Tensile modulus is calculated as the slope in the stress-strain curve for strain values between 0.0005 and 0.0025.

3.6 Compaction testing

To evaluate the compaction behaviour of the reinforcement in material B, compaction tests were performed after the matrix had been removed by burn-off. Samples of commingled glass/PP were placed in a pre-heated oven at temperature over 400°C until the polymer was completely burnt. Four samples composed of three layers of reinforcement each were then lubricated with 10 ml of Elfolna 15 (mineral oil supplied by Elf) to reduce the effect of friction between fibres (i.e. approximating the lubricating effect of the molten matrix during consolidation). The lubricated samples were then compacted between steel platens using a Hounsfield Universal Testing machine whilst the applied forced was recorded and an LVDT measured the platen displacement. Data was then processed to account for the compliance of the rig. The dimensions of the specimens were 110 mm wide and 110 mm long and the compaction rate was 0.5 mm/min.

3.7 Void Content Image Analysis

3.7.1 Preparation of specimens

Sample casting

Mouldings were carefully aligned to ensure that the specimens were not cut parallel to any of the fibre directions, to avoid confusing fibre cross sections with voids. Specimens were then cast into resin for the following reasons:

- To prevent damage to the edge of specimens during grinding.
- To enable the use of automatic polishing facilities or a manual polishing holder.

- To reduce the misalignment of the section plane during grinding.
- To improve the repeatability of the polishing process.

The specimens were fixed at the bottom of the casting pot. Adhesive was used to hold the samples temporarily. Unfilled polyester casting resin gives an appropriate bond to specimens. The specimens were cast in polyester resin in 40 mm mounting rings (about 25 g per ring) using 2-5% by mass of Butanox catalyst. A greater percentage of catalyst may produce cracks in the specimen. A quantity of resin sufficient to yield a specimen thickness of not less than 20mm was used.

The polyester resin used was accelerated: this means that no additional accelerator was necessary. However, in order to get a faster curing of the resin about 2% of additional accelerator NL-49P was introduced.

Cutting

After removing the cured specimen from the mounting rings, the specimen was cut on the two faces, to a thickness not exceeding 14 mm. This allowed the specimen to be in focus under the microscope.

Grinding

Initially the two faces of the specimens were ground using polishing paper to obtain parallel faces (the lower face has to be roughly polished). The grinding operation was carried out on Struers® DAP-7 machine equipped with an automatic holder (Struers® Pedemin-S). The cast samples were ground and washed using waterproof papers from 240, 400, 600, 1200 and 2400 (or 4000) grade. To obtain a good polished surface, at least three polishing papers (e.g., 240, 600 and 1200) with growing grit size were used for not less for three minutes each, the 1200 and 2400 grit for not less than five minutes and the 4000 grit for not less than eight minutes. The grinding operation was carried out using 240 rpm motor speed.

After polishing using grinding paper, if specimen quality was not good enough, the specimens were polished with 1 μm alumina paste consisting of 20% by volume of powder and 80% by volume of water. After that, the sample was polished with a

metallographic solution using a smooth cloth and then a dye penetrant was applied to enhance the contrast between the composite and the voids.

3.7.2 Microscopy analysis

A detailed description of procedure is given in Appendix 3.1. A summary is presented below.

Thresholding using Aphelion Image Analysis

Image analysis software such as Aphelion™ allows one to identify 256 grey levels. These grey levels are used to discriminate between objects in an image using a process called *thresholding*, which separates objects on the basis of their grey level or brightness and creates a resulting binary image.

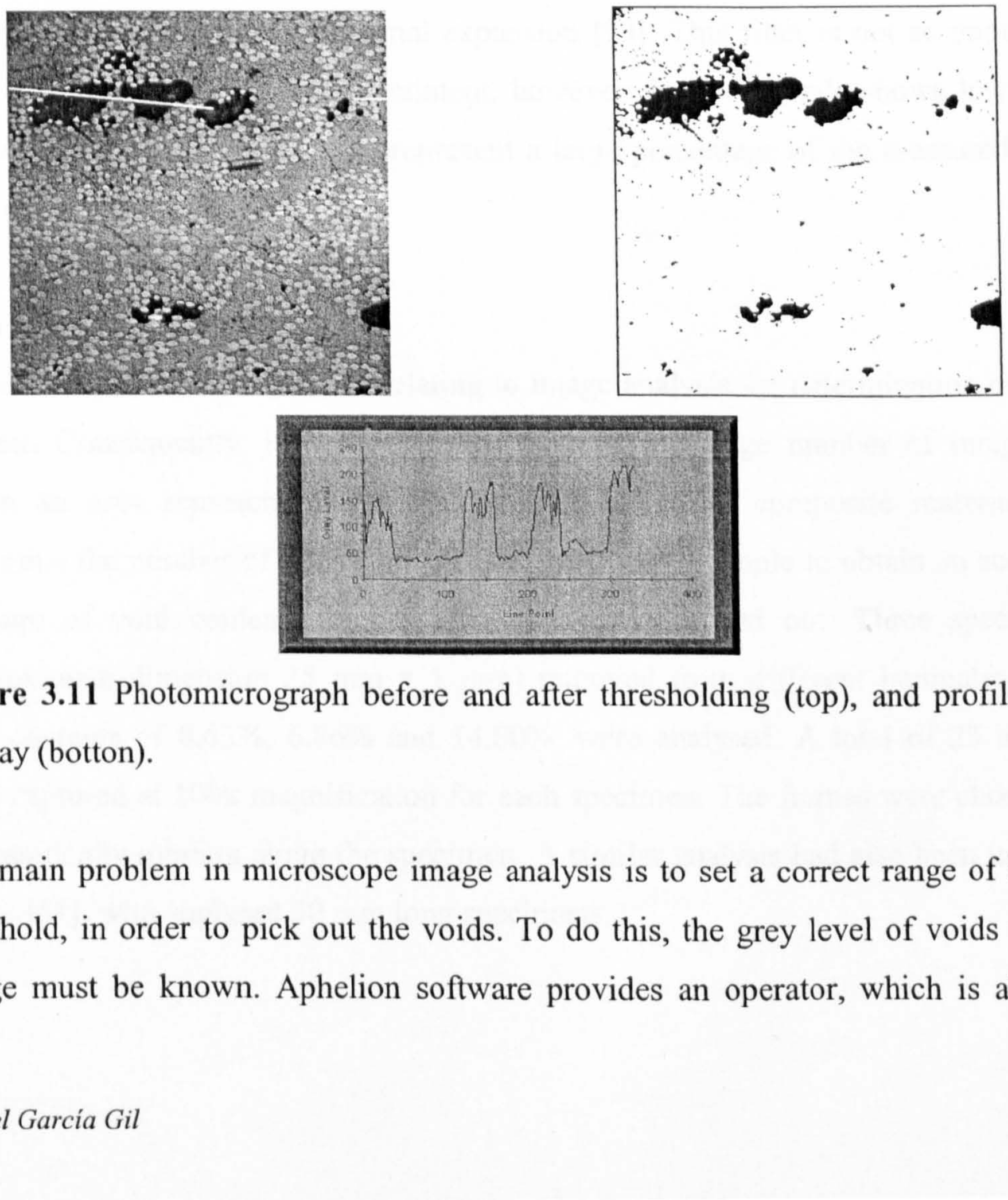

Figure 3.11 Photomicrograph before and after thresholding (top), and profile line display (botton).

The main problem in microscope image analysis is to set a correct range of image threshold, in order to pick out the voids. To do this, the grey level of voids in the image must be known. Aphelion software provides an operator, which is able to

show pixel intensity across an image. Clicking the *Draw a Profile Line* icon, the cursor changes to a crosshair shape and the line button is activated. Drawing a line over the area of interest, when the mouse button is released, a Profile window is displayed, (see Figure 3.11). This window shows the grey level along the line. A range of grey level inside the void is required, so different voids in the image should be checked to obtain representative values of minimum and maximum pixel intensity (grey level).

The filter value varies with magnification. Magnification of 50 requires filtering all regions below an area of 15 pixels, while magnification of 100 requires filtering all regions below 50 pixels. These areas come from filtering all regions with diameter similar to the fibres (e.g., in Twintex E-glass fibres have a diameter of 17 μm, while polypropylene fibres have a diameter of 20-25 μm).

When a filter of objects that discriminates objects by their size is used, micro-voids are not counted. These have a great influence on the properties of composite materials, e.g. coefficient of thermal expansion **[93]**. This filter is not so important when a sample shows high void content, however when a sample shows low void content (<2%), micro voids may represent a large percentage of the measured void content.

Error analysis

There are no accepted standards relating to image analysis for determination of void content. Consequently, it was necessary to analyse a large number of images to obtain an area representing the real void level in the composite material. To determine the number of images required from a single sample to obtain an accurate measure of void content, error analysis has been carried out. Three specimens (approximate dimension 25 mm x 1 mm) removed from different laminates, with void contents of 0.63%, 6.86% and 14.00%, were analysed. A total of 23 images were captured at 100x magnification for each specimen. The frames were chosen by systematically moving along the specimen. A similar analysis had also been used by Wilks **[52]**, who analysed 50 mm long specimens.

Eqn. 3.1 shows the definition of error, where V_C^* is the estimated void content based on the number of images analysed and V_C is the true void content. For the purpose of this analysis, the true void content V_C is taken to be the average void content of the entire cross section that was analysed, and this approach was used within this thesis.

$$error = \frac{\left|V_C^* - V_C\right|}{V_C} \tag{3.1}$$

Figure 3.12 shows the number of images required to estimate the mean void content with a given error. This figure demonstrates that between 18 and 20 images have to be analysed to obtain an error less than 0.15 (15%). This means that around 80 % of the specimen cross section should be analysed.

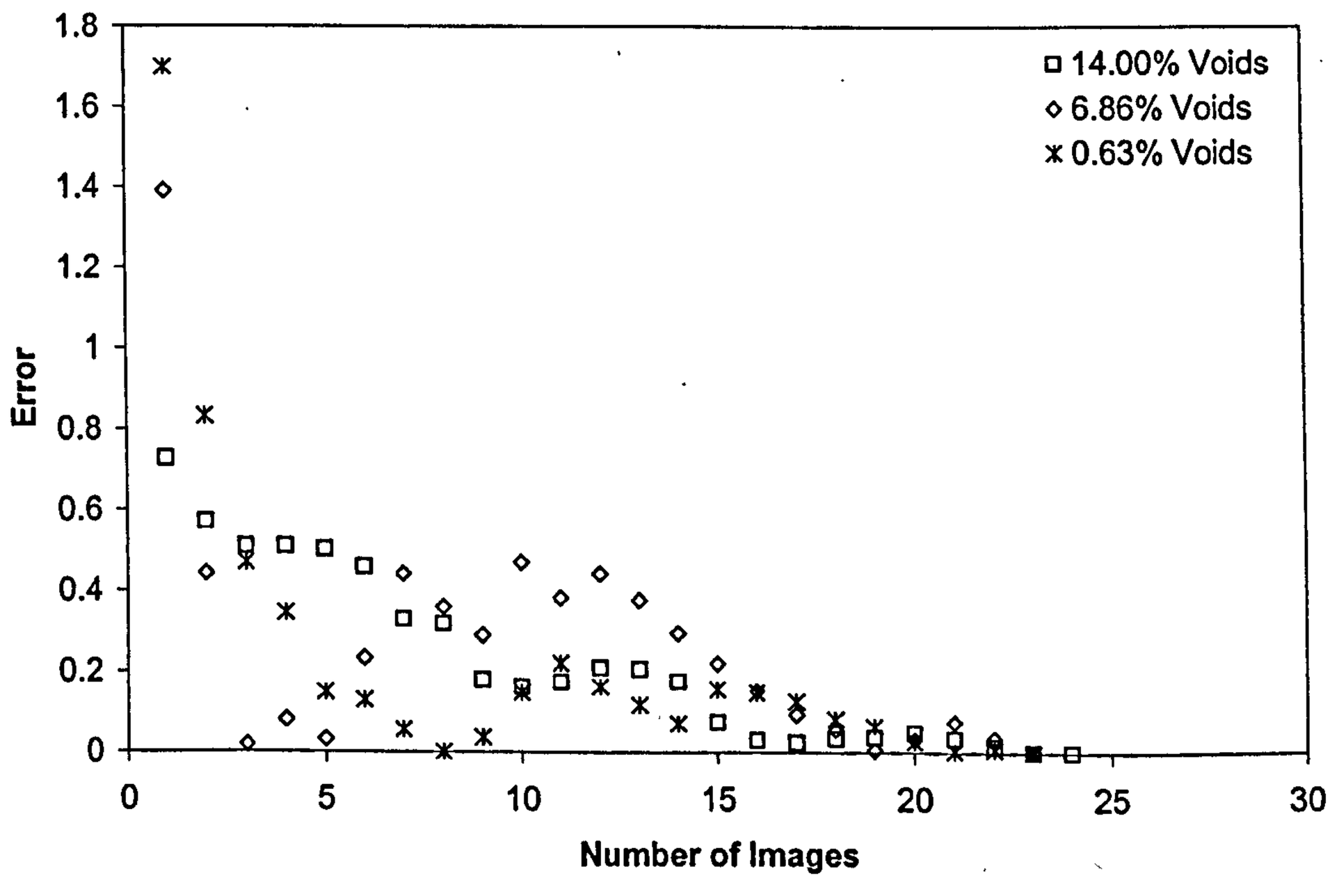

Figure 3.12 Void content error using different numbers of images

3.8 Automated Strain Analysis and Measurement Environment

The Automated Strain Analysis and Measurement Environment (ASAME) system produced by CamSys allows the measurement of strains through a simple process **[94 - 96]**. The strain measurement equipment is an ASAME Target Model. This equipment is a portable, camera-based measurement system that automatically measures the surface geometry and strain distribution over an area of a formed or consolidated part, onto which a square grid has been printed. The equipment used was a Kodak Digital Camera System (DCS420m), with a 25 mm cube (target) used as a reference to edit digital photographs.

The first step is applying a grid to the blank with a grid spacing of 10 mm. Grids can be applied using different methods: electro-chemical etching, silk screening, or photo emulsion. Certain unusual methods are used for specific applications, such as laser etching for plastic or assembling coloured wax cubes for bulk forming simulations. For the results analysed in this work the grid was drawn with a paint marker using a stencil. After gridding, the blank is formed and the component is consolidated.

The next step is to take photographs of the area of interest. In case the component is too large to be photographed in a single image, it has to be divided into different regions. At least two photographs have to be taken of each region (see Figure 3.13). These are taken from different positions. The photographs are then processed to correct any defects in the grid. Defects in the grid can occur for many reasons, including grid application error, or non-grid markings on the blank. Photographs of the measurement area, with the target in the view, are taken from different positions.

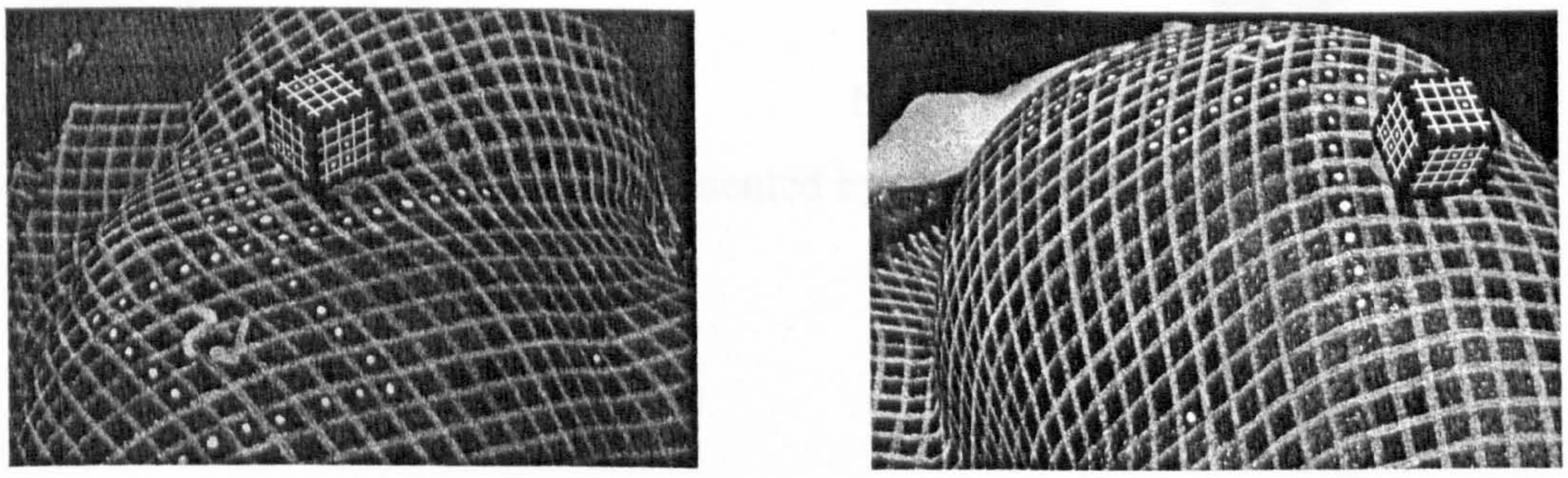

Figure 3.13 Photographs of a part for subsequent analysis.

These digital photographs are then used to determine the 3D coordinates of the intersections of the square grid, Figure 3.14. The 3D coordinates, along with the original grid spacing are used to determine the principal surface strains. Depending on the number of images used to make a measurement, the accuracy of the system changes. In this study two photographs are used and an accuracy of ±2.5% strain is obtained **[95]**.

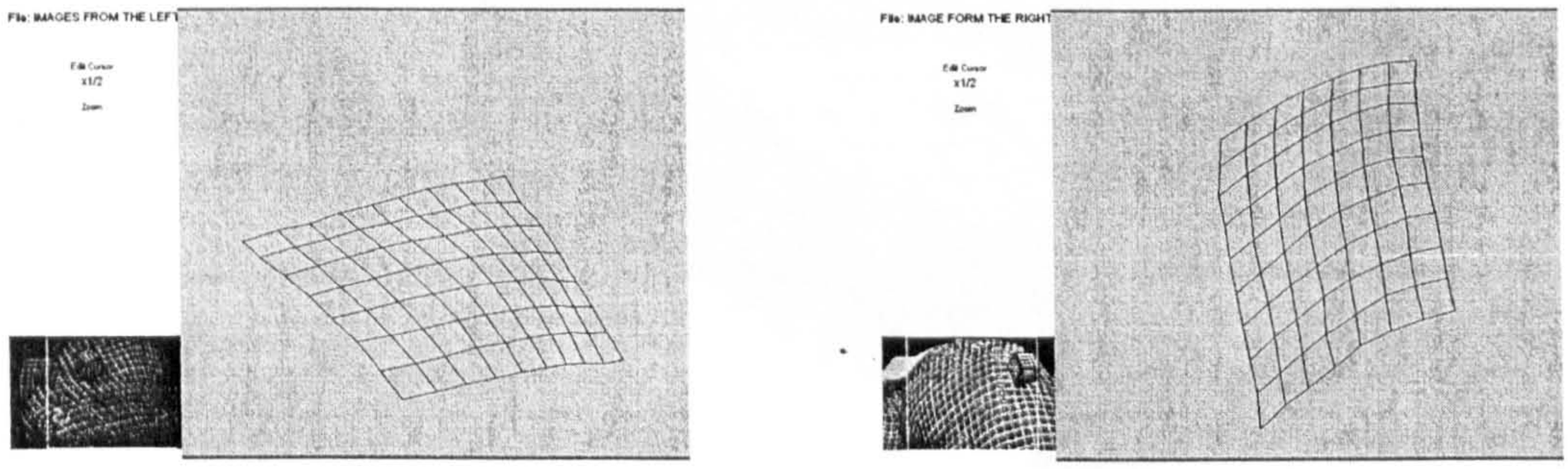

Figure 3.14 Processed digital photographs.

Once photo editing of each pair of photographs is complete the computer automatically calculates the 3D coordinates of the grid intersections and the strain distribution across the measurement area, Figure 3.15. Finally, all of the different parts that form the component are combined leading to the original shape. This 3D shape can then be analysed using the visualisation tools provided by ASAME, Figure 3.16.

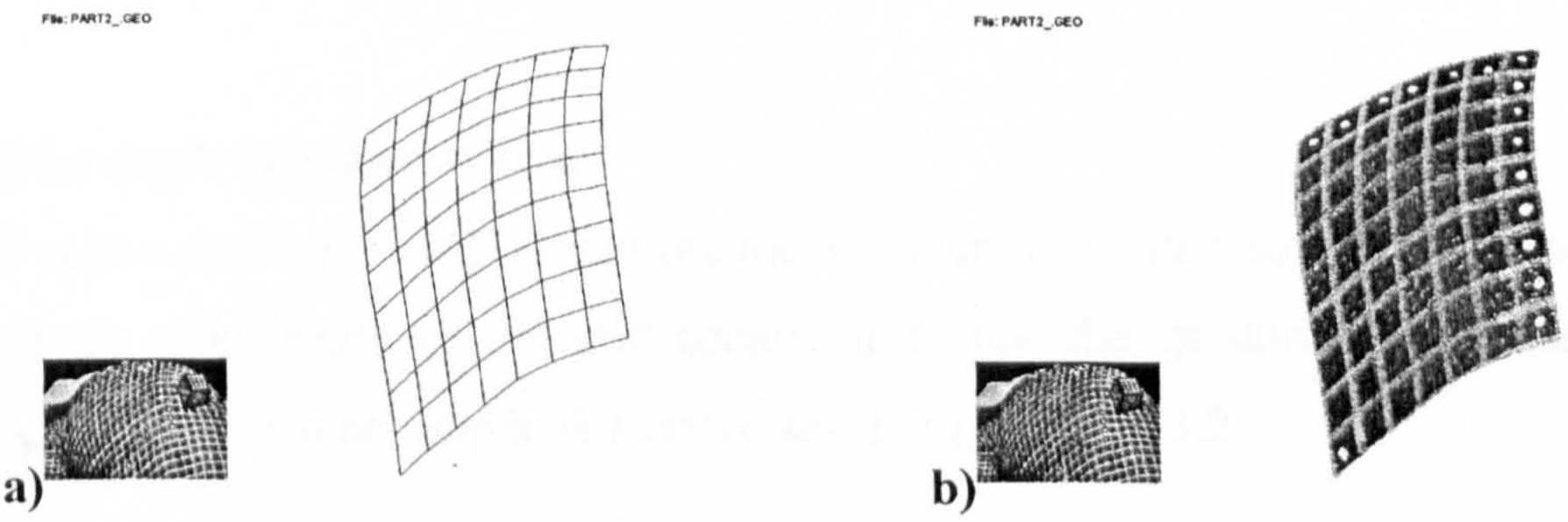

Figure 3.15 3D shape of the part represented by: **a)** grid lines **b)** photograph.

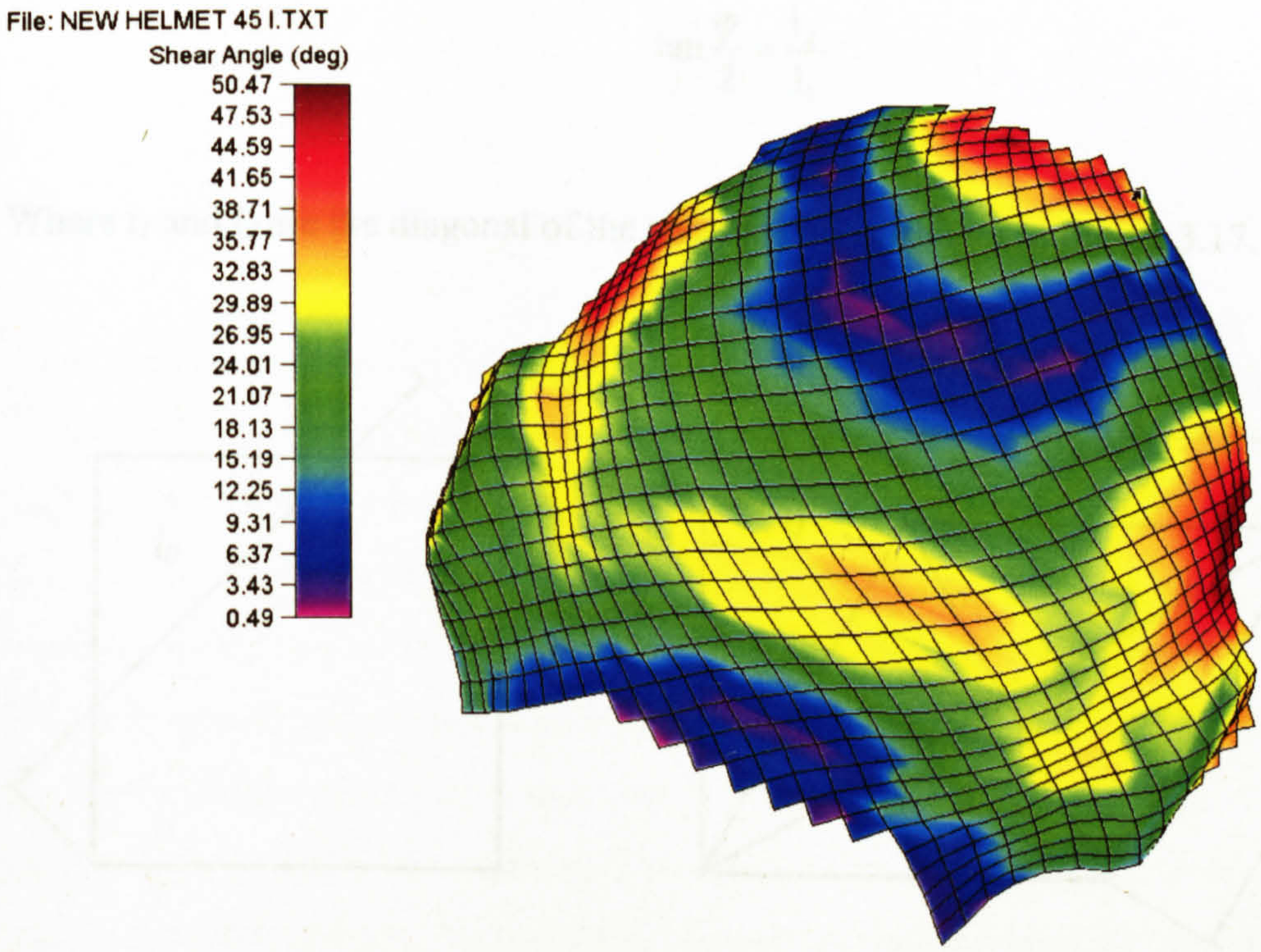

Figure 3.16 Helicopter pilot helmet analysed using ASAME system.

3.8.1 Shear angle measurement

The characterisation of formed textile composite components requires the knowledge of basic parameters such as shear angle, thickness or change in grid spacing. These parameters can be measured using different routes, as explained below.

Shear angle based on strains

As stated above ASAME allows the measurement of surface strains which, assuming that the side length of the grid squares does not change during deformation (see Figure 3.17), can be used to determine shear angles, Eqn. 3.2.

$$\theta = \frac{\pi}{2} - \varphi \qquad \textbf{(3. 2)}$$

Where θ is the shear angle expressed at radians and φ is the fibre angle, calculated as:

$$\tan\frac{\varphi}{2}=\frac{l_2}{l_1} \tag{3.3}$$

Where l_1 and l_2 are the diagonal of the sheared cell as shown in Figure 3.17.

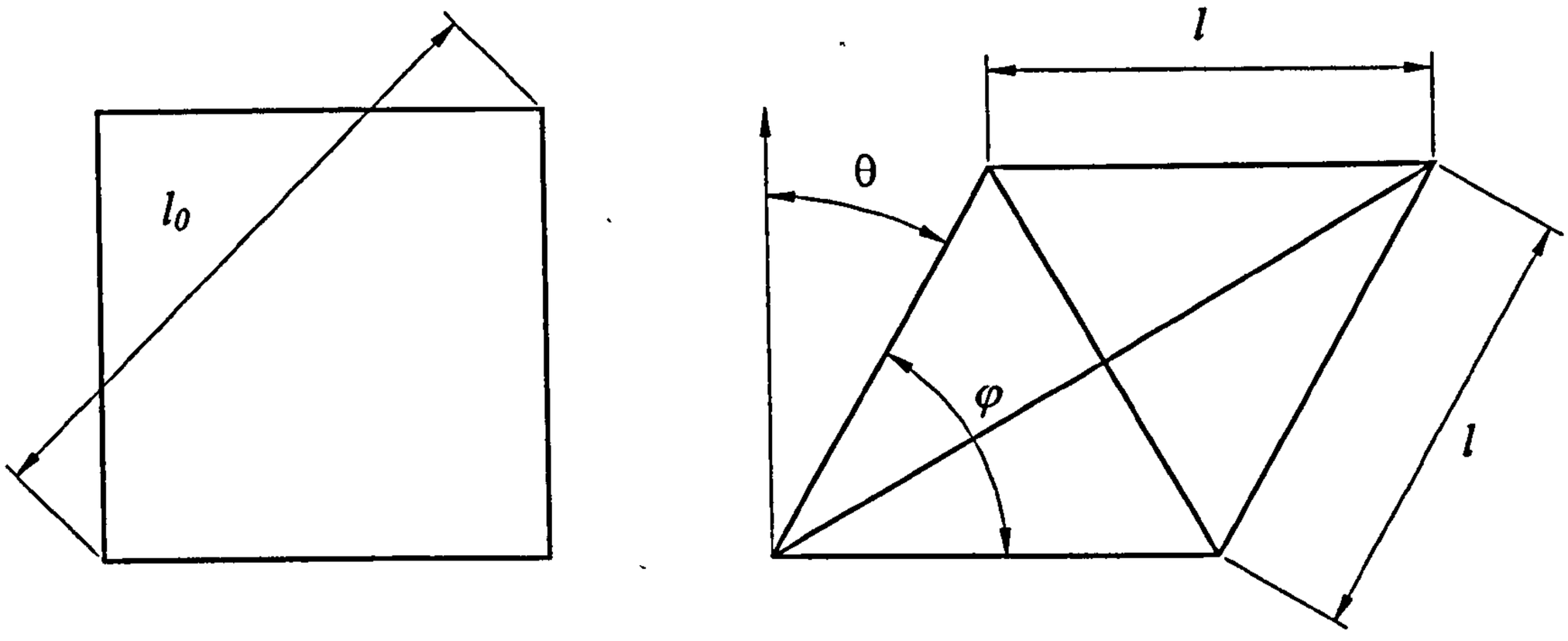

Figure 3.17 Deformation due to in-plane shear.

Using logarithmic strain definition,

$$\epsilon_{true}=\ln\left(\frac{l_i}{l_0}\right) \tag{3.4}$$

The diagonal length can be expressed as:

$$l_i=l_0 exp(\varepsilon_i) \tag{3.5}$$

Eqn. 3.3 and Eqn. 3.5 yield

$$\frac{\varphi}{2}=\tan^{-1}(\exp(\varepsilon_2-\varepsilon_1)) \tag{3.6}$$

Combining Eqn. 3.2 and Eqn. 3.6, the shear angle equation to be implemented by the operator in ASAME is obtained:

$$\theta = 90 - 2\frac{180}{\pi}\tan^{-1}\left(\exp\left(\varepsilon_2 - \varepsilon_1\right)\right) \qquad (3.7)$$

Where ϵ_1 and ϵ_2 are the major and minor strains respectivately.

Shear angle based on the 3D coordinates of the nodes (grid intersections)

Raw data from the ASAME software was processed to calculate the shear angle at each node, corresponding to the average change in included angle with adjacent nodes. The shear angle calculated as a function of the principal strains provides accurate measurements when the deformed square grid keeps the original drawn side length. However, experience demonstrates that the draping of a textile composite on a complicated demonstrator component induces alternative deformation mechanisms such as inter-tow slip or wrinkling. These defects result in a change in the deformed square grid side length, leading to an erroneous measurement of the shear angle. Moreover, comparison of ASAME measurement with predictions from forming or draping simulations requires the use of a consistent method for measurements of shear angle. Understanding the way shear angle is calculated within ASAME using the 3D coordinates of the nodes requires the knowledge of how elements and nodes are defined within ASAME itself. ASAME Reference Manual **[95]** provides an explanation of file formats.

Assuming that a general deformed grid cell has the shape represented in Figure 3.18, the shear angle defined at node 1 can be calculated as:

$$\theta = \frac{\pi}{2} - \varphi \qquad (3.8)$$

Fibre angle can be obtained from the scalar product of two vectors that follow the fibre directions. These are denoted $\vec{a}$ and $\vec{d}$ in Figure 3.18. Fibre angle at node 1 can be calculated as:

$$\varphi = \cos^{-1}\left(\frac{\vec{a}\cdot\vec{d}}{|\vec{a}||\vec{d}|}\right) \qquad (3.9)$$

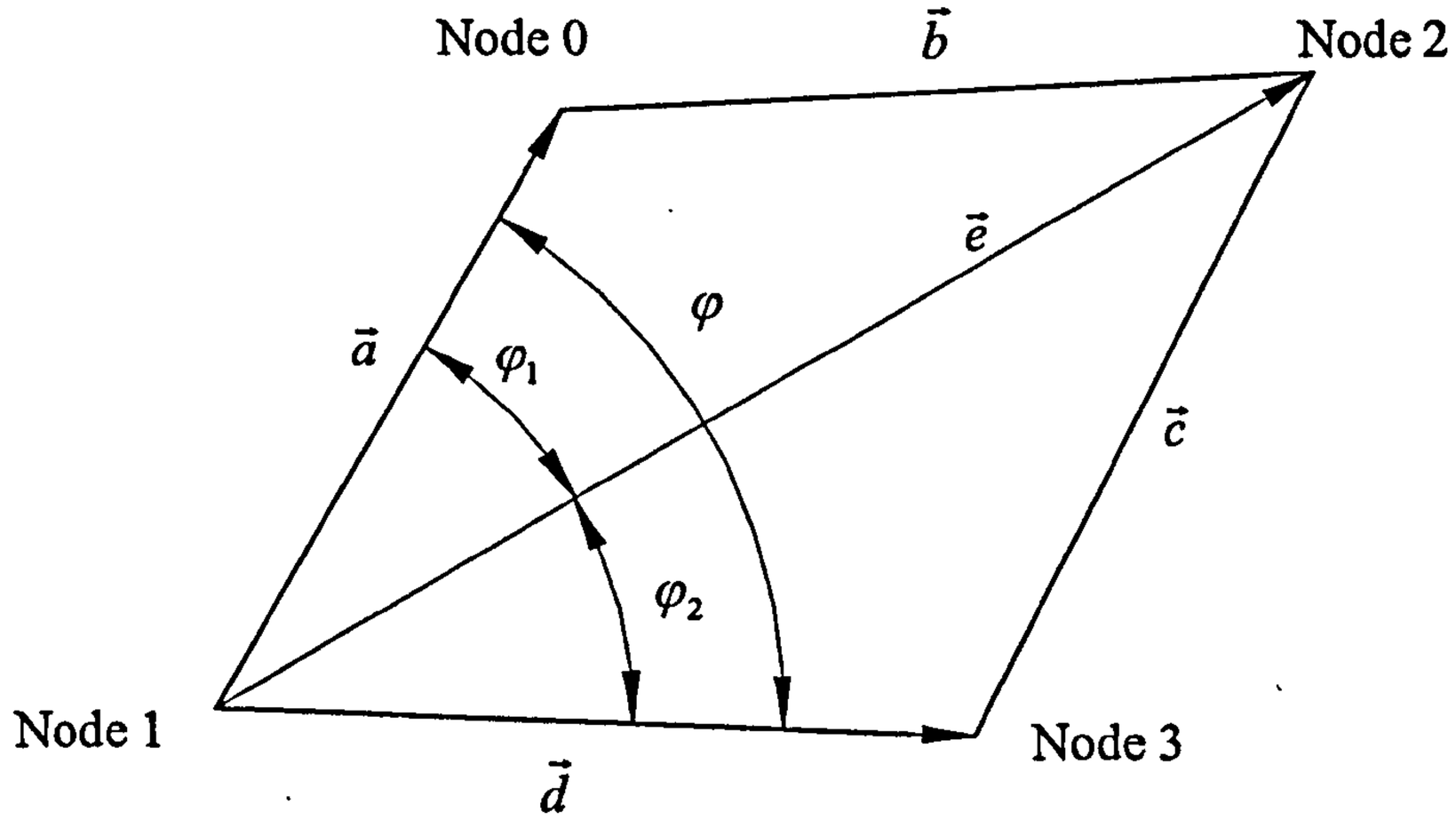

Figure 3.18 Shear angle definition in a deformed element.

An alternative method to calculate fibre angle that accounts for the effect of the curvature of the geometry is to consider fibre angle as the sum of $\varphi 1+\varphi 2$, which is equivalent to Eqn 3.10 in the case of in-plane deformation.

$$\varphi 1+\varphi 2=\cos^{-1}\left(\frac{\vec{a}\cdot\vec{e}}{|\vec{a}||\vec{e}|}\right)+\cos^{-1}\left(\frac{\vec{e}\cdot\vec{d}}{|\vec{e}||\vec{d}|}\right) \quad \textbf{(3. 10)}$$

Although three methods are here presented, the comparison with drape model simulations requires the use of a consistent method. Thus from this point on Eqn. 3.9 Is used to calculate fibre angles.

3.8.2 Thickness measurements

Once the shear angle distribution of a textile composite component is known, the thickness distribution can be calculated. There are two ways to analyse the thickness using ASAME; one is derived directly from the conservation of volume equation and the other is to assume that shearing is the main mechanism of deformation.

Assuming constant side length of the deformed element (Figure 3.17), the constant volume equation can be written as:

$$l_0^2 h_0 = l_1 l_2 h \tag{3.11}$$

Using logarithmic strains $l_i = l_0 e^{\varepsilon_i}$ the thickness of a sheared laminate will be greater or lower than the initial thickness depending on the principal strains. Such an approach is useful to predict thickness when other mechanisms of deformation apart from shear are involved, Eqn. 3.12.

$$h = h_0 \exp(-\varepsilon_1 - \varepsilon_2) \tag{3.12}$$

If grid side length is assumed constant the thickness will always increase as shear angle θ increases:

$$h = \frac{h_0}{\cos\theta} \tag{3.13}$$

A discussion of these two predictive models is presented in Chapter 7.

3.8.3 Extension ratio measurements

Raw data from the ASAME software includes the coordinates of each node, principal strain values and their directions. Grid spacing in each tow direction were calculated, and these were used to calculate the maximum extension ratio (formed grid spacing / initial spacing) at each node and the average extension ratio in each element. These values represent the change in tow spacing due to inter-tow slip or changes in tow crimp, which can be due to:

- Shearing. Localised shearing would result in an increase in thickness. For an inextensible tow, this must result in a decrease in tow spacing. The actual change would depend on the tow path.
- Straightening. Tows may become straightened (un-crimped) locally, resulting in an increase in tow spacing. Perpendicular tows would then be forced closer as crimp would be increased in this direction.
- Component geometry. A convex geometry would result in a decrease in grid spacing, for example a 20 mm radius and a 1 mm thick material would result in 2% reduction in extension ratio.

These mechanisms are discussed further in Chapter 7.

4 Vacuum Forming of Textile Composites

4.1 Introduction

This chapter is concerned with the forming process proposed in this work. The vacuum forming process is characterised by its ability to produce large and complex components in a single operation using a single sided tool and a vacuum bag to form components at low cost [97]. Typical applications include the body of a golf car, an army assault craft, a rigid inflatable boat and wind turbine blades.

Material B and material C have been processed, and void content measured as a function of three main parameters: pressure, time at pressure and temperature. Experimental analysis was used to investigate the isothermal and non-isothermal vacuum processing of commingled fabrics (material B). The quality of flat plaques manufactured using this simple low cost process was assessed by measuring void content using image analysis techniques. These measurements were correlated with mechanical property data to illustrate the effects of processing on subsequent performance.

Finally, flat plaques were sheared and then consolidated to study the effect of deformation on mechanical properties. In addition, the effect of processing parameters on the consolidation of sheared flat plaques was also assessed.

4.2 Effect of processing parameters on void content for glass/polypropylene composites

4.2.1 Effect of time at pressure on void content

Consolidation of the commingled fabric involves coalescence of the molten matrix, compaction of the reinforcement fibre and expulsion of air as the matrix flows. However, at the end of consolidation the composite may still contain entrapped voids.

Laminates composed of three layers of material B were consolidated using an isothermal vacuum forming process at 180°C. Figure 4.1 shows the effect of time at pressure on the void content of these laminates. Error bars indicate 95% confidence interval. Increasing time at pressure decreases void content dramatically from 10% to 1.7% for the first 210 seconds. Applying the vacuum for 300 seconds reduced the void content only marginally more to 1.3%.

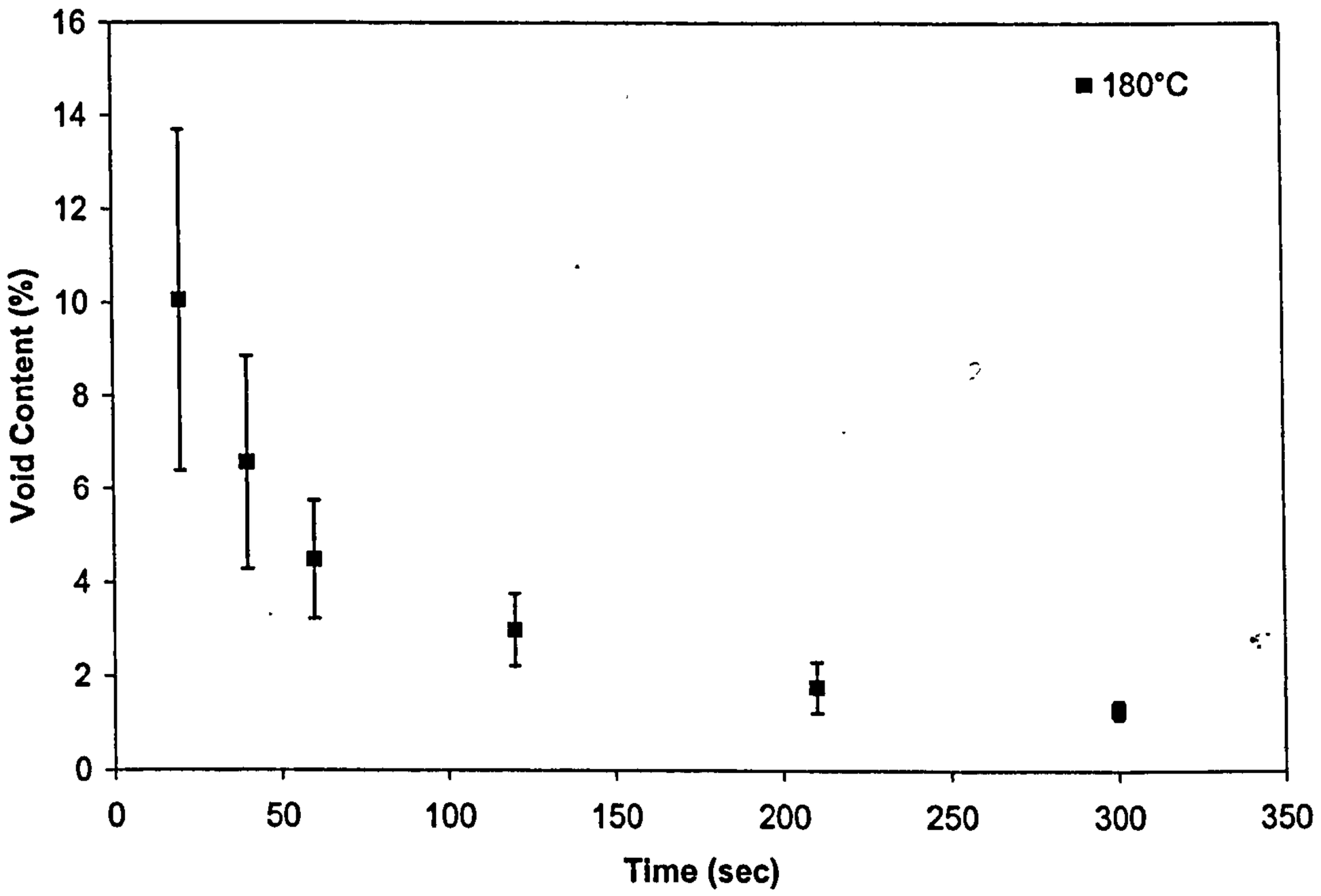

Figure 4.1 Effect of time at pressure on void content of laminates composed of three layers of material B consolidated using isothermal vacuum forming at 180°C. Error bars indicate 95% confidence intervals.

Assuming that the sampling distribution is normal, Eqn. 4.1 shows how error bars are calculated. The second term of Eqn. 4.1 is known as margin of error (MOE), where the standardised normal variable z is obtained from statistical tables, SD is the standard deviation, p is the population and ϕ is the average. For a confidence interval of 95%, $z = 1.96$.

$$l = \phi \pm z\frac{SD}{\sqrt{P}} \qquad (4.1)$$

4.2.2 Effect of processing temperature on void content

To show the effect of processing temperature on void content additional laminates composed of three layers of material B were consolidated isothermally at 195°C. As shown in Figure 4.2, the void content measurements obtained for samples consolidated at 195°C show a reasonably similar trend since the error bars overlap. However, in-situ observations of the laminate consolidated for 20 seconds at 195°C showed a large number of voids on the laminate surface.

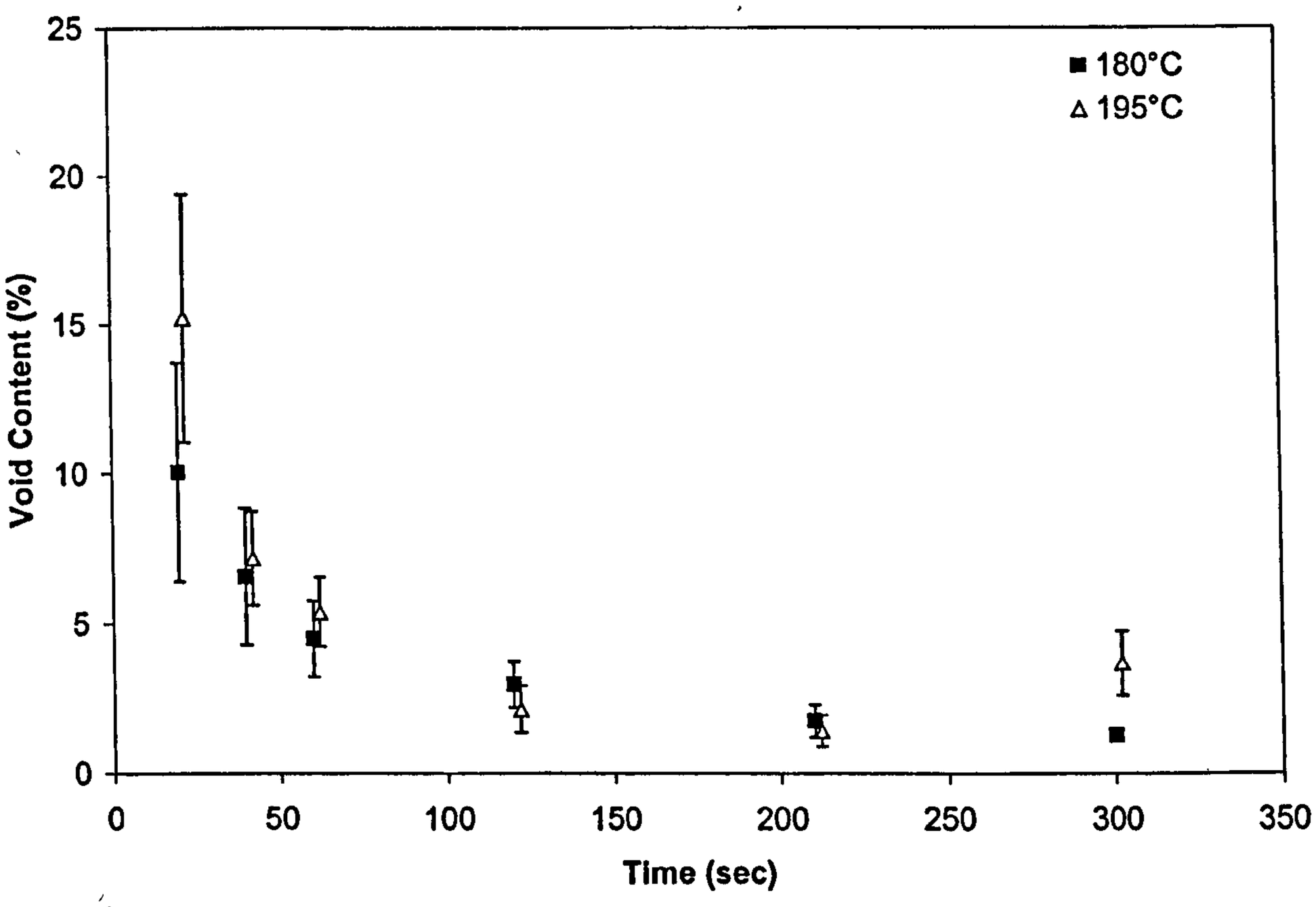

Figure 4.2 Effect of processing temperature on void content of laminates composed of three layers of material B consolidated using isothermal vacuum forming at 180°C and 195°C. Error bars indicate 95% confidence interval.

Void content might be expected to reduce more quickly with time at higher temperature due to a lower viscosity. However, the difference in temperature was not large enough to show a clear trend in this case.

For samples consolidated for longer than 40 seconds a similar void content at both temperatures is observed. However, the laminate consolidated for 300 seconds at 195°C buckled, leading to the appearance of small interstices between fibres and consequently to a higher void content.

The error bars on Figure 4.2 indicate the 95% confidence interval. The confidence interval decreases as time at pressure is increased. This is because voids were more uniformly distributed in samples with low void content.

4.2.3 Effect of pressure on void content

To show the effect of pressure on void content, laminates composed of three layers of material B were formed and consolidated using a non-isothermal vacuum process where the vacuum pressure applied was controlled by the closure of the outlet valve. Figure 4.3 shows the effect of pressure on void content. As pressure increases void content decreases as expected. A more dramatic change is observed for values of pressure between 60 mbar and 500 mbar, where void content decreased from 16% to values under 4%. For levels of pressure over 500 mbar, large changes in pressure did lead to slight changes of void content with values under 1% achieved at 950 mbar. In order to achieve the same level of quality between two laminates consolidated under different pressures, lower applied pressures would require larger times at pressure.

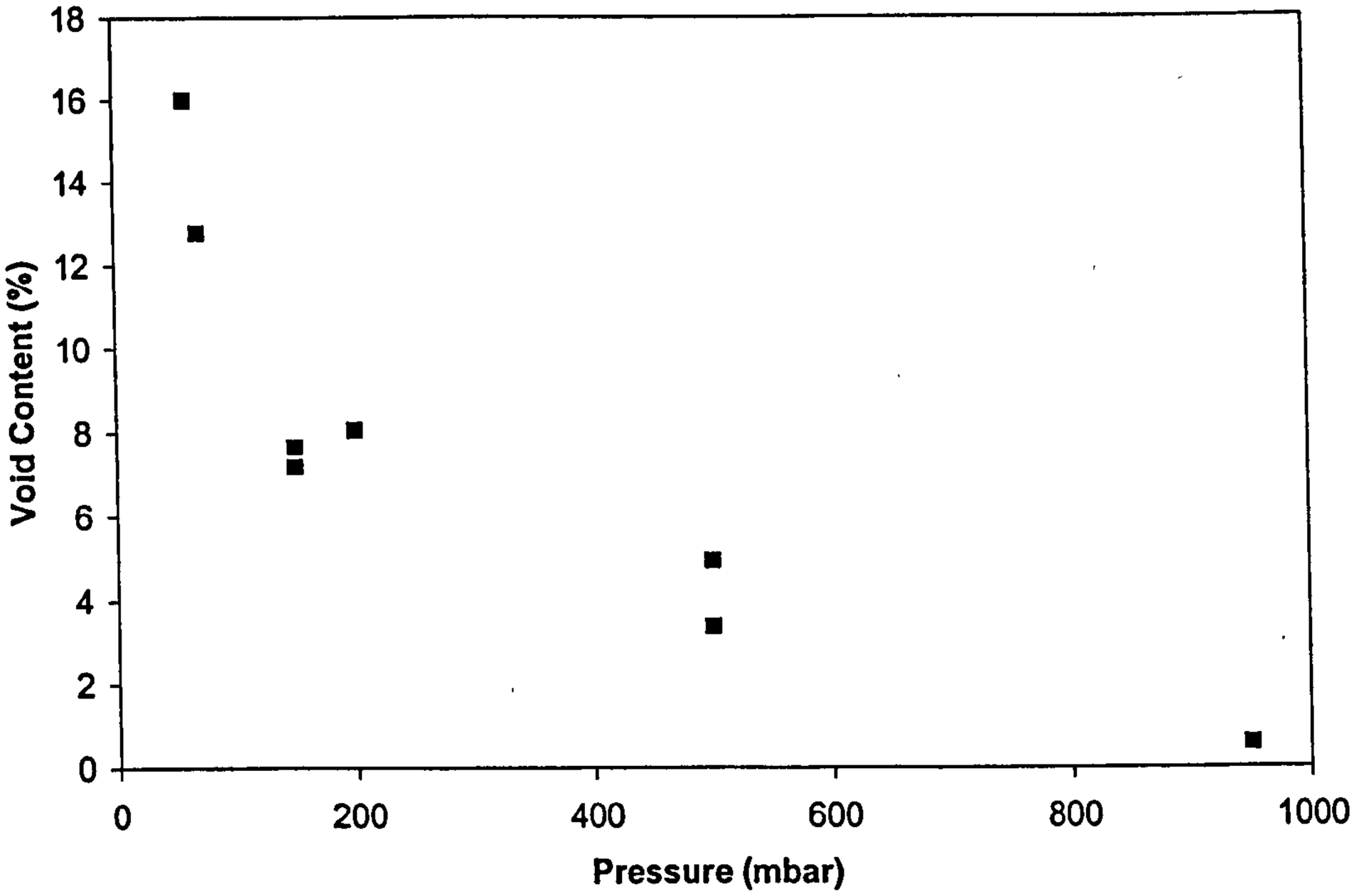

Figure 4.3 Effect of pressure on void content of laminates composed of three layers of material B consolidated using non-isothermal vacuum forming up to 180°C.

4.3 Effect of processing parameters on mechanical properties for glass/polypropylene composites

4.3.1 Flexural properties

Flexural tests were performed on coupons cut from the flat laminates analysed in Section 4.2. Samples were tested following BS 2782 as described in Section 3.4. Thickness ranged from 1.55 to 1.80 mm due to variations in void content. Figure 4.4 shows that flexural strength increases as time at pressure is increased for samples consolidated at 180°C. Error bars represent the 95% confidence interval. Flexural strength is normalised by the manufacturer's quoted value of 280 MPa. A significant increase in the mechanical properties was observed during the first two minutes that the pressure was applied. After that point increasing the time produced a slight increase, although the scatter suggests that this may not be significant.

Figure 4.5 shows one of the main experimental findings in this thesis. Here normalised flexural strength was correlated with void content measurements for the samples processed at 180°C and 195°C. A similar trend was observed for both consolidation temperatures. Samples with a void content below 4% provide flexural strengths in the range 200 MPa to 250 MPa, whilst samples with a high void content tend to an asymptotic value of 140 MPa. It was observed that a void contents over 10% reduced flexural strength by approximately 50% independently of the processing temperature.

Figure 4.6 shows the effect of void content on the normalised flexural modulus of laminates consolidated at 180°C and 195°C. Although no clear trend is observed, a void content of more than 6% decreased flexural modulus by around 30%. Large void content reduces the fibre volume fraction of the laminate, hence a lower flexural modulus could be expected. Flexural modulus is normalised by 13 GPa (the value provided by manufacturer).

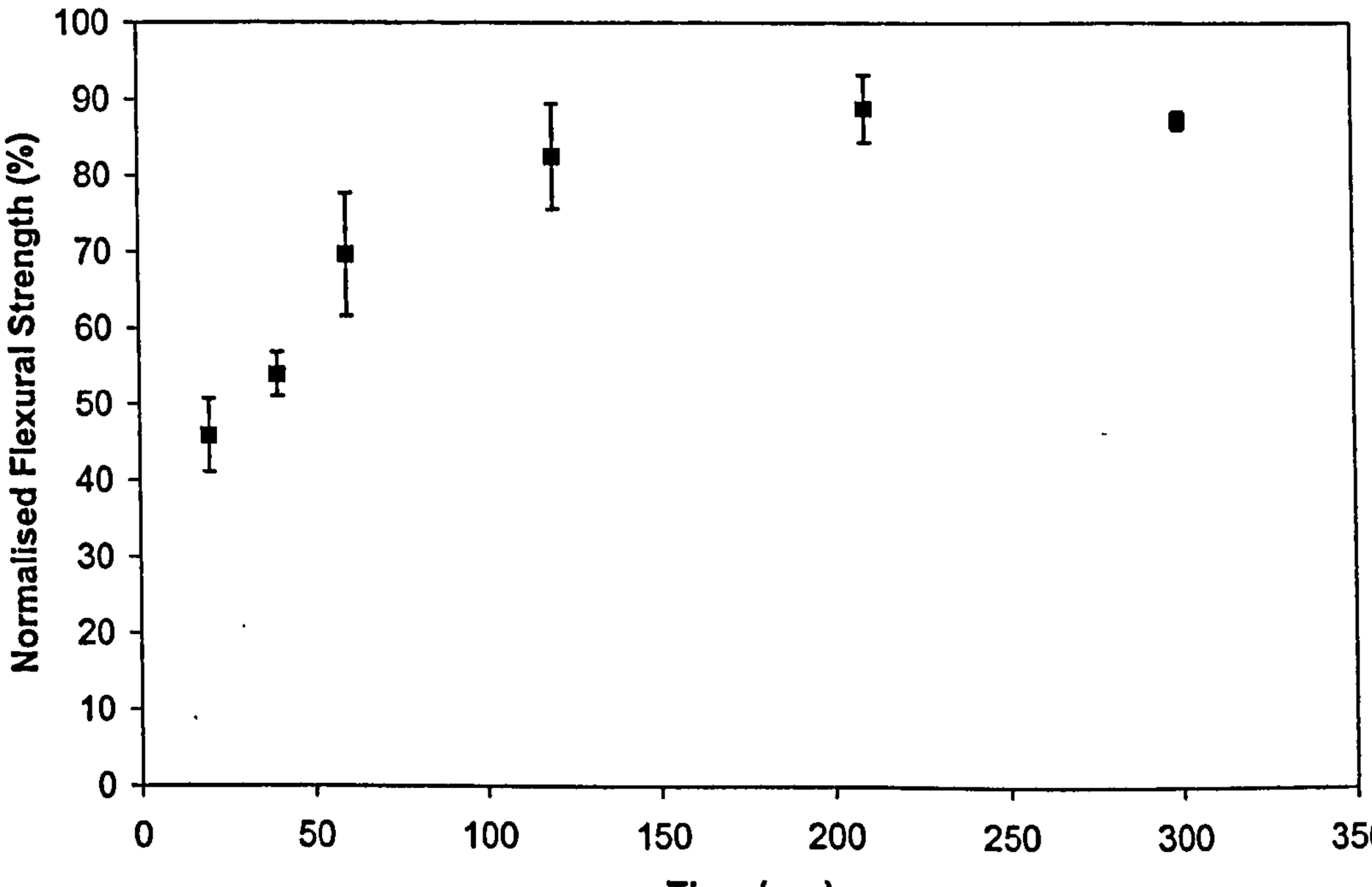

Figure 4.4 Effect of time at pressure on flexural strength of laminates composed of three layers of material B consolidated using isothermal vacuum forming at 180°C. Error bars represent 95% confidence interval. Fibre orientation was 0/90°.

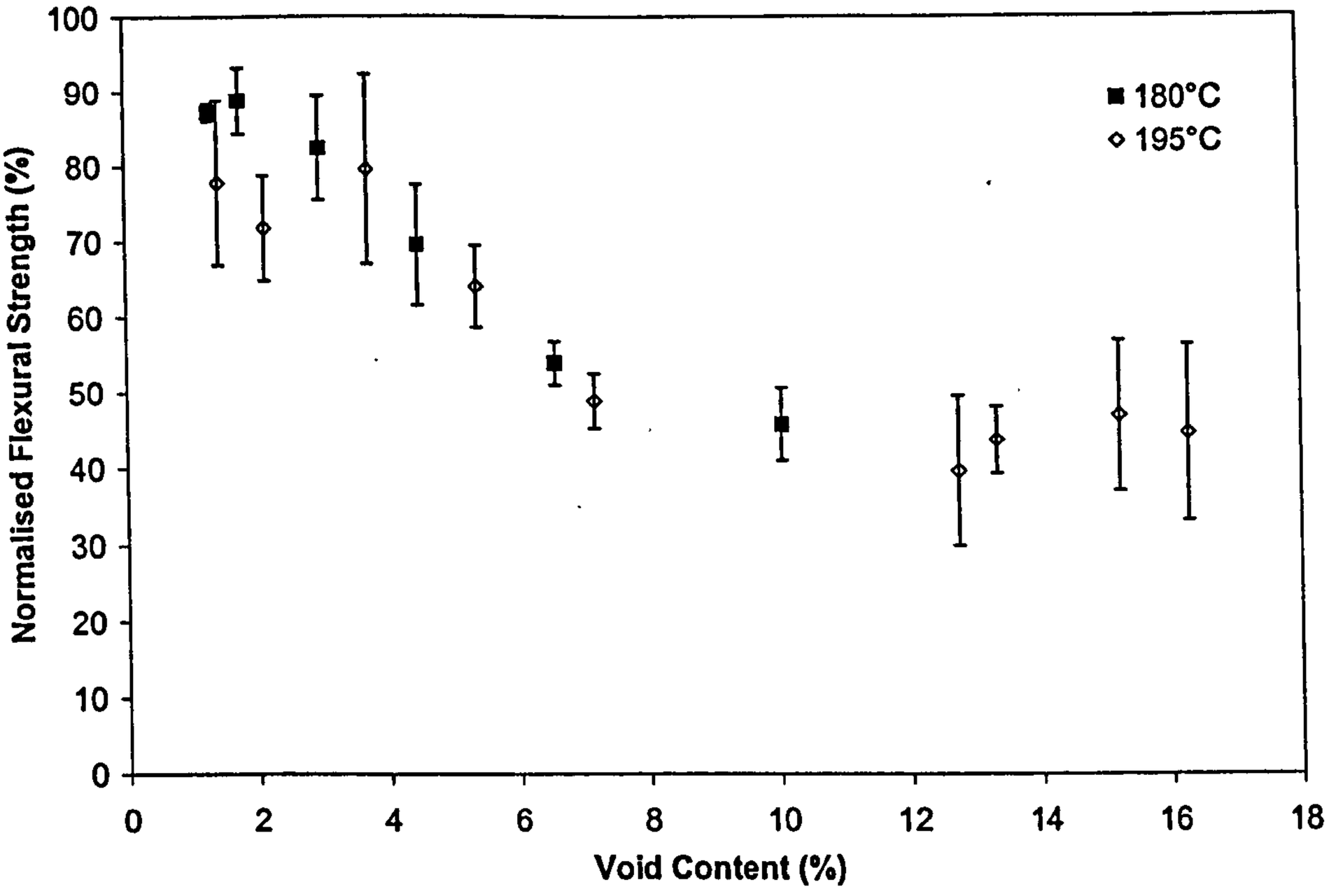

Figure 4.5 Effect of void content on flexural strength of material B laminates consolidated using isothermal vacuum forming at 180°C and 195°C. Fibre orientation was 0/90°.

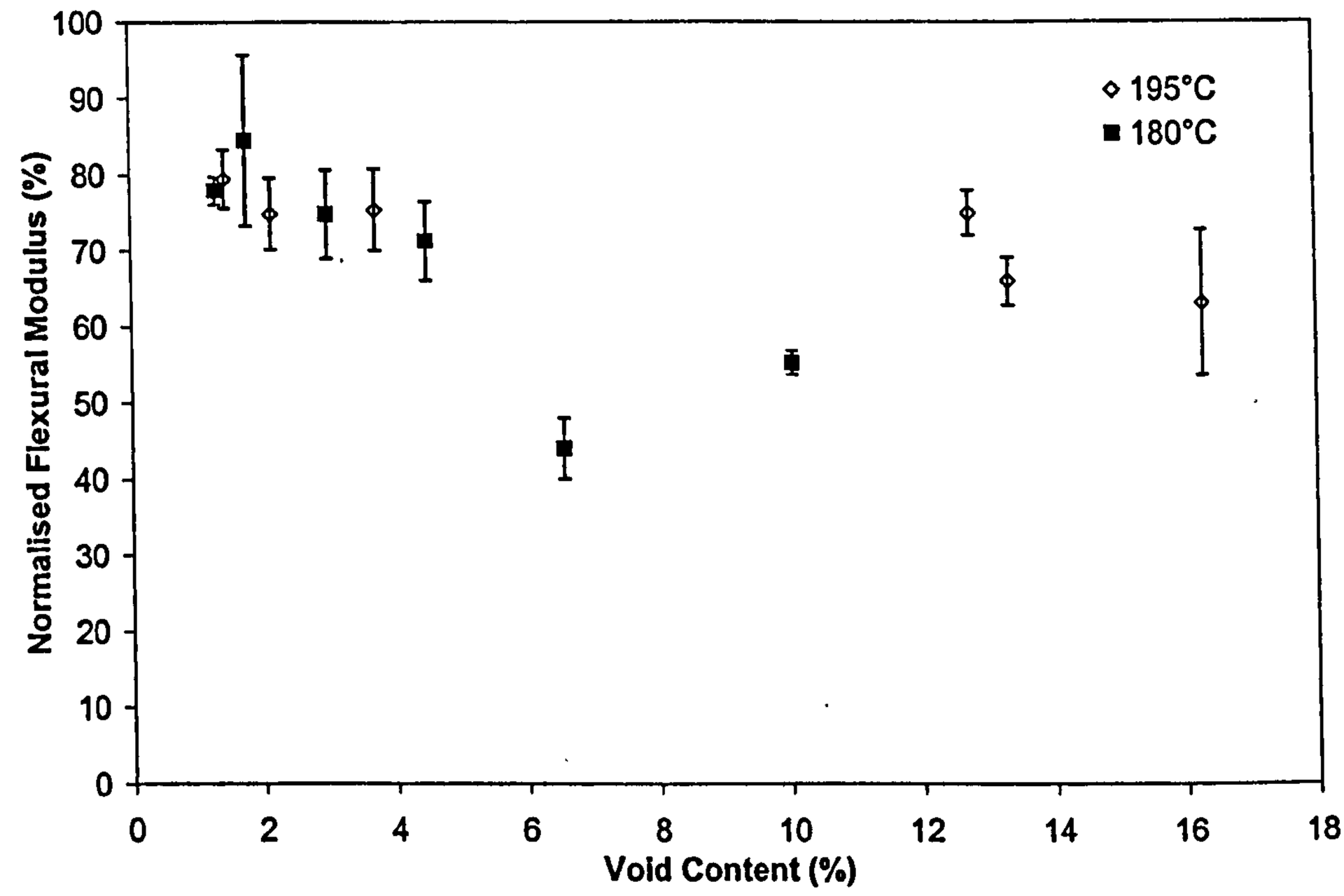

Figure 4.6 Effect of void content on flexural modulus of material B laminates consolidated using isothermal vacuum forming at 180°C and 195°C. Fibre orientation was 0/90°.

4.3.2 Tensile properties

This section is concerned with tensile properties of continuous glass fibre reinforced polypropylene composites produced by vacuum forming. To corroborate the findings in the section above on the relationship between flexural properties and void content, laminates composed of three layers of material B were formed using a non-isothermal vacuum forming process. In order to get high levels of void content the applied pressure ranged from 60 to 1000 mbar, see Figure 4.3.

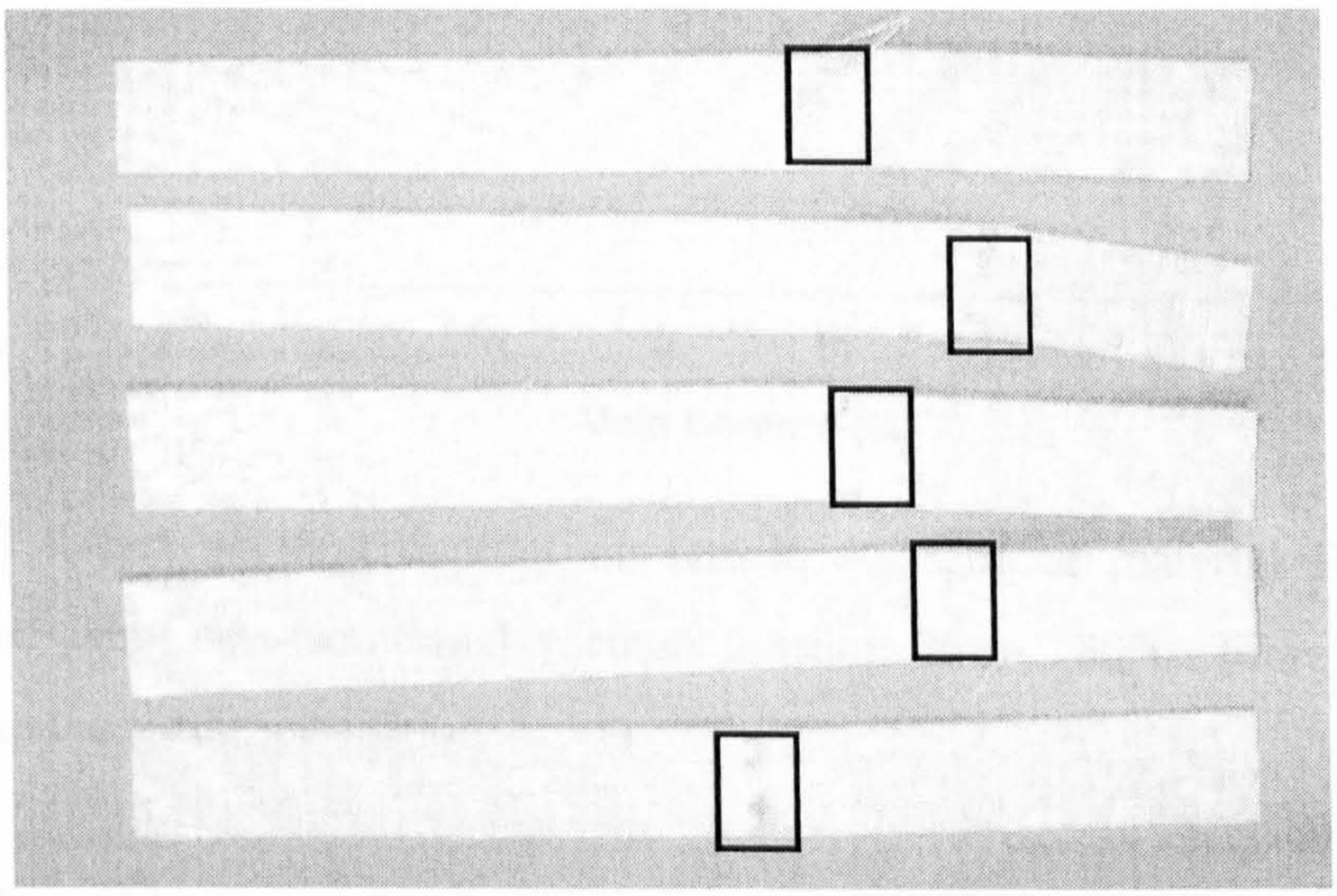

Figure 4.7 Five material B tensile specimens after being tested.

Tensile tests were performed using an Instron Universal Testing machine. Samples were tested following BS EN ISO 527 –4:1997 as described in Section 3.5. Thickness ranged between 1.55 and 1.80 mm due to variations in void content.

Figure 4.7 shows five specimens after testing. Just one of the specimens failed within the gauge length. However, none of them failed at the grips so the results from these specimens were used.

Figures 4.8 and 4.9 show the effect of void content on normalised tensile properties for flat plaques consolidated by a non-isothermal vacuum forming process. Tensile

properties are normalised by manufacturer's values, which are 315 MPa for the tensile strength and 13.6 GPa for the tensile modulus.

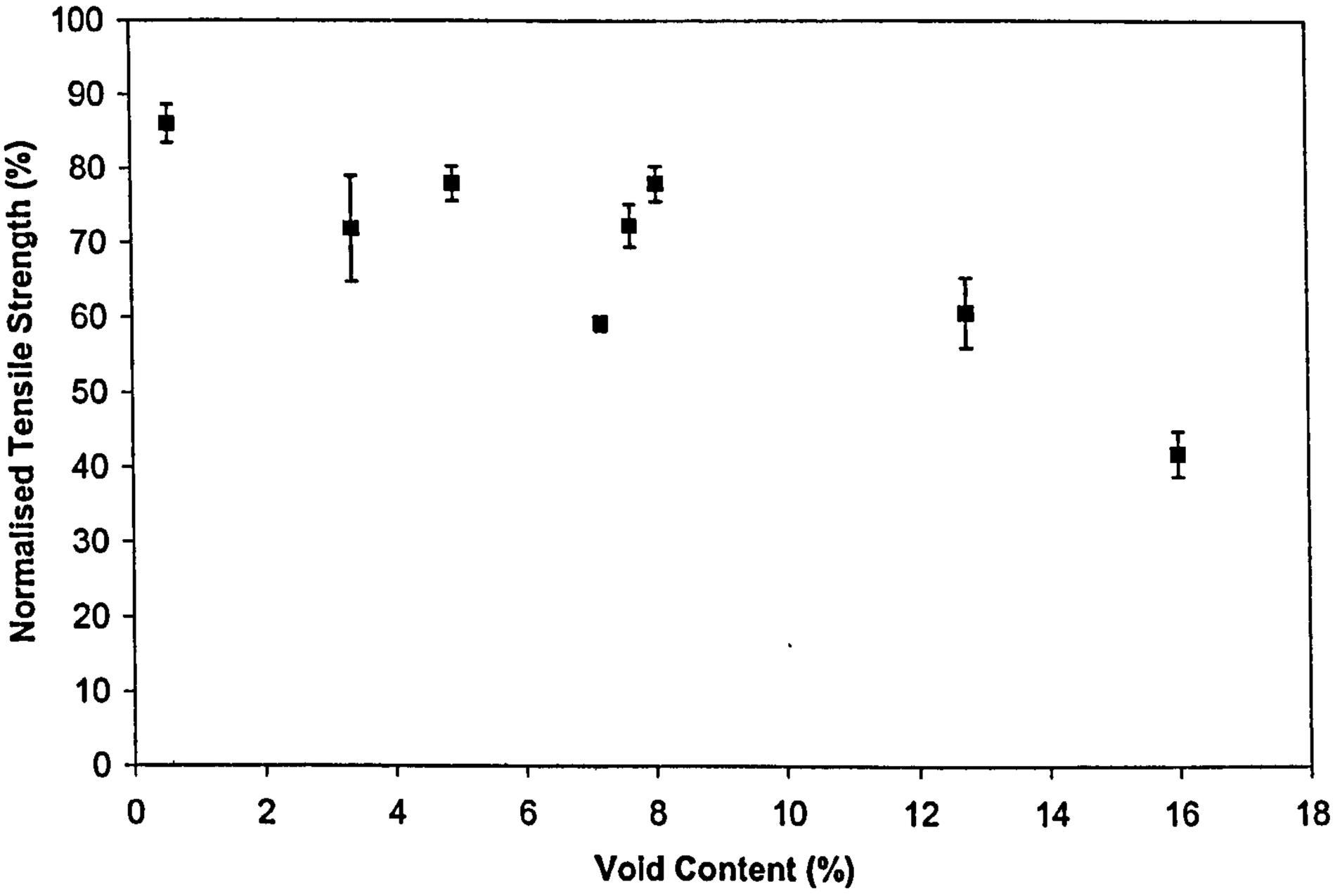

Figure 4.8 Effect of void content on tensile strength of material B laminates consolidated using non-isothermal vacuum forming up to 180°C. Fibre orientation was 0/90° to the loading direction.

As observed in Figure 4.5 for flexural strength, void contents over 10% decreased tensile strength by 50%. However, void contents between 1% and 10% had little effect on the tensile strength, which ranged between 80% and 70% of the maximum value stated by the manufacturer. Fibre strength is dominant in determining the tensile strength of the laminate when fibres are at 0/90° to the loading direction. Hence, higher void contents lead to lower fibre volume fractions and induce stress concentrations around the voids.

Figure 4.9 shows the effect of void content on tensile modulus. Whilst void contents above 13% reduced the normalised flexural modulus by 30%, a 50% reduction in tensile modulus was observed.

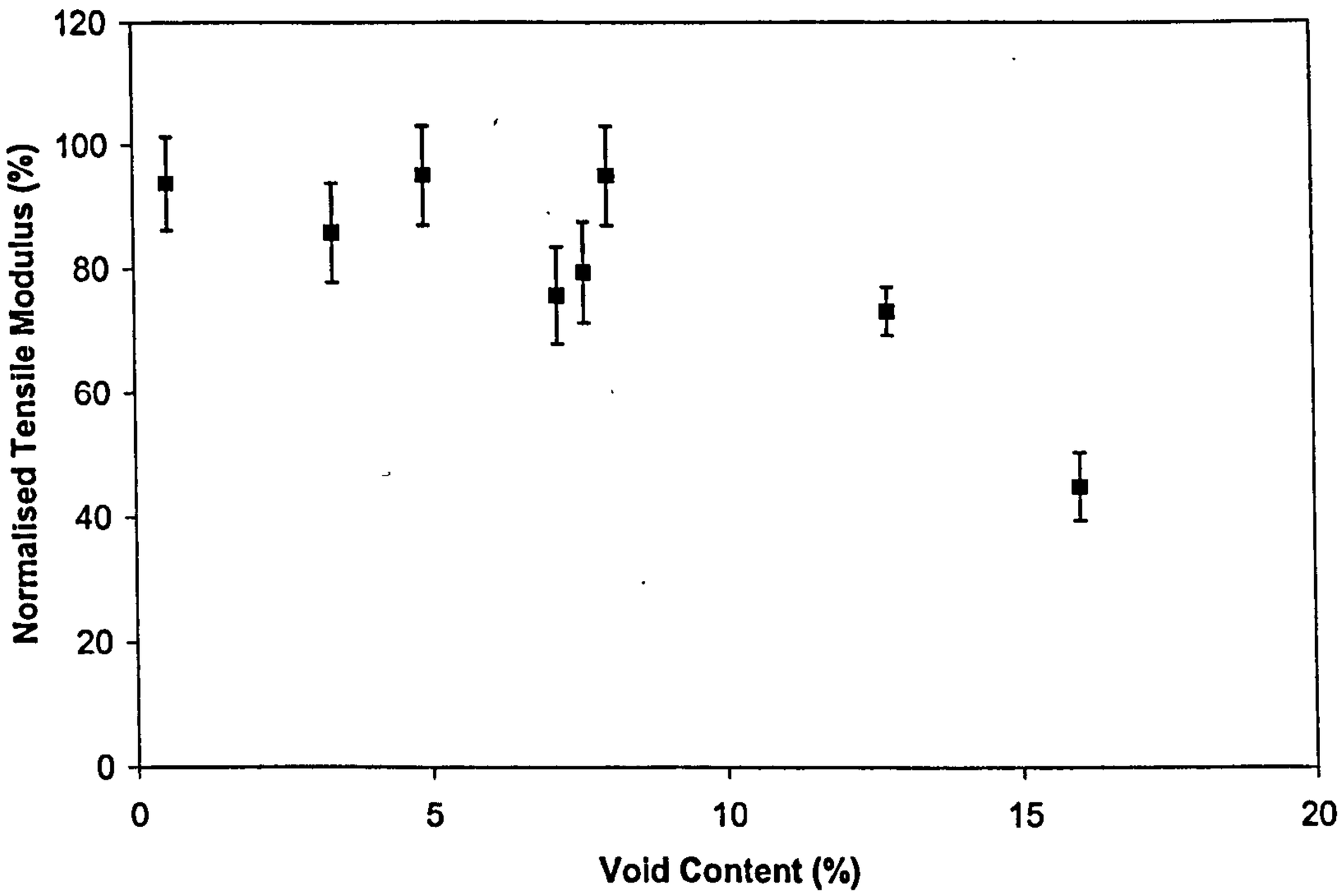

Figure 4.9 Effect of void content on tensile modulus of material B laminates consolidated using non-isothermal vacuum forming up to 180°C. Fibre orientation was 0/90° to the loading direction.

4.4 Sheared glass/polypropylene flat plaques

4.4.1 Effect of shear angle on consolidation

This section is concerned with the effect of in-plane shear on consolidation of flat plaques consolidated using a non-isothermal vacuum forming process, described in Section 3.3.2. Figure 4.10 shows that change in shear angle has little effect on the void content of sheared flat plaques. Figure 4.11 shows a sketch for $\pm(90-\theta)/2$ fibre orientations. During non-isothermal consolidation of sheared flat plaques pressure is applied whilst the material is heated up, therefore no variation in final void content should by expected. In the case of isothermal consolidation the vacuum is applied once the material reaches a certain temperature. However, unless fibre bundles rearrange during shearing no effect on the final void content should be expected for commingled fabrics where fibre volume fraction of fully consolidated laminates remains constant.

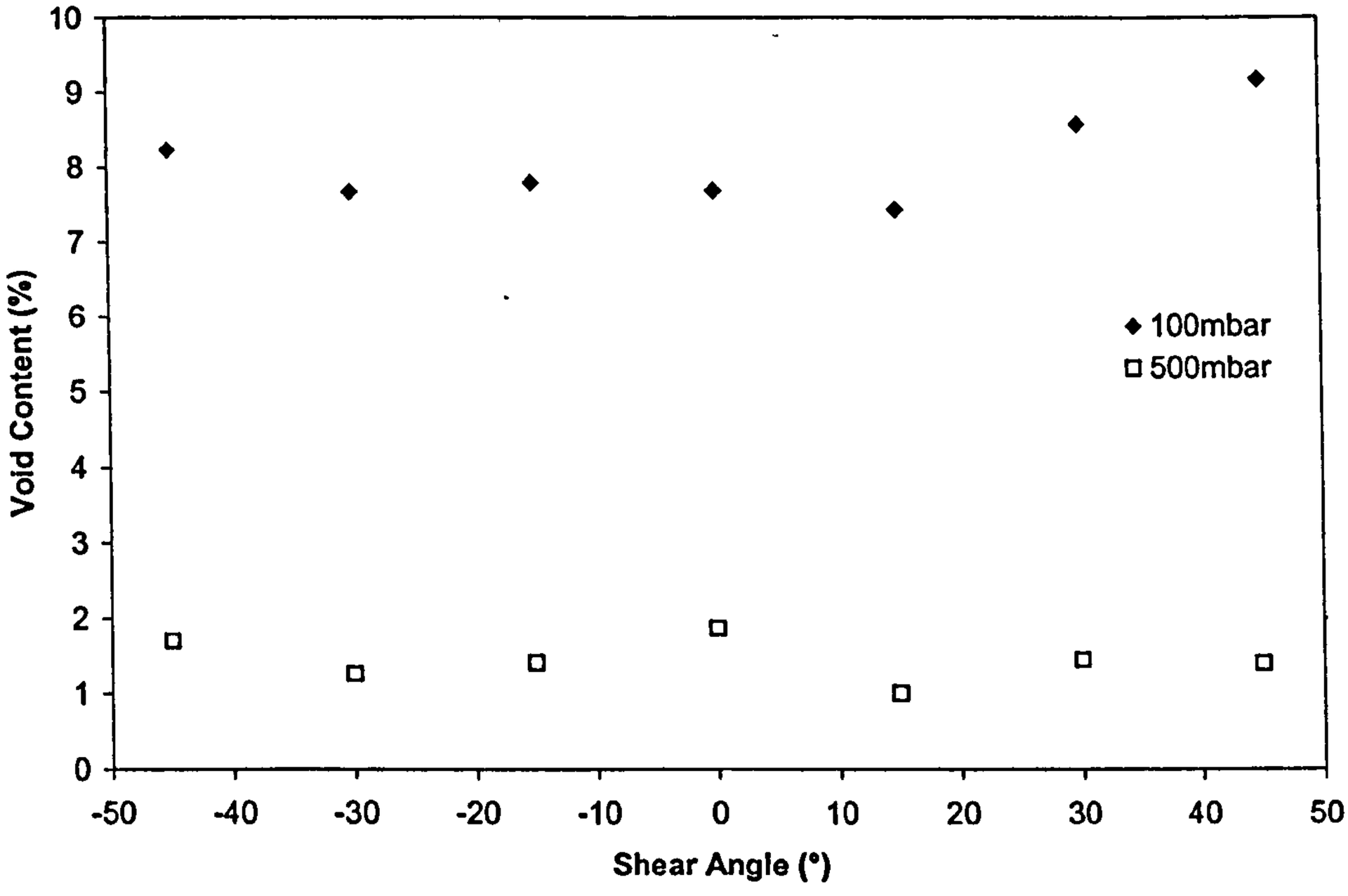

Figure 4.10 Void content measurements for sheared and vacuum consolidated flat plaques composed of three layers of material B.

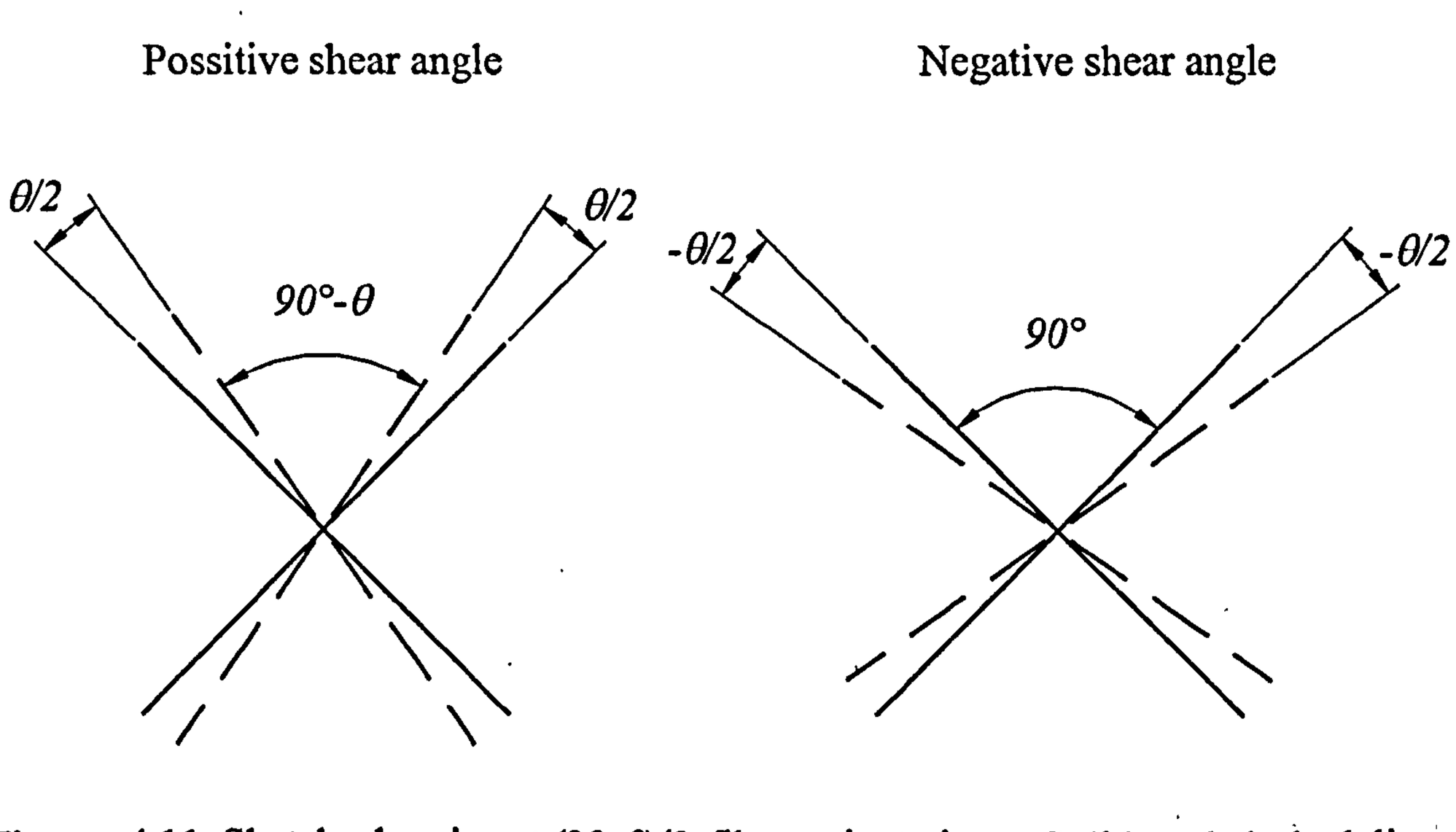

Figure 4.11 Sketch showing $\pm(90-\theta)/2$ fibre orientations. Solid and dashed lines represent the fibre orientation before and after shearing respectively.

4.4.2 Effect of shear angle on mechanical properties

Tensile tests were performed on the sheared flat plaques at $\pm(90-\theta)/2$ to the axis (following the bias direction) using the technique described in Section 3.5. Mechanical properties of samples with three layers were obtained. Thickness ranged between 1.55 mm and 2.44 mm due to variations in void content and changes in shear angle. For a fully consolidated laminate thickness is expected to change with shear angle as:

$$h = \frac{h_\infty}{\cos\theta} \qquad (4.2)$$

Where h_∞ is the thickness of a fully consolidated laminate and θ is the shear angle.

Figure 4.12 shows the effect of void content and deformation on the mechanical properties of two series of sheared flat plaques consolidated at 100 mbar and 500 mbar. As shear angle increases tensile strength of sheared flat plaques increases. This result was expected because as shear angle increases, fibres become aligned with the loading direction and the tensile strength is logically higher. Figure 4.12 also shows that the tensile strength of sheared flat plaques decreases as void content increases, corroborating findings in Section 4.3. In Chapter 6, classical laminate theory and first ply failure criterion are used to predict the elastic and failure behaviour observed in these experiments, and a stress concentration criterion is used to predict the effect of void content on strength.

Figure 4.13 shows the effect of the void content and deformation on the tensile modulus. As expected tensile modulus increases as shear angle increases, as fibres become more aligned with the loading direction. A similar effect of void content on tensile modulus is observed to that presented in Section 4.3, where as void content increases tensile modulus decreases.

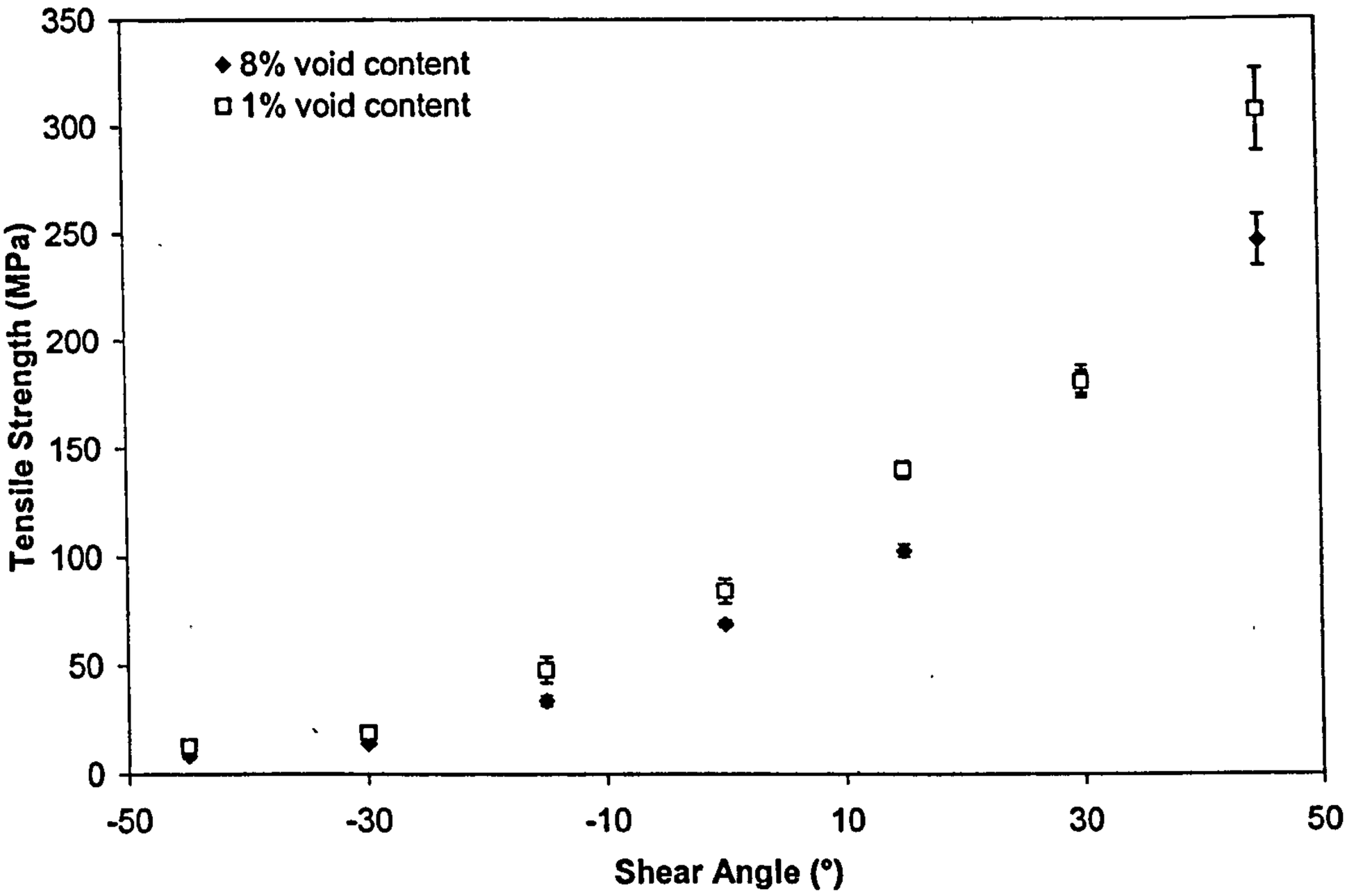

Figure 4.12 Effect of shear angle and void content on the tensile strength. Samples consolidated under 100 mbar and 500 mbar contain approximately 8% and 1% void content respectively.

Figure 4.14 shows the stress/strain curves for sheared flat plaques consolidated at two different pressures. For flat plaques sheared to low shear angles (between 0° and 15°) and consolidated under 100 mbar the ultimate strain is larger than for flat plaques sheared to the same angles and consolidated under higher pressure. However when the shear angle is higher, larger strains were observed for sheared flat plaques consolidated under 500 mbar. For negative shear angles, see Figure 4.15, failure stresses of flat plaques consolidated under 100 mbar are still between 60% and 80% of the value of failure stress of sheared flat plaques consolidated under 500 mbar.

From Figures 4.14 and 4.15 two phenomena are observed. Firstly, for shear angles between 15° and –30° there is a significant realignment of the fibres. The slope of the stress/strain curves first decreases and then increases due to the higher alignment of the fibres with the loading direction. This phenomenon is discussed below. Secondly for a shear angle of –45°, at values of strain above the yield stress, a decrease in stress is observed. This indicates that there is a critical angle where the resin has a more important influence on the stress.

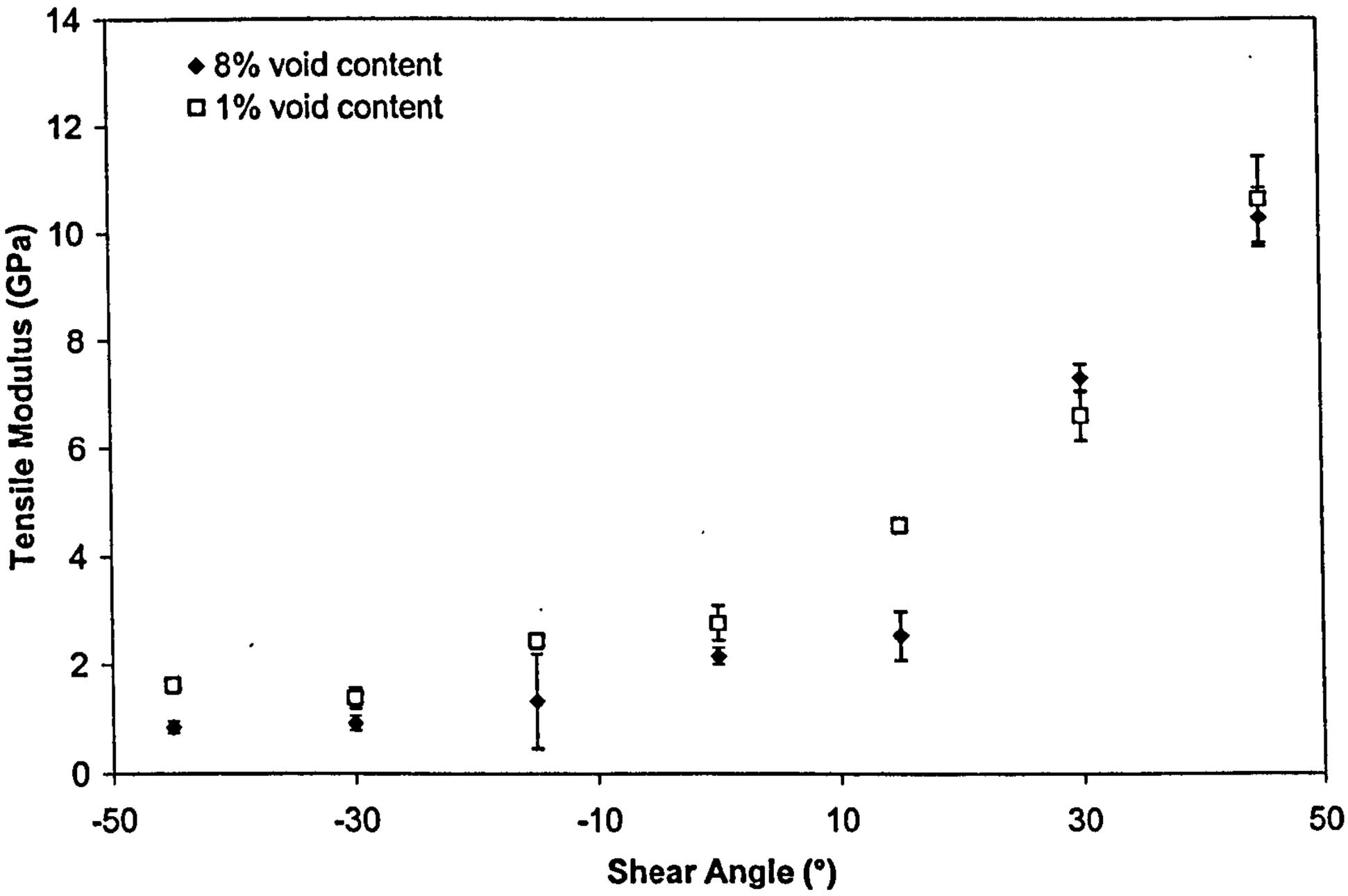

Figure 4.13 Effect of shear angle and void content on the tensile modulus. Samples consolidated under 100 mbar and 500 mbar contain approximately 8% and 1% void content respectively.

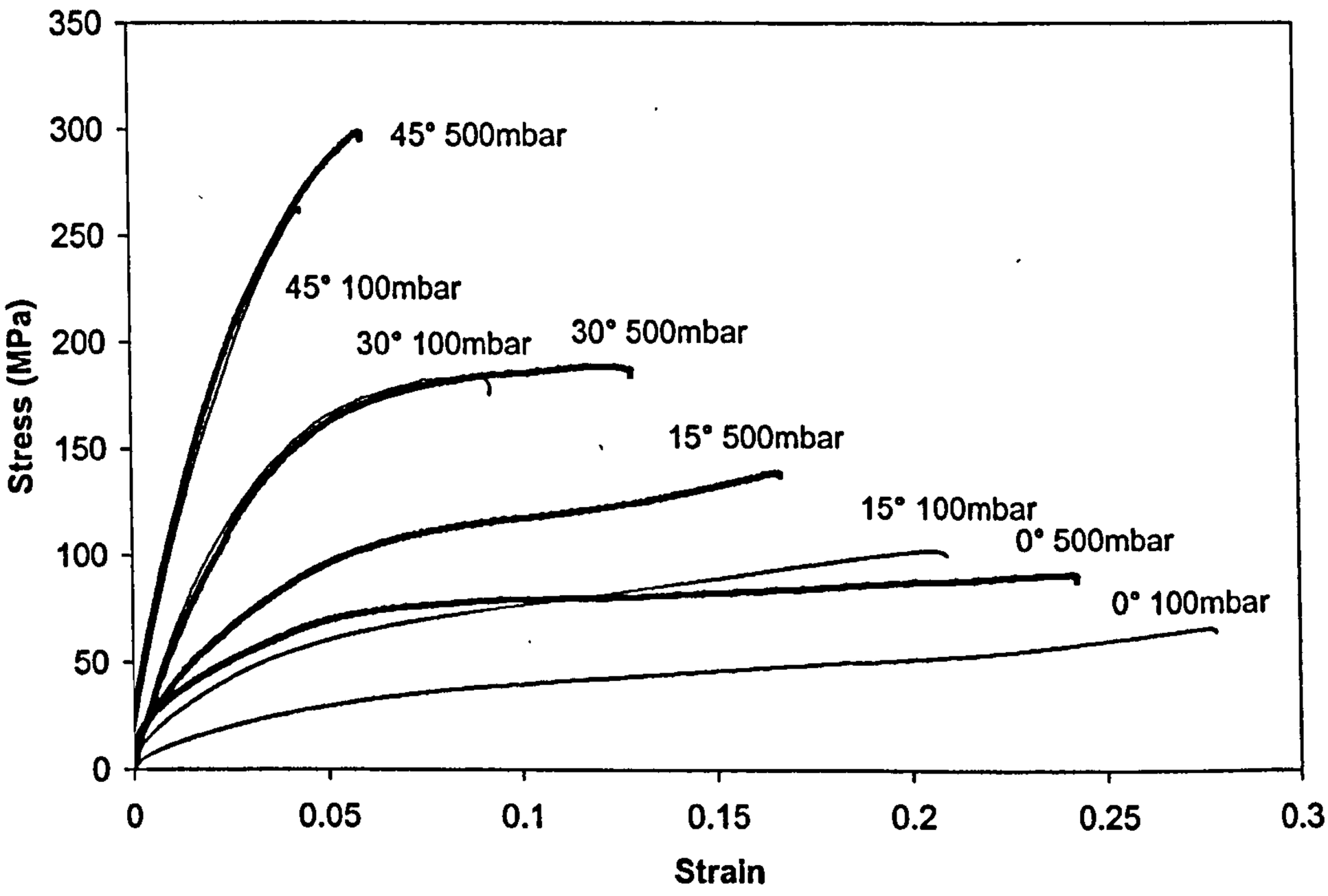

Figure 4.14 Stress-strain curves for material B flat plaques sheared between 0° and 45° and consolidated at 100 mbar and 500 mbar.

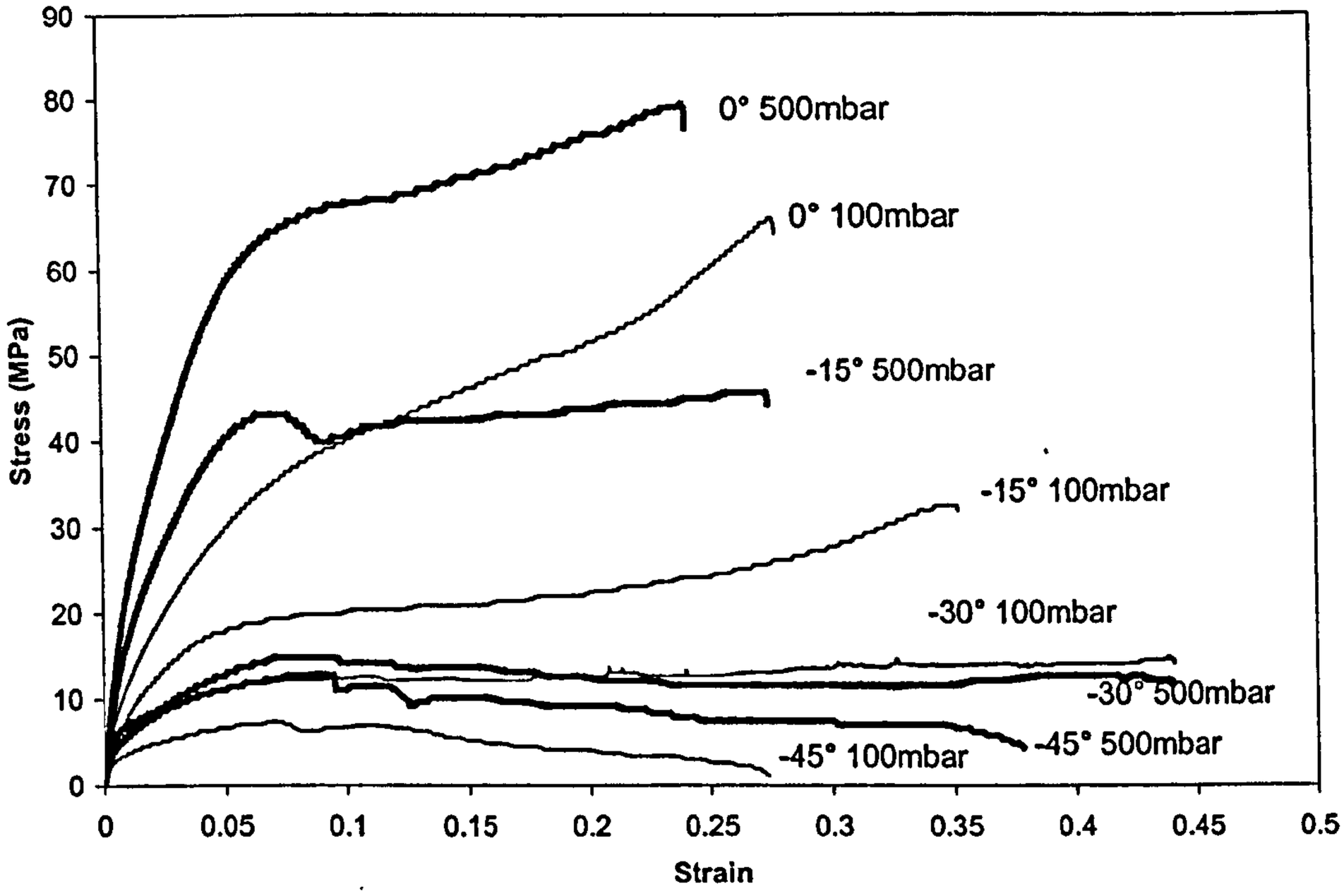

Figure 4.15 Stress-strain curves for material B flat plaques sheared between 0° and -45° and consolidated at 100 mbar and 500 mbar.

4.4.3 Realignment of fibres

This section is concerned with the rotation of fibres as tension is applied. Rotation is defined as the realignment of the fibres towards the loading direction. From the stress-strain curves it is observed that as shear angle decreases the strain measured during the tensile test of the sheared flat plaques increases until a critical angle is reached between –30° and –45°. Here the ultimate strain of the laminate sheared by –45° is lower than the ultimate strain for the laminate sheared by –30°. The main mechanism of deformation during the tensile test that makes these large strains possible is the realignment of the fibres towards the loading direction.

Fibre angle after failure was calculated by measuring the angle between the warp and weft directions on an in-plane digital image using AutoCAD. This angle is compared with the initial fibre angle. Thus, rotation is the difference between the fibre angle before and after testing divided by two. Figure 4.16 shows the realignment of the

fibres as tension is applied depending on the initial shear angle. For flat plaques sheared by 45° no realignment is observed. However as shear angle decreases, a realignment of the fibres by approximately 3° for each 10° of shear is observed until a critical shear angle is reached. No clear dependency with consolidation pressure is observed.

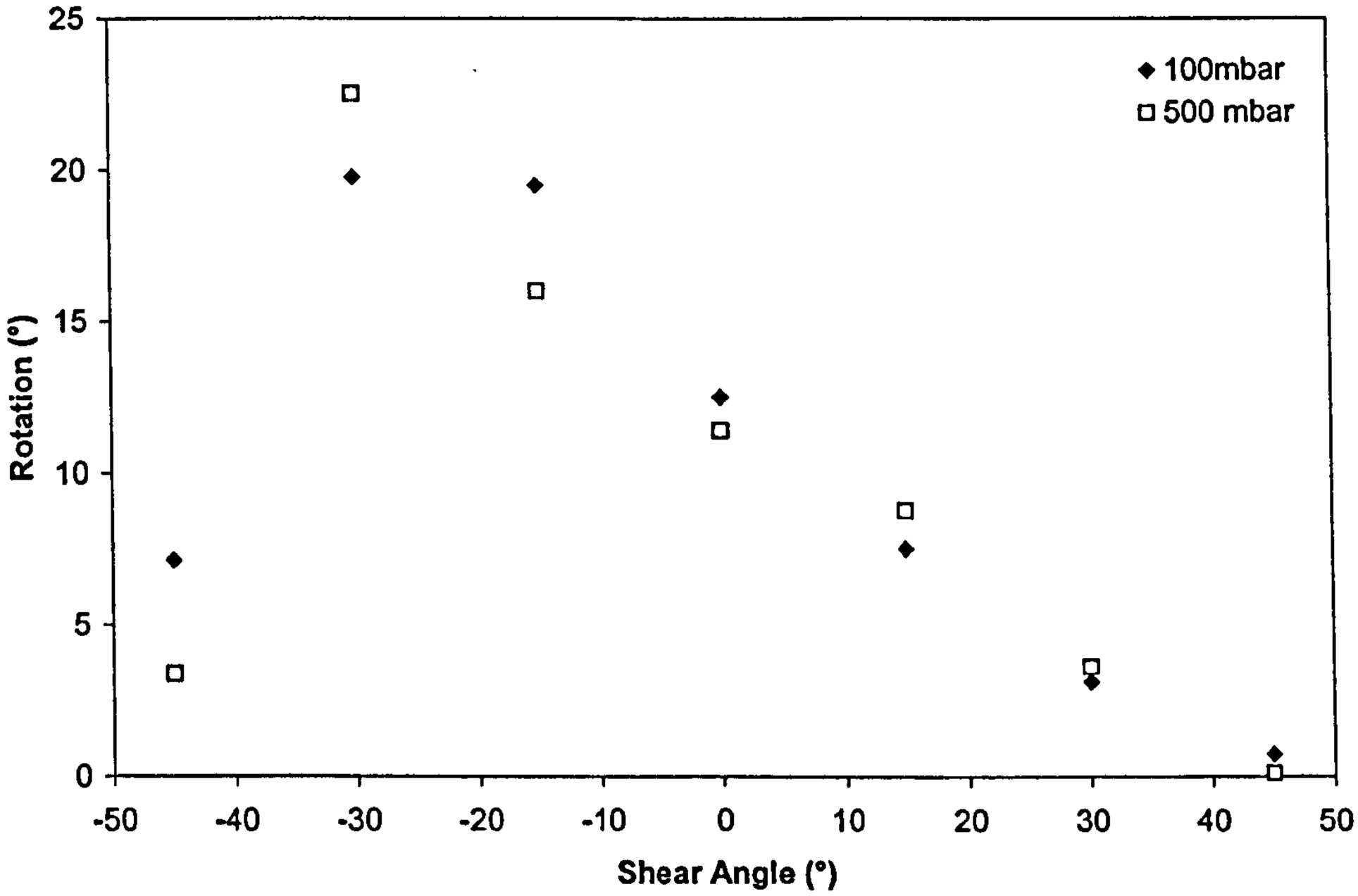

Figure 4.16 Rotation of the fibres observed on sheared flat plaques after testing.

The measurement of the fibre angle after failure may not completely explain the change of fibre angle during testing since it does not take into account the possible relaxation in fibre angle from before to after failure. Analysis of the fibre angle during testing showed that fibre angle relaxes approximately 4° at laminate failure. Figure 4.17 shows the measured shear angle during testing of four 0°sheared flat plaques. Last values of each series show the fibre reorientation after failure. Further analysis is presented in Chapter 6, where realignment of the fibres during testing is predicted.

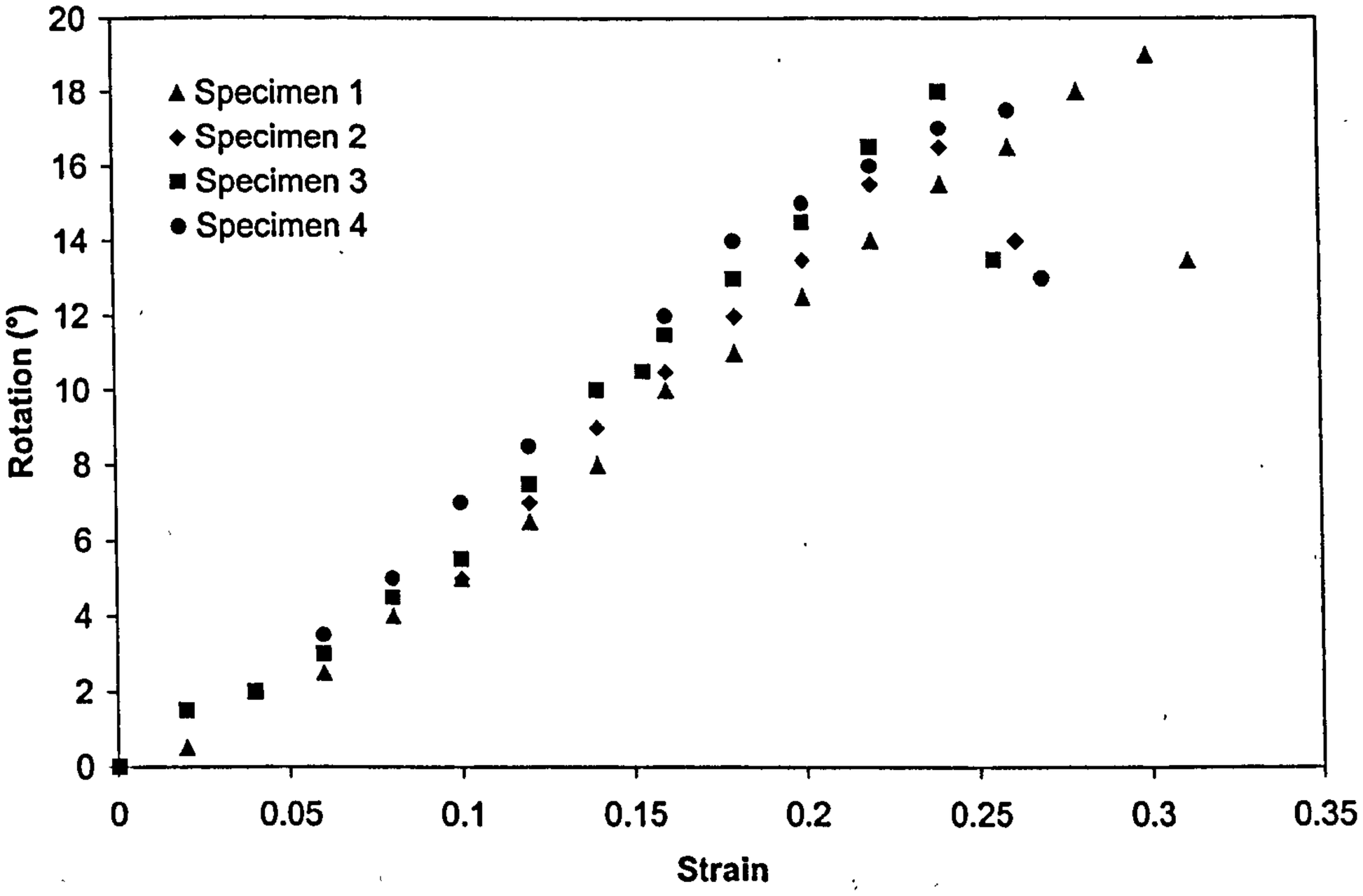

Figure 4.17 Measured fibre angle during testing for four 0° sheared flat plaques. Difference between the last two points of each series represents the relaxation of the fibres after failure.

4.5 Prepreg flat plaques

4.5.1 Void content analysis

This section is concerned with the location of voids within a prepreg laminate consolidated by vacuum forming using the technique described in Section 3.3.4. Figure 4.18 shows a micrograph of a laminate composed of 4 layers of material C consolidated at 180°C for 2 hours. It is observed that large voids are located mainly in the inter-tow region. To analyse whether voids resulted from poor nesting of plies, one layer of material C was consolidated at 180°C for 2 hours. From this laminate two specimens were cut. The first specimen, Figure 4.19, was cut at an angle of 45° with respect to the warp direction. The second specimen, Figure 4.20, was cut along the warp direction for a better understanding of the void distribution. From the analysis of Figures 4.19 and 4.20, voids seem to be located in the spaces between adjacent tows.

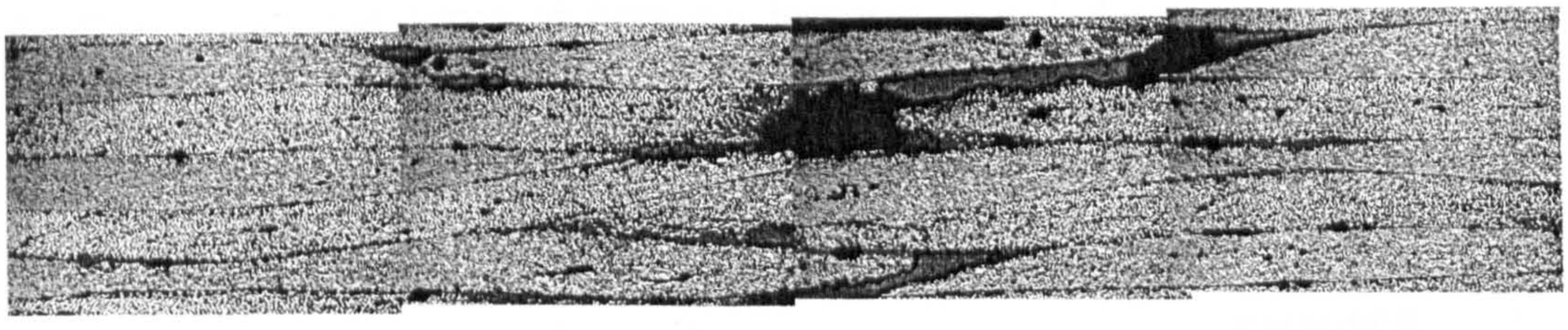

Figure 4.18 Micrograph of a 4 ply specimen consolidated by vacuum at 180°C for 2 hours revealed the void content to be 9.77%.

Figure 4.19 Micrograph of a single ply, at 45° to the warp direction. The micrograph showed 7.98% void content.

Figure 4.20. Micrograph of a single ply along the warp direction.

4.5.2 Effect of void content on mechanical properties

Flexural tests were performed on coupons cut from the flat laminates using the technique described in Section 3.4. Thickness ranged from 1.50 to 1.60 mm. Microscope image analysis was used to determine void content levels.

Figure 4.21 shows the effect of void content on flexural strength of laminates consolidated by vacuum forming at 180°C for times between 2 and 4 hours. Data from commingled glass/polypropylene laminates (material B) consolidated by the isothermal vacuum forming process are included for comparison. As observed for thermoplastic composites, a void content of 10% reduces mechanical properties by 50% compared to the manufacturers' stated value (1880 MPa). However, more tests are needed to establish if the correlation is real. It is observed from void image analysis that vacuum pressure may not be sufficient to consolidate a laminate of

material C, so that times at pressure between 2 and 4 hours do not affect the mechanical properties of the laminates significantly.

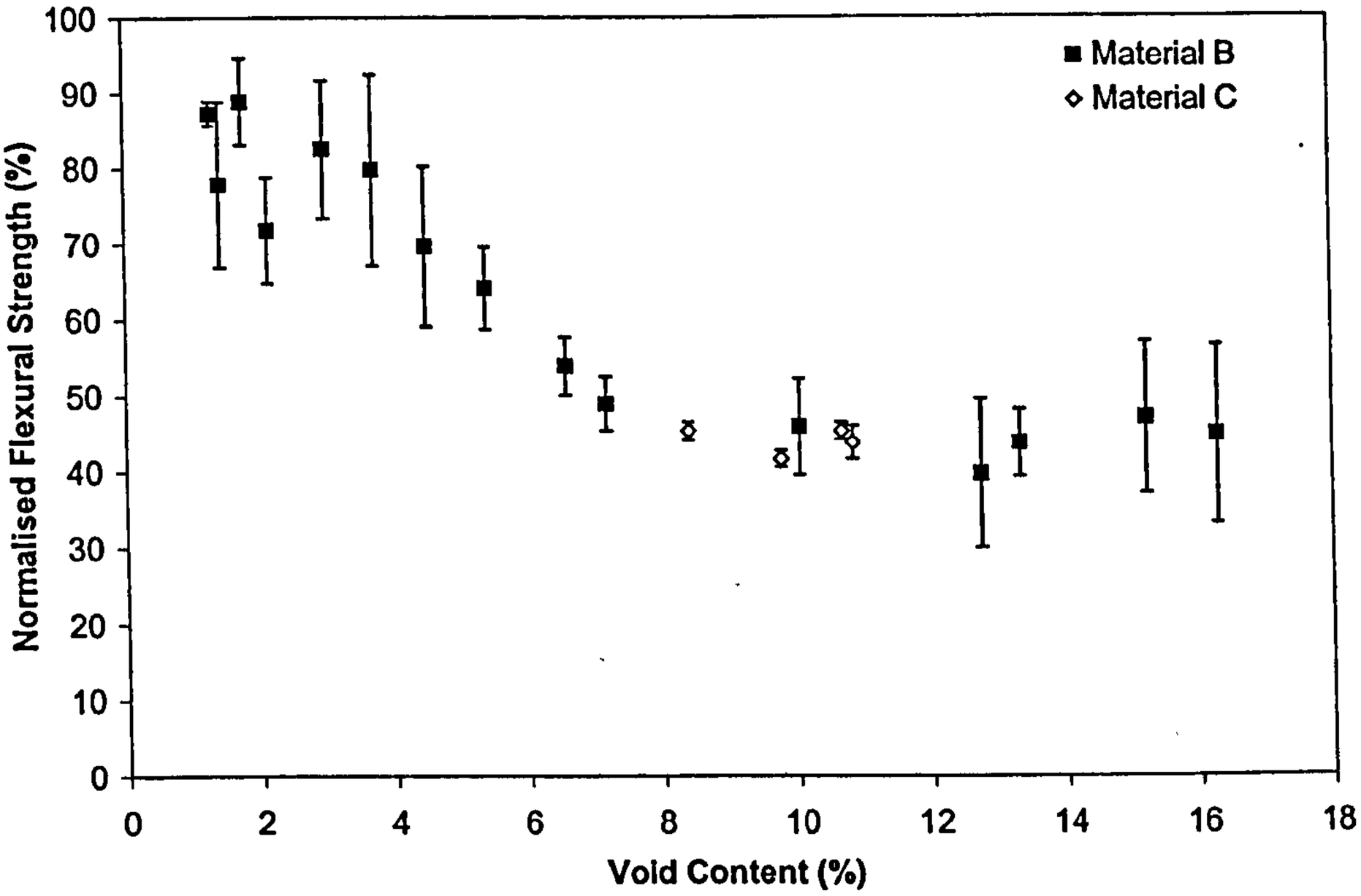

Figure 4.21 Effect of void content on flexural properties of material C with. fibre orientated at 0/90° with the loading direction. Data for material B is included for comparison.

4.6 Conclusions

This chapter has presented experimental data collected during the first 18 months of this research work, which is the basis for predictive models presented in Chapters 5 and 6. A glass/PP commingled thermoplastic and a five-harness satin woven prepreg were tested in three point bending. Additionally, material B was also loaded in tension. Strength was correlated with the void content obtained by an image analysis technique to illustrate the effects of processing on subsequent performance. Measurements from commingled glass/PP consolidated laminates revealed that a void content of less than 2% could be achieved with suitable process parameters applying a pressure of 950 mbar. This value is comparable to that expected for applying a pressure of 30 bar in compression moulding **[2]**. Mechanical testing revealed that low void content does not significantly affect mechanical properties, as would be expected. However for void levels of over 10%, a reduction in flexural

strength of approximately 50% was observed. A similar trend was observed in consolidated sheared flat plaques, where different shear angles did not affect the final void content. Material B and material C show the same loss of performance with increasing voidage. In general, a void content of 10% reduces failure stress by 50%, whatever the material. Hence, a consolidation model that predicts void content as a function of processing parameters is required. Such a model is presented in Chapter 5.

Tensile strength and modulus were correlated with initial shear angle of flat plaques to illustrate the effect of deformation on the mechanical behaviour. Tensile strength and modulus increased as the fibres aligned with the loading directions. Void content measurements showed that the effect on the tensile strength of sheared flat plaques was similar to that observed for un-sheared flat plaques. This experimental data will be used to validate predictive models presented in Chapter 6. Also an existing stress concentration criterion will be applied to model the effect of void content on mechanical properties. Finally, realignment of fibres during and after testing was also observed and measure using image analysis. The importance of this finding relies on the effect of reorientation on the elastic behaviour during testing. A simple model that predicts the reorientation of the fibres during loading is presented in Chapter 6.

5 Consolidation of Textile Composites

5.1 Introduction

Prior chapters addressed the importance of predicting void content as a function of processing parameters. High levels of void content have a detrimental effect on the mechanical properties of textile composite materials. Therefore, this chapter is concerned with the development of a consolidation model capable of predicting void content for commingled materials as a function of pressure, time at pressure and temperature.

The conditions to fully impregnate the bundle are dependent upon both the material properties and the consolidation process parameters. The density of fibre packing, the dimensions of the fibres and their arrangement as well as the viscosity, and the distribution of the matrix affect the flow of the polymer into the interstitial space of the laminate. Due to the high viscosities present in thermoplastic composites, more than two or three orders of magnitude higher in comparison to thermosets, proper wetting and impregnation of the fibre bundles by the molten matrix during production is essential to achieve acceptable materials properties.

5.2 Problem description

A normal processing cycle for a composite laminate made of thermoplastic commingled yarns consists of three main stages. Firstly, the material is heated above the melting temperature of the resin. Secondly, a chosen pressure is applied for a chosen period of time to reduce the thickness of the laminate to the fully consolidated thickness. Thirdly and finally, the material is cooled while maintaining the pressure.

The time to reach full consolidation depends on the time taken to fully impregnate the reinforcing fibre bundles. The time to consolidate is dependent upon material properties and the consolidation process parameters. These include maximum

applied pressure, rate of pressure application, temperature and time. The structure of a fabric, yarn dimensions and shape, number of fibres per yarn, fibre diameters, and quality of commingling affect the rate at which matrix impregnation and fibre wetting occur and therefore influence the time to consolidate.

During the vacuum moulding of commingled fabrics, the flexible fibre structures are impregnated and consolidated during formation into the final component. During the consolidation stage, two main mechanisms take place:

- Autohesion. Once two surfaces of identical material come into intimate contact, a bonding process takes place at the interface.
- Fibre bundle impregnation.

Mei et al. **[98]** studied the kinetics of autohesion for continuous carbon fibre thermoplastic prepreg above the glass transition temperature. They stated that the time required to complete autohesion depends on the processing temperature, with a higher processing temperature leading to a shorter autohesion time. It is assumed in this work that fibre bundle impregnation is the main mechanism of consolidation. Work by Phillips et al. **[99]** on consolidation of woven carbon fibre reinforced polyetherimide supports the validity of this assumption, where intimate contact and autohesion processes consumed only 1% of the total consolidation time. This assumption is also supported by experimental observations during consolidation of commingled yarns carried out by Ye et al. **[51]**. It is also assumed that all the commingled yarns within a laminate are geometrically identical and undergo fibre impregnation simultaneously. The consolidation of the whole laminate can therefore be described by consolidation behaviour of a single representative commingled yarn. It is further assumed that the commingling within a yarn is not homogeneously distributed, so that at the impregnation stage a yarn is composed of cylindrical dry fibre bundles surrounded by a matrix pool. The applied pressure is transmitted hydrostatically by the molten resin to the boundary of each dry fibre bundle.

5.2.1 Evolution of microstructure

To develop a model that represents the consolidation of textile composites, a study of the microstructure in the different stages of consolidation was conducted. A series of laminates were produced applying vacuum pressure for different times at a constant temperature of 180°C to establish the changes in the microstructure during consolidation of material B. Pressure was maintained whilst the laminate was cooled in a tank of water. Samples were cut, polished and analysed by optical microscopy.

The sequence of compaction here is similar to that found by Long et al. **[100]**, and is shown in Figures 5.1 to 5.7. Long et al. established the changes in microstructure during consolidation of balanced 2x2 twill weave of commingled glass/polypropylene tows using constant displacement rate to a predetermined thickness.

1. *Initial coalescence of the molten matrix before application of pressure.*

The microstructures of three plies heated to 180°C without vacuum pressure, followed by cooling, is shown in Figure 5.1.

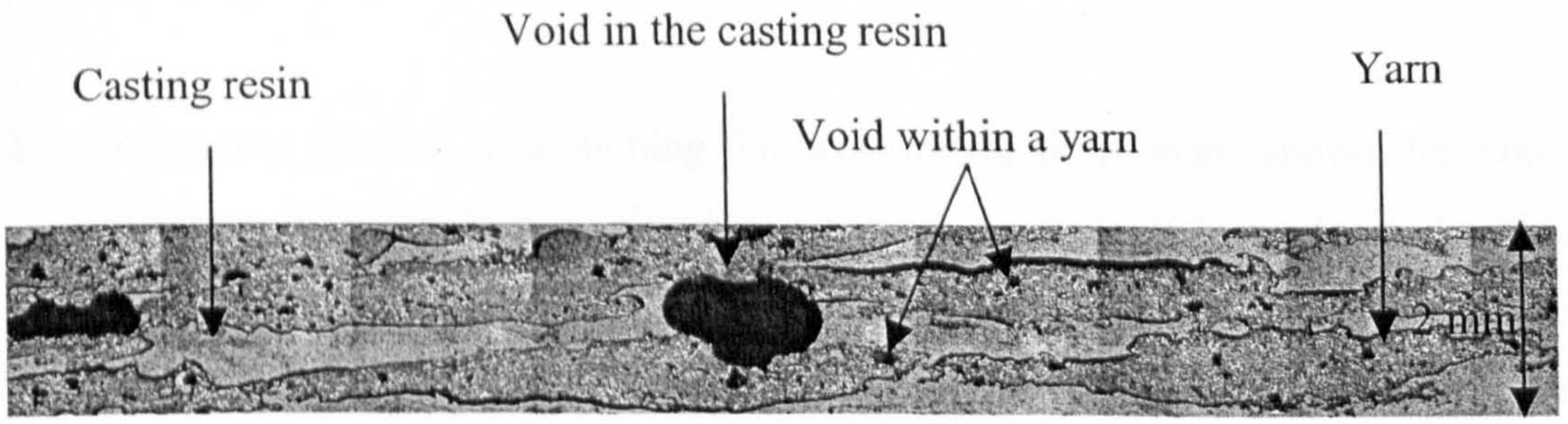

Figure 5.1 Commingled fabric heated to 180°C without application of pressure.

Once the matrix has coalesced, the amount of matrix impregnating the fibre bundles must compensate any reduction in laminate height. Cain et al. **[43]** examined micrographs obtained via staged compaction tests. These micrographs indicated that the matrix remained interspersed within the tows, but large areas of dry fibre existed before the onset of compaction. Micrographs presented here show that those large dry areas do not exist. In contrast, fibres within the tows tend to gather in smaller fibre bundles (agglomeration) each of which surround a void.

2. *Coincident removal of voids from between the plies and within the plies as time at pressure is increased.* Figure 5.2 shows the microstructure of a laminate consolidated for 20 seconds. Voids are evenly located in the inter-tow region and within the tow.

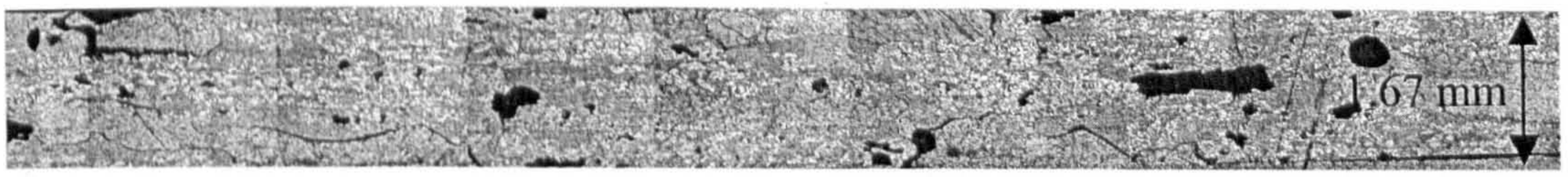

Figure 5.2 Laminate consolidated for 20 seconds with a void content of approximately 10%.

Figure 5.3 shows the microstructure of a laminate consolidated for 40 seconds with 6.5% void content, showing that removal of voids from the matrix and within the fibre bundles has already occurred.

Figure 5.3 Laminate consolidated for 40 seconds with a void content of approximately 6.5%.

3. *Entrapment of voids.* Maintaining the pressure for 60 seconds shows that voids are entrapped by molten matrix. Also, it is shown that voids are located within the fibre bundles and in matrix rich regions. Figure 5.4 shows that a large amount of voids are entrapped within fibre bundles whilst voids initially located in the inter-tow region tend to disappear.

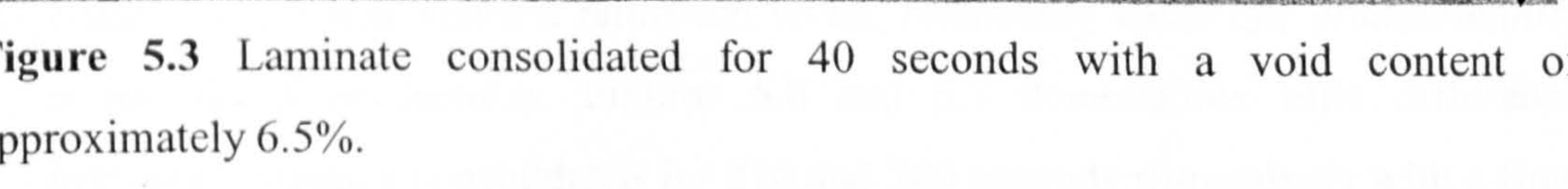

Figure 5.4 Laminate consolidated for 60 seconds with a void content of 4.5%.

4. *Reduction in the void content as time at pressure is increased.* Figure 5.5 shows laminate consolidated for 120 seconds. Voids are located mainly in the fibre bundles and the void content is decreasing as time at pressure is increased.

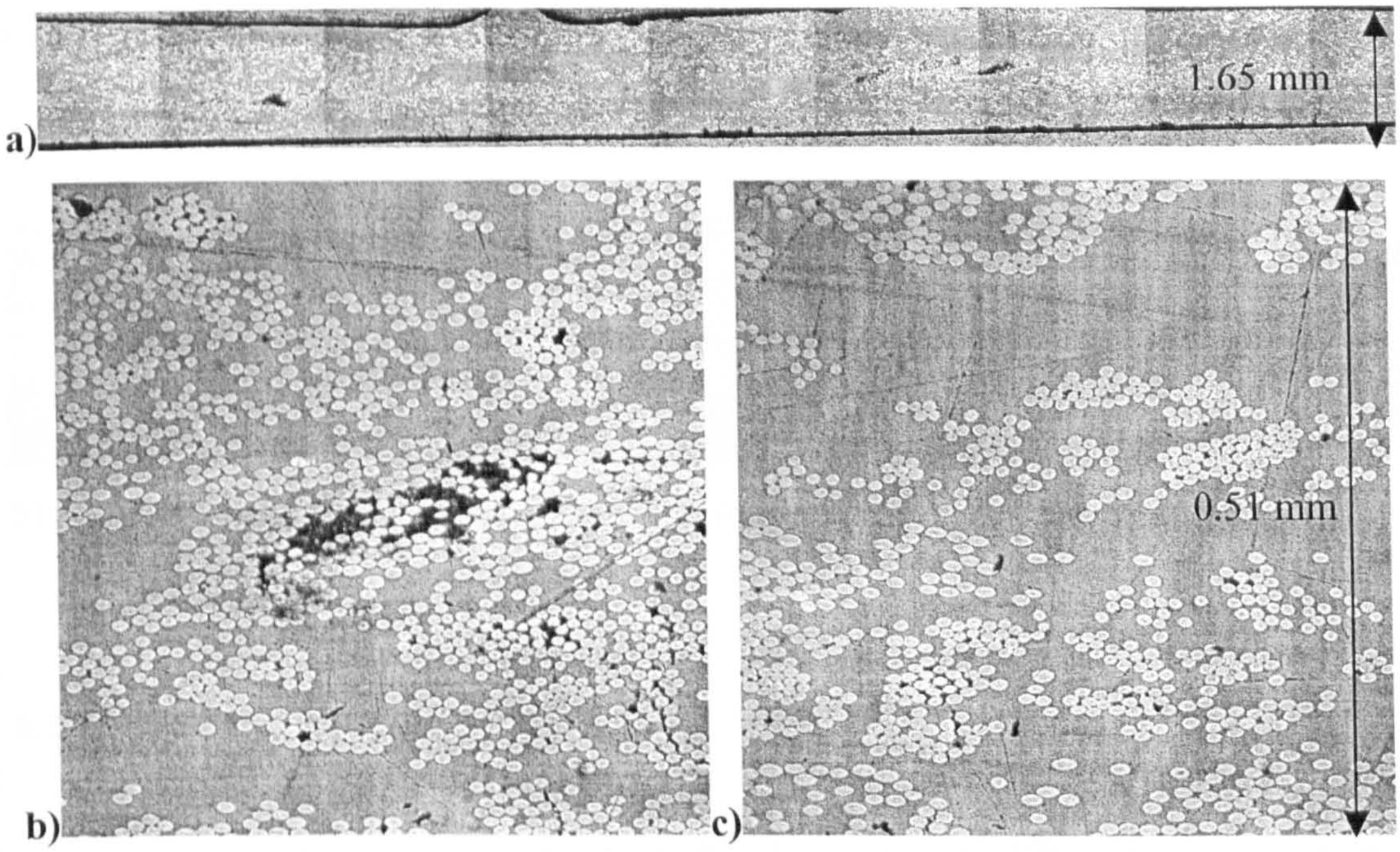

Figure 5.5 These three micrographs correspond to **a)** laminate consolidated for 120 seconds **b)** and **c)** demonstrate that voids are compressed within fibre bundles and in matrix rich regions. Void content is approximately 2.3%.

5. *Once void content nears a minimum value, remaining voids are predominantly within the fibre bundles.* Figures 5.6 and 5.7 demonstrate little difference between laminates consolidated for 210 and 300 seconds respectively with a final void content of 1.3%.

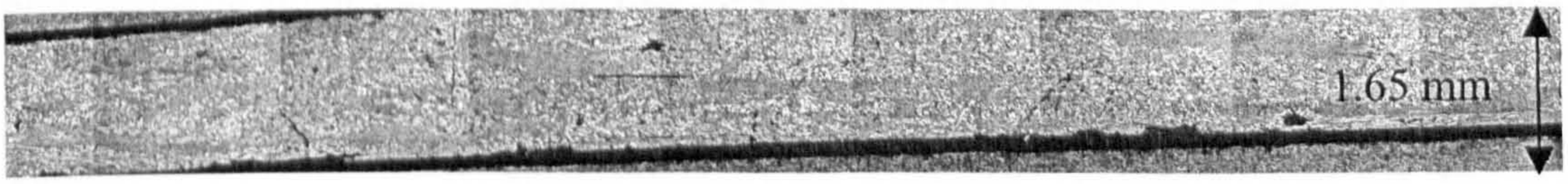

Figure 5.6 Laminate consolidated for 210 seconds. Remaining void content was 1.8%.

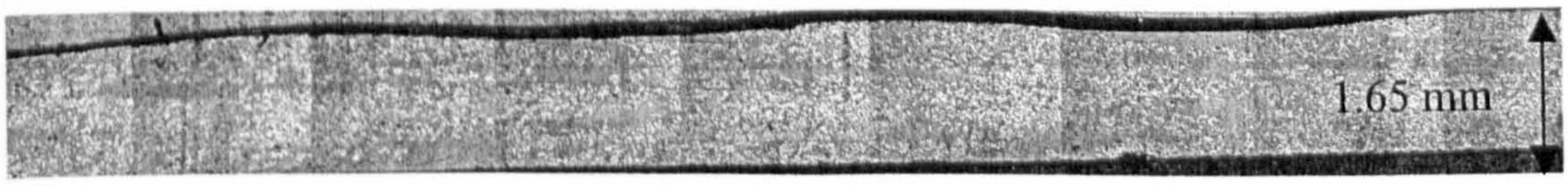

Figure 5.7 Laminate consolidated for 300 seconds with a remaining void content of approximately 1.28%.

Wilks **[52]** stated that remaining voids were predominantly within the matrix rich regions. However, the micrograph presented (Figure 5.8) did not illustrate a fully consolidated laminate and a large amount of voids were also located within the tows.

Figure 5.8 Commingled glass/PP laminate consolidated by pressure forming **[52]**.

5.2.2 Void distribution

The study of the microstructure of the laminate at different stages of the consolidation process also allowed the analysis of the distribution of voids at those same stages. This was required to locate the position of voids in the laminate, and in particular to study the contribution of inter-tow voids to the measured void content. Micrographs presented in the previous section showed that inter-tow voids disappeared during the first two minutes of consolidation. Here an analysis of the void size distribution is presented.

By analysing micrographs of the cross section of laminates at different stages of consolidation it can be observed that large voids are present in the inter-tow section whilst smaller voids are present within fibre bundles, see Figure 5.9. Similar observations were made by Phillips et al. **[99]** who presented micrographs of consolidated woven carbon fibre-reinforced polyetherimide showing large voids between plies as a result of the mechanism of intimate contact.

Micrographs were used to measure void content and analysed using image analysis software. Assuming voids are circular, void radius was calculated based on the void area measurements, and these were grouped by their radii every 10 μm. Data in Table 5.1 supports the theory that these large inter-tow voids disappear during consolidation. In laminates consolidated for two minutes or longer inter-tow voids ($r \geq 10$ μm) were not found. Figure 5.10 shows that the distribution of the voids

located in the inter-tow region with time at pressure is almost linear during the first two minutes of consolidation.

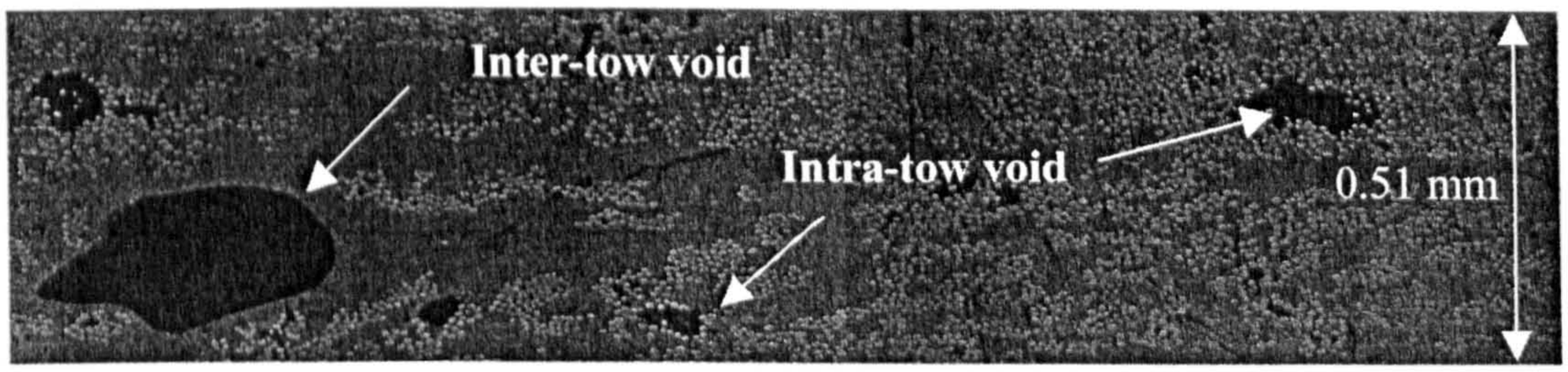

Figure 5.9 Cross-section of a commingled glass/PP laminate consolidated for 40 sec under full vacuum showing a large void in the inter-tow region and smaller voids within a yarn.

Table 5.1 Analysis of the void distribution by radius at different stages of consolidation of material B laminates consolidated by isothermal consolidation at 180°C. Sample size was 20 mm wide and 1.55-1.80 mm thick.

r(μm)	Number of voids						
R<5	9485	9666	11400	6986	10469	6371	
5<r<10	1043	1129	1021	592	1067	460	
10<r<20	246	303	281	118	210	104	
20<r<30	51	61	44	14	30	13	
30<r<40	21	31	11	3	6	3	
40<r<50	14	8	8	2	2	0	Intra-tow voids
50<r<60	14	9	2	2	2	0	
60<r<70	4	6	6	1	0	0	
70<r<80	7	3	1	0	1	0	
80<r<90	2	1	3	0	0	0	
90<r<100	2	2	0	1	0	0	
100<r<110	1	1	3	1	1	0	
110<r<120	3	3	2	0	0	0	
120<r<130	1	0	1	0	0	0	Inter-tow voids
130<r<140	1	1	1	0	0	0	
140<r	10	7	2	0	0	0	
t (sec)	**20**	**40**	**60**	**120**	**210**	**300**	

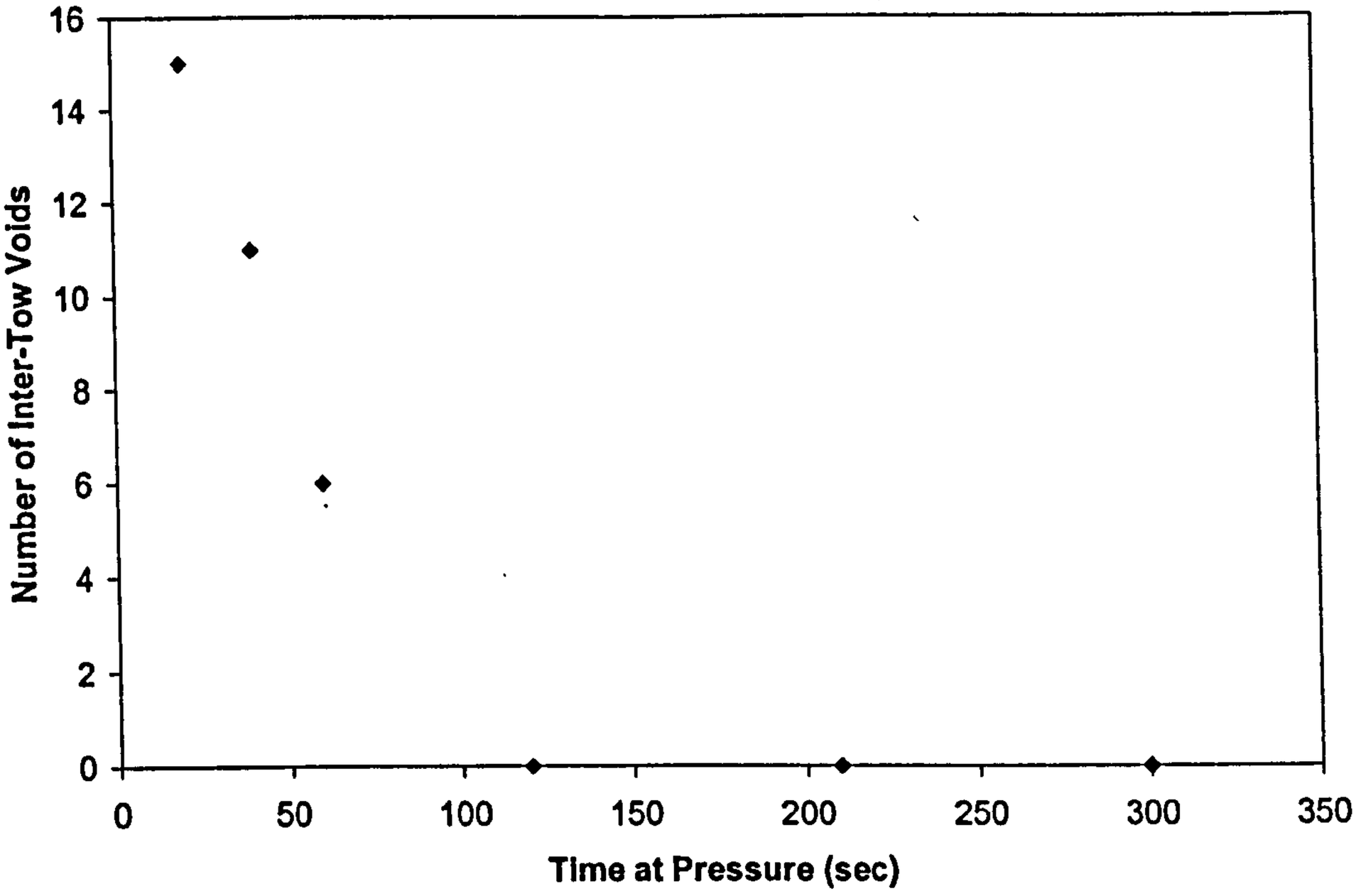

Figure 5.10 Distribution of inter-tow voids with time at pressure.

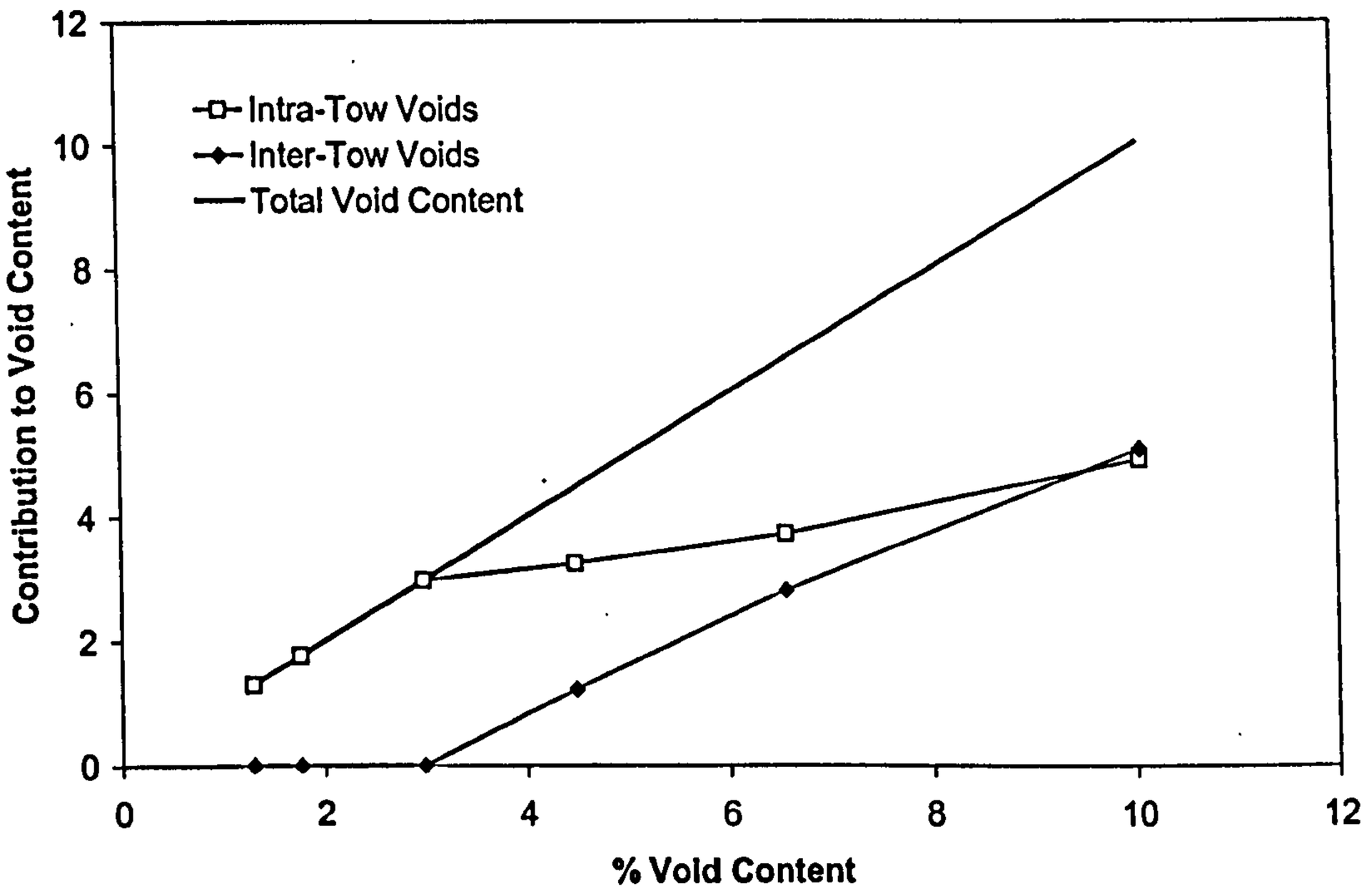

Figure 5.11 Contribution of inter-tow and intra-tow voids to the total void content.

Figure 5.11 shows that the contribution of the large inter-tow voids to the total void content is linear and suggests that the consolidation model should consider two

different problems: the evolution of inter-tow voids and the encroachment of the matrix into fibre bundles to eliminate intra-tow voids.

Lee et al. [46] modelled the evolution of gaps located in the inter-ply region as a flow problem. Representing the irregular ply surface as rectangles of identical size (Figure 5.12) the flow problem is represented by the deformation of these rectangles as a function of processing parameters. By assuming that the volume of these elements remains constant (Eqn. 5.1) the deformation of these elements can be calculated by Eqn. 5.2 where e, f and w are geometric parameters, P_a is the applied pressure, t is time at pressure and μ_{mf} is the viscosity of fibre–matrix mixture.

$$e_0 f_0 = ef \tag{5.1}$$

$$\frac{e_0}{e} = \left[1 + \frac{5P_a}{\mu_{mf}}\left(1 + \frac{w_0}{f_0}\right)\left(\frac{e_0}{f_0}\right)^2 t\right]^{1/5} \tag{5.2}$$

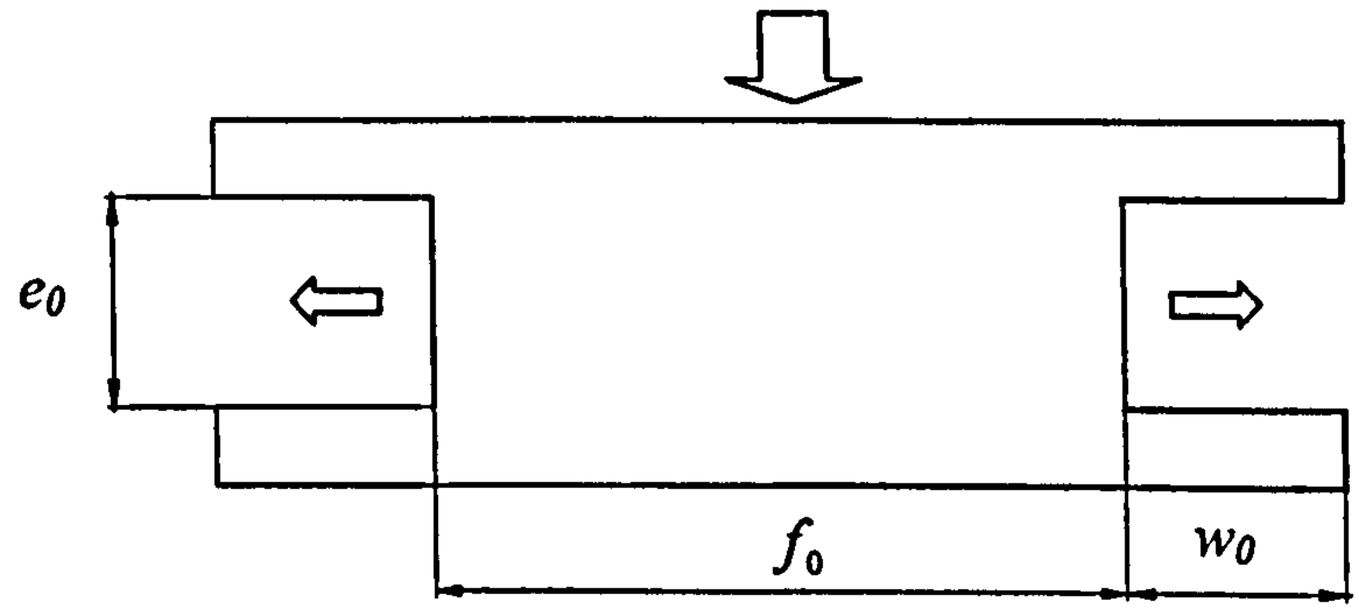

Figure 5.12 Spreading of a rectangular element, which represent a resin bridge (contact between ply surfaces).

Although Lee's model may offer insight into the inter-tow problem, his model was intended to characterise intimate contact and as stated in the previous section this consumes a small proportion of the consolidation time. Additionally, its use to model the evolution of the inter-tow voids presents several problems. First of all, Lee et al. assumed that all of the applied pressure causes the deformation of the rectangular elements (tows in this case), but this assumption is not valid here as deformation of

inter-tow voids and impregnation of the intra-tows dry fibre bundles take place simultaneously. Furthermore, data for the transverse tow viscosity is difficult to obtain and values are highly dependant on the test used. Authors such as Roberts et al. **[101]** and McGuinness et al. **[102]** reported differences of about 1000 times for the same material between results obtained by torsional experiments or by picture-frame tests. As an alternative to this method, a simple geometric model can be used to represent inter-tow void reduction. This model is based in the assumption that voids are eliminated as a result of a change in tow shape. This is further discussed in Section 5.4.1.

5.3 Consolidation Modelling

Van West analysed the isothermal consolidation of commingled material **[33]**, and developed a model to predict laminate height as a function of time under applied pressure. This methodology will be adopted and extended in the present work. It is assumed that compaction is a two-stage process. Firstly, before the matrix coalesces the applied pressure is fully resisted by the fibre bed pressure. Secondly, once the matrix coalesces, the applied pressure is resisted by the sum of the fibre bed pressure, plus the matrix pressure. Three sub-models were used:

1. A compaction submodel, which predicts the deformation of the reinforcement only.
2. A permeability submodel, which determines the property of the fibre bundle that characterises the ease of fluid impregnation.
3. An impregnation submodel, which predicts the encroachment of the matrix into the fibre bundles.

Whilst the ultimate goal is to model and predict the properties of complex components formed under industrial operating conditions, a simplified isothermal process for flat plaques was firstly considered in the present study. This allowed appropriate material models and parameters to be determined, in preparation for a more sophisticated model accounting for heat transfer and the effects of fabric deformation during forming.

Based on general assumptions a sensitivity study was carried out. These assumptions were:

- The matrix is a non-Newtonian fluid.
- Pressure is uniform and remains constant during forming.
- The width and length of the fabric are much larger than the thickness so that matrix pressure is constant in the cross section.
- The consolidation of the whole laminate can be described by the consolidation behaviour of a single representative yarn.
- A yarn is constituted of dry fibre bundles surrounded by the matrix pool. The flow front is considered to advance radially.
- Flow takes place in the direction orthogonal to the fibres.
- Due to the low pressure applied (vacuum pressure), capillary flow must be considered in the impregnation model.
- No void nucleation, migration or dissolution in the matrix is assumed to occur.

The validity and effects of these assumptions will be discussed in Section 5.4.

5.3.1 Compaction sub-model

The empirical models for fibre bed compaction described in Section 2.4.2 represented the deformation behaviour of the laminate for different levels of pressure. However published models were only used for experiments conducted at high pressure (significantly greater than 1 bar). To evaluate the compaction behaviour at pressures of up to 1 bar compaction tests were performed on the reinforcement in material B as described in Section 3.6. Figure 5.13 shows that the pressure required to compact the fibre bed to fibre volume fractions around 35% was less than 0.1 bar indicating that the contribution of the fibre bed compaction is relatively small. The behaviour of the fibre bed may be represented by a power law relationship:

$$P_f = DV_f^B \tag{5.3}$$

where the constants D and B were calculated to be 170 and 7.46 respectively. These values fit the averaged measured fibre pressure for a range of fibre volume fractions between 0.32 and 0.37. Figure 5.13 shows good agreement between the measured and the predicted compaction pressure of lubricated reinforcement within this range.

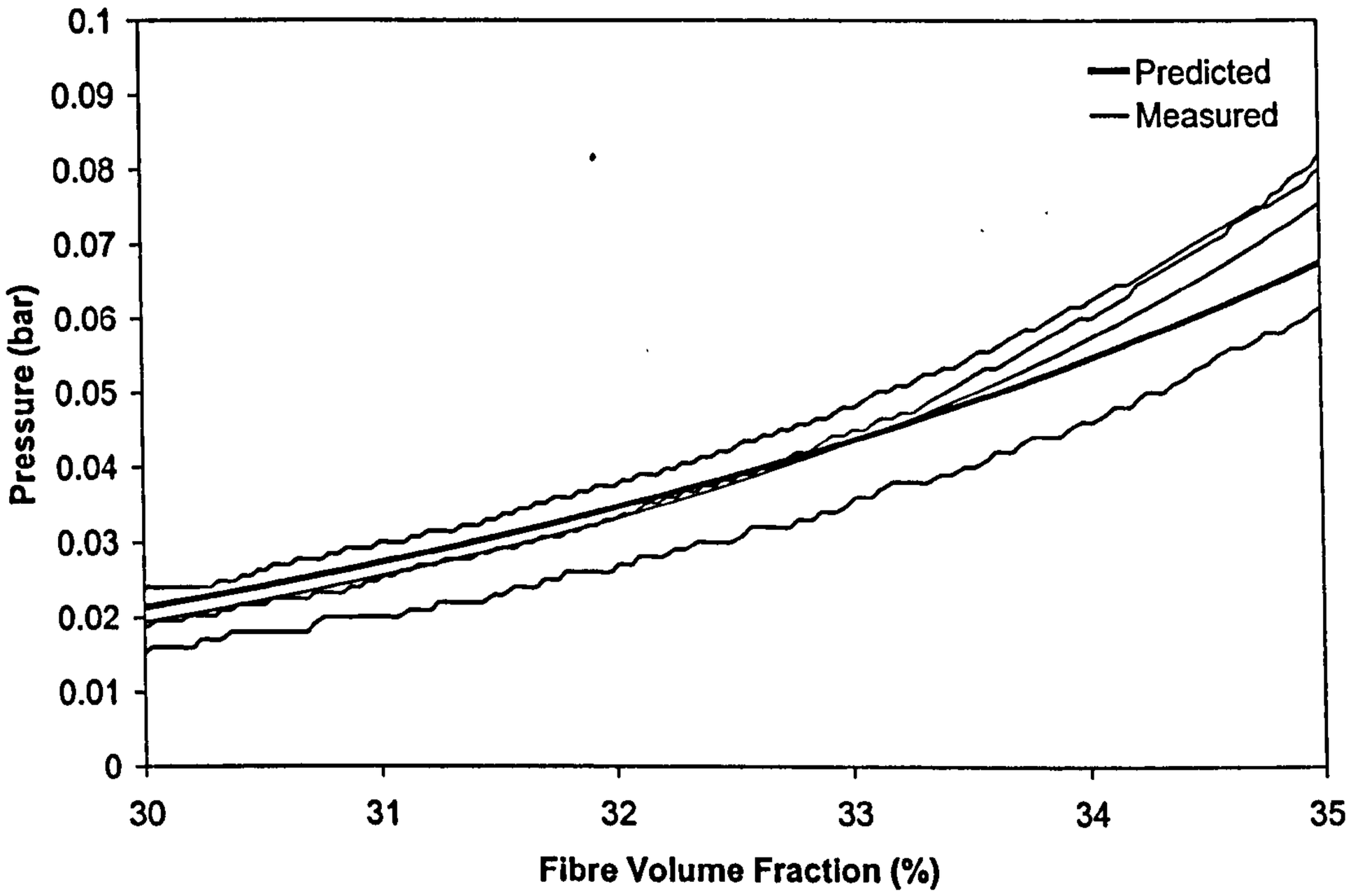

Figure 5.13 Comparison between measured and predicted compaction pressure (Eqn. 5.3) on the reinforcement in material B.

It was observed from experiments that the void content is a function of the total thickness of the laminate. In fact, the void content can be calculated as:

$$V_c = \frac{h - h_\infty}{h} \tag{5.4}$$

Figure 5.14 shows a comparison between the measured void content using microscope image analysis and the predicted void content. A limitation to this

comparison is the changing thickness of the laminate due to the cross-section of the laminate, shown in Figure 5.15.

The current thickness can be obtained from Eqn. 5.4, hence the current fibre volume fraction can be calculated as:

$$V_f = V_{f\infty} \frac{h_\infty}{h} \tag{5. 5}$$

where $V_{f\infty}$ is the fibre volume fraction of a fully consolidated laminate.

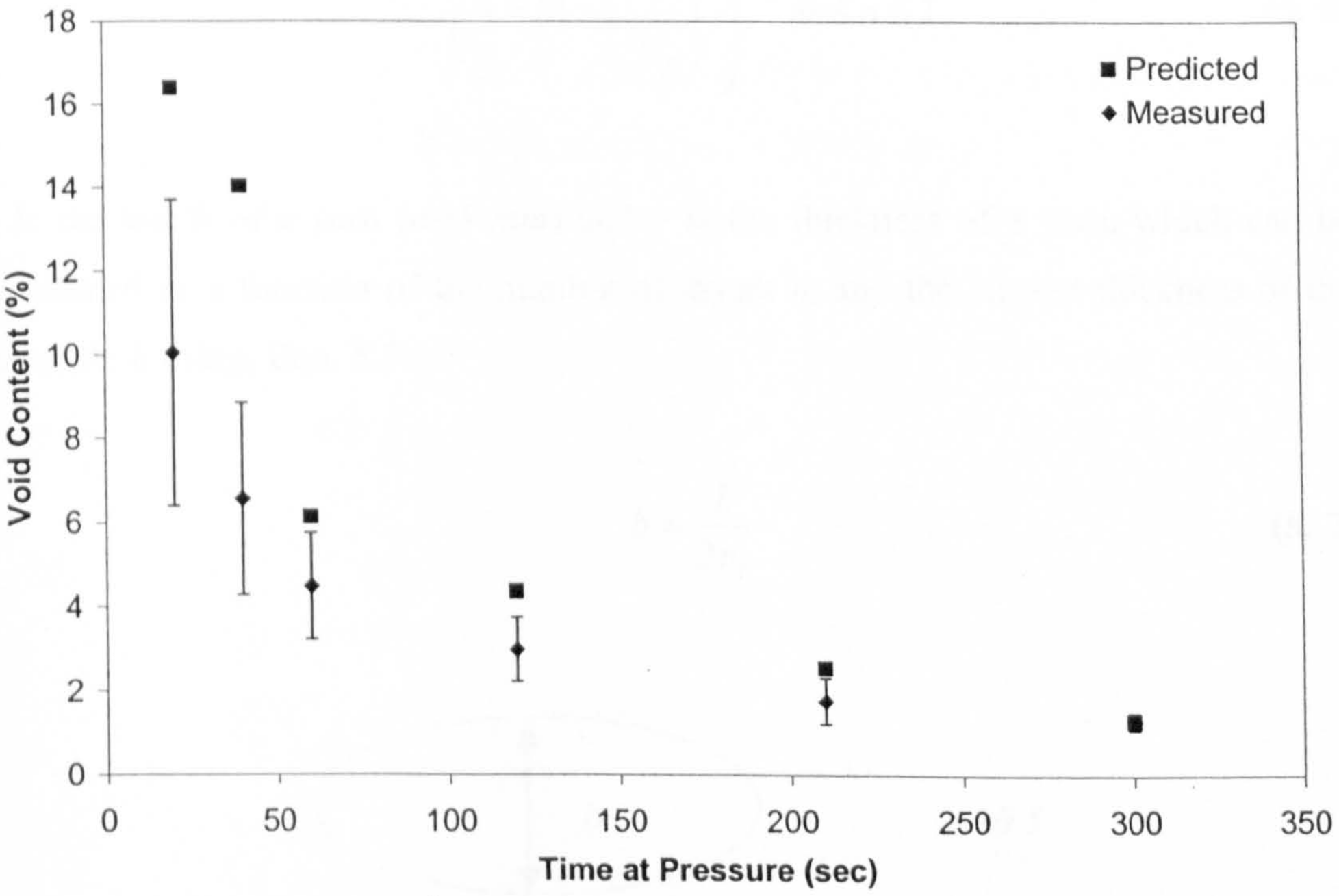

Figure 5.14 Predicted void content based on the current thickness of the laminate.

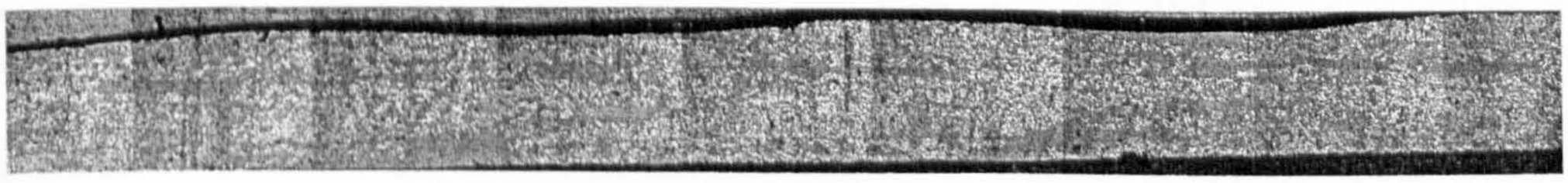

Figure 5.15 Cross-section of a 3 ply glass/PP laminate consolidated by vacuum pressure showing undulations on the surface of the laminate.

Determination of the fibre volume fraction of a yarn

The fibre volume fraction in a yarn v_f differs from the overall fibre volume fraction V_f. Thus, v_f can be calculated from the fibre volume fraction of the laminate. Tow shape is assumed to be defined by an elliptical equation of order n (see Eqn. 5.6), which allows to account for the change in tow shape during consolidation. Figure 5.16 shows how the shape changes with n. As n decreases the shape of the tow becomes rectangular.

$$\frac{y}{b/2} = \left(1 - \left(\frac{x}{a/2}\right)^2\right)^n \qquad 0 \le n \le 1 \tag{5.6}$$

a is the width of a yarn (a=5 mm) and b is the thickness of a yarn, which can be calculated as a function of the number of layers n_l and the current thickness of the laminate h using, Eqn. 5.7.

$$b = \frac{h}{2n_l} \tag{5.7}$$

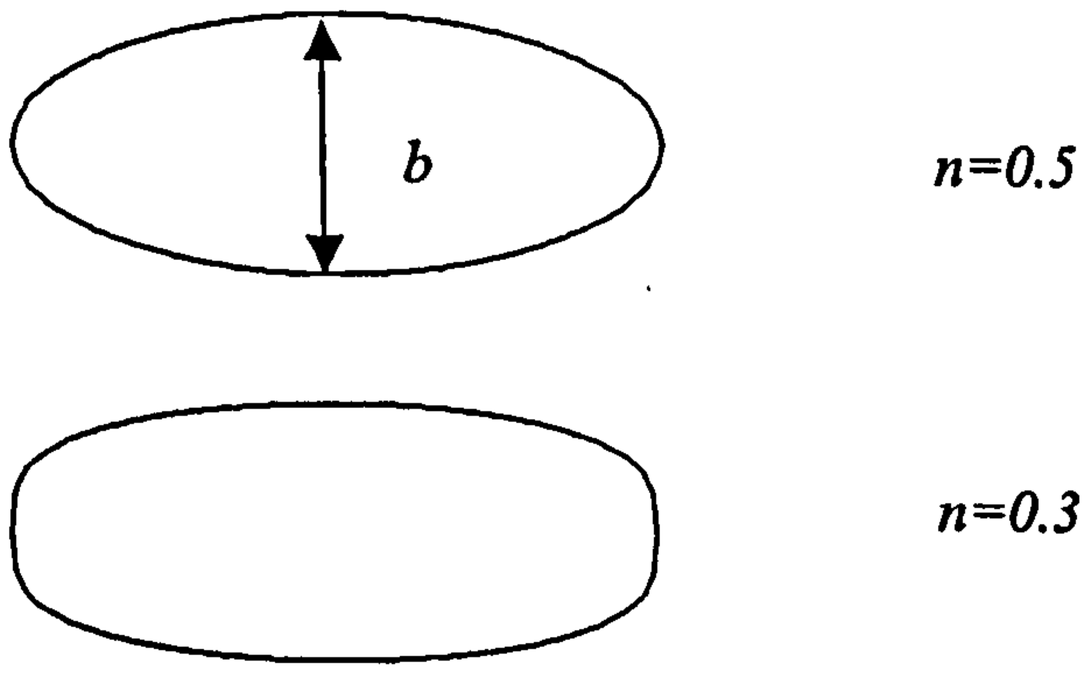

Figure 5.16 Cross-section of the tow as a function of n. As n decreases the shape of the tow becomes rectangular.

Using simple geometric relationships, the fibre volume fraction within a yarn can be calculated using Eqn. 5.8, where the area of the tow cross-section has to be calculated numerically as a function of the exponent n, using a trapezium rule.

$$v_f = \frac{V_f ab}{A_{Tow}} \tag{5.8}$$

5.3.2 Permeability sub-model

Three permeability models were presented in Section 2.4.1. Although Gebart **[40]** presented a model that initially did not require a fitting parameter, an effective fibre radius was introduced in his equation to fit his model to experimental data. Therefore, Gutowski's equation **[103]** is used in the present study. He developed a modified form of the Kozeny-Carman equation to predict the transverse fibre bundle permeability coefficient:

$$K = \frac{r_f^2}{4k'} \frac{\left(\sqrt{\frac{v_a}{v_f}} - 1\right)^3}{\frac{v_a}{v_f} + 1} \tag{5.9}$$

The value of v_a, fibre volume fraction at zero permeability, was calculated to be 0.91 assuming hexagonal close packing of fibres. For glass fibres used in material B the fibre radius is r_f = 9.25 μm. There are no data available that represent the permeability behaviour of the material used in this experiments, so the Kozeny constant, k', was chosen to obtain good agreement with predicted void contents.

5.3.3 Heat transfer sub-model

The consolidation of flat laminates by non-isothermal processes can be solved thermodynamically considering a composite wall consisting of two parallel layers subjected to conduction, where k_1 and k_2 and α_1 and α_2 represent the thermal conductivities and the thermal diffusivities for the aluminium moulding tool and laminate layers, respectively.

The heat conduction problem can be modelled as unidirectional; therefore, it can be described mathematically as:

$$\frac{\partial^2 \Theta_i}{\partial h^2} = \frac{1}{\alpha_i} \frac{\partial \Theta_i}{\partial t} \qquad \textbf{(5. 10)}$$

where Θ is the temperature difference between surfaces, α is the thermal diffusivity and h represents thickness. The unconsolidated laminate consists of glass fibres, pools of polypropylene and air. The exact thermal properties of the laminate will be dependant on the temperature, fibre volume fraction and arrangement of the constituents. The presence of voids in the laminate decreases both the thermal conductivity and the material average density. Consequently, the thermal diffusivity ($k/\rho c$) is also altered.

The bulk properties of the laminate will change as compactions occurs, air is extracted from the laminate and compressed as voids are reduced, and as the temperature of the laminate changes during processing. However, an initial simulation was carried out assuming that thermal properties are time and temperature independent. As Tavman et al. **[55]** suggested, it is assumed that the laminate may be idealised as a rule of mixtures material. In this case, the laminate thermal properties are combined serially, to give the through thickness laminate properties.

The laminate thermal conductivity can be calculated as

$$k_l = \frac{1}{\frac{V_f}{k_f} + \frac{V_m}{k_m} + \frac{V_g}{k_g}} \tag{5.11}$$

and the product ρc

$$\rho_l c_l = V_f \rho_f c_f + V_m \rho_m c_m + V_g \rho_g c_g \tag{5.12}$$

5.3.4 Impregnation sub-model

Bernet et al. [44] considered that the fibre impregnation rate obeys Darcy's law to calculate the time increment Δt necessary for the resin to advance a distance $\Delta r_i = R_i - r_i$, where R_i and r_i are the positions of the resin flow front before and after Δt. Although Bernet's equation is similar to that presented by Friedrich [31], capillary pressure and void pressure were also considered.

Bernet and Friedrich neglected the contribution of the applied pressure to the deformation of the fibre bed by assuming that the fibre bed stays compressed to a given fibre volume fraction, v_f, characteristic of the applied pressure. Both authors considered a constant pressure process where the fibre volume fraction, v_f, remained constant. However, fibre volume fraction keeps changing even for a constant applied pressure; therefore the compaction pressure and the resin pressure change accordingly. By assuming that the fibre volume fraction and the viscosity remain constant at each time step rather than during the whole process, a modified expression for the time increment, Δt, is presented here.

Continuity equations for the solid and liquid phases within a volume element yield [104]:

- Conservation of mass of the fibres

$$\frac{\partial v_f}{\partial t} + \nabla\left(v_f u_f\right) = 0 \qquad \textbf{(5. 13)}$$

- Conservation of mass of the resin

$$\frac{\partial\left(1 - v_f\right)}{\partial t} + \nabla\left[\left(1 - v_f\right)u_r\right] = 0 \qquad \textbf{(5. 14)}$$

Flow within a volume element is expressed by Darcy's Law **[104]**, where u_r and u_f are the velocities of the resin and fibre respectively.

$$u_r - u_f = -\frac{K}{\mu}\nabla P \qquad \textbf{(5. 15)}$$

Assuming that the fibre bed stays compressed to a calculated fibre volume fraction during the time step Eqn. 5.15 leads to:

$$u_r = -\frac{K}{\mu}\frac{\partial P}{\partial r} \qquad \textbf{(5. 16)}$$

and

$$\frac{\partial\left(r u_r\right)}{\partial r} = 0 \qquad \textbf{(5. 17)}$$

From Eqn. 5.17:

$$u_r r = c \qquad \textbf{(5. 18)}$$

Where c is a constant and r is the position of the flow front, which is a function of time only.

Therefore,

$$\frac{c}{r}\partial r = -\frac{K}{\mu}\partial P \tag{5.19}$$

Hence,

$$c\ln\frac{r}{r_0} = -\frac{K}{\mu}\left(P_g - P_c - P_r\right) \tag{5.20}$$

Where P_g is the gas void pressure (in case of a complete vacuum, this is equal to zero), P_c is the capillary pressure and P_r is the resin pressure, which can be calculated as the difference between the applied and the compaction pressures $P_r = P_a - P_f$.

Considering that u_r is the change in the flow front with time Eqn. 5.17 can also be expressed as:

$$c = \frac{dr}{dt}r \tag{5.21}$$

Substituting for c using Eqn. 5.20, a new expression is obtained.

$$r\ln\frac{r}{r_0}\frac{dr}{dt} = -\frac{K}{\mu}\left(P_g - P_c - P_a + P_f\right) \tag{5.22}$$

Solving Eqn. 5.22, the time step Δt necessary for the resin to advance a distance $\Delta r_i = R_i - r_i$ can be calculated as:

$$\Delta t = \frac{\left(1-v_f\right)\mu}{K\left(P_a + P_c - P_g - P_f\right)}\left[\frac{r_i^2}{2}\ln\left(\frac{r_i}{r_0}\right) - \frac{R_i^2}{2}\ln\left(\frac{R_i}{r_0}\right) - \frac{r_i^2}{4} + \frac{R_i^2}{4}\right] \tag{5.23}$$

where μ is the non- Newtonian resin viscosity, v_f is the tow fibre volume fraction, r_0 is the initial agglomeration radius, K is the permeability, P_a is the applied pressure, P_c is the capillary pressure and P_g is the internal void pressure.

Based on experimental observations in Section 5.2 it can be stated that small fibre bundles tend to gather within the yarns. Each of these groups is known as an agglomeration and is assumed to surround a single intra-tow void. Assuming that the commingled yarn contains N_a agglomerations with an initial radius r_0, the total void content of the yarn at a given time step is given by:

$$V_c = \frac{\pi N_a r_i^2 \left(1 - v_f\right)}{A_t + \pi N_a r_i^2 \left(1 - v_f\right)} \tag{5. 24}$$

where A_t, the cross sectional area of the fully consolidated yarn, can be expressed as:

$$A_t = \frac{N_t \pi r_f^2}{v_{f\infty}} \tag{5. 25}$$

where N_t is the total number of reinforcing fibres in the total commingled yarn and r_f is the fibre radius. For material B the number of fibres in a yarn is N_t=1600 and the average initial agglomeration radius was measured at 75 μm from image analysis.

Capillary pressure

P_c is the capillary pressure, defined here as positive when it enhances resin flow. Following Bernet's model **[44, 45]**, the capillary pressure can be estimated theoretically using the Young-Laplace equation:

$$\mathrm{P_c} = \frac{4\beta_{lv}\cos\omega}{\mathrm{d_f}} \frac{\mathrm{v_f}}{1 - \mathrm{v_f}} \tag{5. 26}$$

where β_{lv} is the surface tension of the polypropylene and ω is the contact angle between the solid and the liquid. Capillary pressure can be estimated using β_{lv} = 0.029 $\mathrm{Jm^{-2}}$ and ω = 89° **[105]**. Typical values of capillary pressure are between 50 Pa and 100 Pa for fibre volume fractions of 0.3 and 0.35 respectively. Given that the applied pressure here was typically 95,000 Pa, capillary pressure should have a negligible effect in this case.

Gas pressure

The ideal gas law under general conditions, Eqn. 5.27, expresses the void pressure. In the case of forming using a full vacuum, it is assumed that the ambient pressure is the vacuum, hence P_g equals zero. Otherwise:

$$P_g = P_{atm}\frac{initial\ void\ volume}{current\ void\ volume} = P_{atm}\frac{r_0^2}{r_i^2}\left(\frac{1-v_{f0}}{1-v_f}\right)\frac{T}{T_0} \qquad (5.27)$$

5.3.5 Shear Thinning

Polypropylene behaves in a non-Newtonian manner, so Cain et al. **[42, 43]** incorporated a facility for shear-strain rate dependent viscosity into their model. The scheme suggests that at ultimate compaction, the reinforcing fibres will assume a hexagonal close packing configuration, Figure 5.17. At intermediate stages the fibres will lie in a proportionately packed hexagonal array. This allows construction of a triangular unit cell, with the inter-fibre spacing being denoted by x.

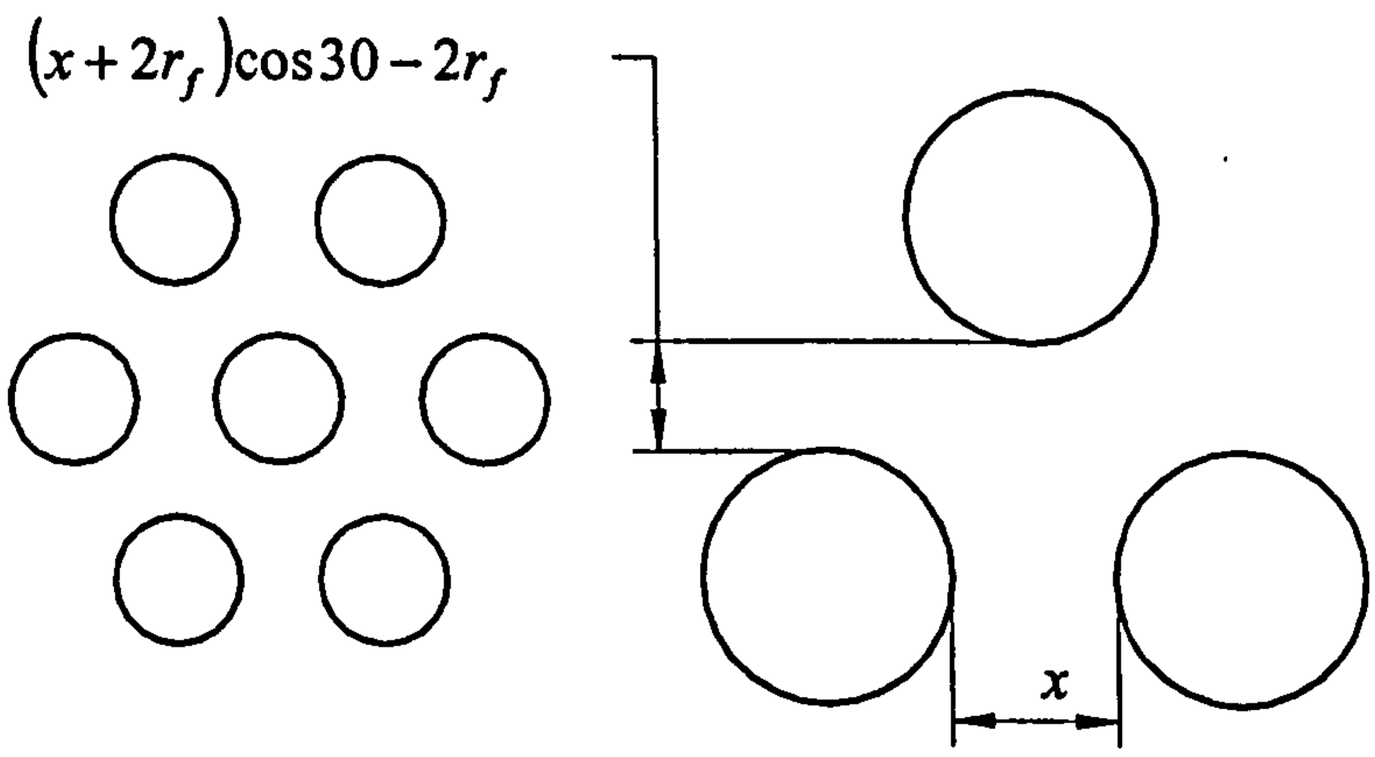

Figure 5.17 Hexagonal packing and triangular unit cell geometry.

Hence, an expression relating x to the instantaneous fibre volume fraction v_f can be derived:

$$\left(\frac{x}{r_f}+2\right)^2 = \frac{\pi}{v_f \cos\frac{\pi}{6}} \tag{5.28}$$

Eqn. 5.28 can be solved for x, giving a measure of the inter-fibre spacing within the bundle. The flow path between fibres can be represented as a rectangular channel, thus Eqn. 5.29 can be used to determinate the matrix shear-strain rate attributable to flow between fibres.

$$\dot{\gamma}_a = \frac{2g+1}{g}\left(\frac{2V}{x}\right) \tag{5.29}$$

Here, g is the power law index, which is fitted to the viscosity and V is the flow velocity, which can be determined from the flow front radius r_i, the flow front radius at the previous time step R_i, the fibre volume fraction within a yarn v_f and the duration of the time step Δt.

Harrison et al. **[106]** presented a generalised Newtonian model describing the shear rate and temperature dependence of the viscosity for the grade of polypropylene used in material B. The Carreau-Yasuda model was used:

$$\mu = a_T \mu_o \left\{1+\left(\lambda_{cy} a_T \dot{\gamma}\right)^i\right\}^{(m-1)/i} \tag{5.30}$$

Where μ is the viscosity, μ_o is the zero shear rate viscosity and m, i and λ_{cy} are additional fitting parameters. Chhabra et al. **[107]** stated that the Careau-Yasuda model was appropriate for the very low shear strain rate, where the power-law model was inappropriate. However, Figure 5.18 shows that m has approximately the same value as g in Eqn. 5.29 for the range of shear strain rates where the polymer showed a shear thinning behaviour. The shift factor a_T is calculated by

$$\log(a_T) = A\left(\frac{1}{T} - \frac{1}{T_{ref}}\right) \tag{5.31}$$

With $A = \Delta H/2.303R$, ΔH is the flow activation energy, R the Boltzmann gas constant and T_{ref} the reference temperature (in °K).

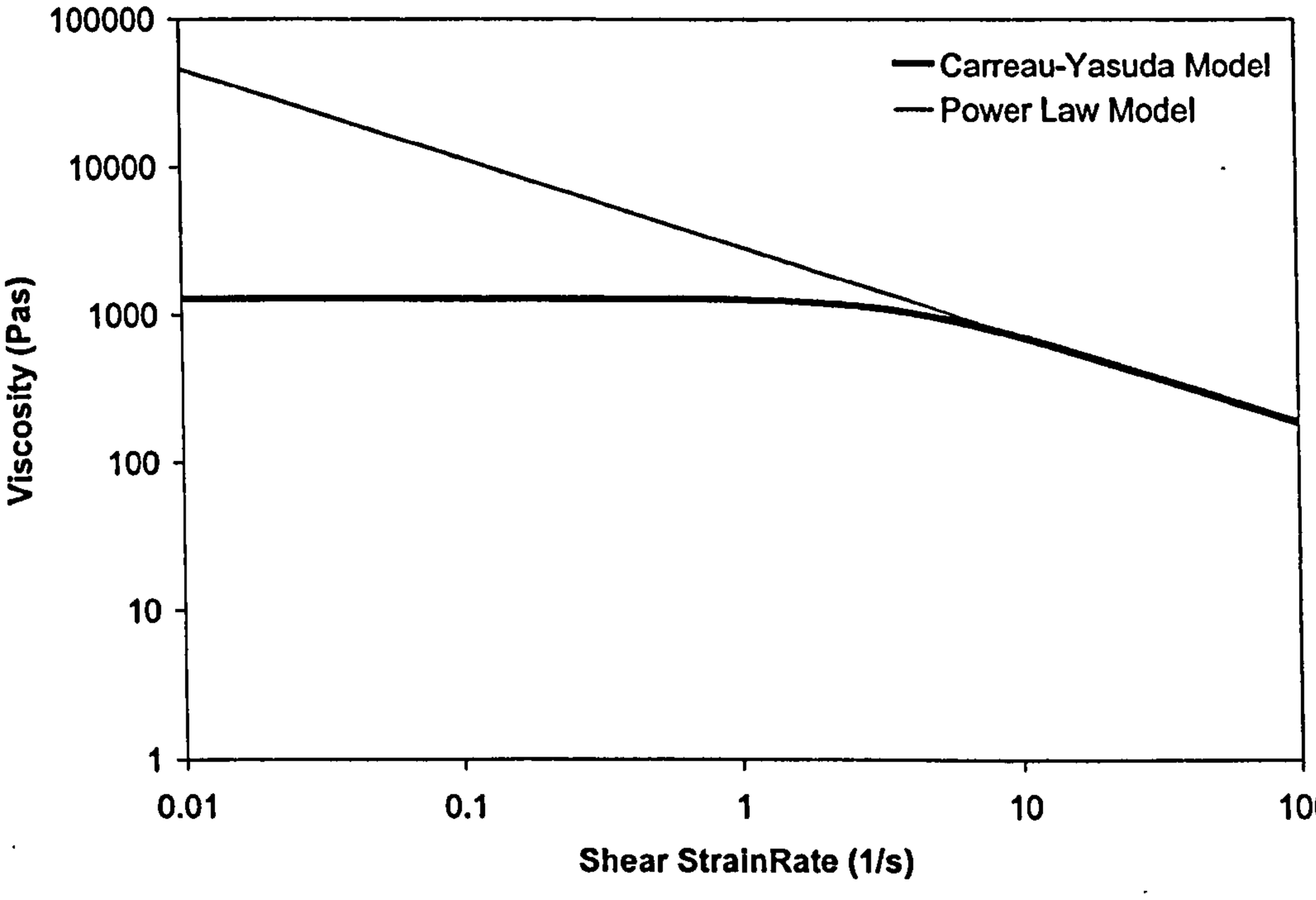

Figure 5.18 Comparison between Carreau-Yasuda and power law model with n=0.4.

Table 5.2 Parameter values for fitted Carreau-Yasuda model.

Parameter	Value
η_o (Pas)	840
λ_{cy}	0.16
m	0.4
i	2
ΔH (kJ/mol)	37.95
T_{ref}(K)	473
R (kJ/mol/K)	$8.31\ 10^{-3}$

Parameter values used in the Carreau-Yasuda model are given in Table 5.2 along with the parameters for Arrenhius equation (Eqn. 5.31).

An explanation of how the different sub-models are implemented in a spreadsheet at each time step is presented below.

Firstly, several parameters provided by the manufacturer are required in addition to the boundary conditions. Then, fibre volume fraction and area of the tow are calculated to obtain fibre volume fraction within the yarn and void content in the inter-tow region. The calculated material temperature is then used to obtain the viscosity of the resin, and pressures (compaction, capillary and gas) are calculated. When a full vacuum is not applied, pressure inside the voids could lead to the equilibrium of pressures, consequently stopping the advance of the flow front. This issue is further studied in Section 5.5. Finally, the time step to advance the flow front is calculated using Eqn. 5.23.

5.4 Vacuum forming

5.4.1 Isothermal case

The aim of the model is to predict void content as a function of processing parameters. A comparison between measured and predicted void content is shown in Figures 5.19 and 5.20, where the effect of different empirical permeability constants and number of agglomerations is observed. An increase in the empirical permeability constant results in a decrease in permeability (Eqn. 5.9), so the void content is increased for a given time at pressure. An increase in the number of agglomerations increases the initial void content. This is because each agglomeration is assumed to be of the same size, and each contains a void at its centre. Due to the absence of full vacuum (950 mbar are applied) the gas pressure inside the voids is also considered.

When the empirical permeability constant equals 40 and the number of agglomerations is 12, the predicted void content shows acceptable correlation with the measured void content for time at pressure greater than 100 s (see Figure 5.21). Below this time, the contribution of inter-tow voids must also be considered as described below. Shear strain rates predicted by the model ranged from 0.05 s^{-1} to 0.5

s^{-1}, which correspond to viscosity values of around 1200 Pas. These values indicate the lack of importance of shear thinning for the case considered here.

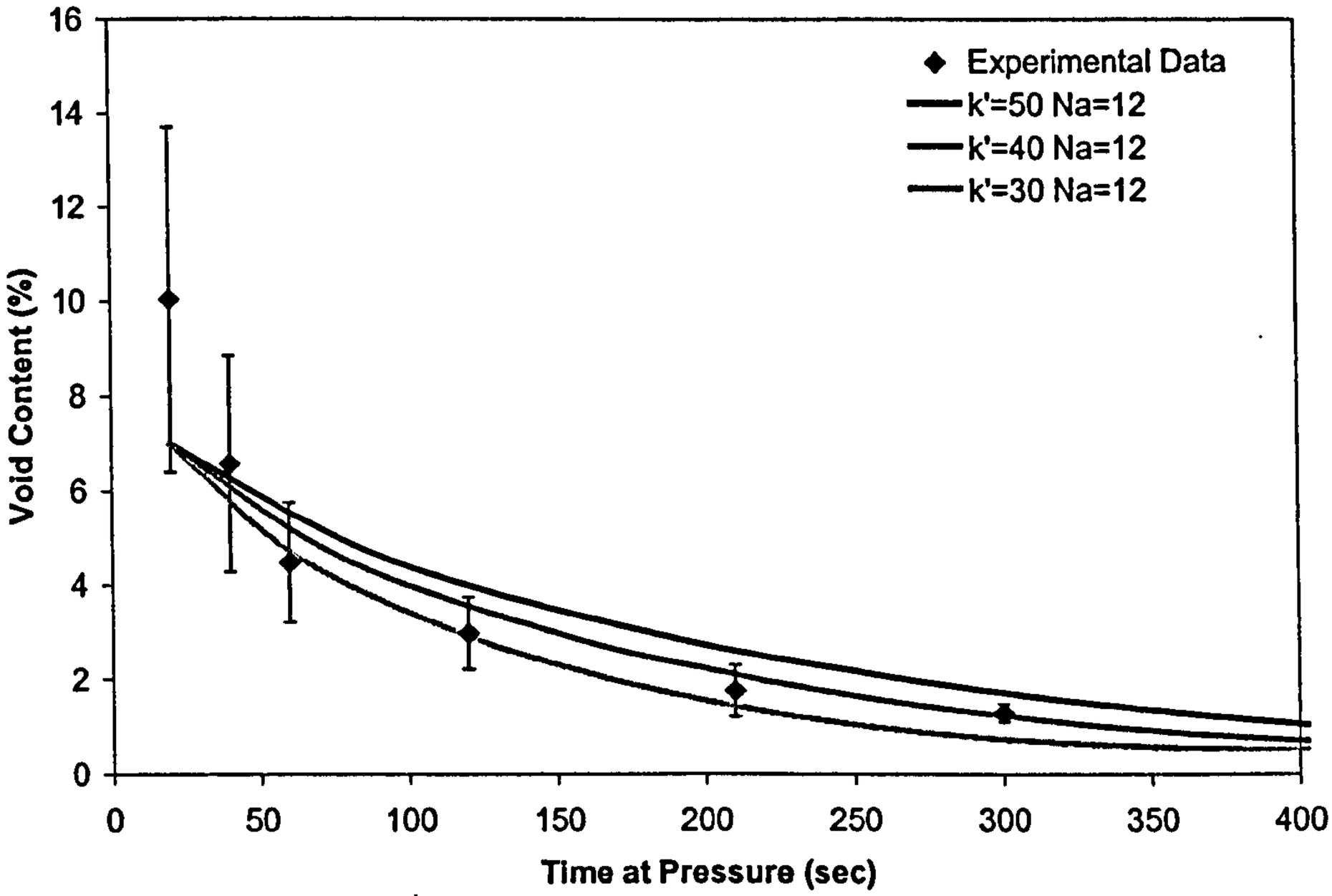

Figure 5.19 Comparison between predicted and measured void content. Effect of permeability constant on predicted void content.

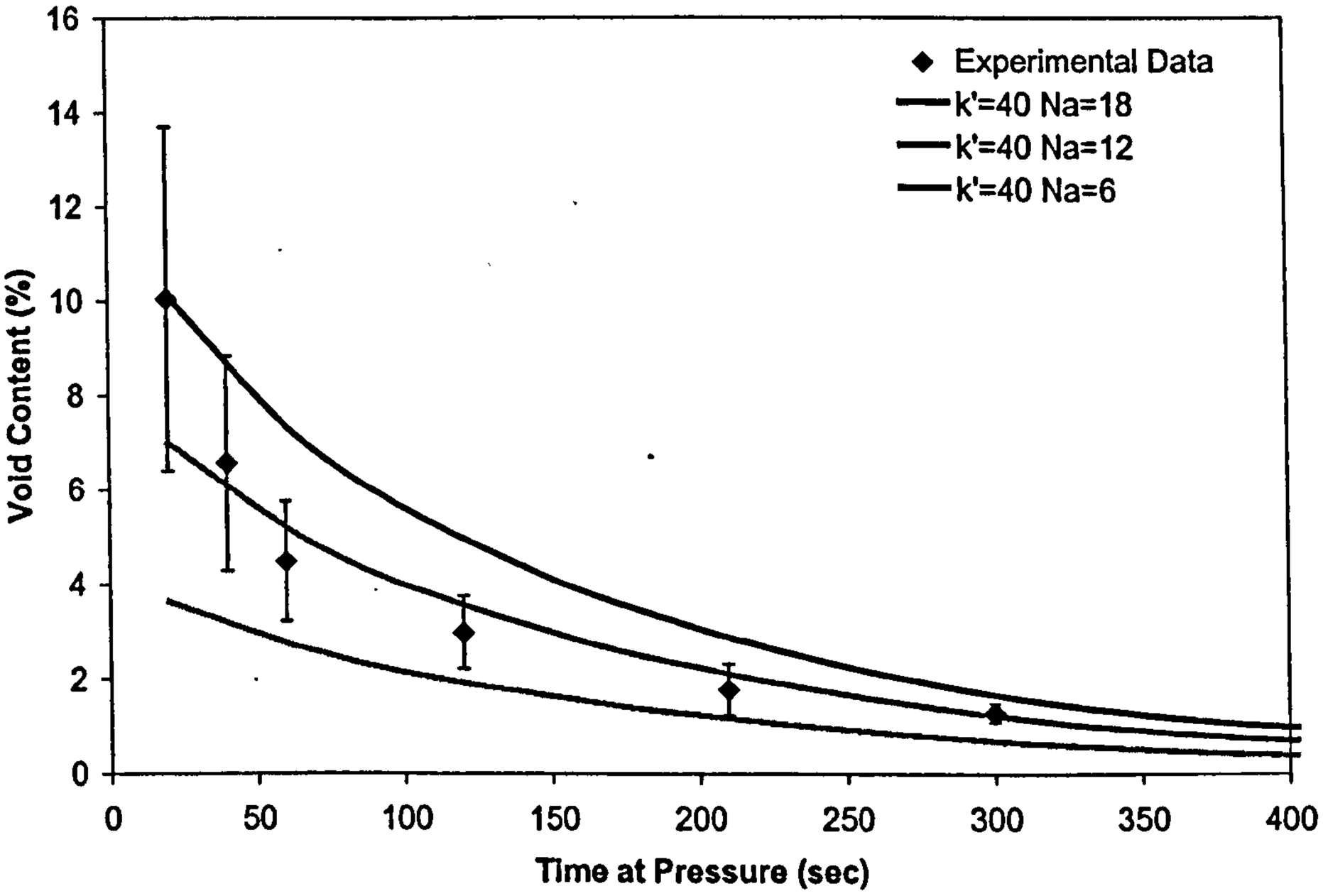

Figure 5.20 Effect of number of agglomerations on predicted void content.

It should be noted here that the assumption that the number of agglomeration is constant during the process is not valid. Within the model, initially each agglomeration is assumed to surround a void within the tow, so that a reduction in the number of voids would suggest a reduction in the number of agglomerations.

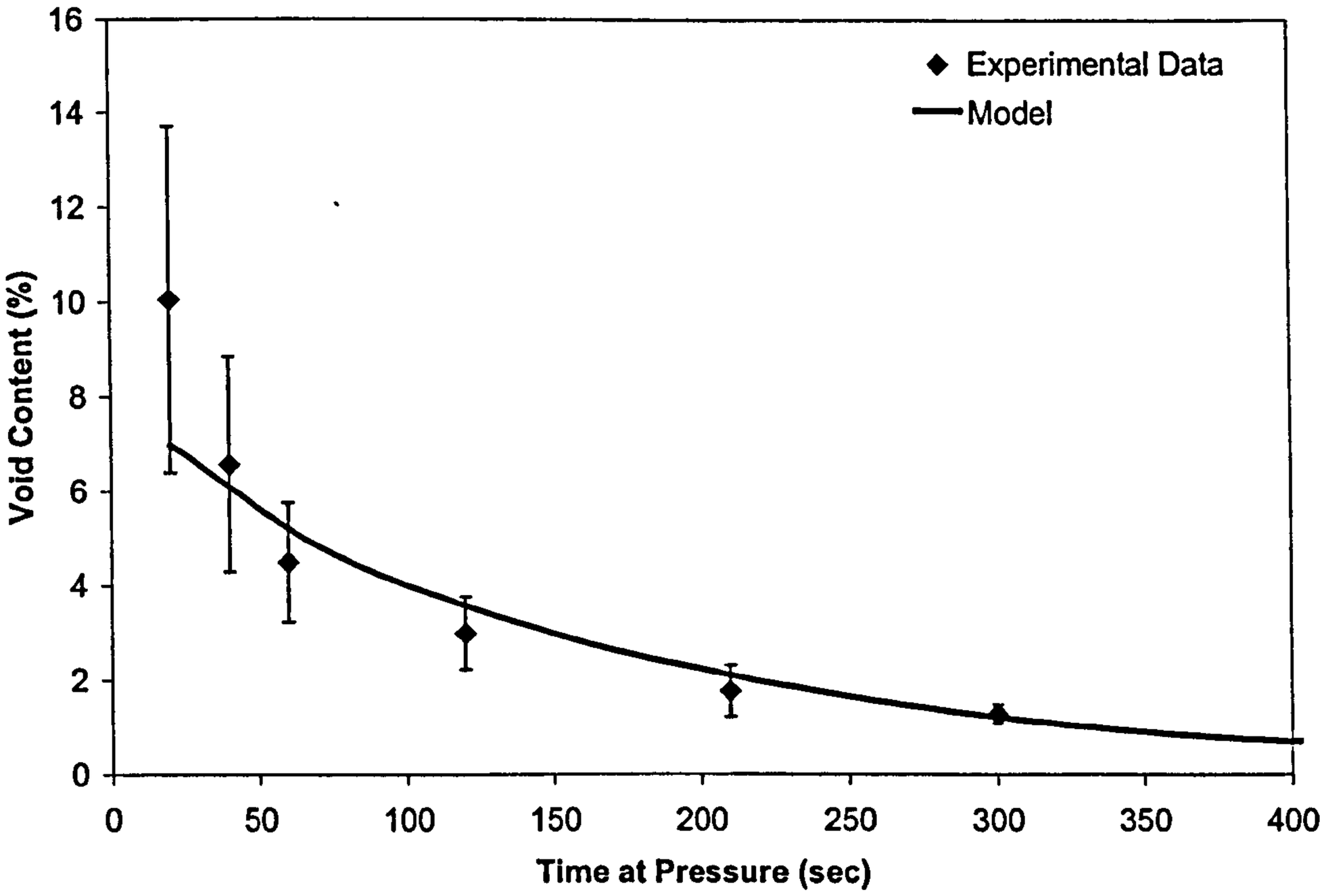

Figure 5.21 Comparison between predicted and measured void content (k'=40, N_a=12).

In Section 5.2.2 a model developed by Lee et al. [46], which represented the inter-tow void content, was presented. Alternatively, the evolution of the inter-tow voids could be explained by a simple geometric concept, which relies on the tow shape during consolidation. The inter-tow void content could be the result of a change in that elliptical shape - i.e. n is not a constant.

Therefore, the inter-tow void content can be calculated as:

$$V_{C\ Inter-tow} = \frac{ab - Area\ of\ the\ tow}{ab} \tag{5.32}$$

where the area of the tow has to be calculated numerically as a function of the exponent n using a spreadsheet and where:

$$A_{Tow} = \frac{N_t \pi r_f^2}{v_{f\infty}} + \pi N_a r_i^2 \left(1 - v_f\right) \tag{5.33}$$

The initial value of n was estimated to be 0.1. As n decreases the shape of the tow becomes rectangular. Figure 5.22 shows a comparison between measured and predicted inter-tow void content. As consolidation evolves the tow cross-section changes (i.e. the exponent of the tow shape equation decreases) until the inter-tow void content equals zero (rectangular tow shape). Good agreement is observed.

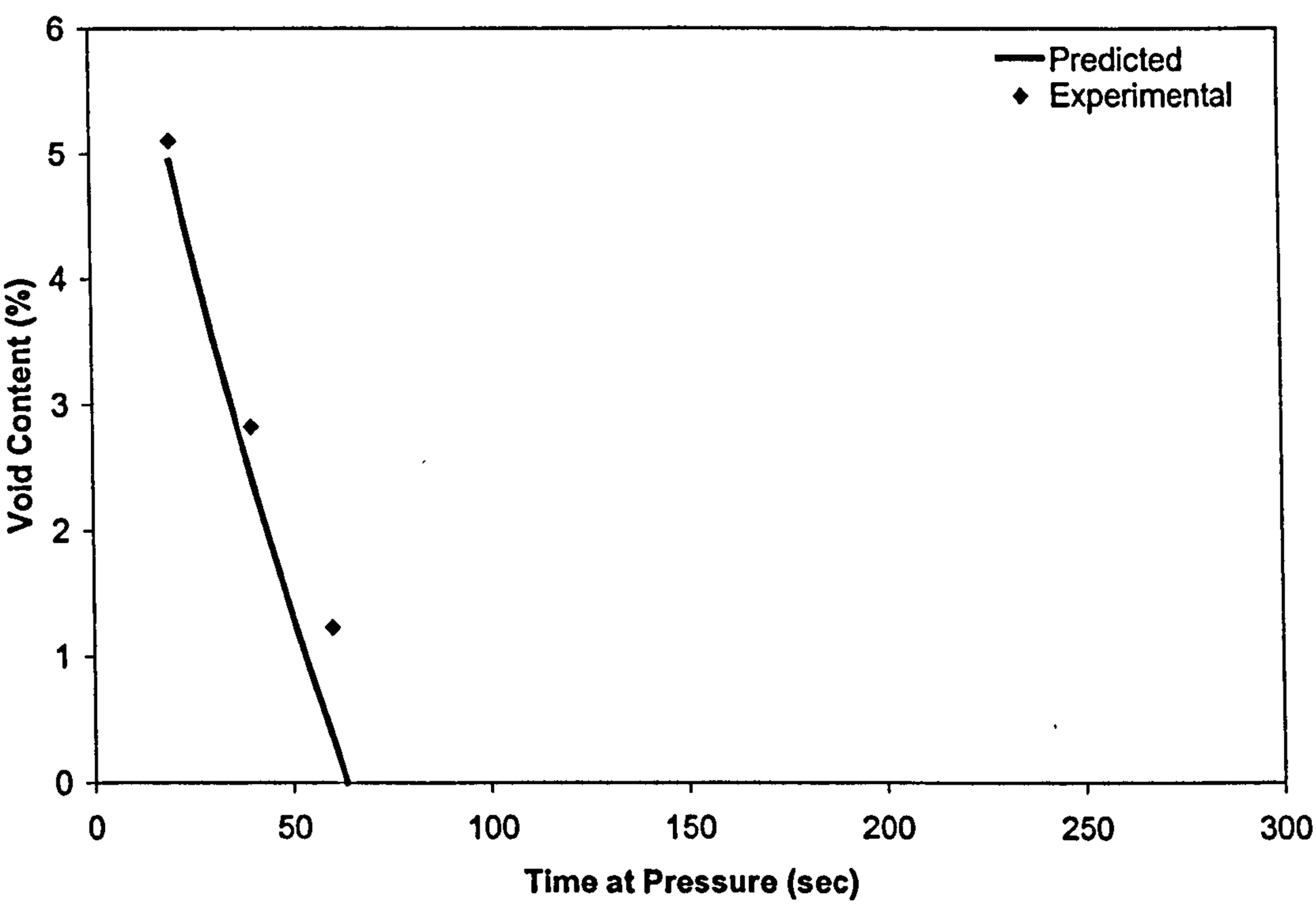

Figure 5.22 Comparison between the measured and the predicted inter-tow void content (Eqn. 5.32).

Assuming that the total void content of the laminate is the sum of the inter-tow void content $V_{C\ Inter\text{-}Tow}$ and intra–tow void content $V_{C\ Tow}$ the predicted void content is presented in Figure 5.23, where the fitting parameters are k'=40 and N_a=12. During the first 60 seconds of consolidation the void content is the sum of the inter-tow and intra-tow void content. However, after 60 seconds the tow shape becomes virtually

rectangular and no voids are located in the inter-tow region. Good correlation between the measured and predicted void content is observed.

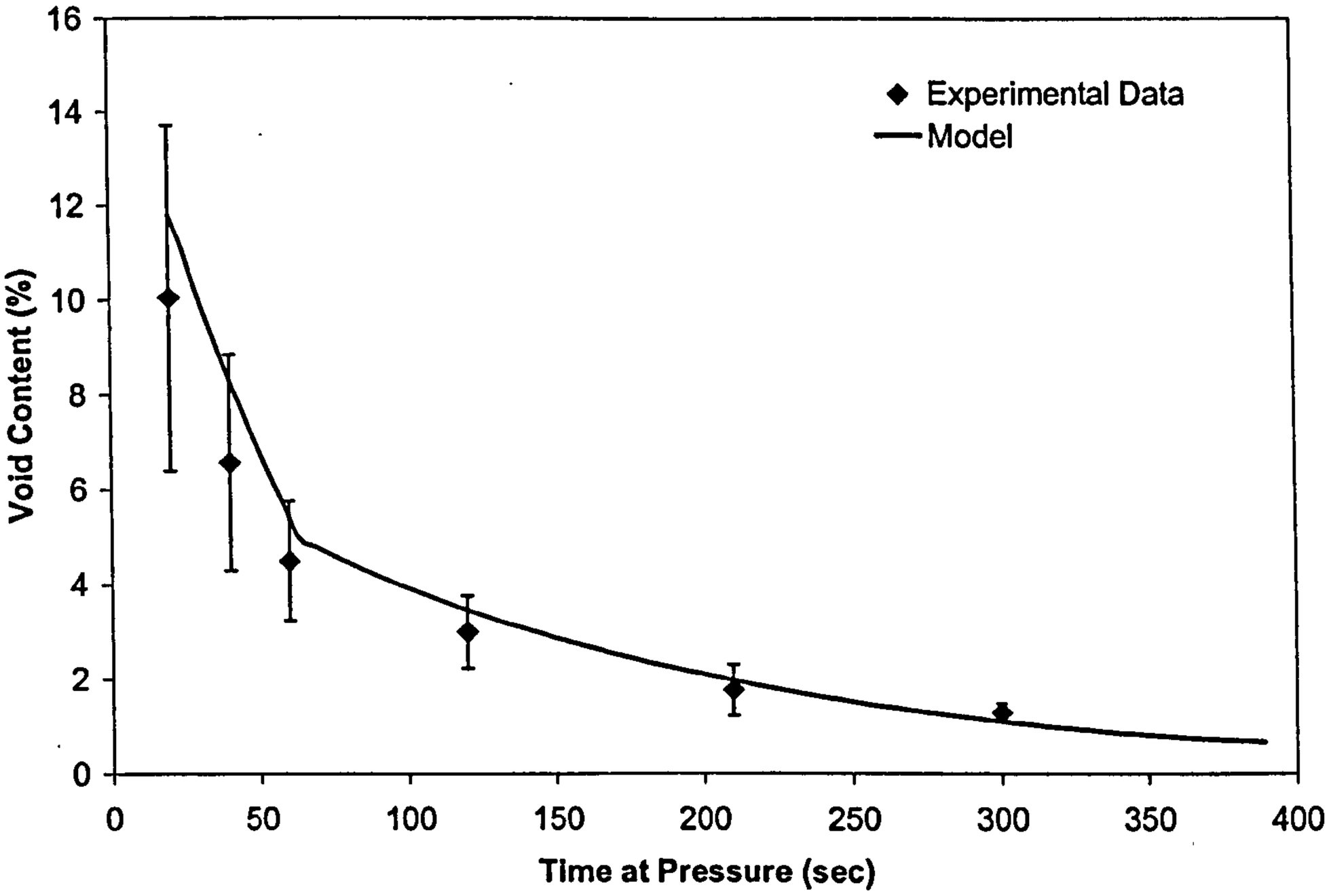

Figure 5.23 Modified consolidation model, incorporating void content due to inter-tow voids.

5.4.2 Non-isothermal case

A consolidation model that predicts void content during an isothermal vacuum forming process was presented in the previous section. However, for industrial applications void content has to be predicted under non-isothermal conditions.

Table 5.3 Constants values for heat transfer model

Material	k (W/mK)	ρ (kg/m^3)	c (J/kgK)
Glass	1	2550	840
Polypropylene	0.288	900	1090
Air	0.034	0.783	1021

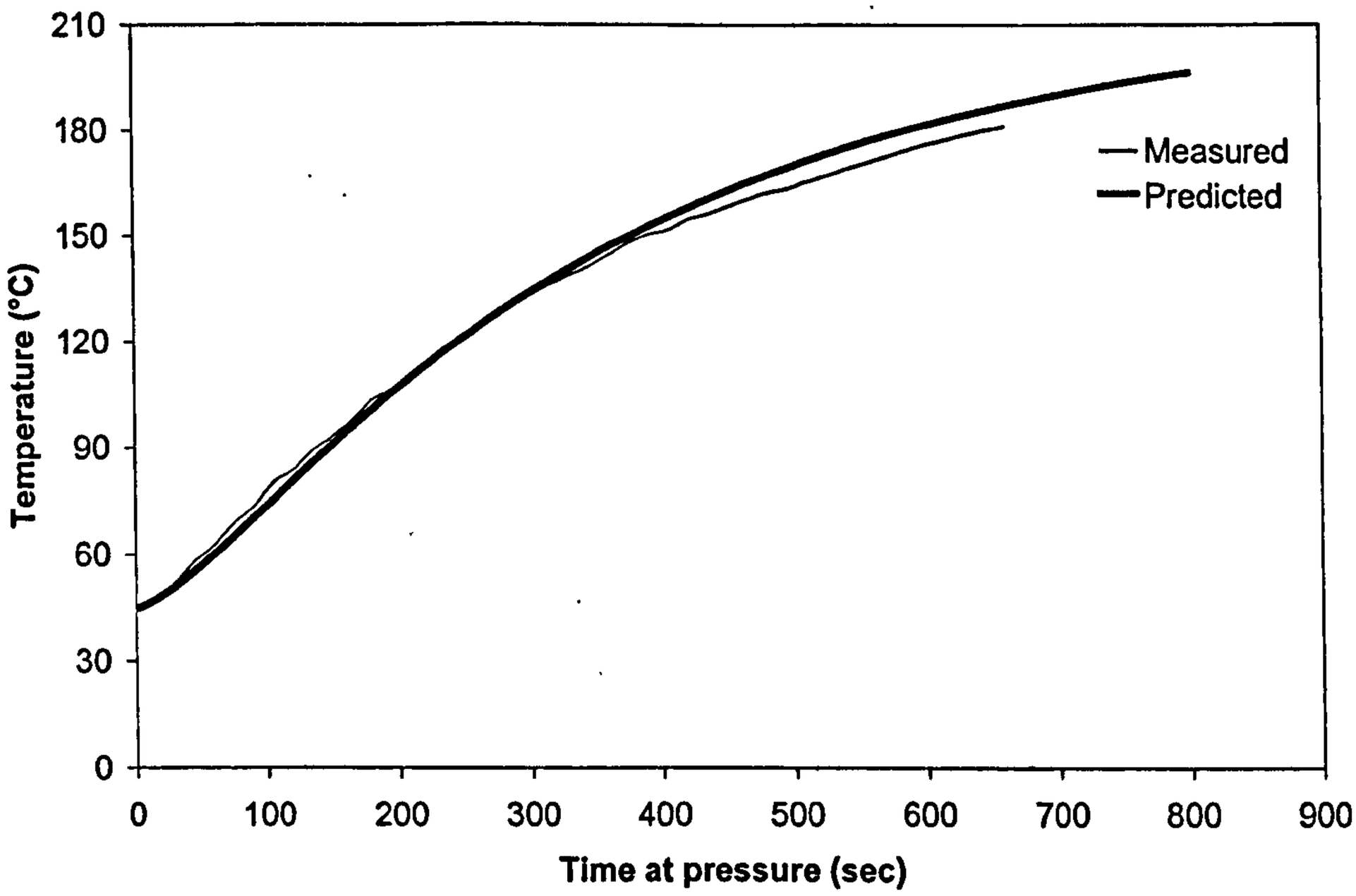

Figure 5.24 Predicted and measured laminate temperature for 3 layers of material B consolidated by a non-isothermal vacuum forming process.

The constants used in these simulations are shown in Table 5.3. Solving Eqn. 5.10 using finite difference analysis, Figure 5.24 shows a comparison between the measured and the predicted material temperature in the middle of 3 layers of material B during a non-isothermal vacuum forming process. Excellent agreement is observed between measured and predicted material temperature.

By updating the viscosity value with the predicted material temperature at each time step, the remaining void content after a non-isothermal vacuum forming process can be calculated. Figure 5.25 shows the predicted values for void content when a non-isothermal case is analysed. Fitting parameters k' and N_a are 40 and 12 respectively as used in the isothermal model. The contribution of the inter-tow voids was also accounted for as described previously. Predictions showed that inter-tow void content contributed 4.7% to the final void content of a laminate content consolidated under 100 mbar. However, no contribution was observed for laminates consolidated under pressures above 300 mbar. Excellent agreement between the measured and the predicted void content was observed.

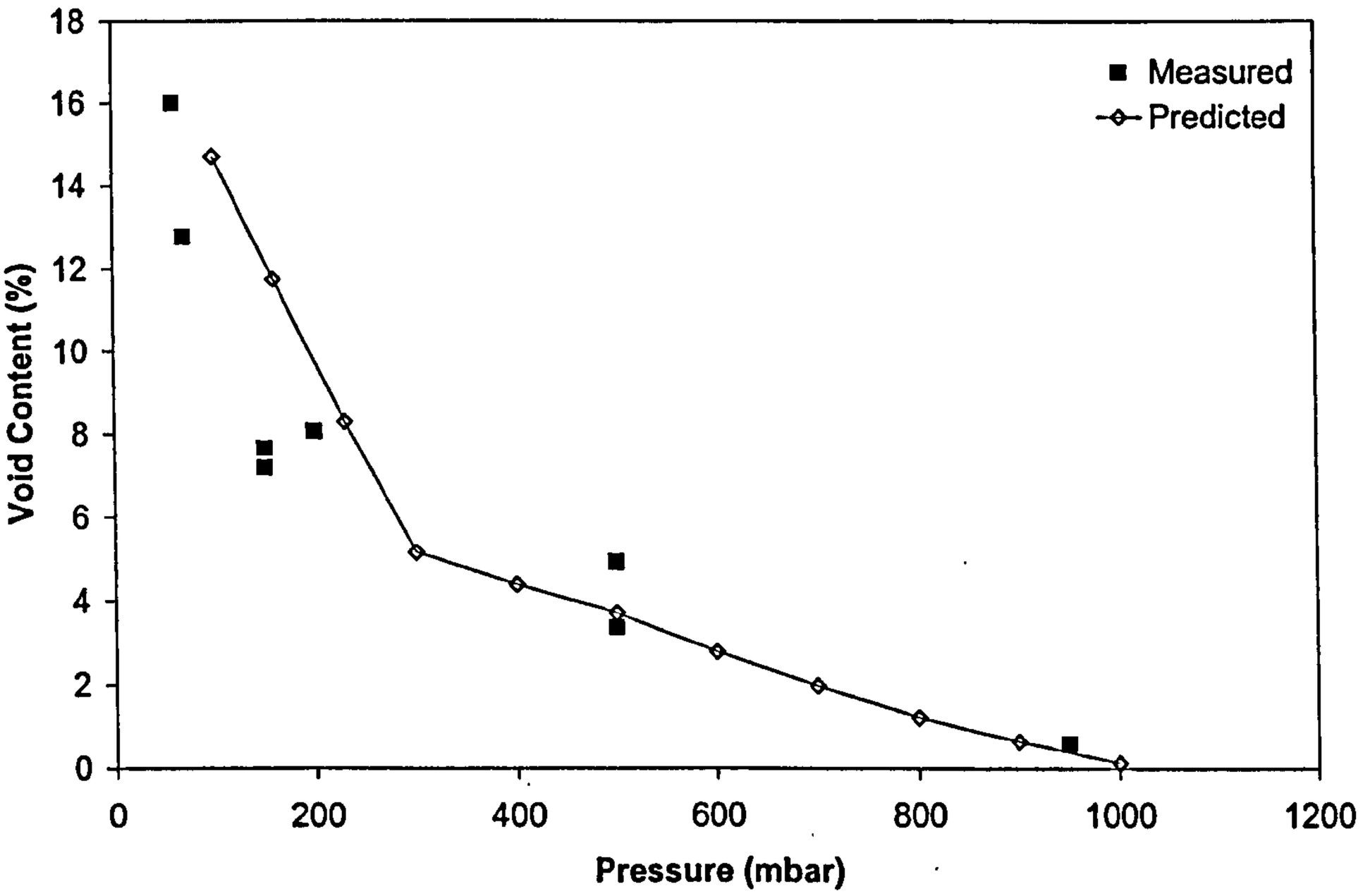

Figure 5.25 Predicted void content for material B laminates consolidated under different levels of pressure using non-isothermal vacuum forming.

As stated in Chapter 3, experimental work showed that the material temperature was uniform across the thickness of three layers of material B. However, thick laminates could present a non-uniform material temperature across the thickness of the laminate. Due to this difference, the melting point is reached successively from the surface in contact with the vacuum bag towards the surface in contact with the tool. This facilitates the movement of the voids or entrapped air through the rooms or pockets situated in the region of the laminate with lower temperature, which are attracted by the vacuum pressure applied. Therefore, the application to thick laminates of the consolidation model presented here should account for the temperature profile at each time step of the consolidation.

5.5 Pressure forming

This section is concerned with the prediction of void content for laminates formed by positive pressure forming processes such as compression moulding. Special attention

is given to the effect that the application of vacuum (in addition to positive pressure) has on the final quality of these flat plaques.

In the case a full vacuum is applied during processing, the term P_g in Eqn. 5.23 equals zero. Considering the same fitting parameters used for the isothermal vacuum forming process, Figure 5.26 shows the effect of increasing the applied pressure on the void content. Thus as the applied pressure increases, the time to obtain a certain void content decreases.

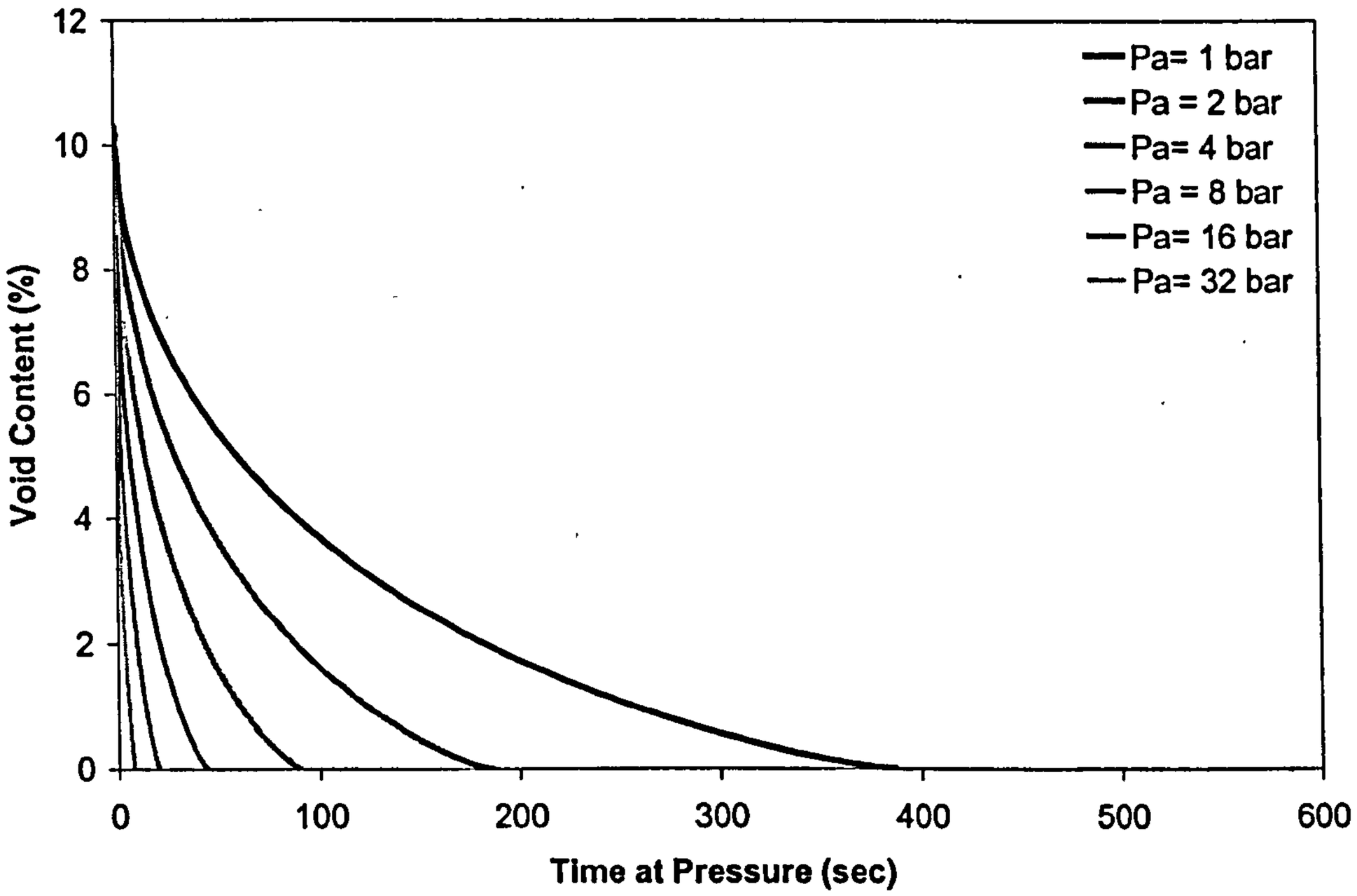

Figure 5.26 Void content as a function of time at pressure for flat plaques consolidated by positive pressure forming with vacuum at 180°C.

Figure 5.26 is contrasted with Figure 5.27 which shows the predicted void content for pressure forming without a vacuum, where pressures over 15 bar are necessary to obtain flat plaques of the same quality as those consolidated under vacuum pressure. For a certain level of pressure, void content decreases until the pressure inside the void is too high to allow the impregnation of the fibre bundle leading to a remaining void content. However, Leterrier et al. **[53]** showed that if the applied pressure is maintained for certain time at pressure voids may dissolve into the resin. Nevertheless, the remaining void content decreases as the applied pressure increases

in such a way that to obtain fully consolidated laminates the applied pressure has to be extremely high.

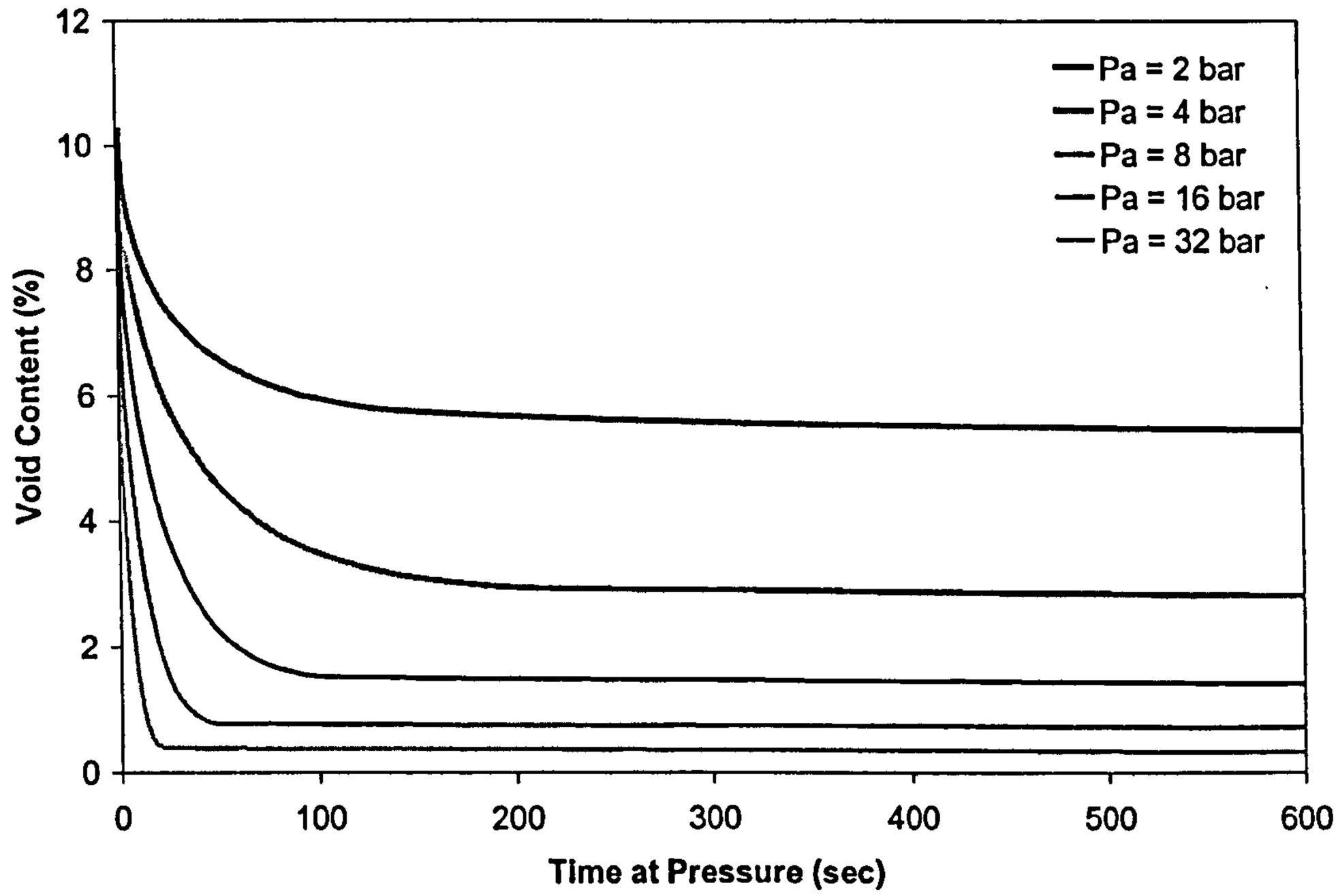

Figure 5.27 Void content as a function of time at pressure for flat plaques consolidated by positive pressure forming without vacuum at 180°C. The absence of vacuum during consolidation leads to partially consolidated flat plaques.

5.5.1 Remaining void content

This section is concerned with analytical calculation of the remaining void content for an isothermal forming process under constant applied pressure. As stated above changes in processing temperature over the melting point of the resin affect the time at pressure to obtain minimum void content.

If a full vacuum is not applied, the pressure inside the voids increases as the flow front advances until the pressure inside the fibre agglomeration is too high for the resin to advance, Eqn. 5.34.

$$P_a + P_c - P_g - P_f = 0 \qquad (5.34)$$

where P_a is the applied pressure, P_c is the capillary pressure (Eqn. 5.26), P_g is the pressure inside voids (Eqn. 5.27) and P_f is the compaction pressure (Eqn. 5.3), and the only unknown parameters are the fibre volume fraction and the flow front radius.

Neglecting the contribution of the capillary pressure, $P_c \approx 0$, the square of the radius of the circular fibre agglomeration can be expressed as:

$$r_i^2 = \frac{\left(1-v_{fo}\right)P_{atm}r_0^2}{\left(P_a - DV_f^B\right)\left(1-v_f\right)} \tag{5.35}$$

where V_{f0} is the initial laminate fibre volume fraction, P_{atm} is the atmospheric pressure, r_0 is the initial void radius, D and B are compaction pressure parameters and V_f and v_f are the final laminate and tow fibre volume fraction, related by Eqn. 5.8. Thus, Eqn. 5.36 is used to calculate the minimum possible void content, which is related to the laminate fibre volume fraction by Eqn. 5.4 and 5.5.

$$V_c = \frac{\pi N_a r_i^2\left(1-v_{f\infty}\right)}{A_t + \pi N_a r_i^2\left(1-v_{f\infty}\right)} \tag{5.36}$$

Figure 5.28 shows a comparison between the predicted remaining void content using the consolidation model and the predicted void content using Eqn. 5.36. Excellent agreement was found between the data. As expected, higher applied pressures lead to lower remaining void content.

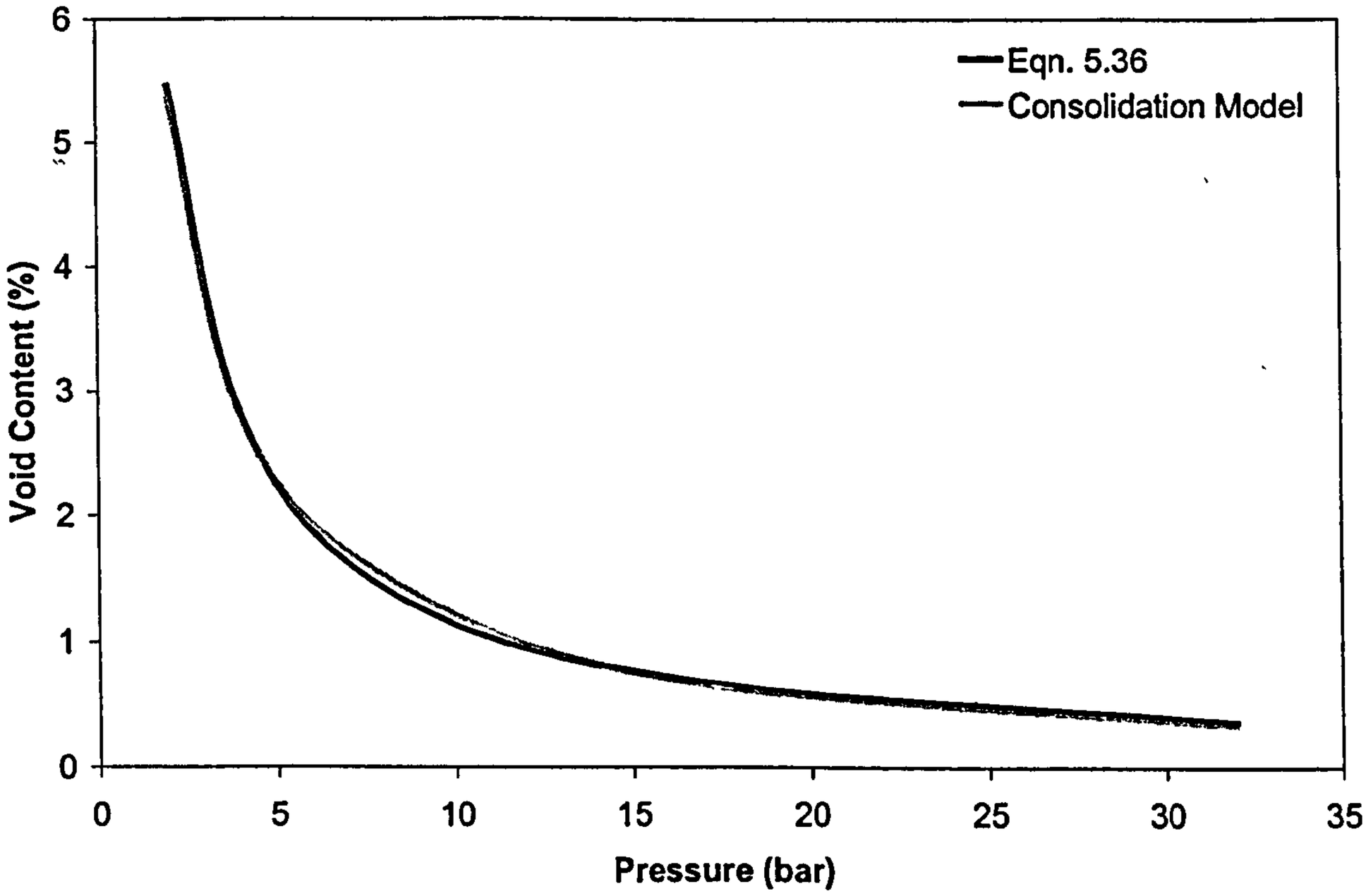

Figure 5.28 Remaining void content as a function of applied pressure for material B laminates consolidated by positive pressure forming.

5.6 Effect of in-plane shearing on consolidation

During draping of textile composites the primary mechanism of deformation is in-plane shear, thus the consolidation model should be able to predict void content as a function not only of processing parameters but also of deformation. Work by Cain et al. **[42]** incorporated the effect of in-plane shearing into their consolidation model by modifying fabric geometric parameters based on experimental observations. These changes are summarised below:

- Assuming conservation of volume, laminate thickness increases:

$$h^{\theta} = \frac{h}{\cos\theta} \qquad (5.37)$$

- The sheared fabric tow-pitch changes as:

$$S^{\theta} = S\cos\theta \tag{5.38}$$

where h^{θ} and S^{θ} are the instantaneous thickness and tow-pitch of a laminate sheared by an angle θ. As a result of in-plane shearing the tow shape changes, the tows become closer and the inter-tow space equals zero.

Micrograph image analysis did not show fibre rearrangement, therefore the compaction model and the permeability model are assumed to remain unchanged. However, as Cain et al. suggested, the pressure required to consolidate a laminate to a given thickness will increase as shear angles increases because of the increase in fibre volume fraction.

Fibre rearrangements within the tow as a result of change in tow shape were not observed during experimental observation of the microstructure of sheared flat plaques (see Figure 5.29), therefore the assumption of circular voids is still assumed to be valid.

Figure 5.30 shows the predicted void content versus time at pressure for two flat plaques formed by three layers of material B and sheared by angles of 0° and 30°. No difference was observed in the quality (void content) of the laminates. This is supported by the experimental data presented in Section 4.4.1.

The consolidation model can be rearranged to model the compaction of flat plaques at a constant rate as Cain et al. did, Eqn. 5.39. Figure 5.31 shows the effect of shearing in the consolidation of flat plaques at a constant rate. As expected, to achieve a specified thickness the pressure increases as shear angle increases.

$$P_a = P_g + P_f - P_c + \frac{(1-v_f)\mu}{K\Delta t}\left[\frac{r_i^2}{2}\ln\left(\frac{r_i}{r_0}\right) - \frac{R_i^2}{2}\ln\left(\frac{R_i}{r_0}\right) - \frac{r_i^2}{4} + \frac{R_i^2}{4}\right] \tag{5.39}$$

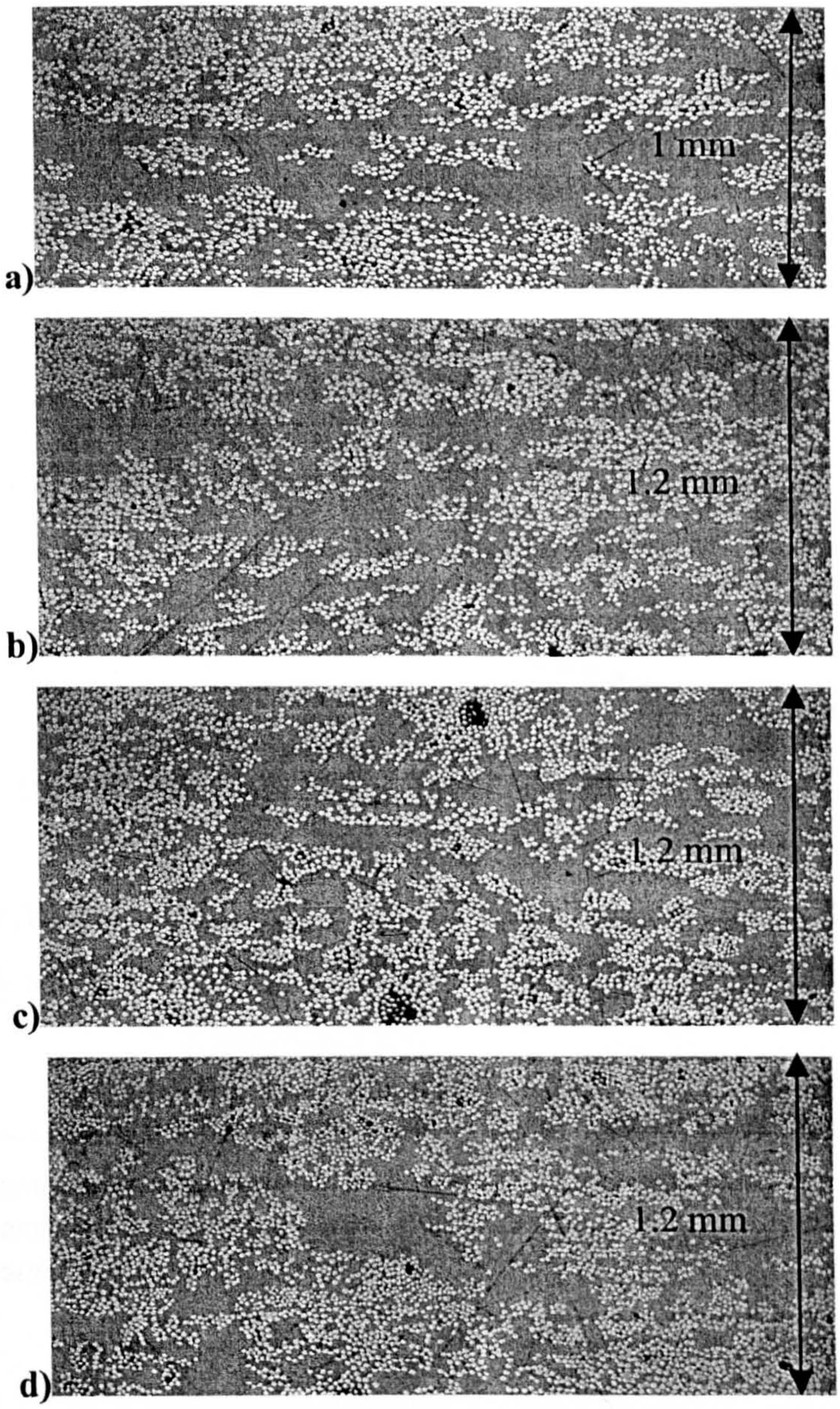

Figure 5.29 Micrographs corresponding to a) 0°, b) 15°, c) 30° and d) 45° sheared flat plaques consolidated under 500 mbar of pressure. Fibre volume fraction remains constant, $V_f \approx 0.35$.

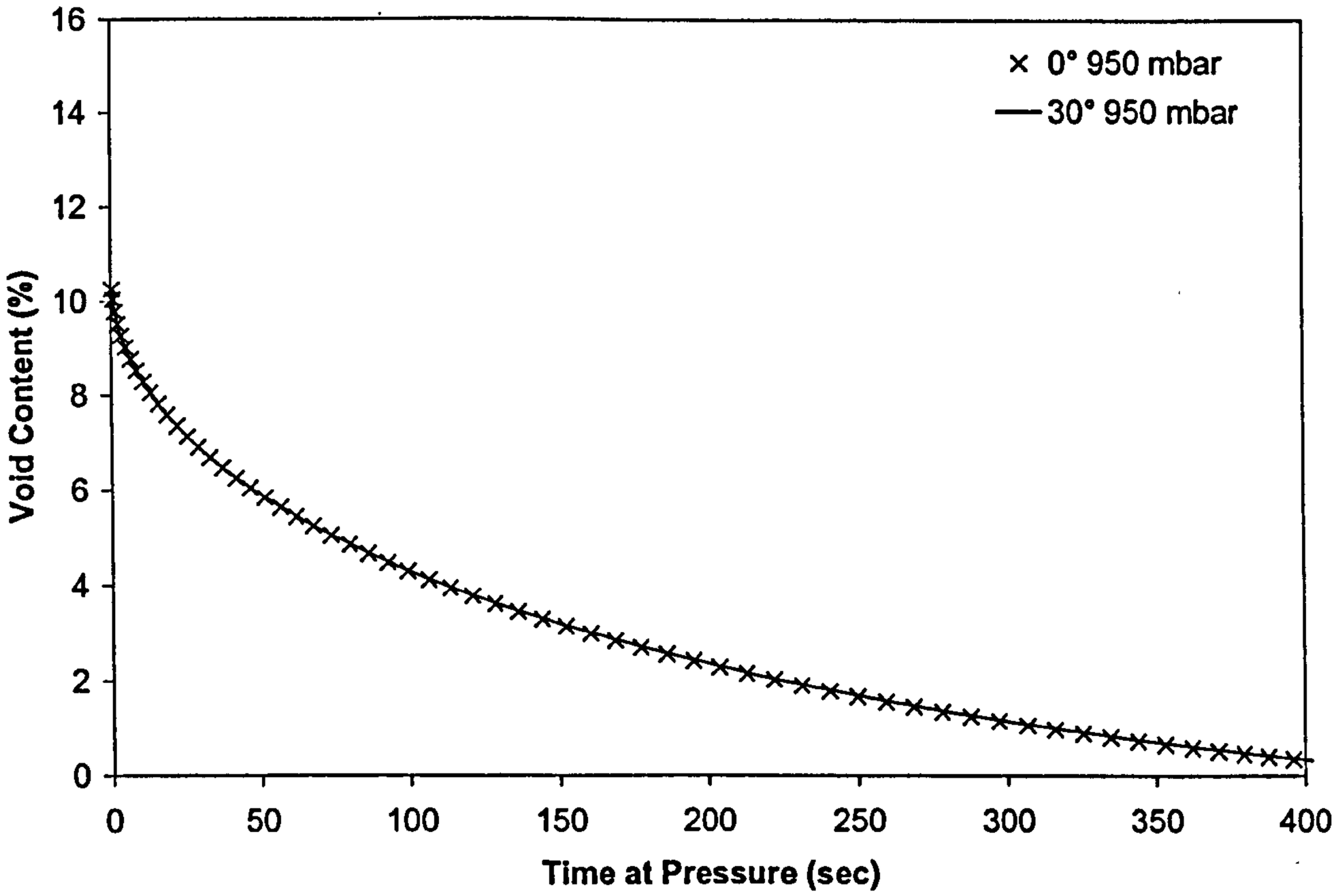

Figure 5.30 Effect of deformation on the consolidation model for flat plaques consolidated by an isothermal vacuum forming process at 180°C.

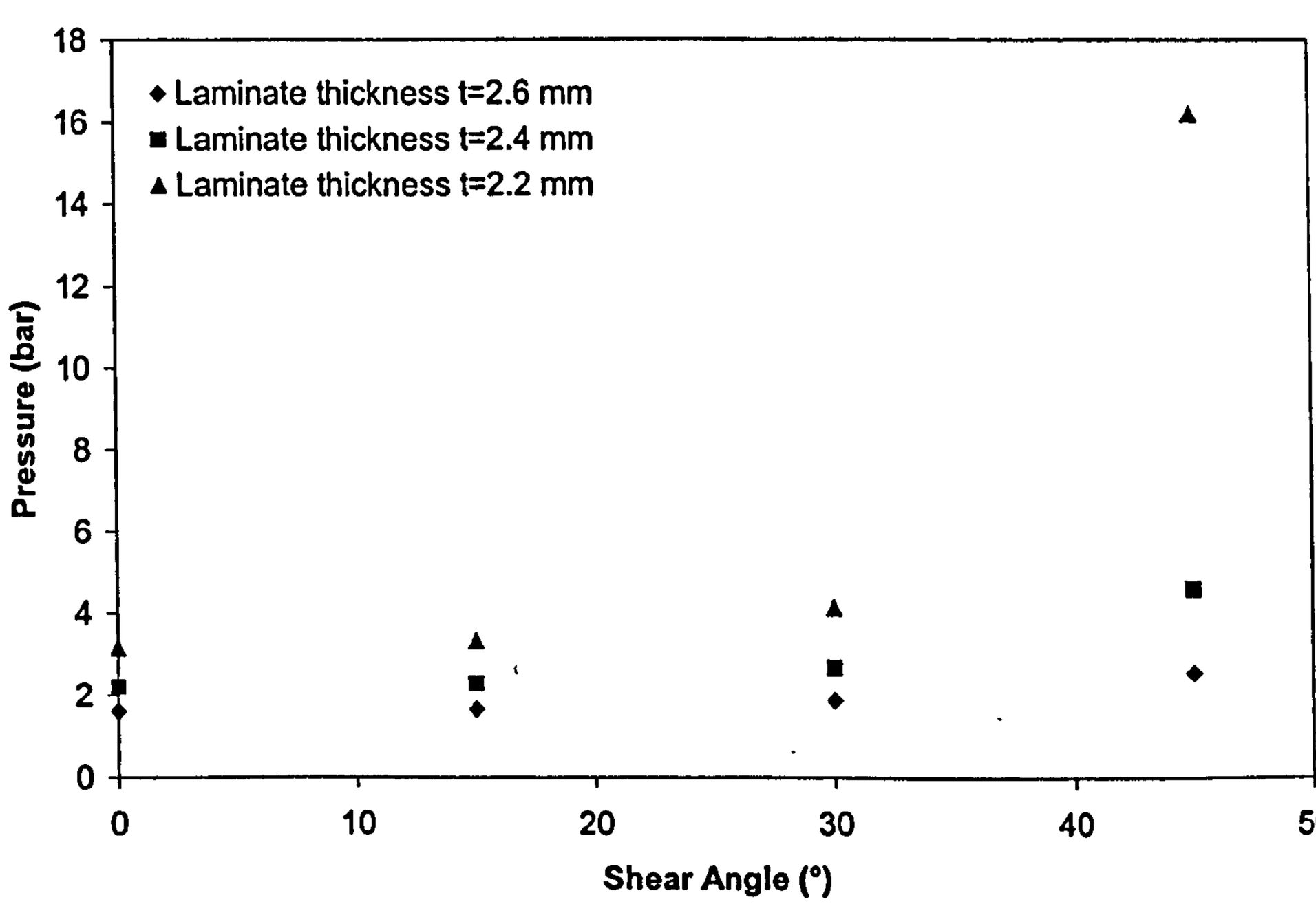

Figure 5.31 Predicted pressure required to consolidate flat plaques to different thickness depending on the shear angle. Forming process used was pressure forming at 180°C and a constant compaction rate of 1 mm/min.

5.7 Conclusions

A model that predicts void content as a function of processing parameters such as pressure, time at pressure and processing temperature has been developed and validated using data obtained from vacuum consolidation of a glass/PP commingled thermoplastic. Analysis of micrographs from consolidated flat plaques was used to study the evolution of the microstructure during different stages of consolidation. The presence of large macrovoids in the inter-tow region, particularly during the first minute of consolidation, led to the consideration of two consolidation problems: evolution of inter-tow voids and encroachment of the matrix into fibre bundles.

Although several models that predicted the encroachment of the matrix into fibre bundles were studied, none of them represented properly the consolidation stages observed in the micrographs. An existing model based on Darcy's law was modified to account for the effect of shear thinning, although in the isothermal vacuum forming process the viscosity was approximately constant (at the appropriate temperature) as shear strain rates were less than $1s^{-1}$. Capillary pressure was also accounted for, but this had little effect on the predicted void content. Sensitivity studies revealed the effect of the number of agglomerations, N_a, and the empirical permeability constant, k', on the predicted void content. An increase in the number of agglomerations and the empirical permeability parameter increased the void content and the time at pressure required to obtain full consolidation.

Despite the difficulties found to present a suitable model that would predict the evolution of the inter-tow voids, a simple geometrical analysis based on the change in tow shape showed reasonable agreement between measured and predicted void content. However, a more thorough analysis of the change in tow shape under different processing conditions should be the subject of further work.

Based on the intra-tow consolidation model, different processing conditions were explored. Increasing the applied pressure whilst maintaining the vacuum pressure showed a reduction in the time to obtain fully consolidated laminates. In contrast with the vacuum assisted pressure forming process the prediction of the void content under normal positive pressure conditions (without vacuum pressure applied to the

laminate) showed that unless extremely high pressures are applied an unacceptable remaining void content would be obtained. A simple model that predicted the remaining void content as a function of the applied pressure was also presented.

Finally, the effect of deformation was accounted for by the change of geometrical parameters such as thickness and tow width. Micrographs did not show a change in fibre arrangement due to in-plane shear deformation. In terms of void content, a negligible effect of deformation on consolidation for sheared flat plaques using a vacuum forming process was observed, as expected by experimental evidence since fibre volume fraction remained constant and no rearrangement of fibres within the tow was observed.

6 Prediction of Mechanical Properties of Textile Composites

6.1 Introduction

This chapter is concerned with prediction of the effect that void content and deformation have on the mechanical properties of composite laminates. Chapter 4 addressed the importance of predicting void content due to the effect on the mechanical performance of composite components. The shape of the curve of flexural strength versus void content (see Figure 6.1) may be explained from the theory of linear elastic fracture mechanics or simple stress fracture criteria. However, linear elastic fracture mechanics could be more appropriate for prepreg materials, where inter-tow voids are similar to sharp cracks (see Figures 4.18 and 4.19), than for commingled materials where voids are more circular.

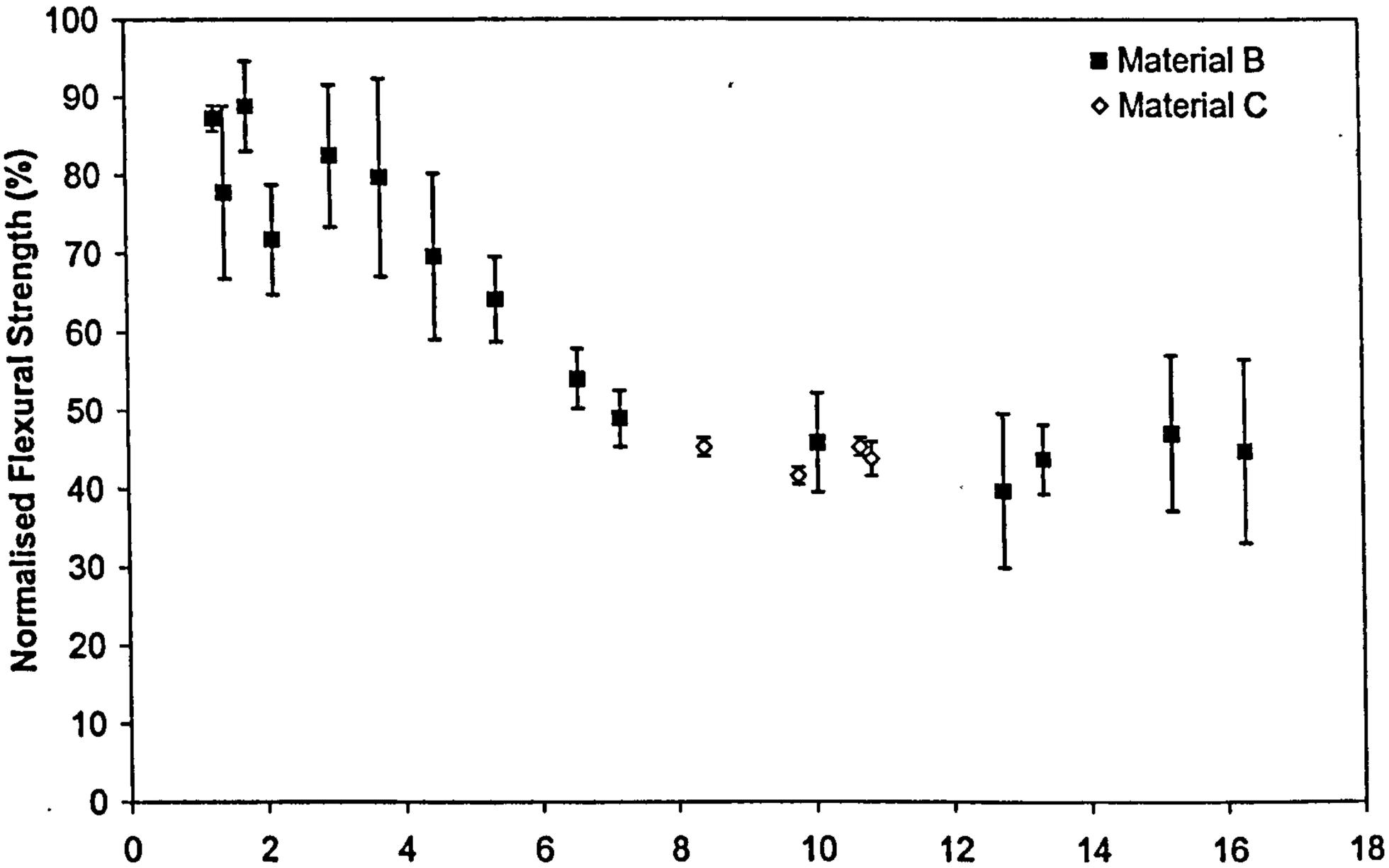

Figure 6.1 Effect of void content on mechanical properties of material B and C flat plaques consolidated under vacuum at 180°C and 195°C with fibres at 0/90°.

Two simple stress criteria that predict the effect of void content on mechanical properties assuming circular voids are presented. The criteria result in a two-

parameter model that is capable of predicting strength without resorting to classical concepts from linear elastic fracture mechanics.

An approach is presented for predicting the elastic and first ply failure behaviour of components manufactured from textile reinforced composite materials where the manufacturing process and component shape necessitate in plane deformation of the textile. Simple models are used for mechanical properties, based primarily on the properties of the reinforcement and matrix phases, and combined with classical laminate theory to enable modelling of multilayered laminates where the angles between tows may notionally take any value between 0° and 90°. Comparisons with experimental data from tensile tests on angle ply laminates manufactured at a range of ply angles are presented.

6.2 Theoretical analysis of the effect of void content on composite strength using stress fracture criteria

Whitney et al. **[64]** developed two related criteria based on stress distribution for predicting the uniaxial tensile strength of laminated composites containing through thickness discontinuities of general shape. The criteria discussed in Section 2.5.1 resulted in a two-parameter model that is capable of predicting void content without resorting to classical concepts from linear elastic fracture mechanics. The two parameters are the strength of a fully consolidated laminate and a characteristic dimension.

The first approach assumes that the failure occurs when the stress at some distance away from the void is equal or greater than the strength of a fully consolidated laminate. It is also assumed that the characteristic distance ψ_1, where the stress is equal to the strength of the fully consolidated laminate, is independent of laminate geometry and stress distribution.

Assuming circular voids and a uniform distribution of voids in the laminate, the consolidation model is able to predict the void radii for each level of void content

assuming that the number of agglomerations in a yarn is 12 as used in the previous chapter. With these assumptions, the point stress failure criterion becomes

$$\frac{\sigma}{\sigma_\infty} = \frac{2}{2+\zeta_1^2+3\zeta_1^4} \tag{6.1}$$

where σ_∞ is the strength of a fully consolidated laminate (provided by the manufacturer), σ is the predicted laminate strength for a specific void content and

$$\zeta_1 = \frac{r}{r+\psi_1} \tag{6.2}$$

A second approach was developed by assuming that the failure occurs when the average stress over some distance away from the void is equal or greater than the strength of a fully consolidated laminate. The physical argument for the average stress criterion resides in the assumed ability of the material to redistribute local stress concentrations. As in the point stress criterion the characteristic distance ψ_2 is assumed to be independent of laminate geometry and stress distribution.

As in the point stress criterion, for the case of a circular hole of radius r and uniform distribution of voids, the stress failure criteria is given by Eqn. 6.3.

$$\frac{\sigma}{\sigma_\infty} = \frac{2(1-\zeta_2)}{2-\zeta_2^2-\zeta_2^4} \tag{6.3}$$

where in this case

$$\zeta_2 = \frac{r}{r+\psi_2} \tag{6.4}$$

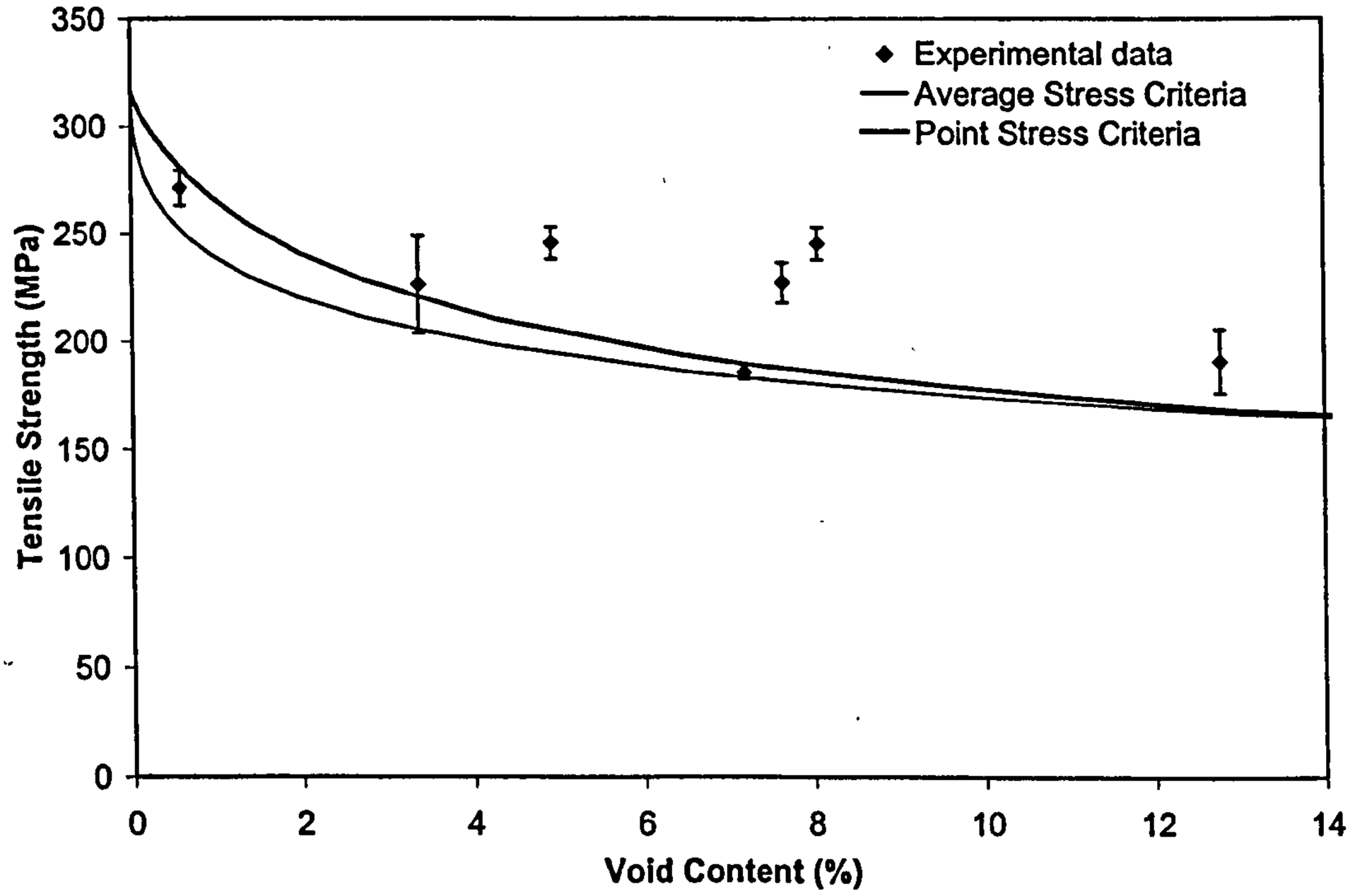

Figure 6.2 Comparison between measured tensile strength, point stress criterion and average stress criterion for different levels of void content on commingled glass/PP (material B) consolidated laminates, σ_∞=315 MPa.

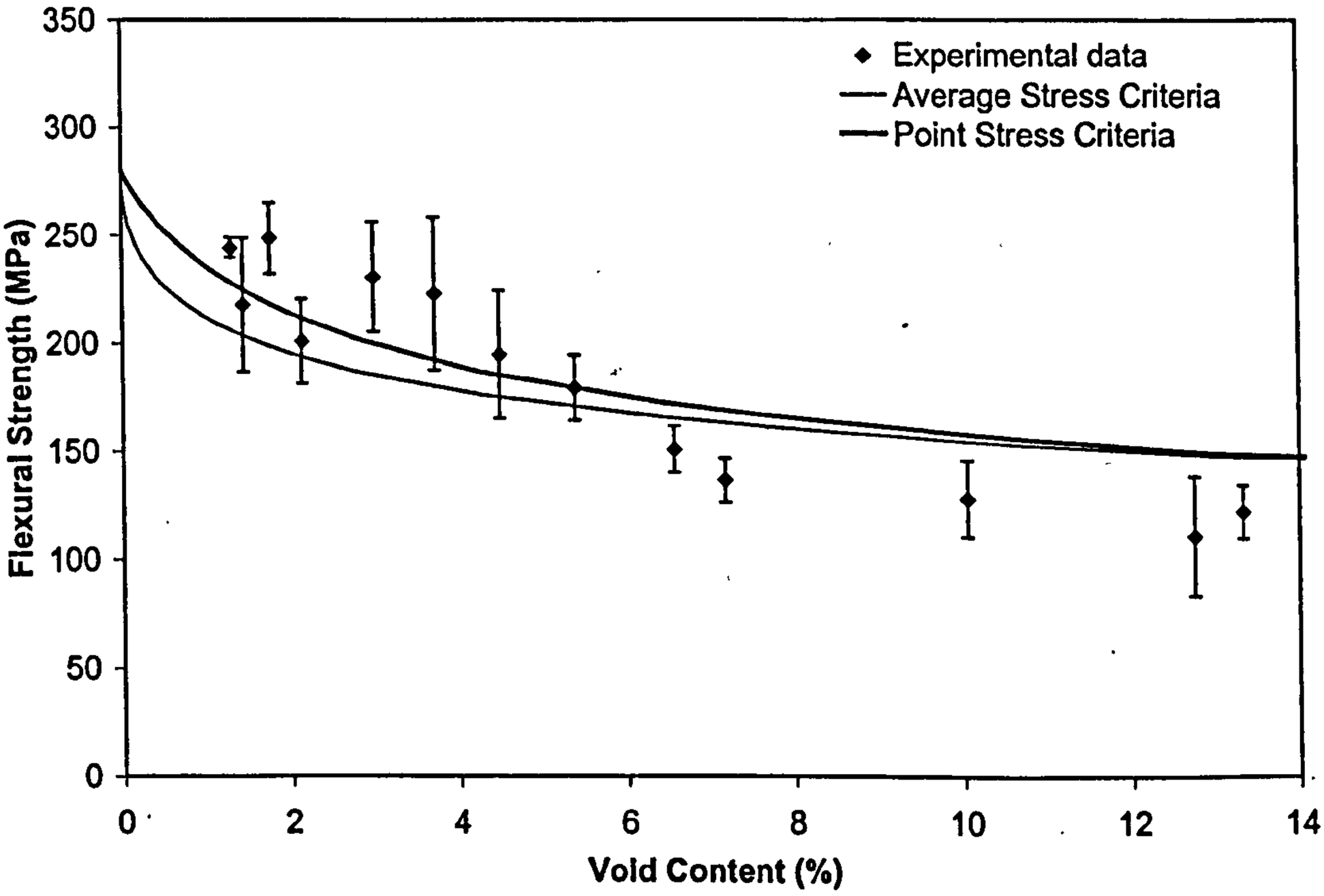

Figure 6.3 Comparison between measured flexural strength, point stress criterion and average stress criterion for different levels of void content on commingled glass/PP (material B) consolidated laminates, σ_∞=280 MPa.

Figures 6.2 and 6.3 show comparisons between the predicted and experimental strengths from these criteria. Values of ψ_1 and ψ_2 equal 25 μm and 60 μm respectively. These values were calculated as an average of the values that minimise the error between predicted and experimental data.

It is difficult to decide which model should be used because reasonable agreement between experimental data and predictions is observed for both criteria. However, the point stress criterion looks marginally better.

Although the Whitney stress criteria are intended for predicting the uniaxial tensile strength of composite laminates, the validity of the approach for flexural properties was initially dubious since a non-uniform distribution of voids could affect the results. However, such an effect was not observed during testing.

6.3 Theoretical analysis of the effect of deformation on mechanical properties

6.3.1 Laminate theory and failure stress criterion

In this section, classical laminate theory (CLT) is used to determine elastic behaviour and the maximum stress failure criterion is used to predict first ply failure of sheared flat plaques.

Balanced twill weave fabric is assumed to be composed of two unidirectional lamina (without considering crimping of the yarns), hence to calculate the behaviour of a composite laminate, mechanical properties of the constituent unidirectional lamina are required. The constants E_1, E_2, ν_{12} and G_{12} describe the elastic behaviour since the laminate is assumed to be thin, i.e. through-thickness and out of plane stresses are neglected. The micromechanical methods used to determine properties of unidirectional composite are well described by Hull **[108]** and Halpin **[109]**. Although several micromechanical methods are available **[109]**, their application to twill weave fabric would require a large amount of validation work for unidirectional lamina. Unfortunately, unidirectional laminae are difficult to produce from the

constituents in the textile composite used here; moreover, a simple micromechanical model based on the elastic properties of the constituents is desirable. The rule of mixtures is used to determine lamina stiffness in the fibre direction, E_1. A similar equation is used to find Poisson's ratio.

$$E_1 = v_f E_f + (1 - v_f) E_f \tag{6.5}$$

$$\upsilon_{12} = v_f \upsilon_f + (1 - v_f) \upsilon_m \tag{6.6}$$

Halpin-Tsai equations are used to calculate transverse stiffness.

$$E_2 = \frac{E_m (1 + \xi \eta v_f)}{(1 - \eta v_f)} \tag{6.7}$$

where

$$\eta = \frac{\left(\frac{E_f}{E_m} - 1\right)}{\left(\frac{E_f}{E_m} + \xi\right)} \tag{6.8}$$

Although the parameter ξ is usually calculated experimentally, the difficulties to produce unidirectional lamina required the use of a value suggested by Halpin **[109]**, $\xi = 2$.

For the constituent phases of the composite (i.e. isotropic glass and polypropylene), the shear modulus is calculated as:

$$G = \frac{E}{2(1 + \upsilon)} \tag{6.9}$$

Subsequently, the Halpin-Tsai equations are used to find the shear modulus of the composite using $\xi = 1$, as suggested by Halpin **[109]**.

$$G_{12} = \frac{G_m(1+\xi\eta v_f)}{(1-\eta v_f)} \tag{6.10}$$

where

$$\eta = \frac{\left(\frac{G_f}{G_m}-1\right)}{\left(\frac{G_f}{G_m}+\xi\right)} \tag{6.11}$$

Similarly, micromechanical approaches were taken to define the strength of a unidirectional lamina. Since most long fibre composites have fibre volume fractions between 30% and 70%, it is evident that the fibre strength is dominant in determining the axial strength of the composite. Hence, the on-axis tensile failure stress, σ_{1u}, can be determined using the relationship in Eqn. 6.12, derived from the rule of mixtures,

$$\sigma_{1u} = v_f \sigma_{fu} \tag{6.12}$$

where σ_{fu} is the failure stress of the fibre reinforcement. In determining the transverse failure stress, a method was used which assumes that fibres make no positive contribution, but in fact weaken the material. The relationship is defined by Eqn. 6.13, and has been shown to give reasonable agreement with experimental data [1].

$$\sigma_{2u} = \sigma_{mu}\left[1-2\left(\frac{v_f}{\pi}\right)^{\frac{1}{2}}\right] \tag{6.13}$$

No micromechanical model is implemented to calculate the shear failure stress. Instead a constant value from manufacturer's data is used (τ_{12u}=22.5 MPa).

When lamina are bonded together forming a laminate, interactions occur between the layers such that further theory is required to predict the response to an applied load. Classical laminate theory (CLT) is used, and the implementation is described below.

To predict the mechanical behaviour of flat plaques of a single layer of fabric sheared by an angle θ°, the material was analysed as a laminate composed of two lamina at ±(90-θ)/2° to the loading direction. Hence for a laminate made from three layers of woven fabric, six laminae are present. For a laminate comprising lamina with orthotropic symmetry in a plane stress state, i.e. $\sigma_3=\tau_{23}=\tau_{31}=0$, Eqn. 6.14 can be used to describe the elastic behaviour in terms of the laminate compliance matrix [S].

$$\begin{bmatrix}\varepsilon_1\\ \varepsilon_1\\ \gamma_{12}\end{bmatrix}=\begin{bmatrix}S_{11} & S_{12} & 0\\ S_{12} & S_{22} & 0\\ 0 & 0 & S_{66}\end{bmatrix}\begin{bmatrix}\sigma_1\\ \sigma_2\\ \tau_{12}\end{bmatrix} \qquad \textbf{(6. 14)}$$

Where

$$S_{11}=\frac{1}{E_1};\ S_{12}=-\frac{\upsilon_{12}}{E_1};\ S_{22}=\frac{1}{E_2};\ S_{66}=\frac{1}{G_{12}}$$

In order to determine the response to a load applied in an arbitrary direction, *x*, in the plane of the lamina, a transformation must be applied using an appropriate transformation matrix [T], defined in Eqn. 6.15.

$$[T]=\begin{bmatrix}c^2 & s^2 & 2cs\\ s^2 & c^2 & -2cs\\ -cs & cs & c^2-s^2\end{bmatrix} \qquad \textbf{(6. 15)}$$

$$\begin{bmatrix}\sigma_1\\ \sigma_2\\ \tau_{12}\end{bmatrix}=[T]\begin{bmatrix}\sigma_x\\ \sigma_y\\ \tau_{xy}\end{bmatrix} \qquad \textbf{(6. 16)}$$

Where $c=cos\ \phi$ and $s=sin\ \phi$ if ϕ is the angle between the loading (x) direction and the fibre (1) direction (in this case $\phi=\pm(90-\theta)/2$). This matrix is used to transform the stress matrix (Eqn. 6.16) and similarly the modified transformation [T'] defined in Eqn. 6.17 is used to transform the engineering strains from the loading axis system to the lamina axis system as in Eqn. 6.18.

$$[T']=\begin{bmatrix} c^2 & s^2 & cs \\ s^2 & c^2 & -cs \\ -2cs & 2cs & c^2-s^2 \end{bmatrix} \tag{6.17}$$

$$\begin{bmatrix} \varepsilon_1 \\ \varepsilon_2 \\ \gamma_{12} \end{bmatrix} = [T'] \begin{bmatrix} \varepsilon_x \\ \varepsilon_y \\ \gamma_{xy} \end{bmatrix} \tag{6.18}$$

To express the elastic behaviour of a lamina fully in terms of the stresses and strains in the loading direction, these matrices are concatenated to form the transformed compliance matrix [S_t] as indicated in Eqn. 6.19.

$$\begin{bmatrix} \varepsilon_x \\ \varepsilon_y \\ \gamma_{xy} \end{bmatrix} = [T']^{-1}[S][T] \begin{bmatrix} \sigma_x \\ \sigma_y \\ \tau_{xy} \end{bmatrix} = [S_t] \begin{bmatrix} \sigma_x \\ \sigma_y \\ \tau_{xy} \end{bmatrix} \tag{6.19}$$

The laminate compliance matrix is the inverse of the laminate stiffness matrix [C], i.e. $[S]=[C]^{-1}$. This relationship is required when calculating the behaviour of a laminate from the engineering constants and hence compliance matrices of the constituent lamina, since this is performed by the addition of the terms in the stiffness matrices with respect to their thickness according to Eqn. 6.20. Note that the summation includes $2n$ lamina since each fabric layer is modelled as two lamina.

$$C_{ij} = \frac{\sum_{k=1}^{2n} (C_{ij} h_k)}{\sum_{k=1}^{2n} h_k} \tag{6.20}$$

Once the stiffness matrix for the whole laminate, $[C_{lt}]$, is known then elastic behaviour can be described, and the engineering constants for the laminate obtained by finding the matrix inverse of $[C_{lt}]$, which is equal to $[S_{lt}]$, and using the relationships used to define the compliance matrix in Eqn. 6.14. To determine the failure behaviour, the principal stresses in each of the lamina must be determined. Since it is assumed that the strains in the loading axis system are equal in each layer, the strain in the lamina axis system for the k^{th} ply with its 1 direction at an angle ϕ from the loading x direction can be found using Eqn. 6.21.

$$\begin{bmatrix} \varepsilon_{1k} \\ \varepsilon_{2k} \\ \gamma_{12k} \end{bmatrix} = [T'] \begin{bmatrix} \varepsilon_x \\ \varepsilon_y \\ \gamma_{xy} \end{bmatrix} \tag{6.21}$$

This result would enable the use of a strain based failure criterion, but to enable the use of a stress based criterion the stresses in the ply can be found from the strains using the stiffness matrix for that ply as in Eqn. 6.22.

$$\begin{bmatrix} \sigma_{1k} \\ \sigma_{2k} \\ \tau_{12k} \end{bmatrix} = [C]_k \begin{bmatrix} \varepsilon_{1k} \\ \varepsilon_{2k} \\ \gamma_{12k} \end{bmatrix} \tag{6.22}$$

A vast number of predictive failure theories for composite laminates are currently available. Since the early 90's several experts have tried to compare them with each other in a study known as the World-Wide Failure Exercise. As a result, two special editions of Composites, Science and Technology have been produced and third issue is in-press **[110 - 111]**. However the maximum stress criterion is the most simple failure criterion and one of the most widely used failure theories. No consideration has been made of compressive or shear behaviour. The maximum stress theory states that failure occurs when at least one of the stress components along the principal material axis exceed the failure strength in that direction, Eqn. 6.23.

$$\sigma_1 \geq \sigma_{1u}$$
$$\sigma_2 \geq \sigma_{2u} \qquad \textbf{(6. 23)}$$
$$\tau_{12} \geq \tau_{12u}$$

Since the relationship between the stresses in the lamina axis system and those in the loading axis system is known, the criterion can be applied such that the stress in the x direction resulting in failure in a lamina within the laminate can be found. The input data used in the model is summarised in Table 6.1.

Table 6.1 Mechanical property model input parameters, with constituent properties supplied by Saint-Gobain Vetrotex.

Parameter	Glass fibre	Polypropylene	UD Lamina
Young's modulus, E_1(GPa)	73	1.6	26.5
Poisson's ratio, ν_{12}	0.22	0.35	0.3
Axial failure stress σ_{1u} (MPa)	2000	38	700
Transverse failure stress, σ_{2u} (MPa)		38	12.5
Shear failure stress τ_{12u} (MPa)			22.5[a]
Fibre volume fraction v_f			0.35

[a] Value for UD Twintex R PP75 1500 supplied by Vetrotex Saint-Gobain.

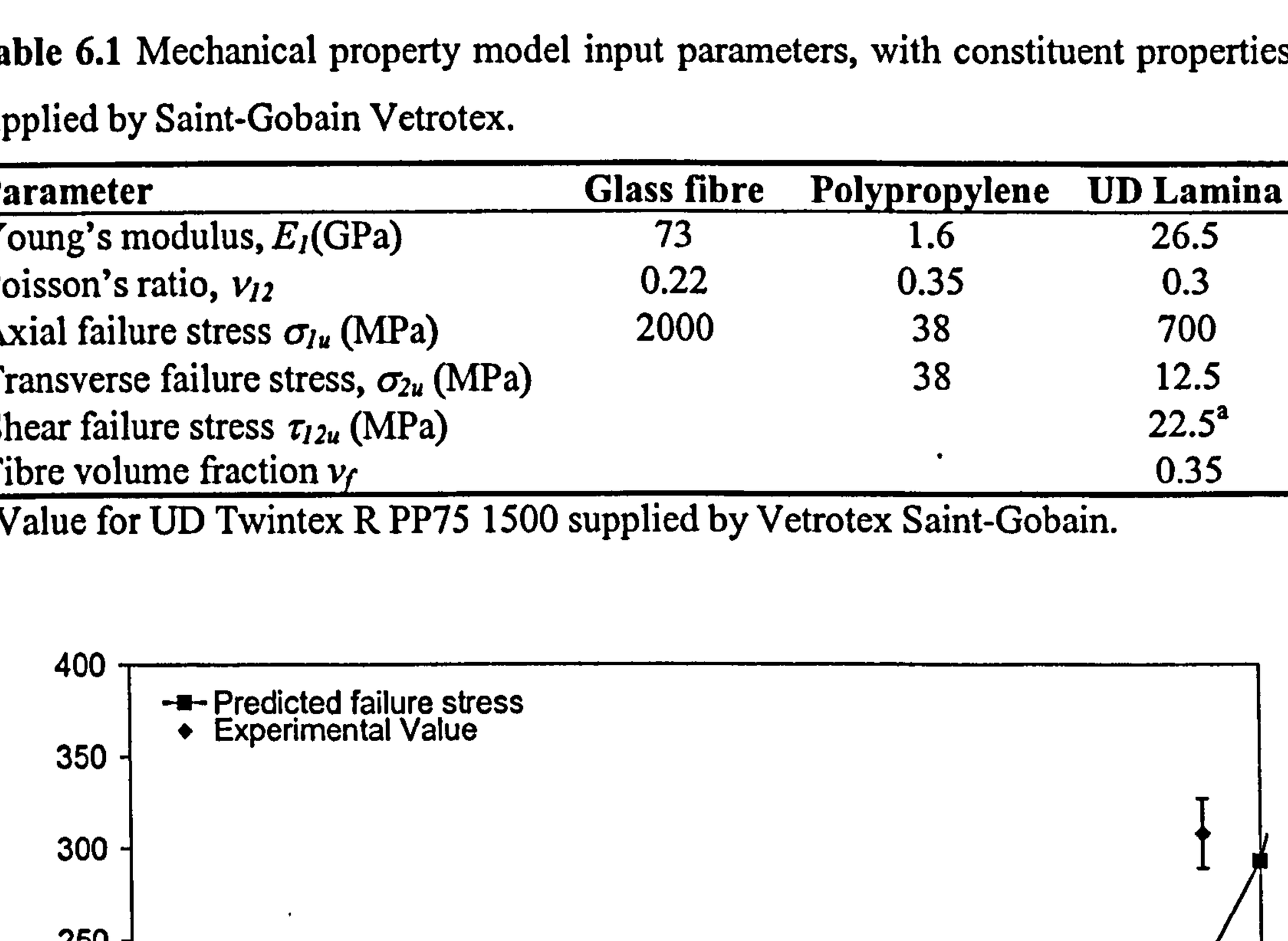

Figure 6.4 Comparison between the measured and predicted laminate failure stress of sheared glass/polypropylene plaques.

Figure 6.4 shows a comparison between the predicted and the measured tensile strength for the range of sheared flat plaques. Reasonable agreement between experiments and prediction is observed. The discrepancy can be explained by two considerations. Firstly, the maximum stress criterion does not consider any stress interaction under a biaxial state of stress and predicted initial failure values are compared with measured ultimate failure values. Secondly, fibre reorientation towards the loading direction was observed during testing. This matter is further analysed in Section 6.3.3. The observed fibre realignment led to an increase in shear angle and therefore, a higher predicted laminate failure stress can be expected. It should be noted that the predictions indicate that the failure mechanisms for $\theta>0°$ is shear failure while this becomes transverse failure for values of $\theta \leq 0°$, when using the values presented in Table 6.1.

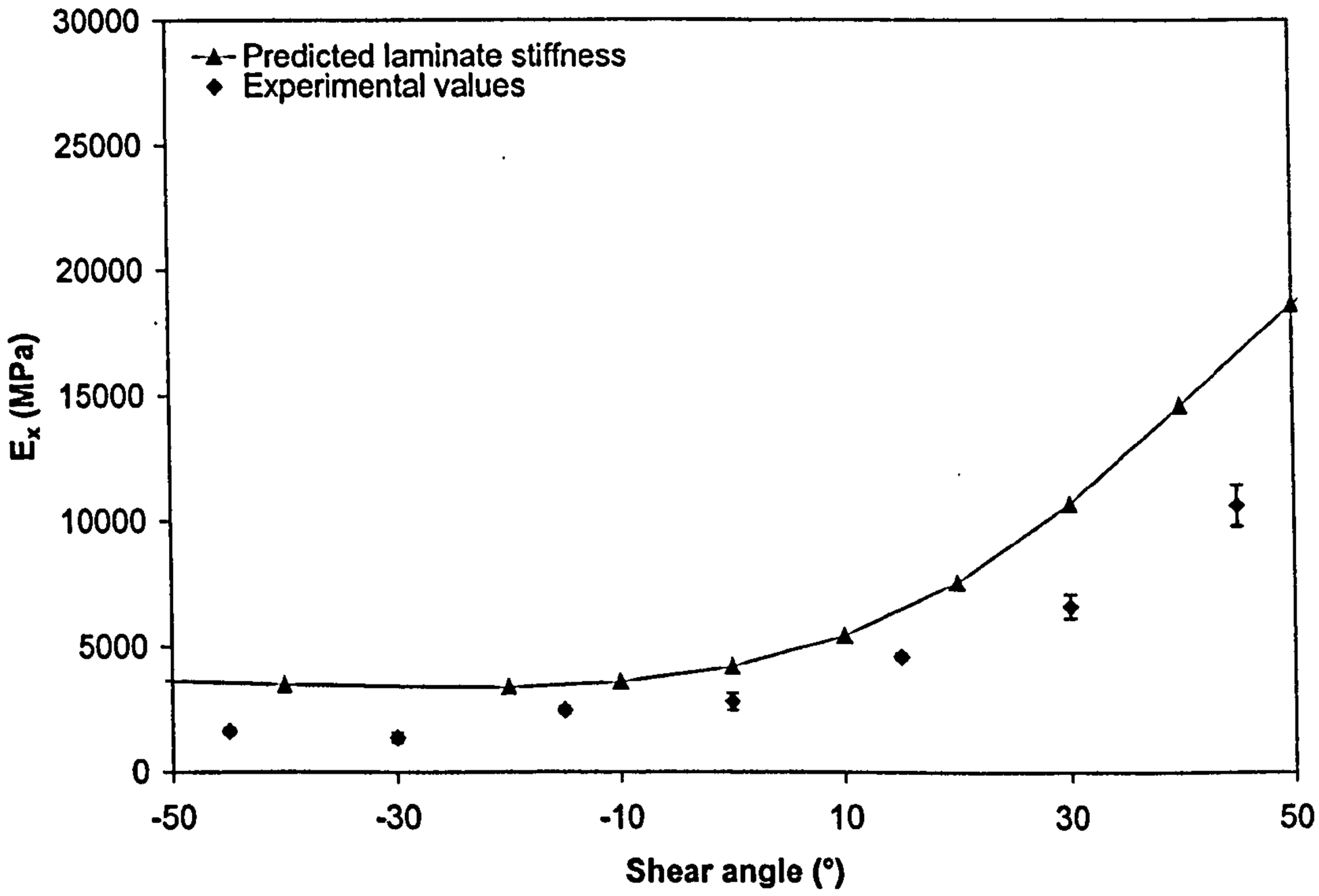

Figure 6.5 Comparison between the measured and predicted tensile modulus of sheared flat plaques.

Figure 6.5 show a comparison between experimental and predicted tensile modulus, calculated as $E_x = 1/S_{11}$. Although CLT overestimates the tensile modulus of the sheared flat plaques, the shapes of the predicted and experimental curves are similar.

CLT predicts an increase in the tensile modulus between –30° and –45° due to Poisson's effect. This trend matched that of the experimental results, where the tensile modulus of the flat plaques sheared by –45° is higher than the tensile modulus of the flat plaques sheared by –30°. The difference between measured and predicted tensile modulus may be due to fibre reorientation towards the loading direction or the undulations of the yarns typical of fabric materials. The effects of waviness are analysed in Section 6.3.2. CLT was more accurate for the case of un-crimped materials, as studied by Crookston et al. **[82]**.

The effect of void content on the predicted mechanical properties was also accounted for. A void content of 8.5% corresponds to a fibre volume fraction of 0.32. Figures 6.6 and 6.7 show the effect of reducing fibre volume fraction on predicted tensile strength and tensile modulus.

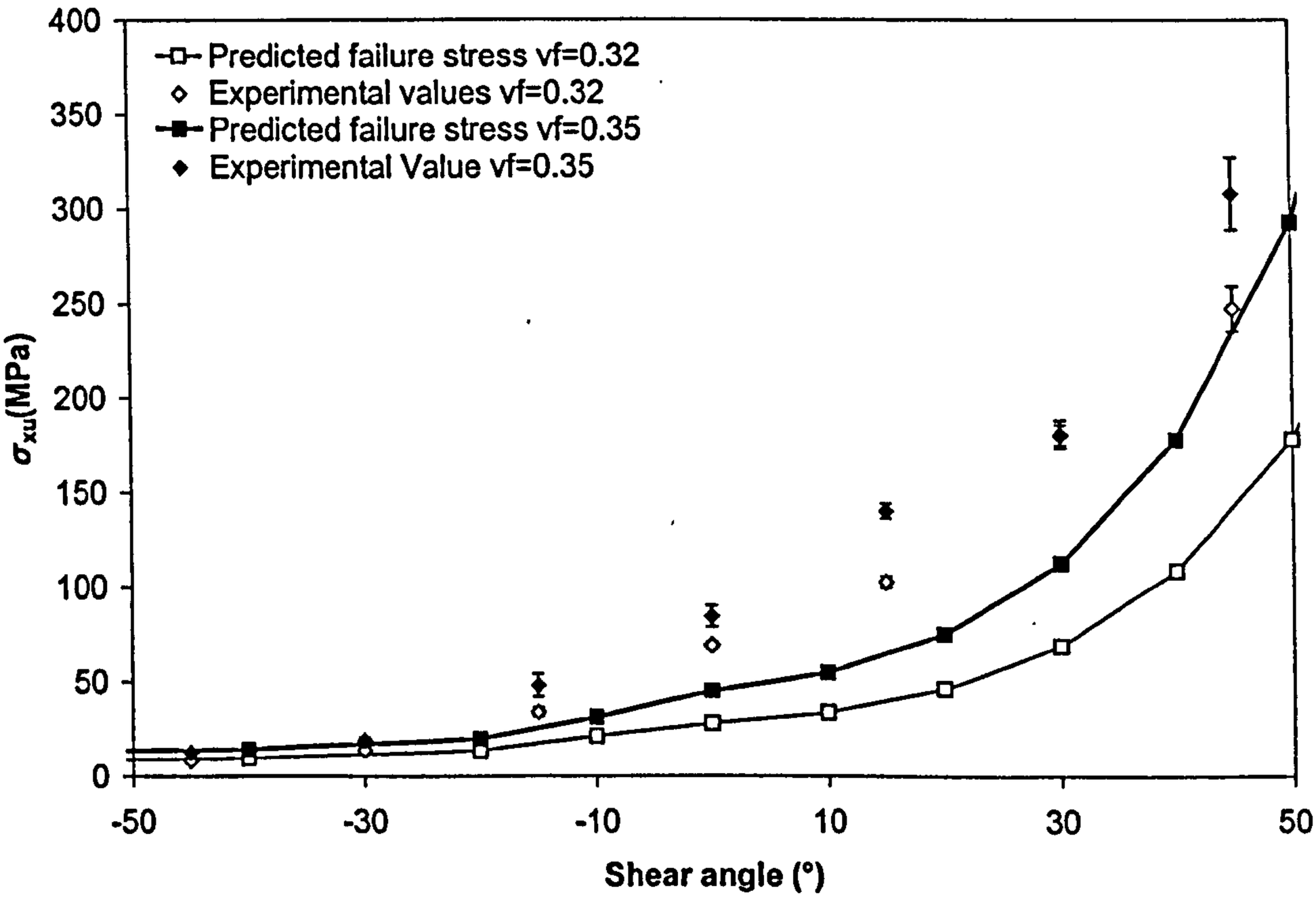

Figure 6.6 Comparison between the measured and predicted tensile strength of sheared flat plaques using Whitney point stress criteria and reduced fibre volume fraction.

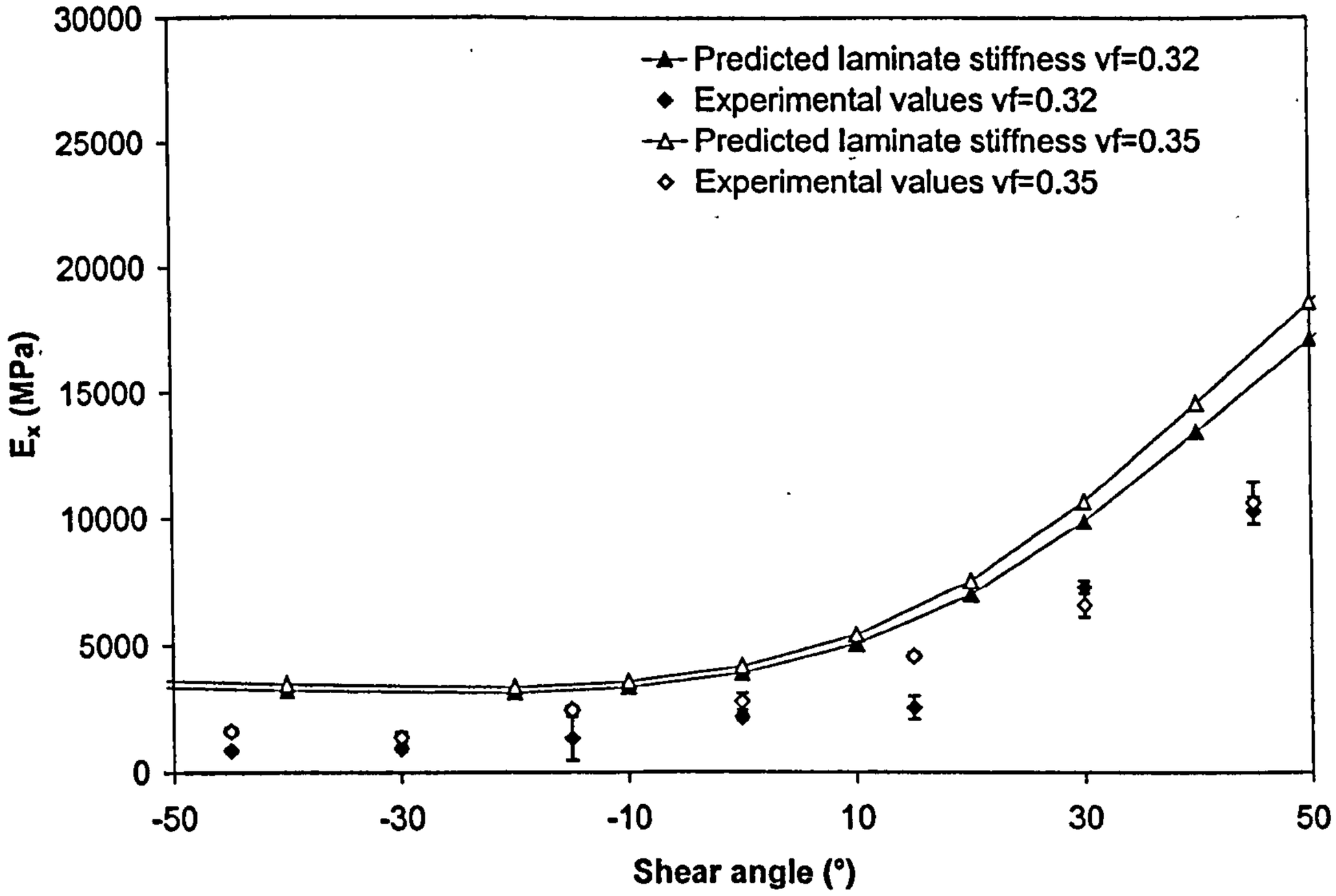

Figure 6.7 Comparison between the measured and predicted tensile modulus of sheared flat plaques with different void contents.

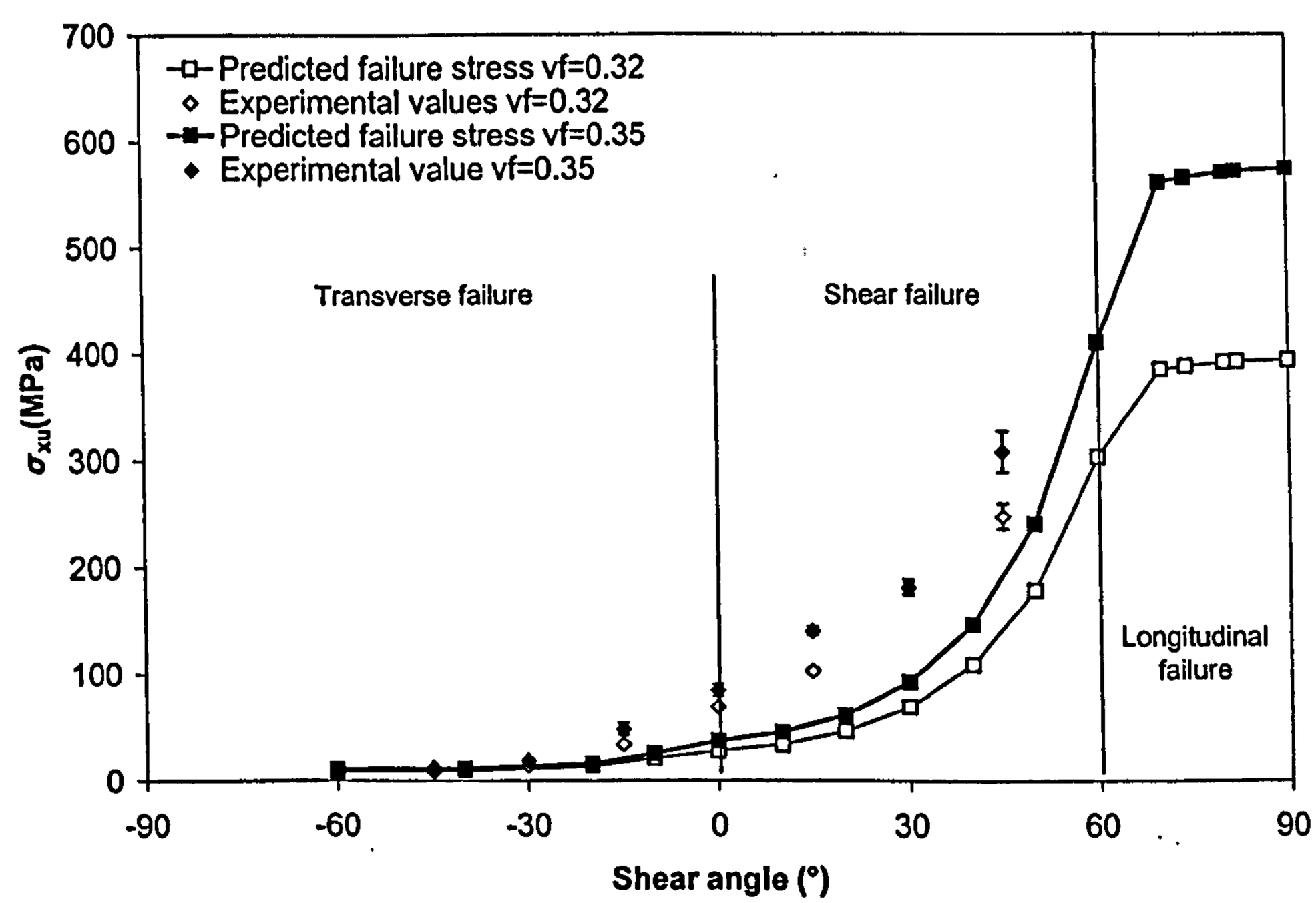

Figure 6.8 Comparison between the measured and predicted tensile strength of sheared flat plaques and changes in the failure mechanism.

Although reasonable agreement between measured and predicted tensile modulus for flat plaques with 8.5% void content is observed by just reducing the fibre volume fraction accordingly with the void content, the Whitney point stress criteria was also used to show the effect of void content on the tensile strength. Figure 6.6 shows that levels of void content around 8.5% significantly reduce the predicted tensile strength of sheared flat plaques similarly to the experimental observations.

Figure 6.8 shows a comparison between measurements and the predictions of tensile strength and the failure mechanism in different ranges of shear angle. For flat plaques sheared against the loading direction (negative shear), the predicted failure mechanism was transverse to the fibre direction. For flat plaques sheared towards the loading direction there are two predicted failure mechanisms. Flat plaques sheared by less than 60° are predicted to fail by shear failure and laminates sheared by more than 60° would fail by longitudinal failure.

6.3.2 Effects of fibre misalignment/waviness

Fibre waviness can occur in many types of reinforcement but is found mostly in woven fabrics due to the crimp between the warp and weft yarns. The simplest model presented in Chapter 2 uses the load bearing efficiency of the reinforcement based on Krenchel's [72] efficiency factor within the modified rule of mixtures:

$$E_1 = \eta E_f V_f + E_m(1 - V_f) \qquad (6.24)$$

The efficiency factor is based on the orientation of the fibres with respect to the direction of loading. The efficiency of a fibre path following a sine wave is described by:

$$\eta = \frac{1}{L}\int_0^{2\pi} \cos^3\theta dx \qquad (6.25)$$

Where the length of the fibre over one cycle is:

$$L = \int_0^{2\pi} \frac{1}{\cos\theta} dx \tag{6.26}$$

The angle subtended by the fibre with the longitudinal axis is:

$$\theta = \tan^{-1}\left[\left(\frac{2\pi}{\lambda}\right)\varsigma\cos\left(\frac{2\pi x}{\lambda}\right)\right] \tag{6.27}$$

The full derivation for the efficiency factor is provided by Turner [74].

Waviness is determined as the ratio between the amplitude ς, which is estimated as a quarter of the thickness of a fully consolidated laminate considering the middle section, and the wavelength λ (four times the tow-pitch of a 2x2 twill weave textile). For material B, $\varsigma = 0.125$ mm and $\lambda = 20$ mm. The laminate efficiency factor for a sinusoidal fibre distribution was calculated by integration of Eqn. 6.25 and has a value of 0.9969, which does not fully explain the difference between measured and predicted tensile modulus observed in Section 6.3.1.

6.3.3 Fibre reorientation during tensile testing

Section 4.4.3 stated that fibres realigned towards the loading direction during tensile testing of sheared flat plaques affecting the elastic behaviour of the laminate. Assuming that realignment corresponds to pure shear of the fabric within the laminate, fibre realignment can be calculated as a function of the strain and the initial shear angle. The rotation of the fibres during testing can be calculated as follows:

$$\Delta\phi = \sin^{-1}\left((1+\varepsilon)\cos\left(45+\frac{\theta}{2}\right)\right) - \left(45+\frac{\theta}{2}\right) \tag{6.28}$$

where $\Delta\phi$ is the rotation angle, θ is the initial shear angle and ε is the measured strain during testing.

Figures 6.9 and 6.10 show the fibre realignment or rotation of fibres during testing and after failure of both 0° and 30° sheared flat plaques consolidated by vacuum forming under 950 mbar. In the same charts fibre realignment is predicted using Eqn. 6.28.

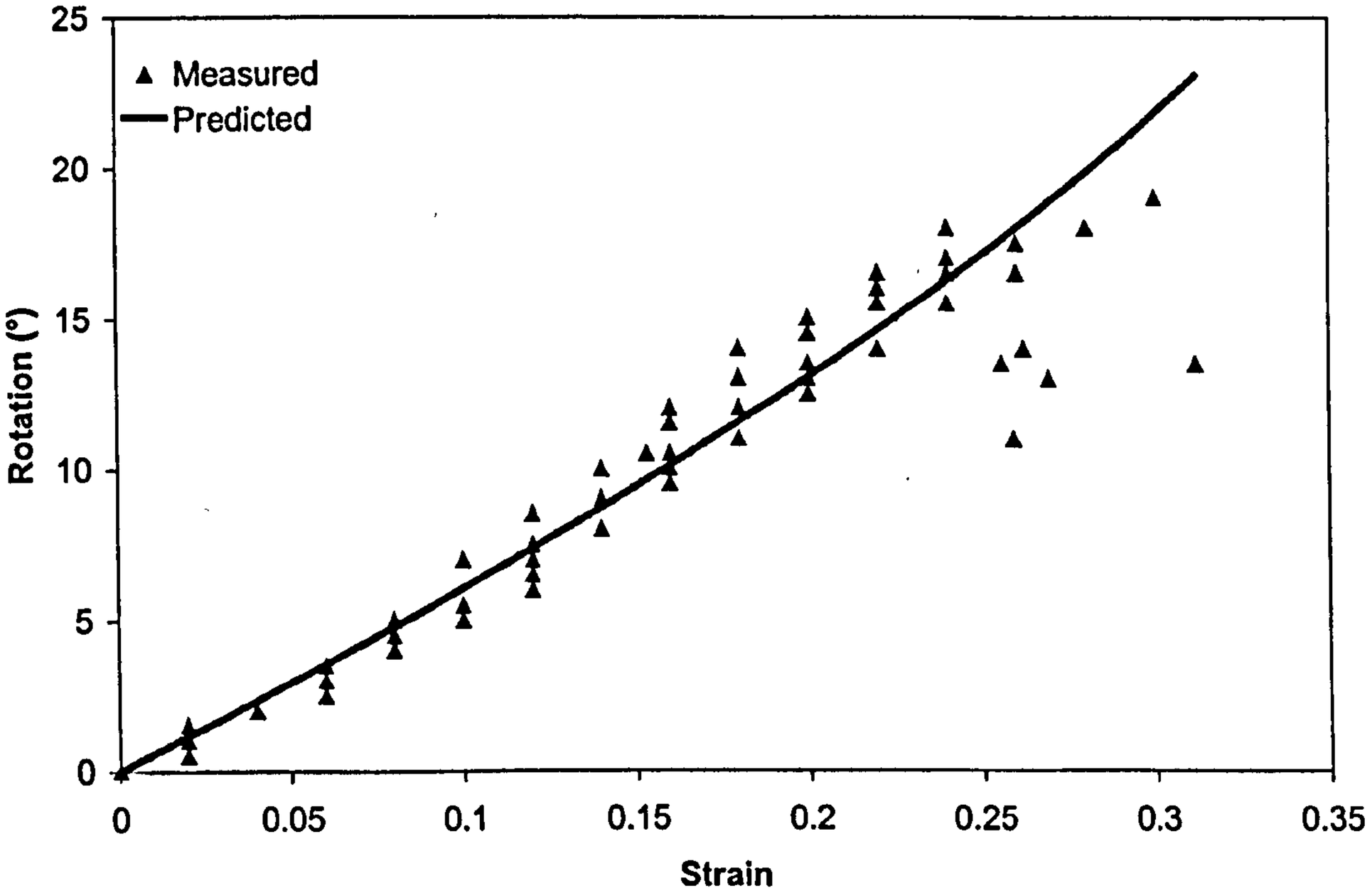

Figure 6.9 Measured and predicted fibre realignment of a 0° sheared flat plaque.

For flat plaques previously sheared by 0° (fibres at ±45° with respect to the loading direction) or less, fibre angle can be predicted by assuming pure shear as the main mechanism of deformation. For flat plaques previously sheared by an angle greater than 0° other mechanisms of deformation may inhibit the fibre realignment. However, the discrepancy is relatively small.

Void content has shown an important effect not only on the mechanical properties but also on the strain at failure (Figures 4.14 and 4.15). One could expect that high levels of void content produce generally higher strains inhibiting the ability of fibres to rotate. However sheared laminates with initial high shear angles showed that high void content produced a premature failure at a lower strain. In conclusion, fibre

realignment showed a clearer relation with the initial shear angle than with the strain at failure. This finding should be the subject for further investigation.

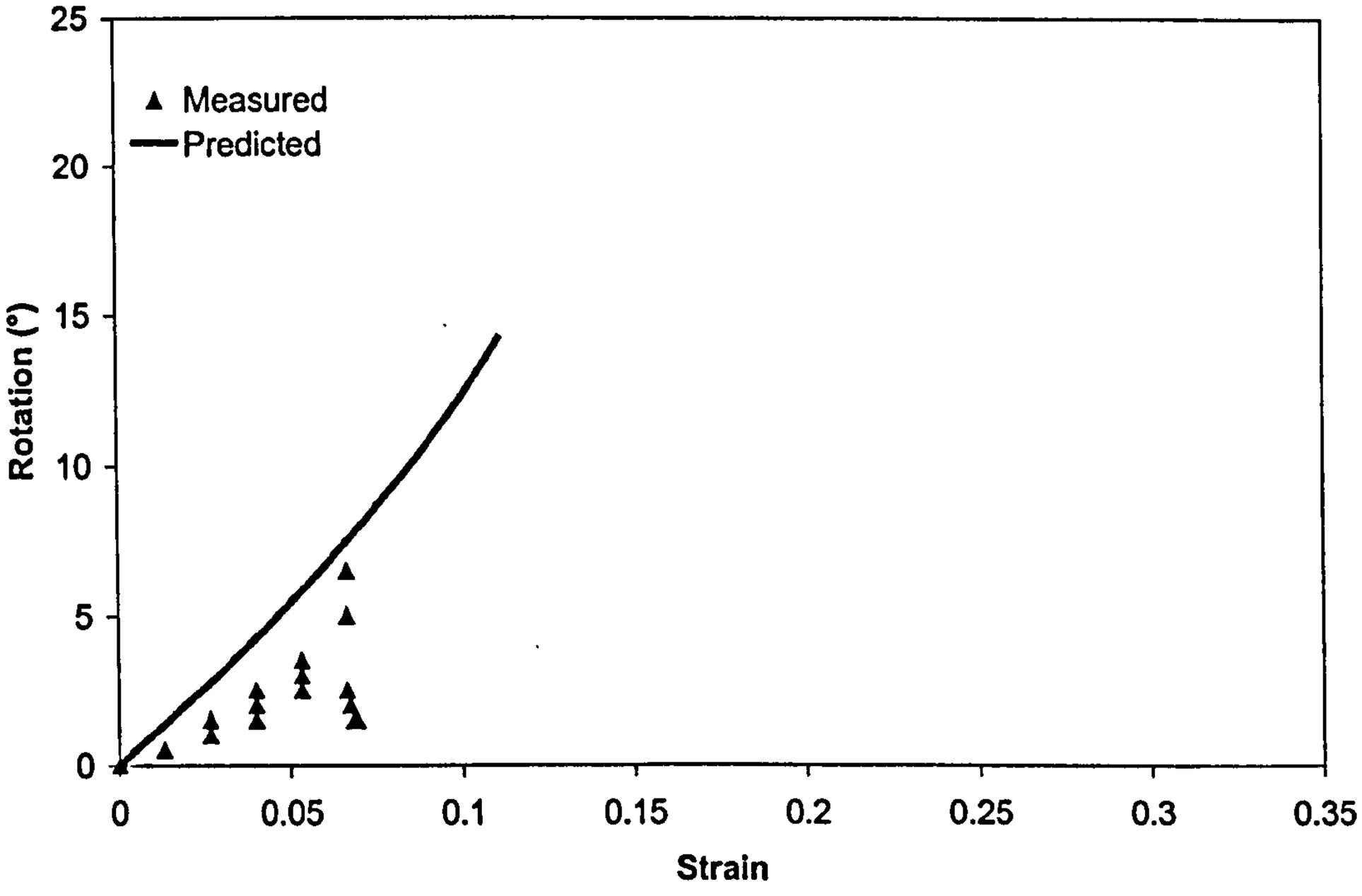

Figure 6.10 Measured and predicted fibre realignment of a 30° sheared flat plaque.

6.4 Conclusions

Two related criteria based on stress concentration for predicting the strength of laminated composites presented in Chapter 4 were discussed. The criteria resulted in a two-parameter model that is capable of predicting void content without resorting to classical concepts from linear elastic fracture mechanics. The two parameters are the strength of a fully consolidated laminate and a characteristic dimension. The use of such models has been demonstrated. Particularly encouraging is the use of the Whitney point stress criterion to predict the effect of void content on the tensile strength of sheared flat plaques. Excellent agreement between the measured and predicted effect of void content on tensile and flexural strength was observed for material B.

Chapter 4 also presented experimental data that showed the effect of in-plane shear on mechanical properties. Here, an approach was presented for modelling the elastic and failure behaviour of components manufactured from textile reinforced composite materials where the manufacturing process and component shape necessitate in plane deformation of the textile. A minimum amount of data from the constituent materials is required as input to these models. Balanced twill weave fabric was assumed to be composed of two unidirectional laminae neglecting the effect of crimp, hence micromechanical methods were used to determine properties of unidirectional laminae, with laminate properties obtained using classical laminate theory. Failure was predicted using the maximum stress failure criterion. Reasonable agreement between measurements and prediction were observed and the discrepancy was explained by fibre realignment with the loading direction and by the fact that predicted initial failure values were compared with measured ultimate failure values. Assuming that pure shear is the main mechanism of fabric deformation during tensile testing, the realignment of the fibres during testing observed in Chapter 4 was also predicted. Good agreement between measurements and predictions was observed.

7 Characterisation of Formed Materials

7.1 Introduction

In recent years, considerable effort has been dedicated to the development of analytical tools and computer codes capable of modelling forming of textile composites. To determine the validity of these simulations, it is necessary to compare predictions with experimental observations. However, such verification has been lacking, due to difficulty in obtaining measured data for the deformed fibre architecture. Kinematic draping simulations assume that the composite is deformed as a pin-jointed net with shearing of the yarns as the main mechanism of deformation. However, it is well know that other mechanisms of deformation are present during the draping of a textile composite over a component. For example, relative movement of the yarns may drastically alter the fibre pattern on the component.

This section is concerned with the fabric deformation during forming of complex components. The components used were a flanged hemisphere and a helicopter pilot helmet supplied by QinetiQ, both laid up by hand and consolidated under vacuum. The vacuum forming process was described in Chapter 3. One objective of this section is to study the effect of deformation on consolidation.

As stated in Chapter 3, the ASAME (Automated Strain Analysis and Measurement Environment) system allows the measurement of different parameters such as thickness, fibre pattern and extension ratios of formed materials. It is well known that kinematic drape models do not take slippage (relative movement between adjacent yarns) into account, thus comparisons between measured shear angles and those predicted by a kinematic drape model are carried out. The models used are described in the following section.

Materials used for these experiments were material B, material C and material D. The only major difference between prepreg materials (C and D) was the tow width

and spacing, with a 3.2 mm spacing weave used for the hemisphere (material C) and a 1.5 mm spacing weave used for the helmet (material D).

7.2 Drape Model

An existing draping model developed initially by Long **[112]** and extended by Souter **[113]** was used to study the deformation of textile composites over the surface of demonstrator components. This is a kinematic model based on geometric principles, where the textile composite is modelled as a pin-joined net that can only deform by pure shear. This pin-joined net is then mapped onto the tool surface following initial fibre paths (generator paths, see Figure 7.1a). Figure 7.1b shows the unique draped fibre pattern predicted by the kinematic drape model. This method is fully explained by Long **[112]**.

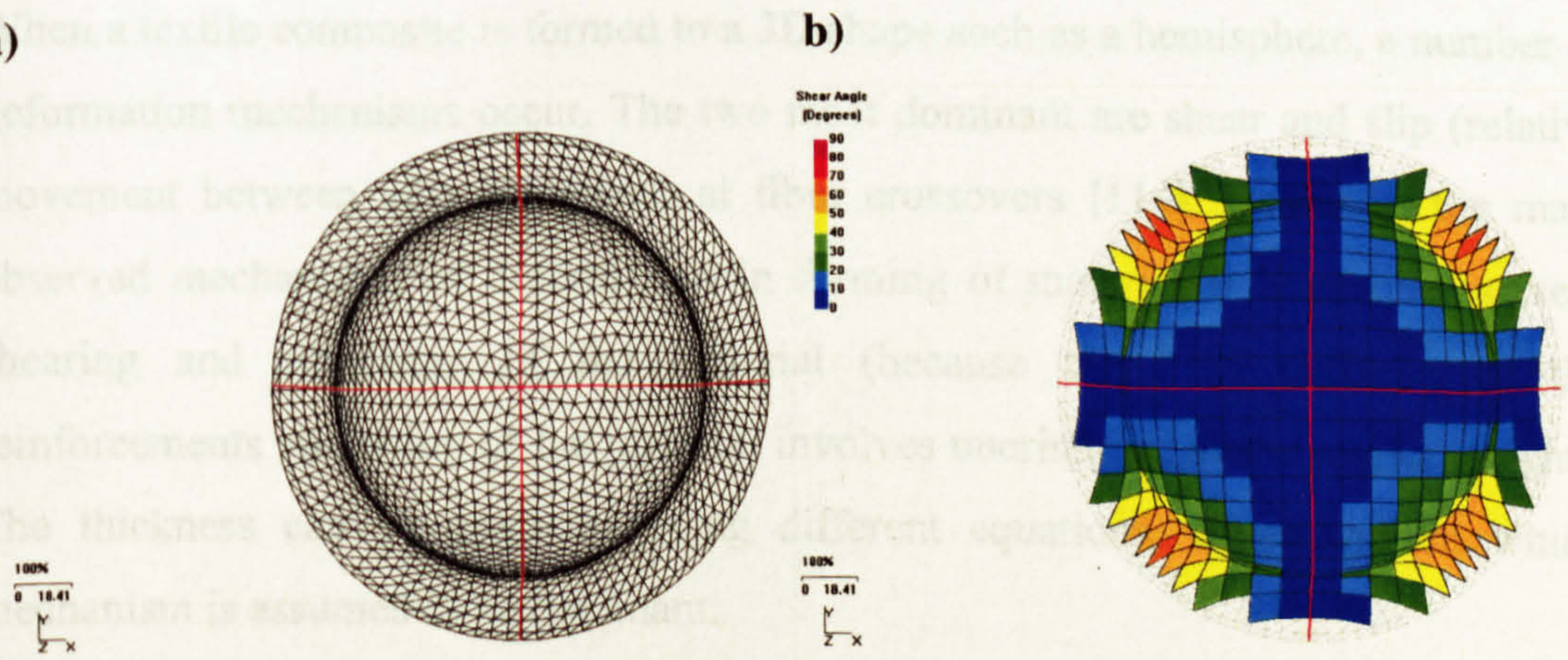

Figure 7.1 Illustration of kinematic drape model **a)** Initial geodesic generator paths, intersecting at first point of ply/tool contact **b)** Unique draped fibre pattern determined from these paths.

7.3 Hemisphere

Several hemispheres were formed using the non-isothermal vacuum forming technique at 180°C described in Chapter 3. The materials used in these experiments were a double layer material B laminate formed and consolidated in a female

hemisphere, whose dimensions are shown in Figure 7.2, and a single layer material C formed and consolidated in the same female hemisphere.

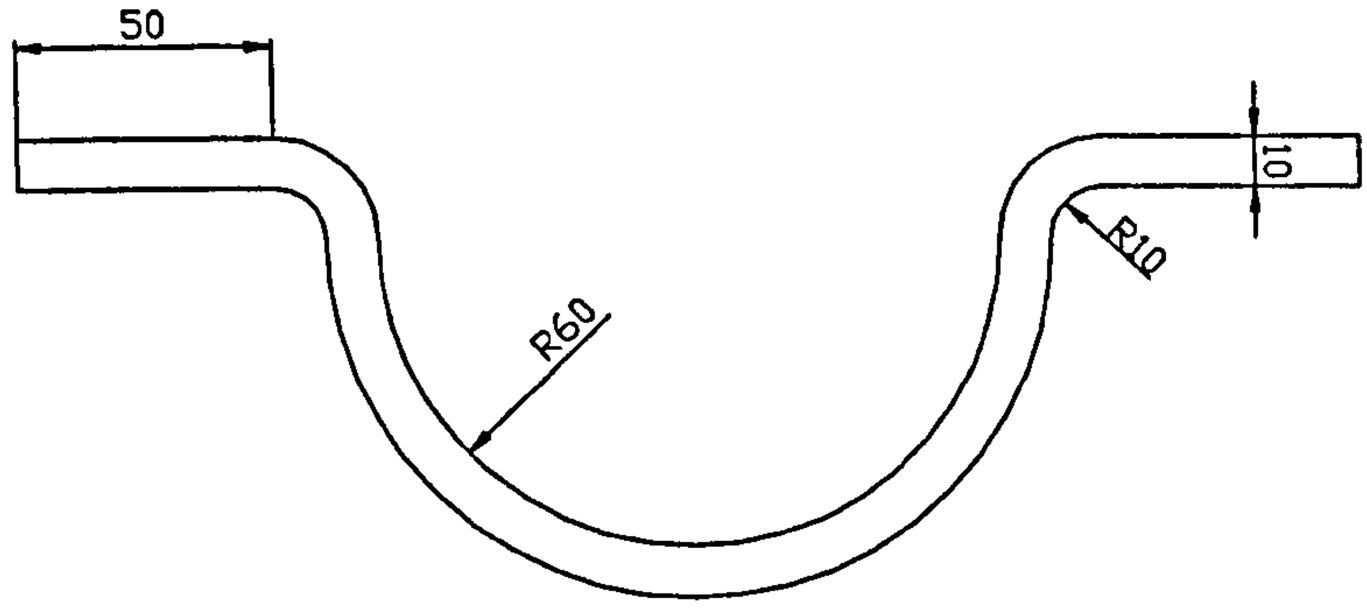

Figure 7.2 Dimensions of the female hemisphere used for non-isothermal consolidation of materials B and C.

7.3.1 Thickness

When a textile composite is formed to a 3D shape such as a hemisphere, a number of deformation mechanisms occur. The two most dominant are shear and slip (relative movement between adjacent yarns) at fibre crossovers **[114]**. However, the main observed mechanisms of deformation in forming of material B hemispheres were shearing and stretching of the material (because the high stiffness of the reinforcements stretching of the material involves uncrimping of the reinforcement). The thickness can be predicted using different equations, depending on which mechanism is assumed to be dominant.

Assuming conservation of material volume, and that the main mechanism of deformation is shearing of the fabric, the thickness h is defined by the well established Eqn 7.1:

$$h = \frac{h_0}{\cos\theta} \qquad (7.1)$$

Where h_0 is the initial thickness.

However, when stretching of the fabric through uncrimping of the yarns also occurs, the thickness can be defined as:

$$h = h_0 e^{-\varepsilon_1 - \varepsilon_2} \tag{7.2}$$

Eqn. 7.2 assumes constant volume and accounts for other deformation modes such as relative movement of the yarns because it is based on measured logarithmic values of the principal strains.

The thickness of the hemispherical mouldings along a path in the high sheared region (see Figure 7.3) was measured using a point micrometer to compare values with the predicted thickness based on different mechanisms of deformation. Thickness values under the thickness of a flat plaque with the same number of layers (1 mm) were measured in the pole region as a result of the lay-up. Figure 7.4 shows the measured and predicted (kinematic drape model) thickness of the material B hemisphere based on shearing in the same region as the measured values. Measured values were obtained using a point micrometer.

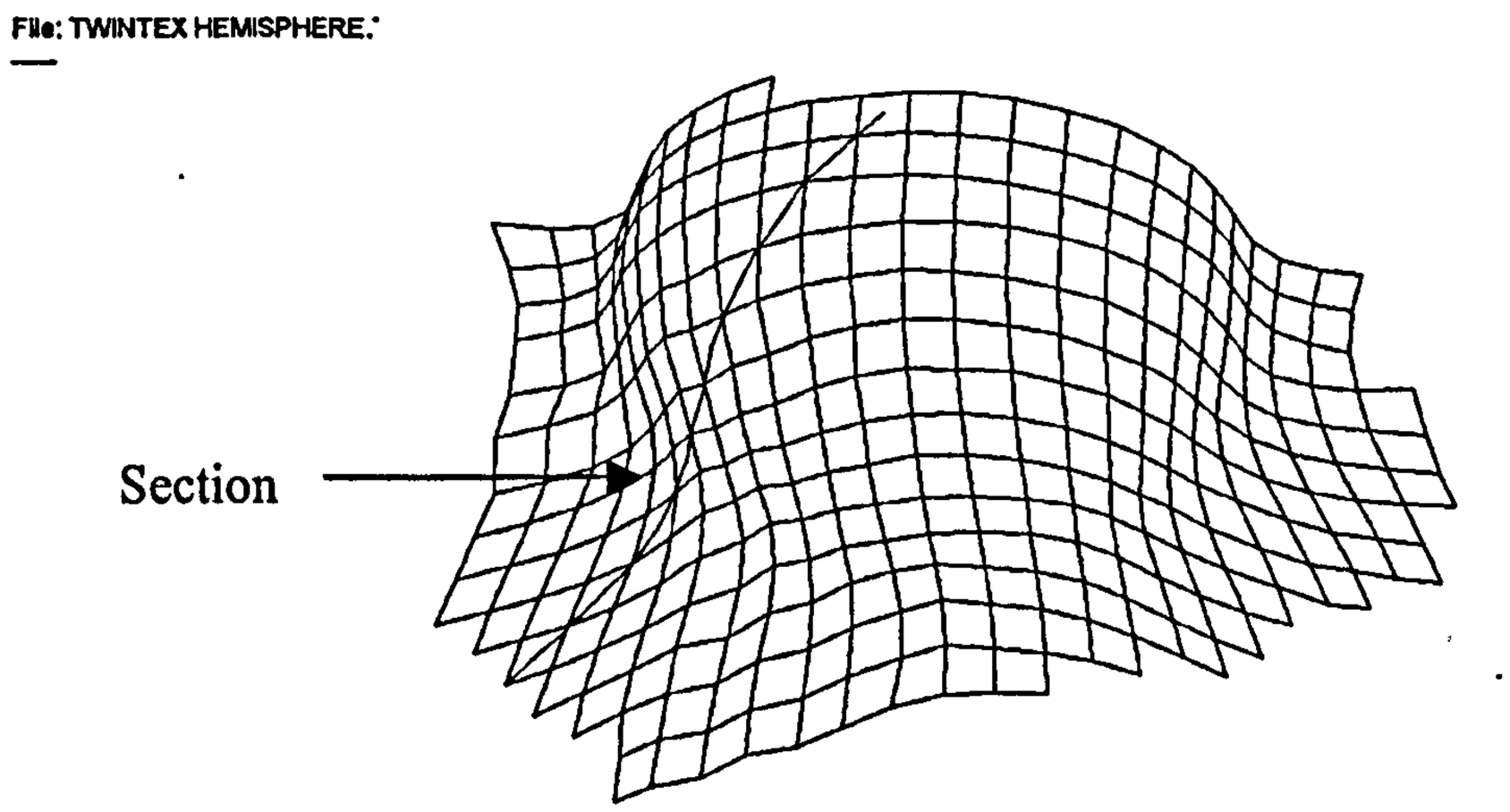

Figure 7.3 Path along the highly sheared region for material B hemisphere.

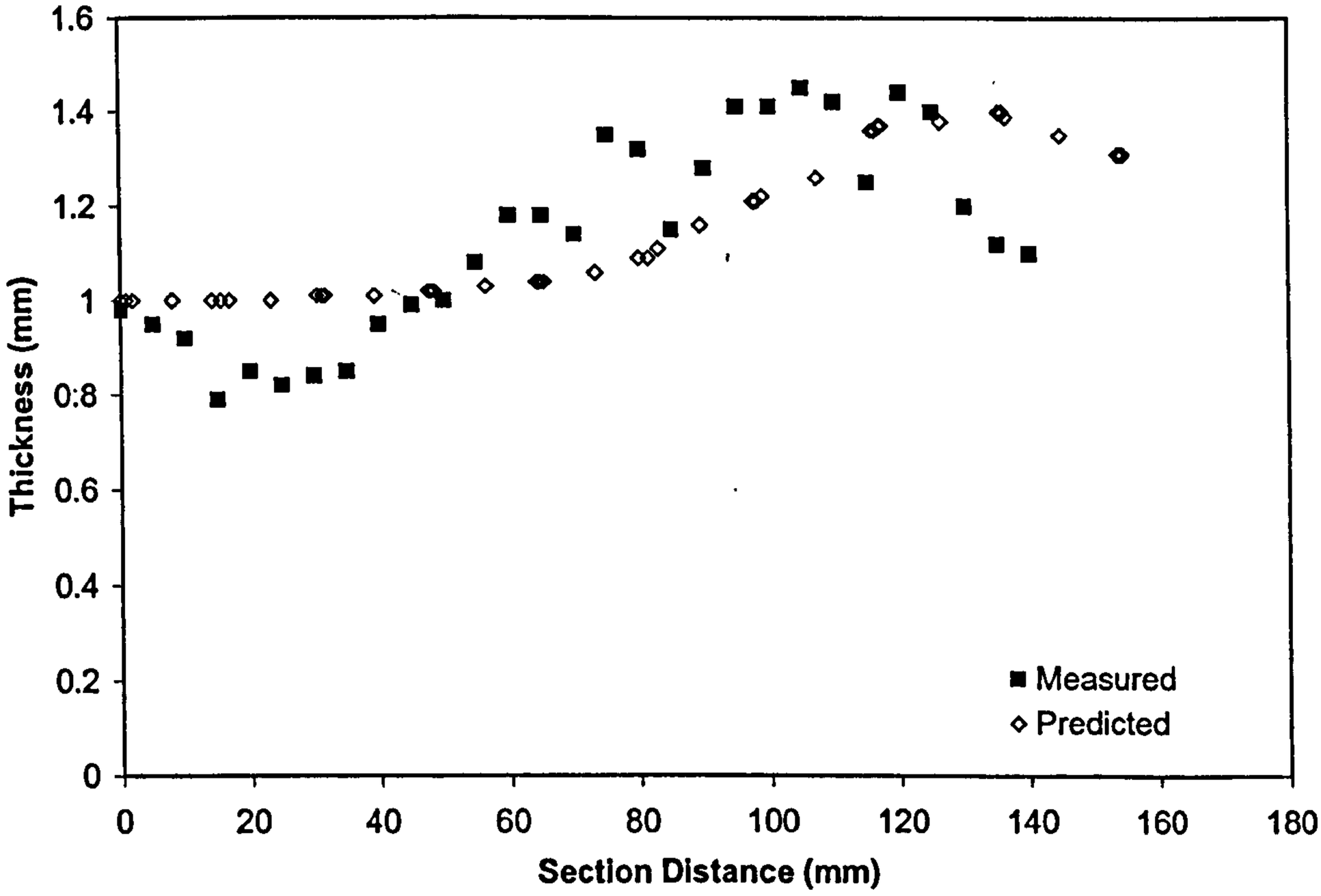

Figure 7.4 Thickness predicted for material B hemisphere based on shearing using computed values of shear angle. Section distance is measured from the pole of the hemisphere.

Figure 7.5 shows the same measured thickness and the predicted thickness when stretching occurs. Comparing the graphs, the predicted thickness based on principal strains shows better correlation with the measured thickness, particularly for values under 1mm (measured thickness of a fully consolidated flat plaques with the same number of layers). However, assuming that shearing is the dominant mechanism, the material thickness must always be greater than the initial thickness of the material.

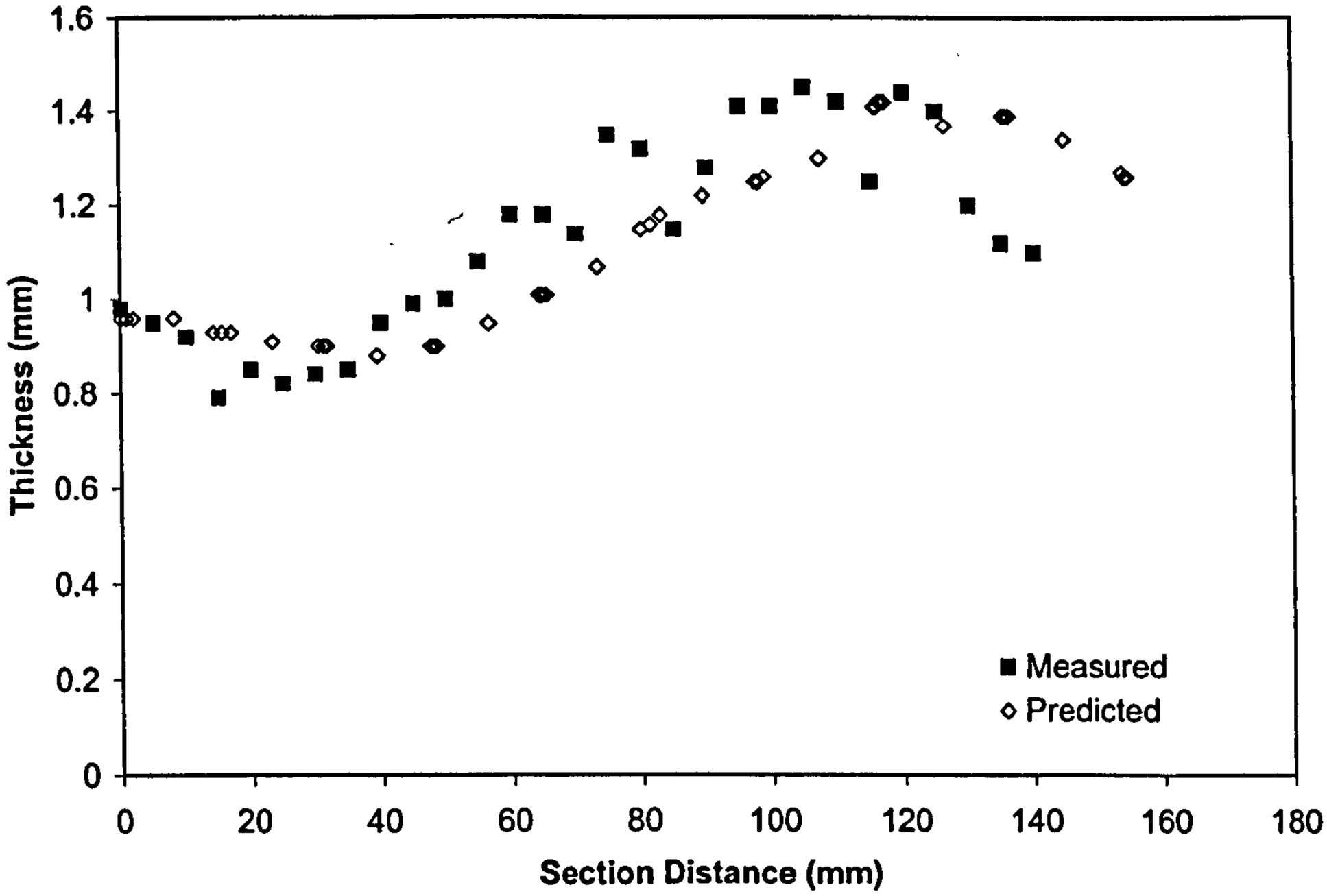

Figure 7.5 Thickness predicted for material B hemisphere based on stretching using computed values of true strain. Section distance is measured from the pole of the hemisphere.

7.3.2 Shear angle

Using the ASAME system described in Chapter 3, Figure 7.6 shows the shear angle distribution of material B on a hemisphere. Figure 7.7 shows the shear angle distribution for a hemisphere formed using prepreg AS4/8552 (material C). The distributions are reasonably symmetric between quadrants, and maximum shear occurs along the bias axis of each quadrant. However, prepreg appears to exhibit higher levels of shear than the commingled fabric in the highly deformed region. The maximum shear angle for the prepreg was 55°, compared to 46° for the commingled fabric. This difference may be due to the different fibre architecture between both materials. Further details are presented in the following section.

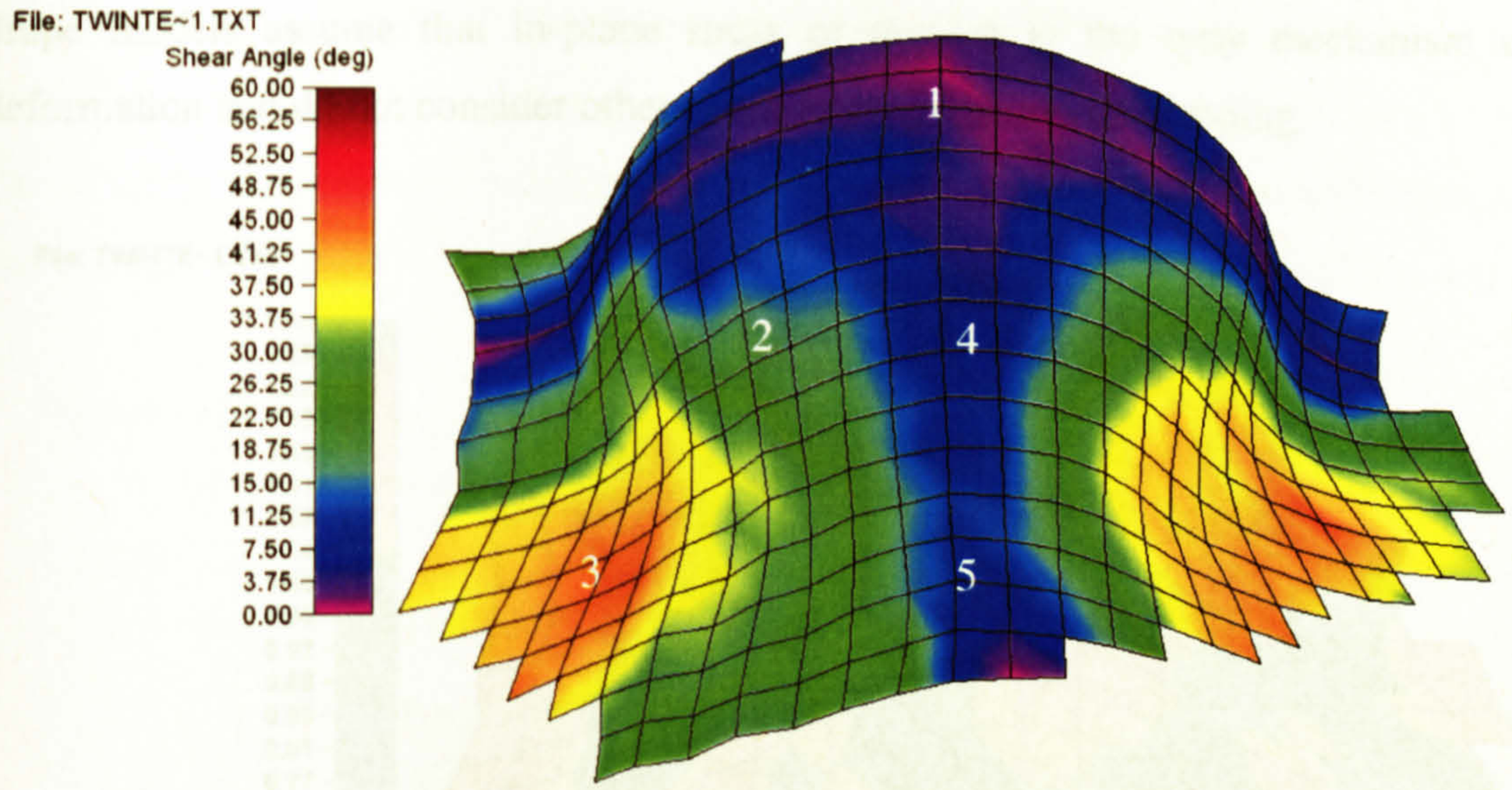

Figure 7.6 Shear angle distribution for material B hemisphere. Numbers indicate the locations of coupons analysed for void content.

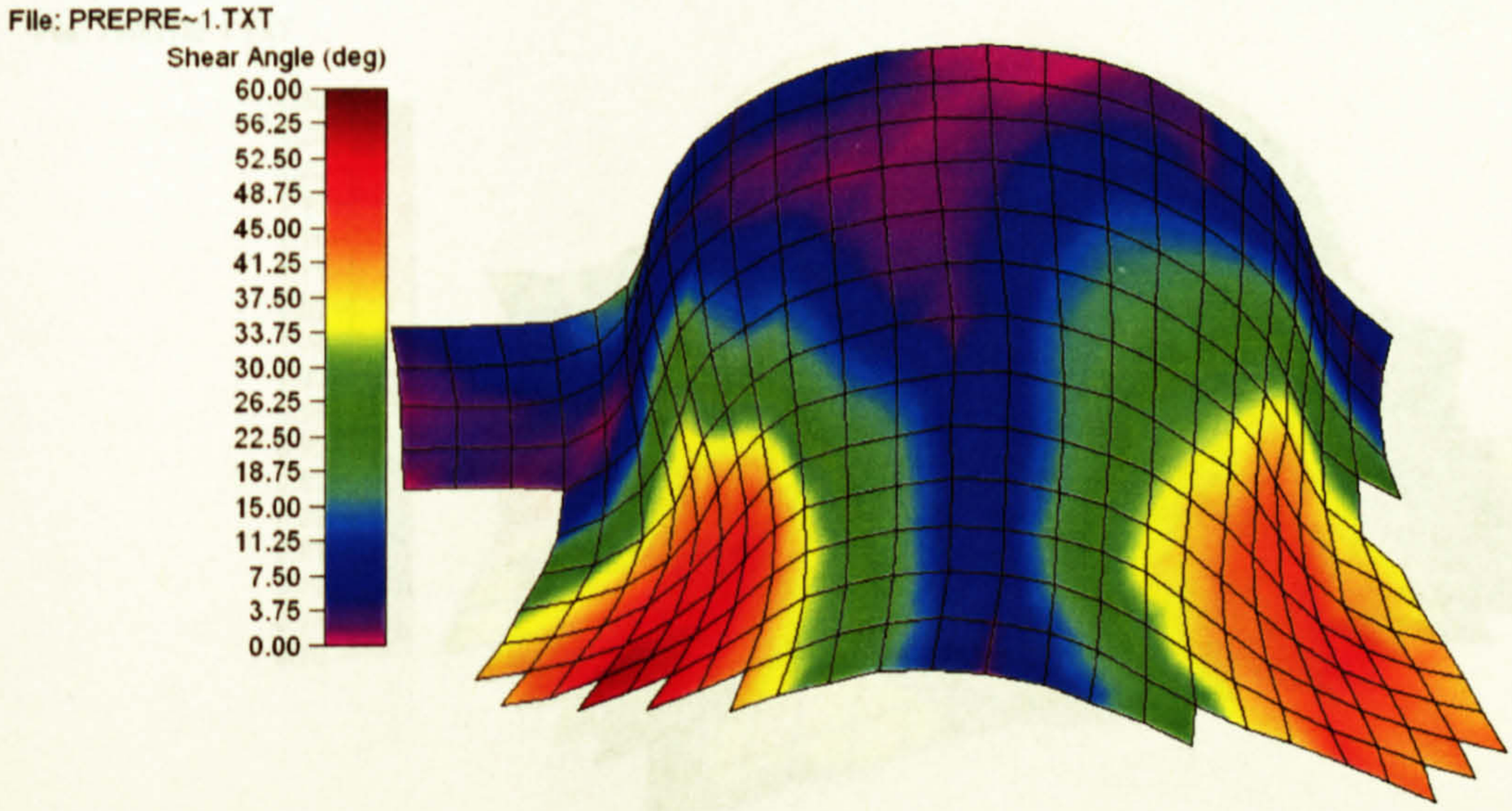

Figure 7.7 Shear angle distribution for material C on a hemisphere.

7.3.3 Extension ratio

This section is concerned with the deformation mechanisms during forming of a component. Extension ratio is defined as the ratio between the final and initial grid spacing, indicating relative displacement of adjacent tows during forming. It is measured in the fibre directions, denoted as direction x and direction y. Kinematic

drape models assume that in-plane shear of textiles is the only mechanism of deformation and do not consider others such as slippage and uncrimping.

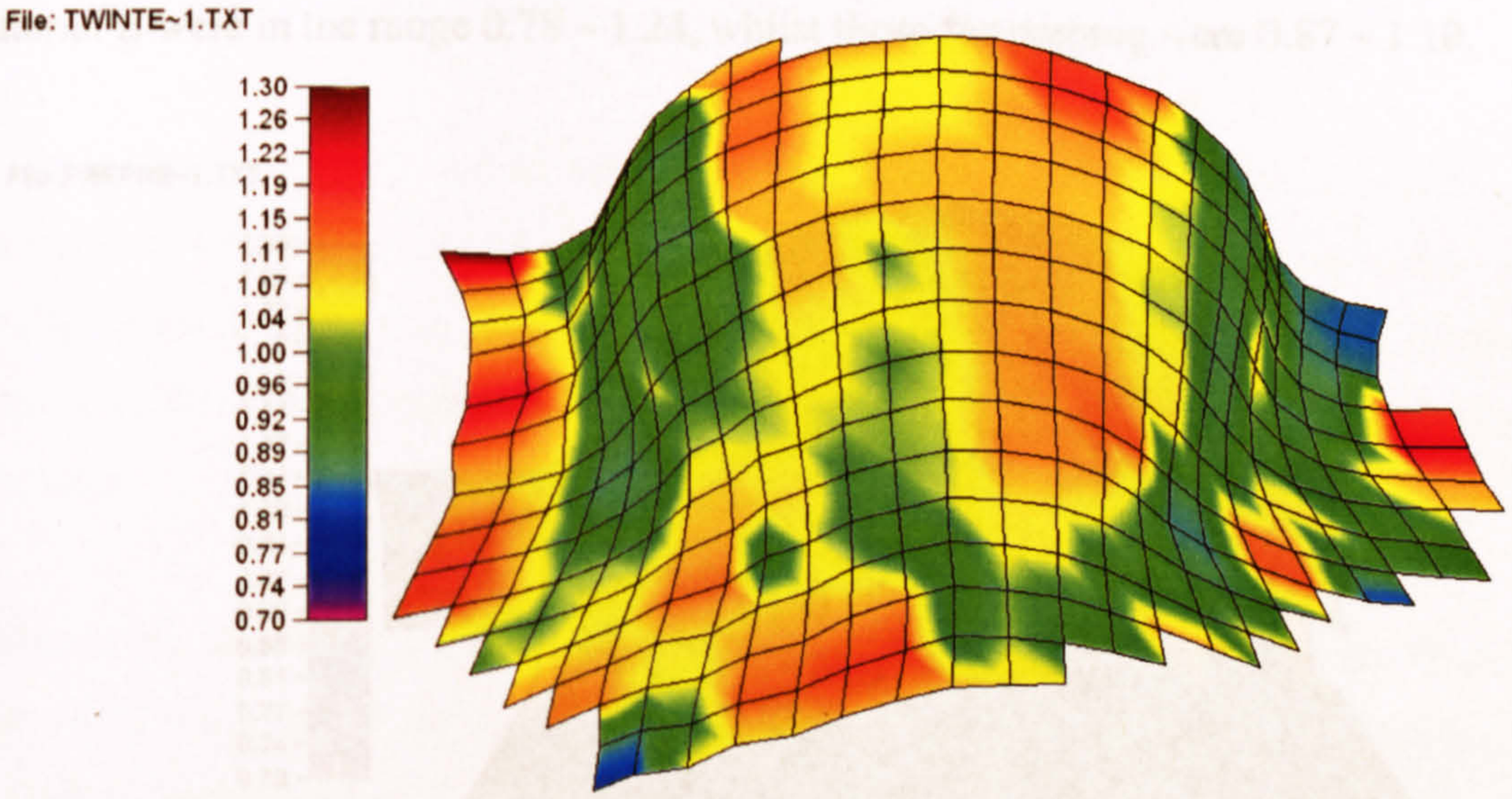

a)

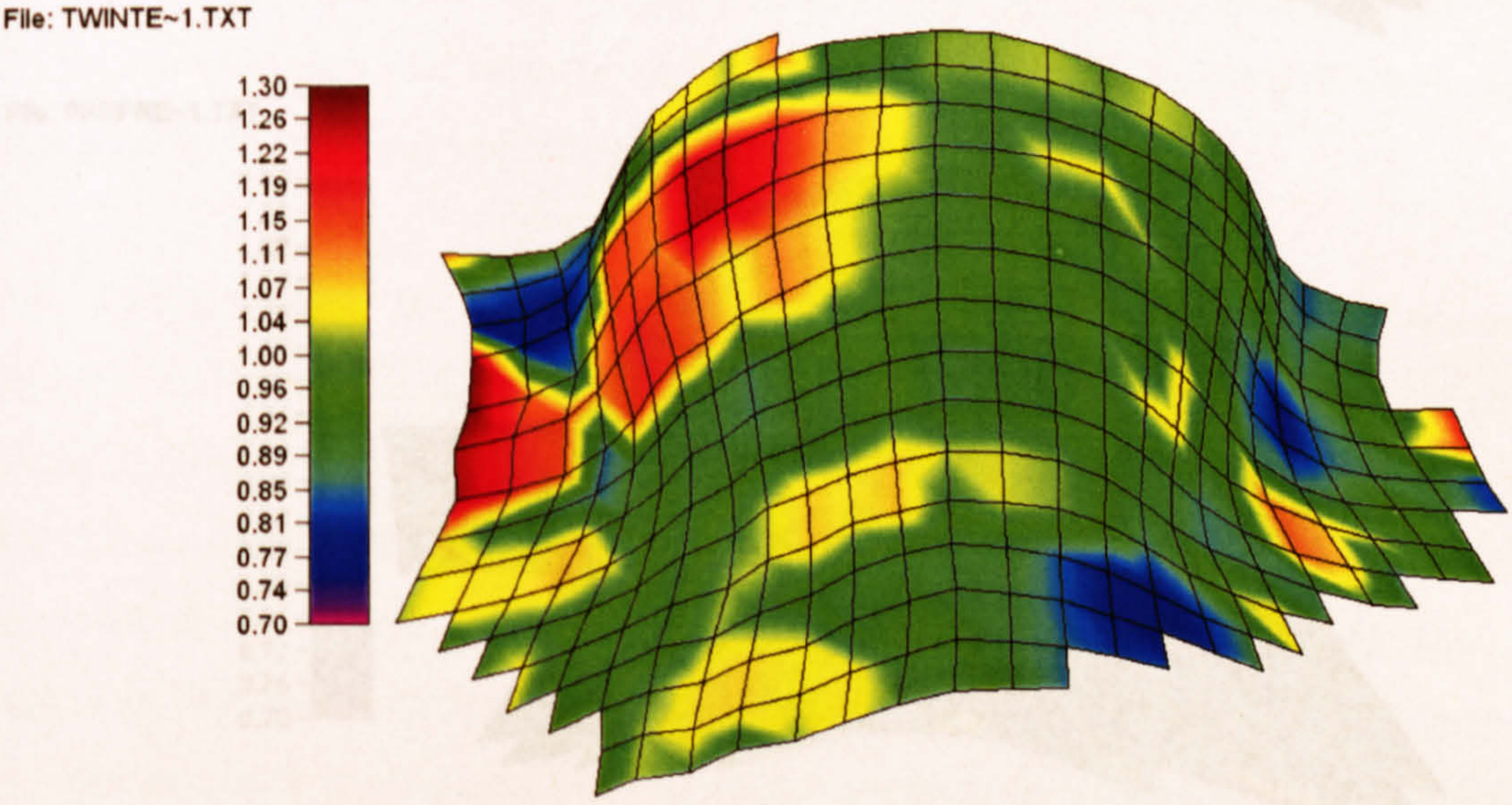

b)

Figure 7.8 Extension ratio distribution along both grid directions for a female hemisphere formed and consolidated using commingled fabric **a)** direction x **b)** direction y.

Figures 7.8 and 7.9 show the extension ratio distribution for a hemisphere formed and consolidated using material B and material C respectively. It is observed that the extension ratio is positive on the region close to the pole of the hemisphere and negative on the part close to the flange. Positive extension ratio is due to the lay-up

of the material over the tool. The material is pushed down into the tool leading to the uncrimping of the yarns in the region close to the pole. However yarns close to the flange are pushed together producing a negative extension ratio. Extension ratios for material B were in the range 0.78 – 1.24, whilst those for prepreg were 0.87 – 1.10.

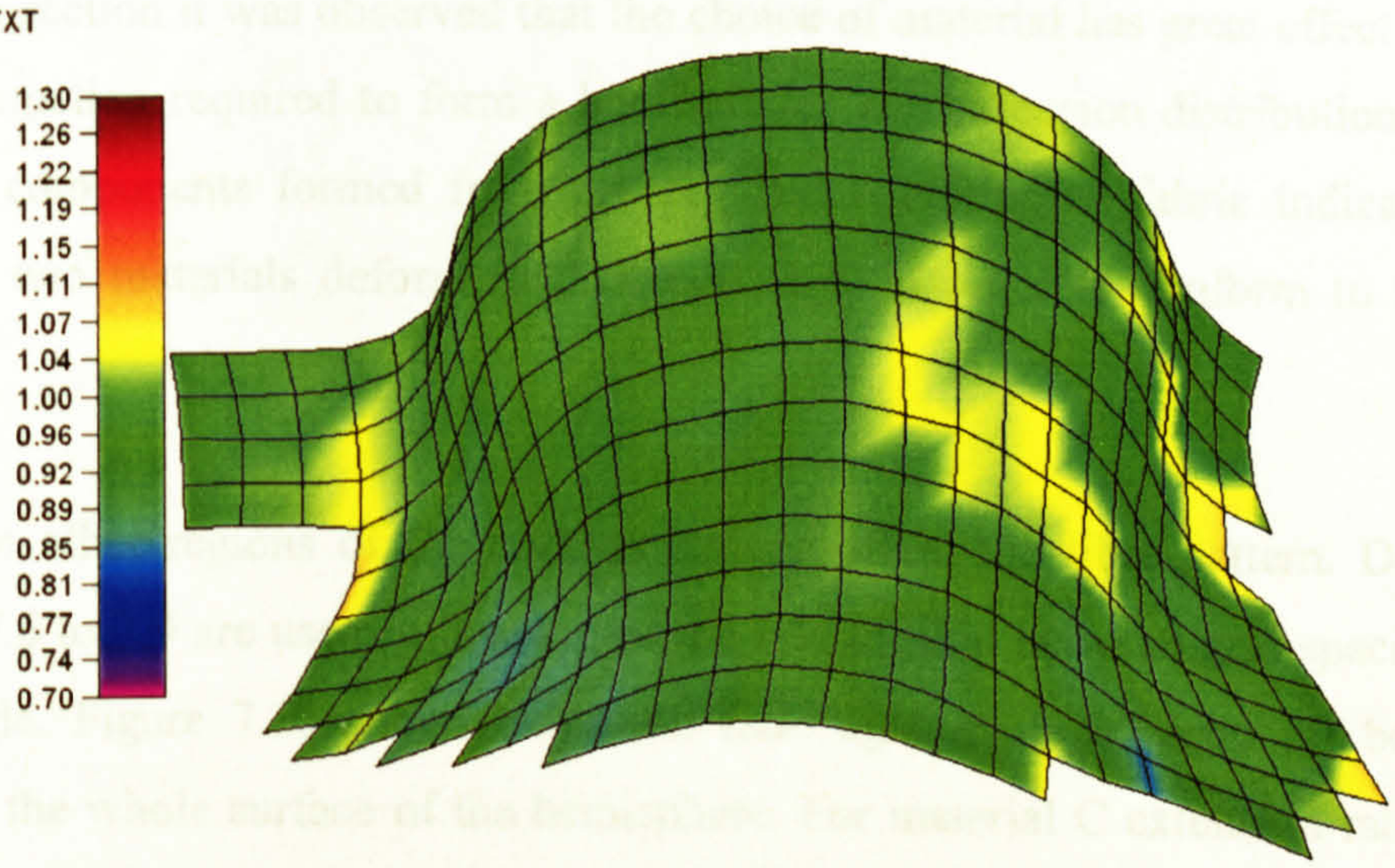

a)

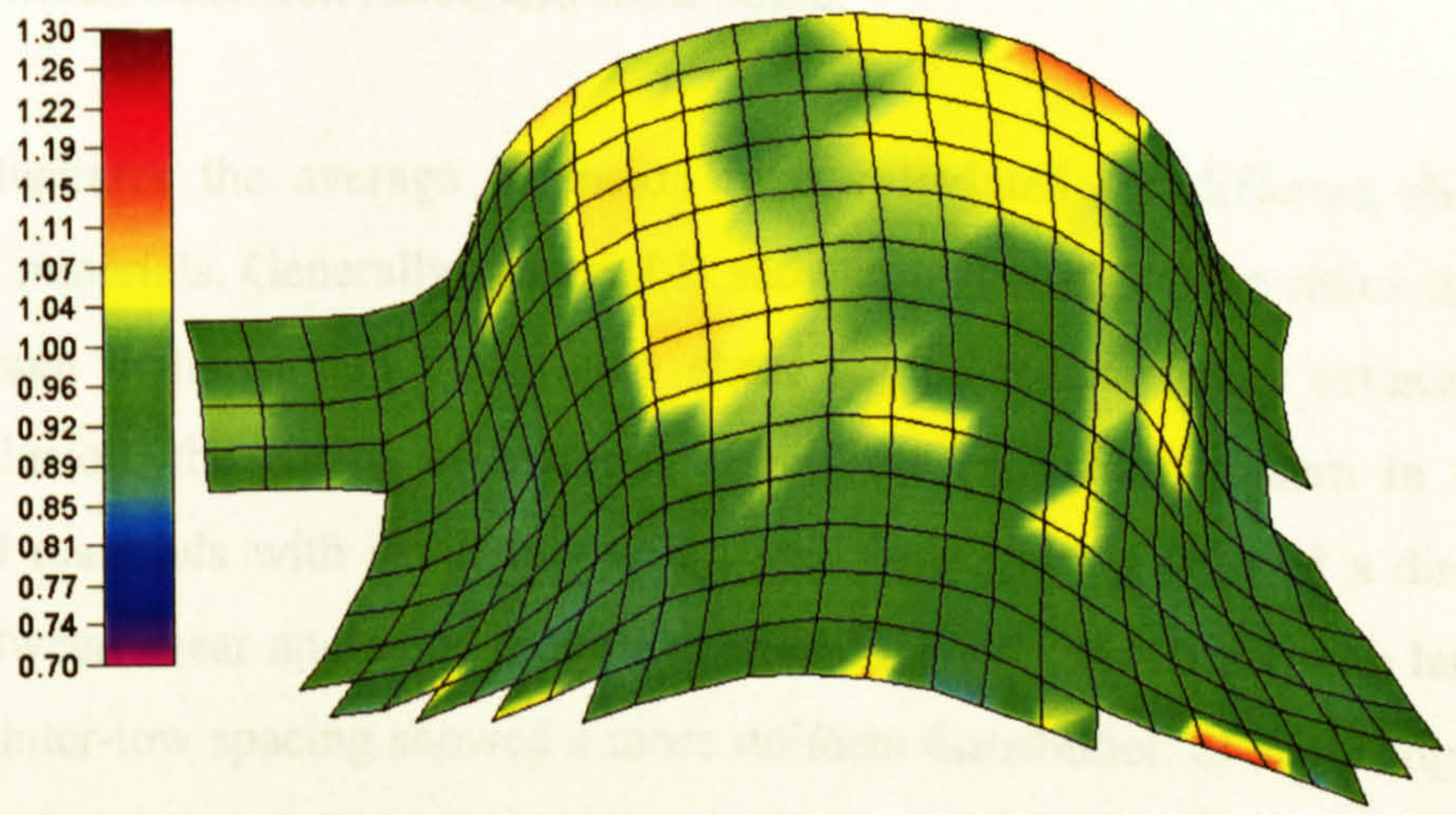

b)

Figure 7.9 Extension ratio distribution for a female hemisphere formed and consolidated using material C **a)** direction x **b)** direction y.

Due to their textile structure these materials undergo extension in different ways. Whilst material B has a large tow width and inter-tow spacing, material C has a small tow width and little inter-tow spacing **[116]**. This inter-tow spacing in the material B textile structure facilitates the relative movement between tows leading to higher extension ratios. Similar trends are observed in each direction for the same material.

Higher changes in grid spacing were observed for material B than for prepreg, which would explain the lower shear angles observed for material B. Extension ratios different to 1 indicates that other mechanism of deformation different to pure shear occur leading to lower shear angles.

In the previous section it was observed that the choice of material has great effect on the shear deformation required to form a hemisphere. The extension distribution in hemispherical components formed from prepreg and commingled fabric indicates again that the two materials deform in different ways in order to conform to the geometry.

Deformation in other regions of the hemisphere can affect the fibre pattern. Data from Figures 7.6 to 7.9 are used to investigate the relationship between grid spacing and shear angle. Figure 7.10 shows extension ratio against shear angle for both materials over the whole surface of the hemisphere. For material C extension ratios under 1 are observed in the high sheared regions. However, material B did not show a clear trend between extension ration and shear angle.

Figure 7.11 illustrates the average extension ratio calculated for different shear angles for both materials. Generally, material B showed higher extension ratios than material C, which demonstrated that higher shear angles induce lower extension ratios. In conclusion, the choice of material affects the final fibre pattern in the component and materials with small tow width and fibre spacing showed a direct relationship between shear angle and extension ratio. However, materials with large tow width and inter-tow spacing showed a more uniform distribution of shear angles and extension ratios.

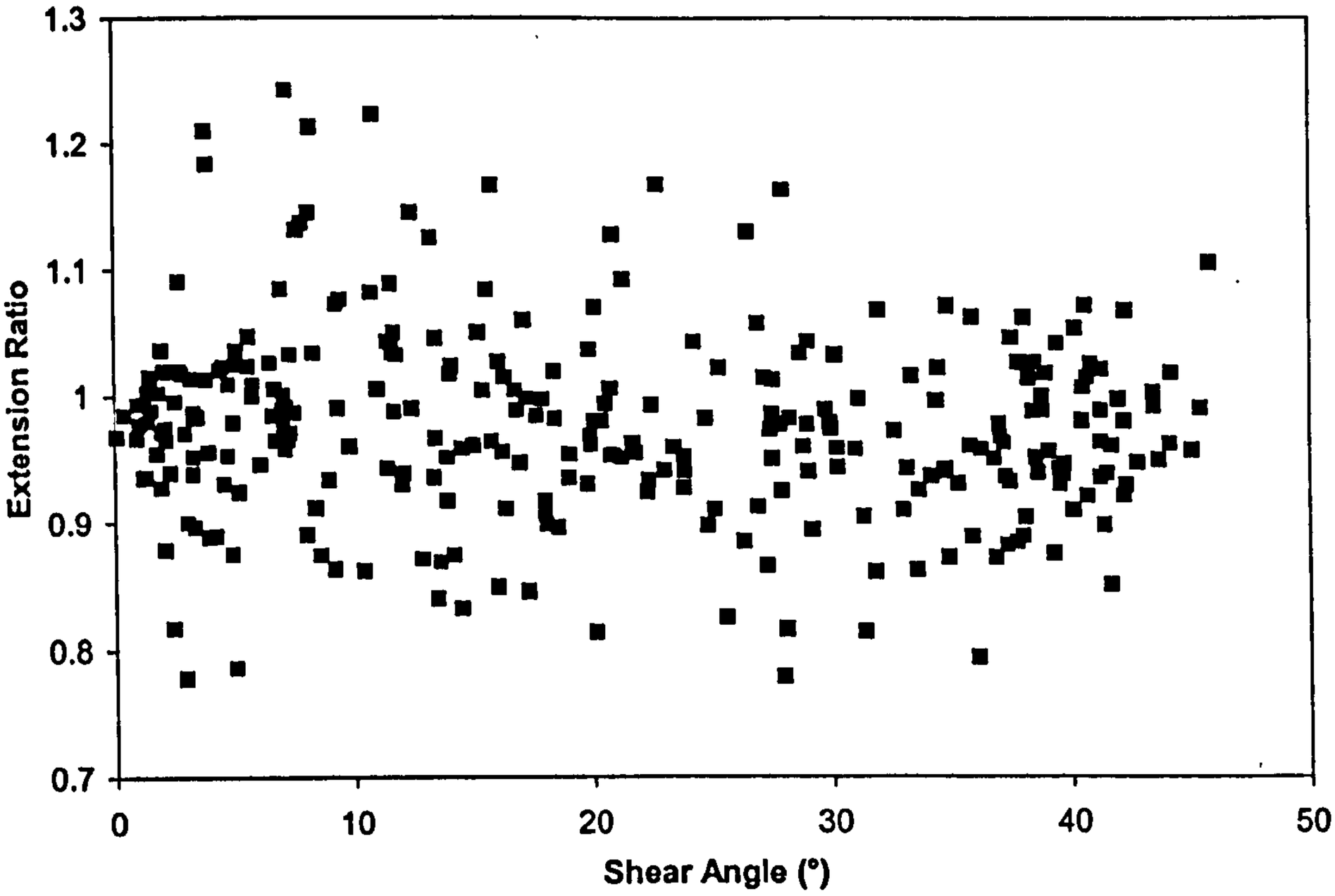

a)

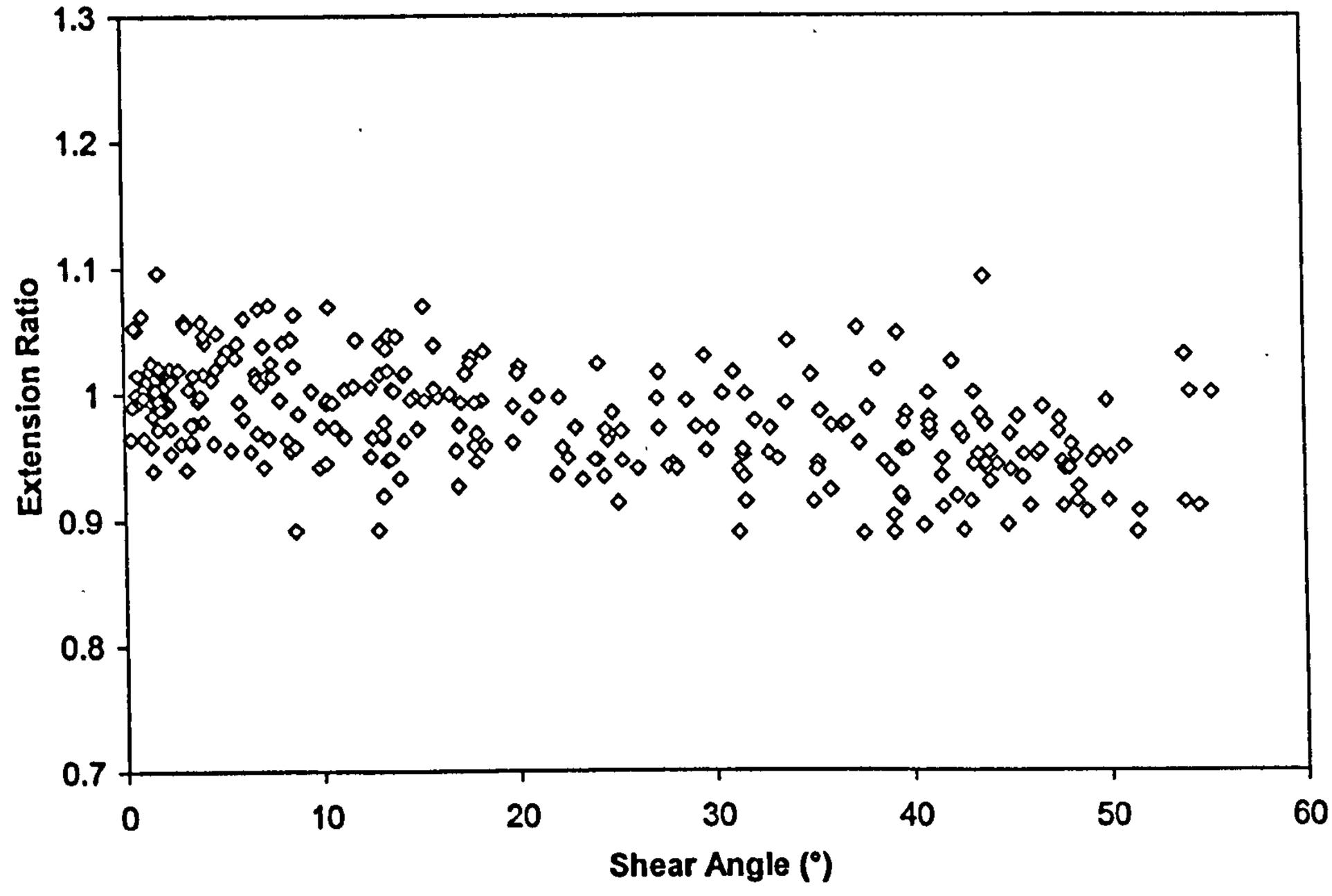

b)

Figure 7.10 Extension ratio in the direction y plotted against shear angle over the surface of the: **a)** material B hemisphere **b)** material C hemisphere.

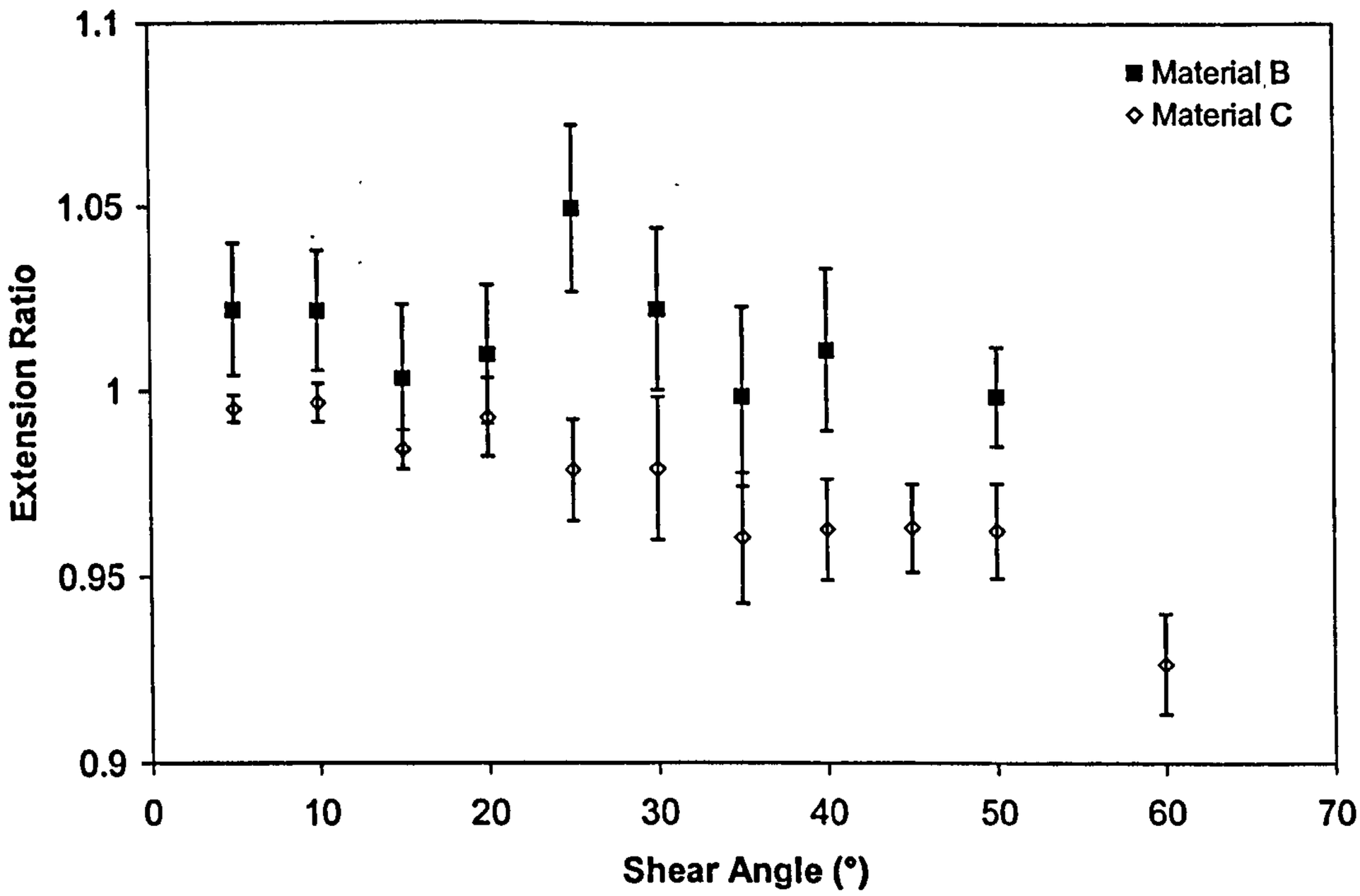

Figure 7.11 Extension ratio versus. shear angle for material B and material C hemispheres. Error bars indicate 90% confidence limits.

7.3.4 Void content

With the aim of studying the effect of deformation on consolidation, void content analysis was carried out on samples taken from the material B hemisphere. Five coupons were cut from different locations, shown in Figure 7.6.

Values in Table 7.1 show the void content for the five different locations on the hemisphere. Clifford et al. **[115]** performed experiments on sheared flat plaques of two plies of preconsolidated material B obtained by compression moulding (without a vacuum). It was stated that for shear angles lower than 40°, void content decreased as the shear angle increased, with a subsequent increase in void content at higher angles possibly due to delamination. Figure 7.12 suggest that a similar trend was observed for coupons taken from the hemisphere. Although physical evidence of delamination was also found in the highly sheared region of the hemisphere (Figure 7.13), such a mechanism was not observed in sheared flat plaques presented in Section 4.4.

Poor correlation is observed between the measured and predicted void content of sheared flat plaques, as described in Section 5.6 where in-plane shearing showed no effect on void content. The complex geometry of the tool and the use of flexible vacuum bag could produce an uneven distribution of pressure during the consolidation process, which may explain the variation in void content measurements observed here. Highly sheared regions are located close to the flange where a maximum extension of the vacuum bag is required to provide enough pressure and consolidate the material. Consequently, large voids are located in those regions producing large margins of error between predictions and experiments.

Table 7.1 Void content for hemisphere consolidated at 180°C by non-isothermal vacuum forming process. Void content is stated along with 95% confidence interval.

Position	Approx. Shear Angle	% Void Content
1	5°	5.4±2.2%
4	7°	6.4±2.5%
5	10°	6±1.2%
2	20°	4±1.1%
3	45°	6.4±4.1%

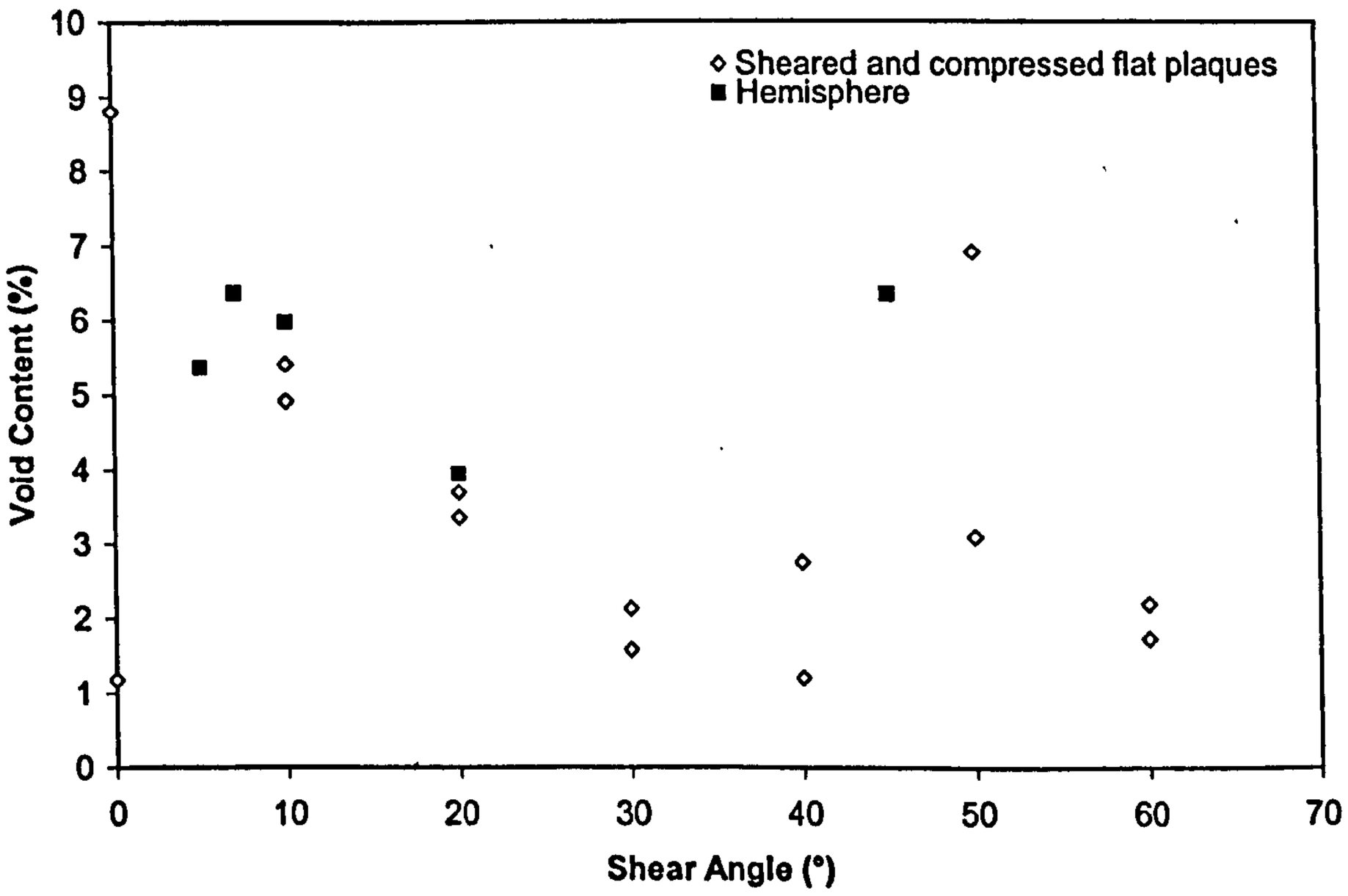

Figure 7.12 Void content versus shear angle for hemisphere and for sheared and compressed material B flat plaques **[115]**.

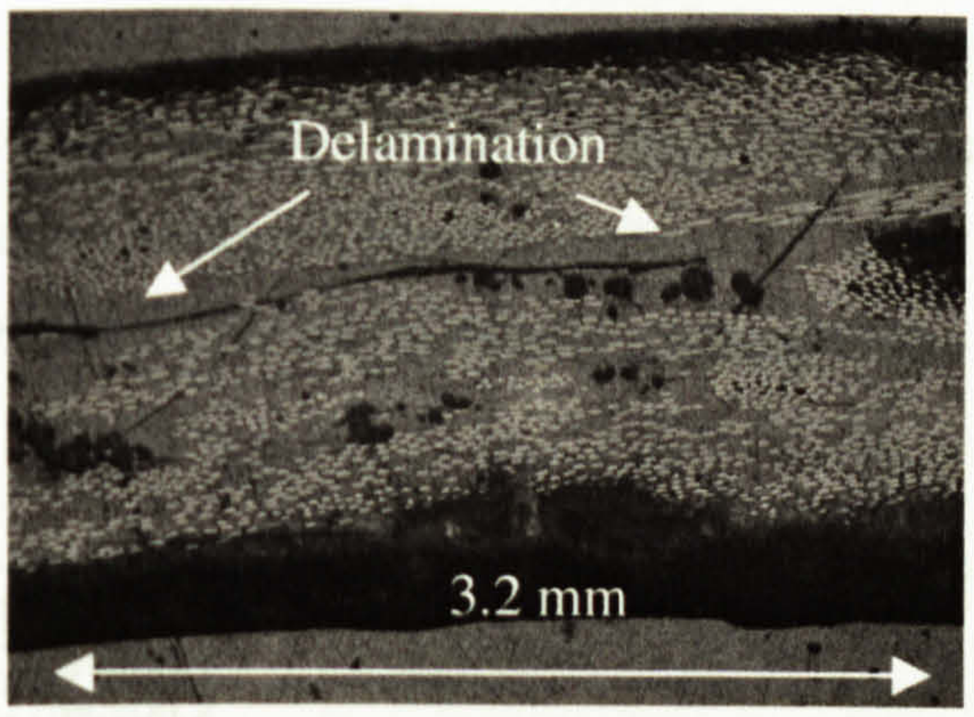

Figure 7.13 Micrograph of coupon 3 at a shear angle of 45° for material B hemisphere.

7.3.5 Comparison between ASAME and Kinematic Drape Model

This section is concerned with validation of software packages capable of modelling the forming process for textile composites. To validate the simulations carried out using the kinematic drape model, the real fibre pattern has to be known.

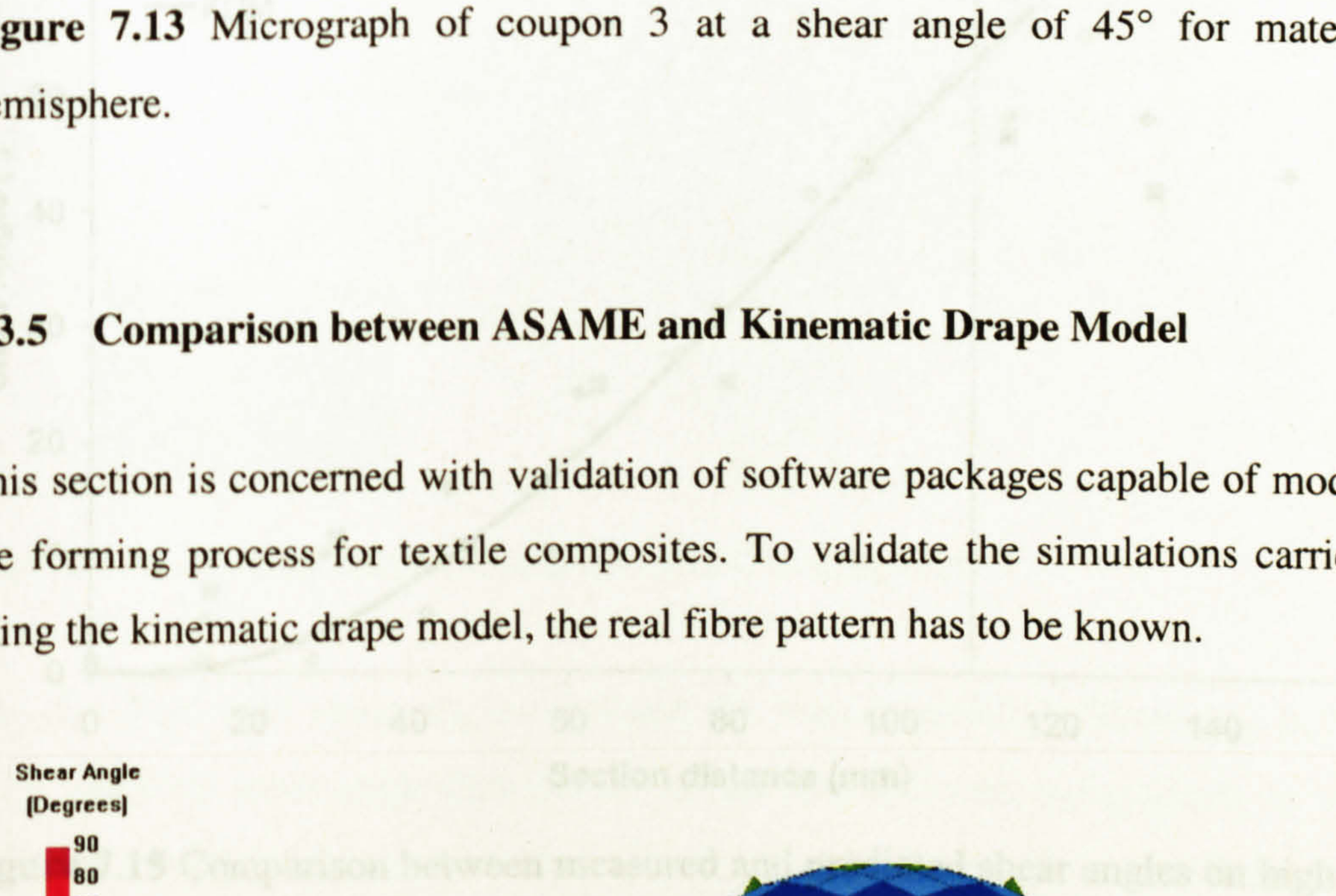

Figure 7.14. Fibre pattern predicted by kinematic drape model. This fibre distribution is representative of both material B and material C, as kinematic drape model ignores material properties.

Figure 7.14 shows the fibre pattern predicted by a kinematic drape model, which ignores material properties, whereas Figures 7.6 and 7.7 show the pattern measured using ASAME on both material B and material C hemispheres.

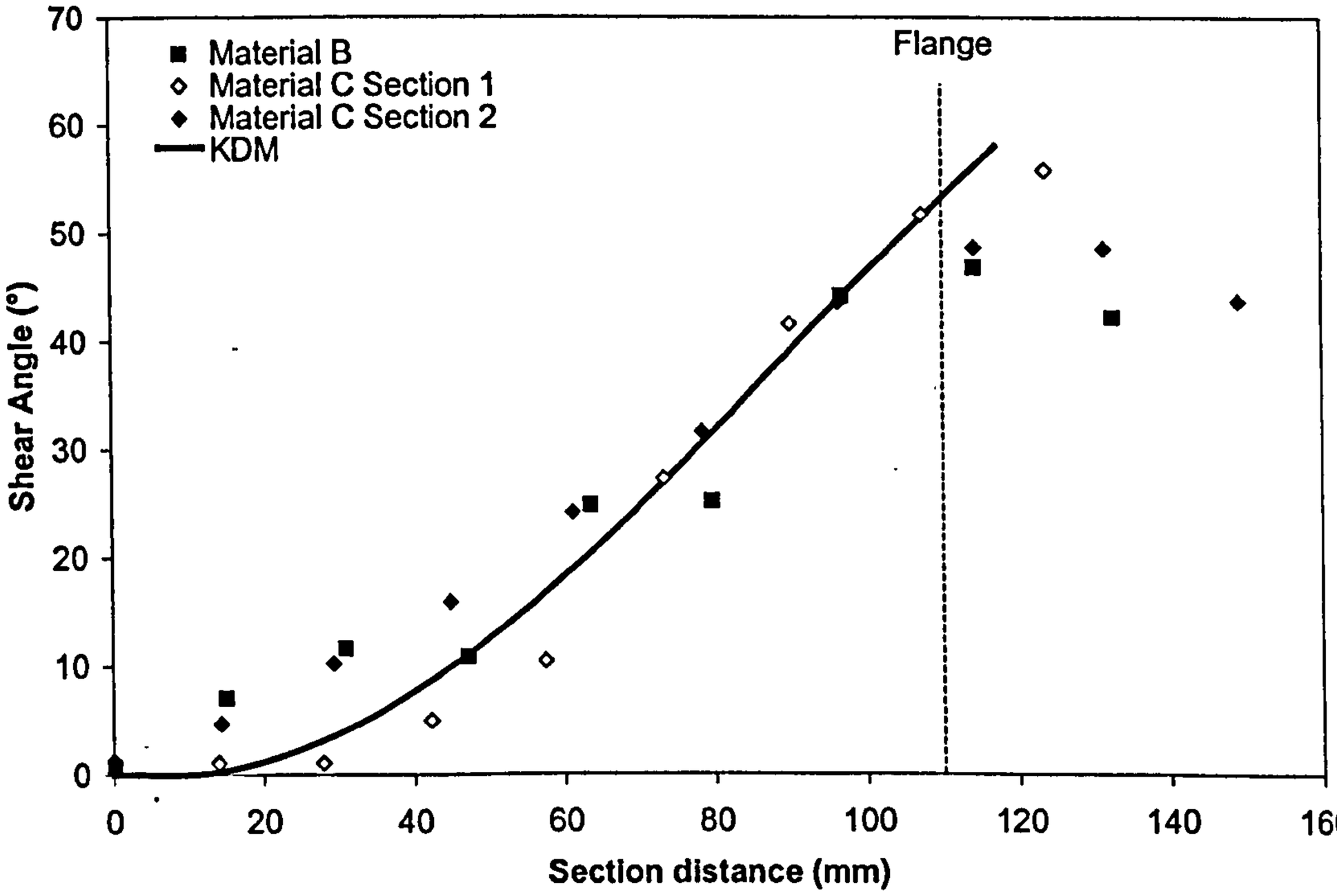

Figure 7.15 Comparison between measured and predicted shear angles on high shear regions.

Figure 7.15 shows the comparison between the measured shear angle both on a balanced twill weave fabric (material B) hemisphere and a prepreg (material C) hemisphere and the predicted shear angle from the kinematic drape model. Measured shear angle is obtained using ASAME system as described in Section 3.8.1 and predicted shear angle is calculated in the same way using drape model raw data.

Figure 7.7 shows the fibre pattern for a female hemisphere formed and consolidated using material C. Due to the lay up procedure used to form the hemisphere, applying force in one direction and then in the orthogonal direction, a different fibre pattern could appear in different quadrants. In order to get a better validation of the kinematic drape model two high shear sections in adjacent quadrants are analysed, as shown in Figure 7.16. For both materials shear angle increases as predicted by the kinematic drape model until a maximum shear angle is reached at the start of the

flange region (around 110 mm). The kinematic drape model offer a better approximation to the predicted maximum shear angle for material C than material B as a result of the different fibre architecture as mentioned in the previous section.

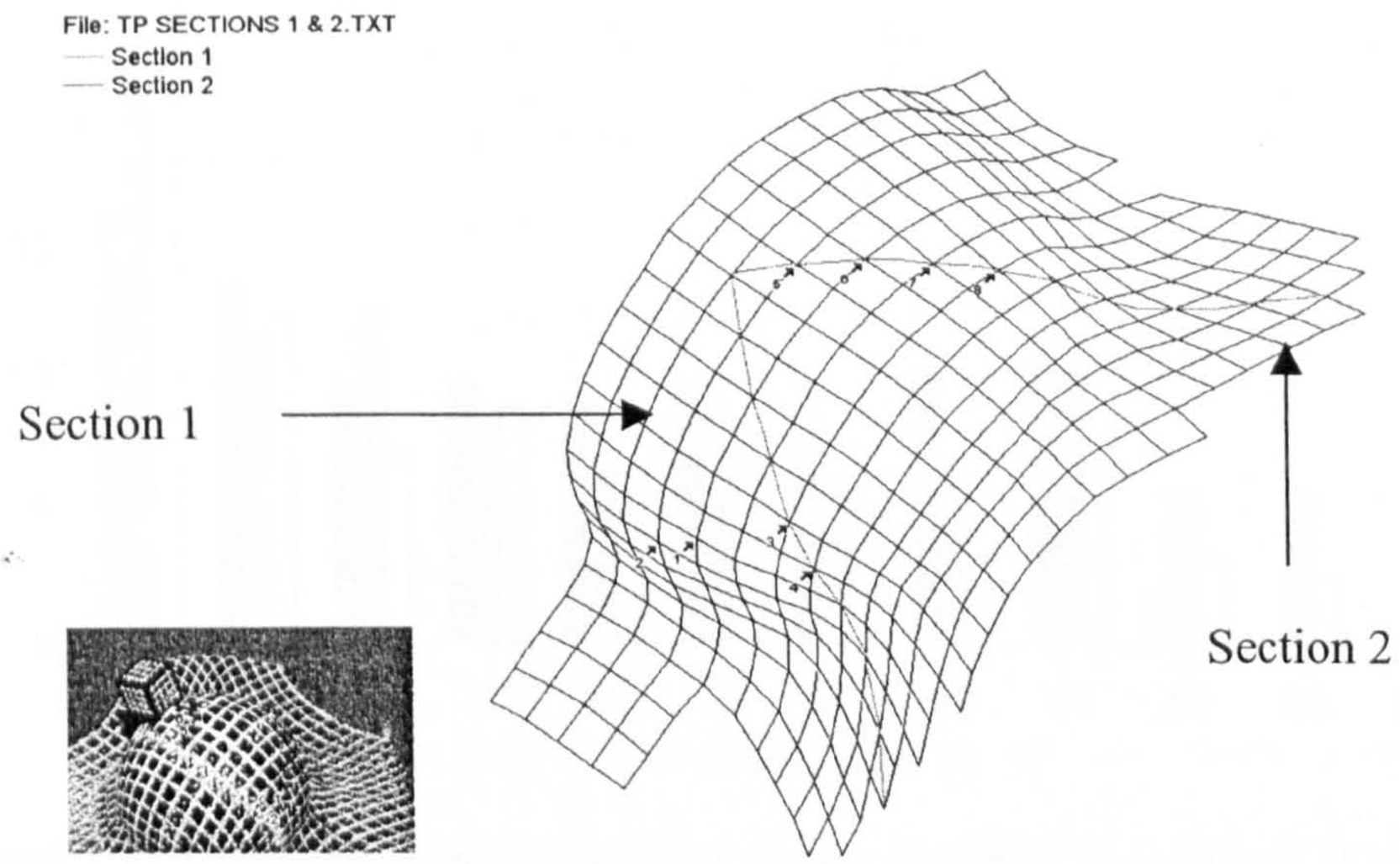

Figure 7.16 Sections analysed on a material C hemisphere.

The distribution in shear angles obtained for both materials is illustrated in Figure 7.17. Showing shear angle distribution in this way different components as well as different materials can be compared. Clearly lower shear angles were obtained more frequently for the material C than for material B, although the range of angles was higher for material C. Also included is the distribution predicted by a kinematic drape simulation. This covers a wider range of angles than achieved with either material. Lower shear angles (<5°) were predicted more frequently than in the experimental measurements, probably related to the difficulty in laying up the material symmetrically (i.e. in practice each quadrant was pre-sheared by a small amount). The predicted distribution is most similar to that obtained using the prepreg, probably due to the tight weave style (tow width and pitch values are almost equal for the prepreg). However from Figure 7.17 it can be concluded that material B is easier to form over the hemisphere geometry than material C since achieving higher shear angles required the application of higher forces.

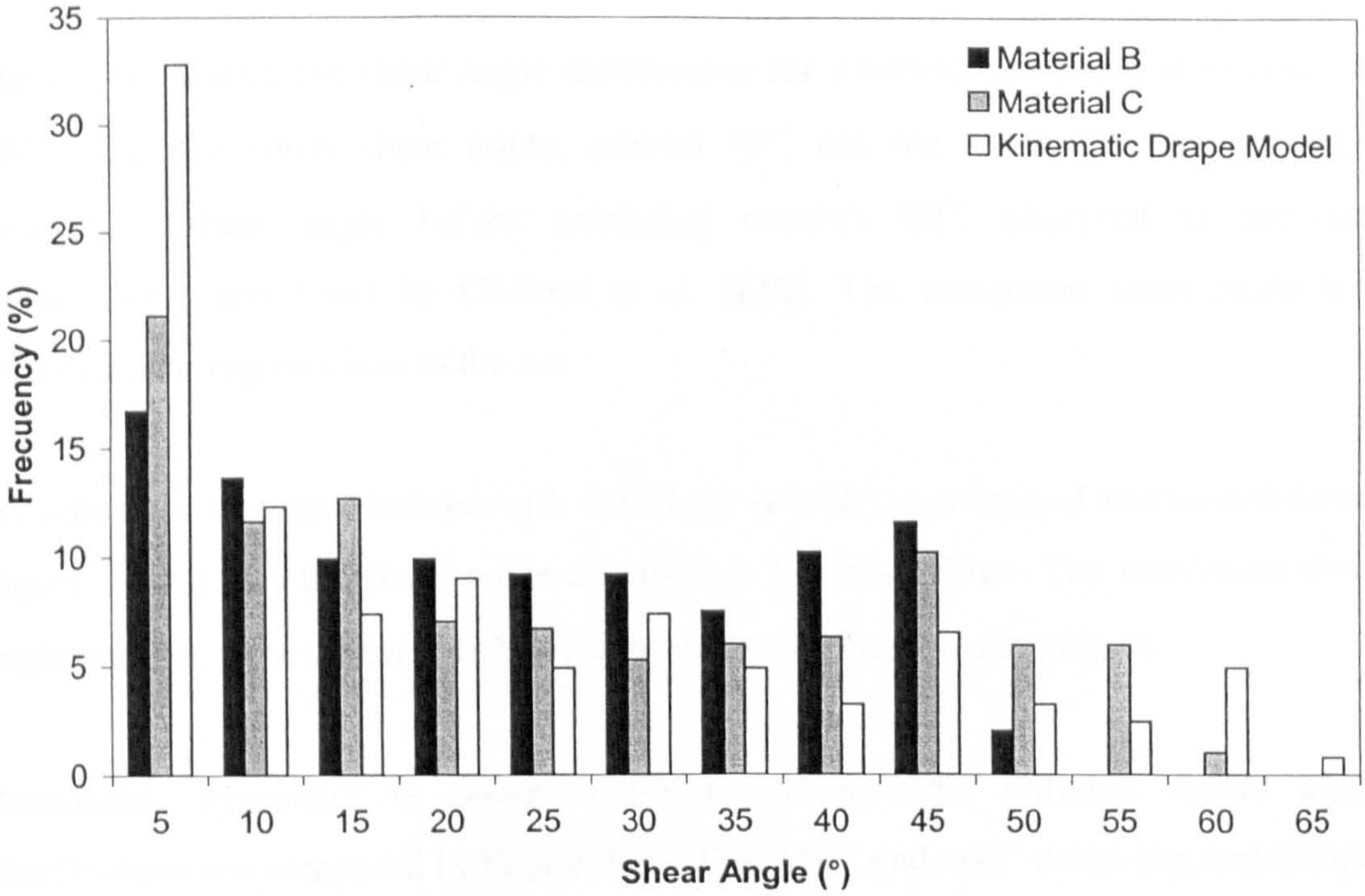

Figure 7.17 Histogram comparing shear angles obtained for material B and material C hemispheres with kinematic drape simulation.

7.4 Helmet

7.4.1 Shear Angle

Helmet mouldings were produced with material D using non-isothermal vacuum forming process as described in Chapter 3. Samples were formed with tows initially at ±45° to the axis of symmetry (from the back of the head to the front). However a significant amount of wrinkling was observed, hence a second sample was produced by stretching the material preferentially across the component, resulting in initial tow paths at ±60°. Finally, a third helmet with tows at 0/90° was formed and consolidated to assess the ease to form a different fibre orientation.

Figure 7.18 shows the shear angle distribution for a helmet produced with fibres at ±45°. A symmetrical fibre pattern (around the centre-line) was observed and the maximum shear angle, 53°, was located on the forehead of the helmet where a significant amount of wrinkling was observed.

Figure 7.19 shows the shear angle distribution for a helmet produced with fibres at ±60°. The maximum shear angle, around 50°, did not reach the locking angle (maximum shear angle before wrinkling occurs), 60°, observed in previous experiments carried out by Clifford et al. **[116]**. The maximum shear angle was located in the region close to the ear.

As stated above a third helmet with the fibres at 0/90° was formed and consolidated. Figure 7.20 shows the shear angle distribution for this helmet. The maximum shear angle, around 43°, is located to both sides of the forehead of the helmet.

Reasonable symmetry is observed for the three fibre patterns. Shear angle distributions are compared in Figure 7.21. The 0/90° and ±45° cases are surprisingly similar, although the latter covers a broader range of angles. The ±60° is dominated by values below 45 degrees. Maximum shear angles were 53°, 50° and 43° for helmets with fibres at ±45°, ±60° and 0/90° orientations respectively, corroborating the experimental observation that the lowest effort during lay-up was that with fibres at 0/90°.

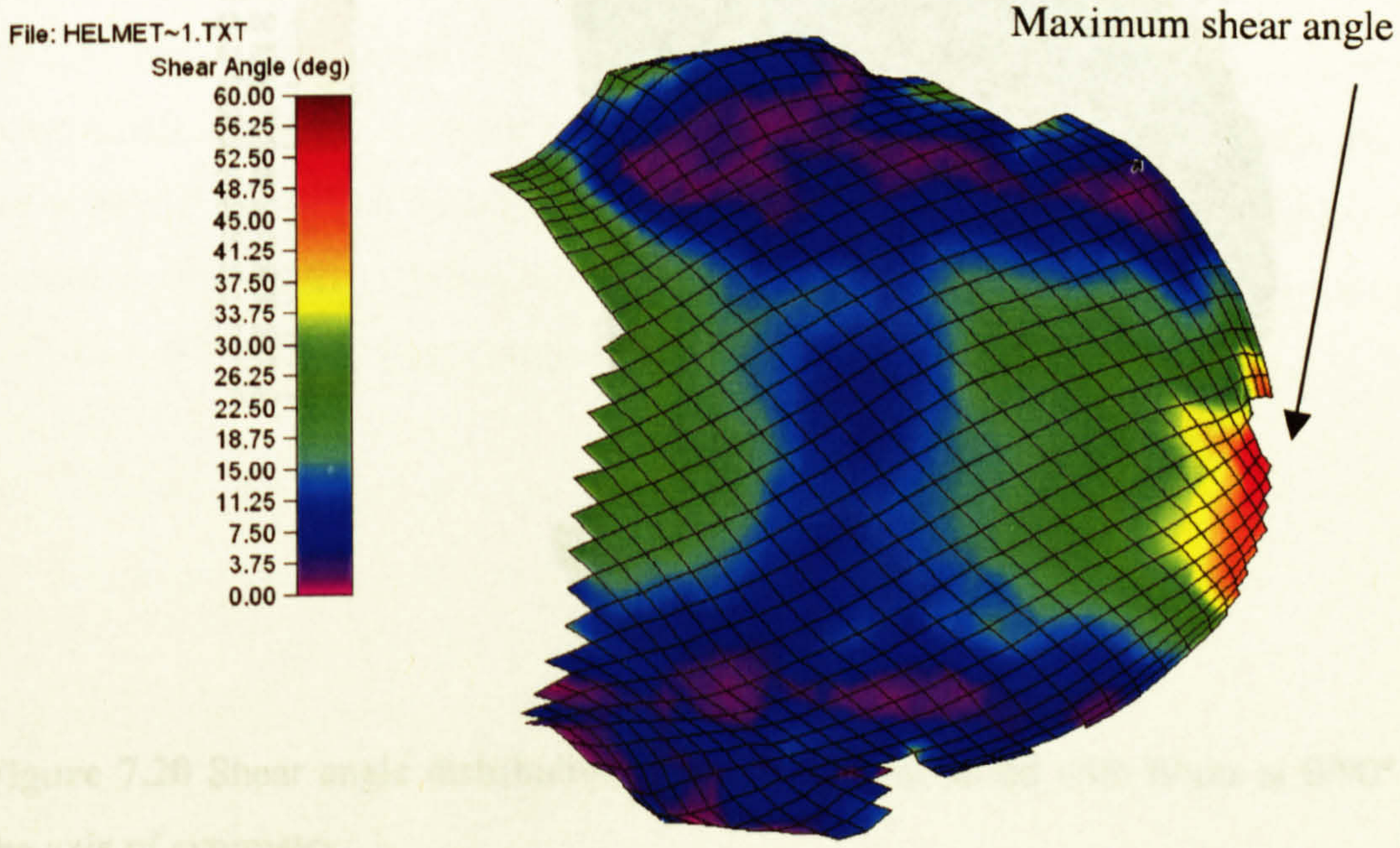

Figure 7.18 Shear angle distributions for a helmet produced with fibres at ±45° to the axis of symmetry.

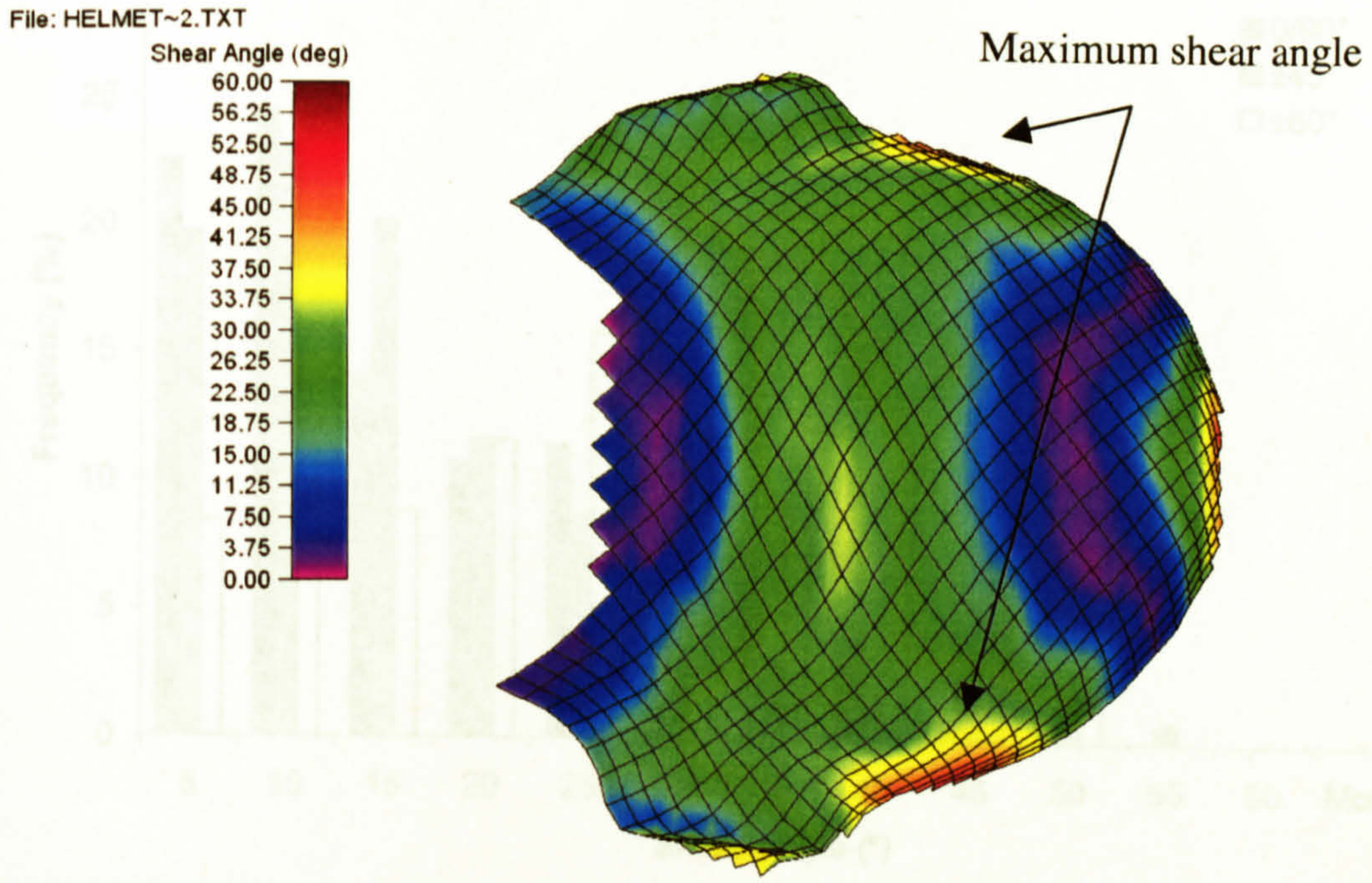

Figure 7.19 Shear angle distributions for a helmet produced with fibres at ±60° to the axis of symmetry.

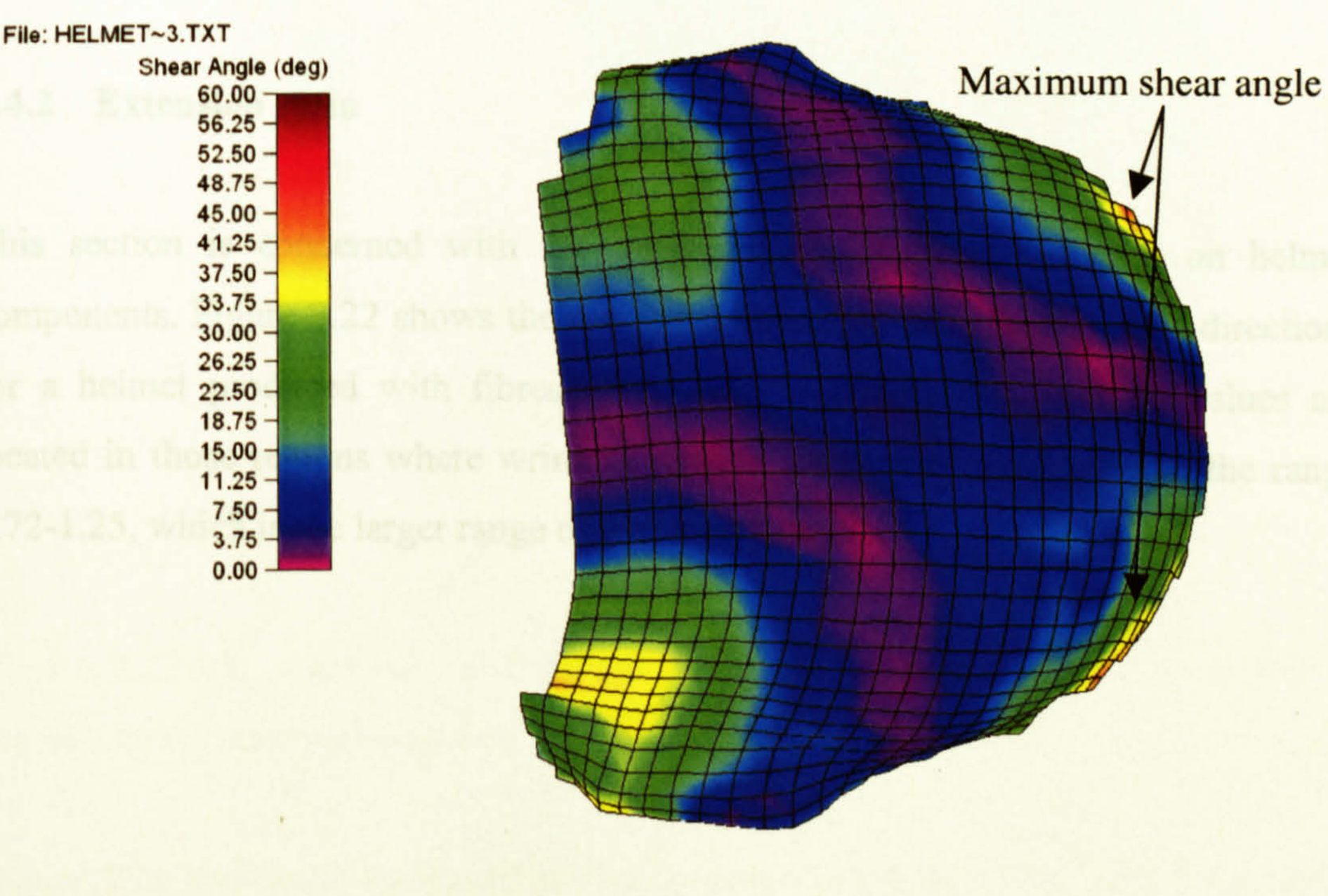

Figure 7.20 Shear angle distributions for a helmet produced with fibres at 0/90° to the axis of symmetry.

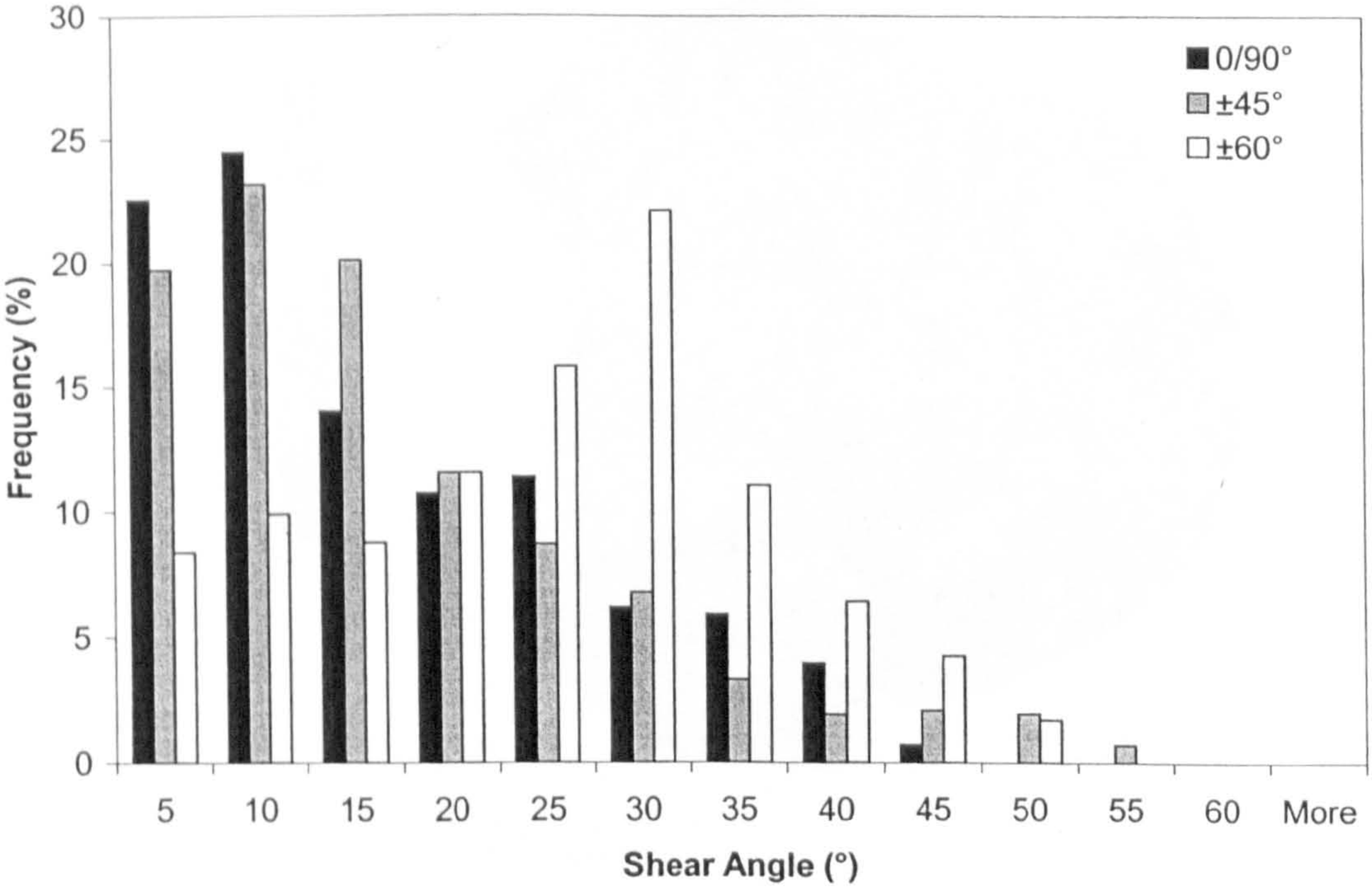

Figure 7.21 Histogram comparing shear angles obtained for prepreg helmets with material initially at 0/90°, ±45° and ±60°.

7.4.2 Extension ratio

This section is concerned with the measurement of extension ratio on helmet components. Figure 7.22 shows the measured extension ratio in both grid directions for a helmet produced with fibres at the ±45° orientation. Minimum values are located in those regions where wrinkles appear. Extension ratios were in the range 0.72-1.25, which is the larger range of the three helmets.

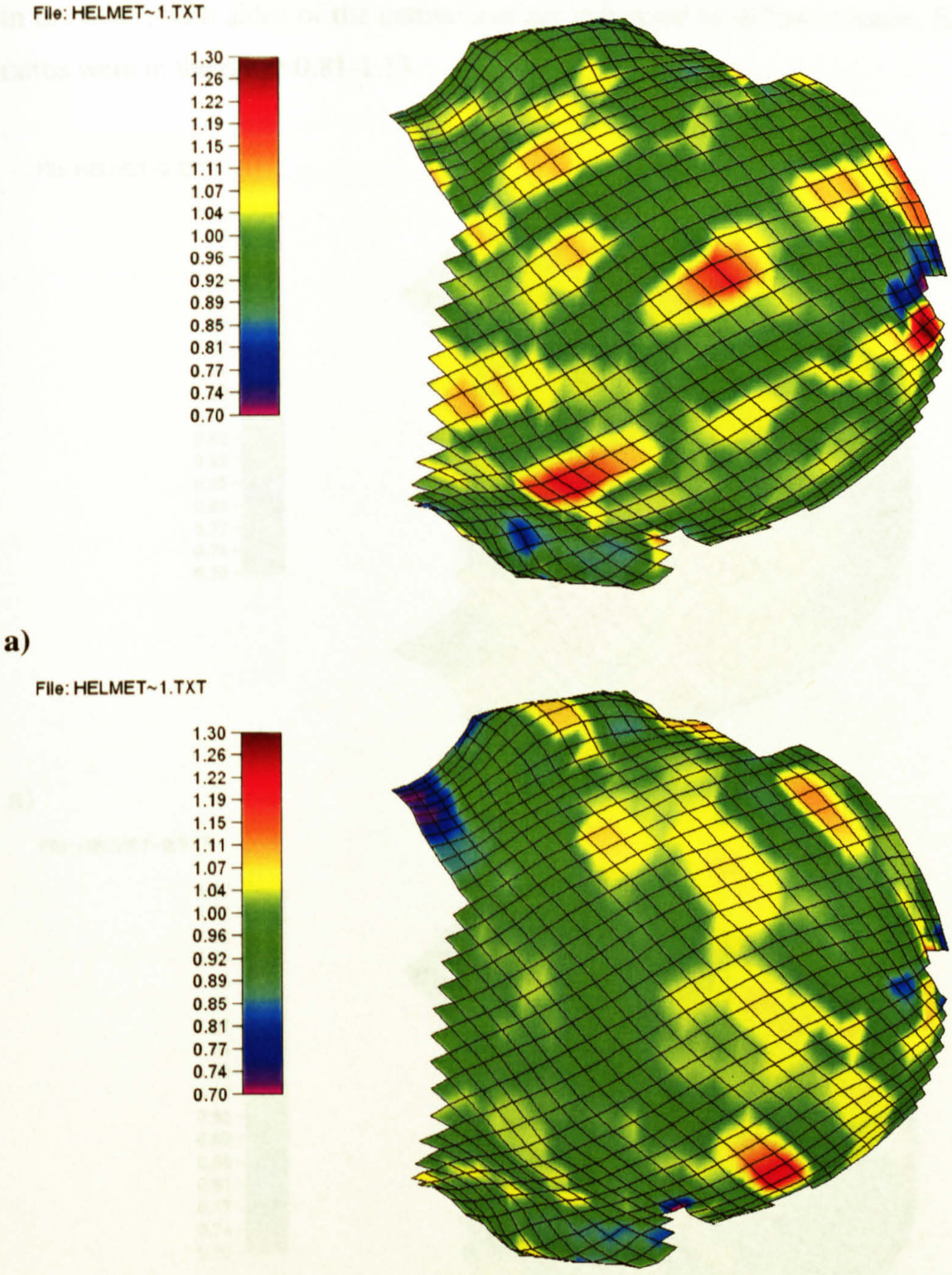

Figure 7.22 Extension ratio distribution for helmet produced with fibres at ±45° to the axis of symmetry **a)** direction x **b)** direction y.

Figure 7.23 shows the measured extension ratio in both grid directions for a helmet produced with fibre at ±60°. Extension ratios over 1 close to the right ear lead the conclusion that the force applied along one of the grid directions was larger than the other, possibly due to the special lay up procedure used to avoid wrinkling. By stretching the material across the helmet in two stages, first in one direction and then

in the other, both sides of the component are subjected to different loads. Extension ratios were in the range 0.81-1.13.

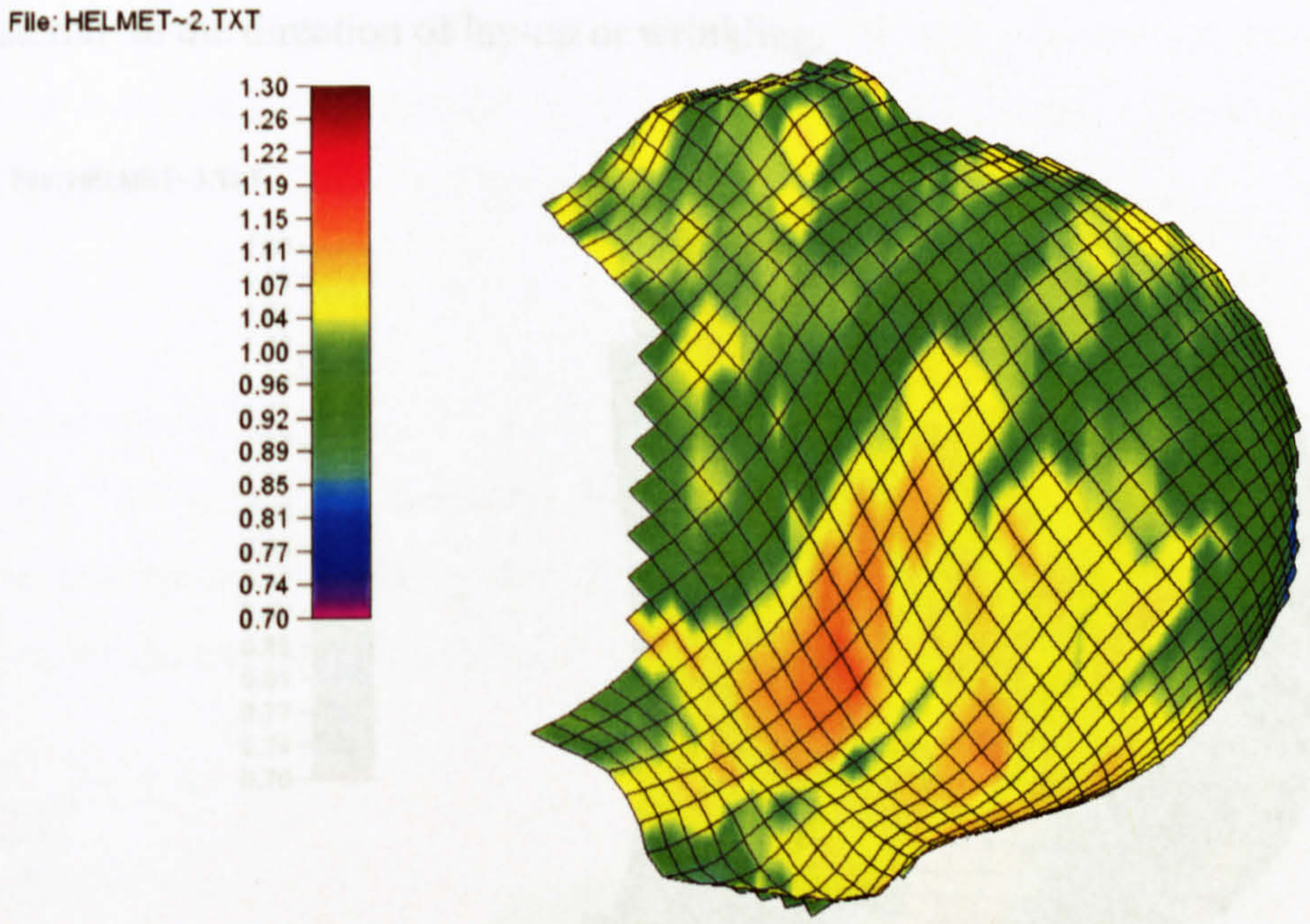

a)

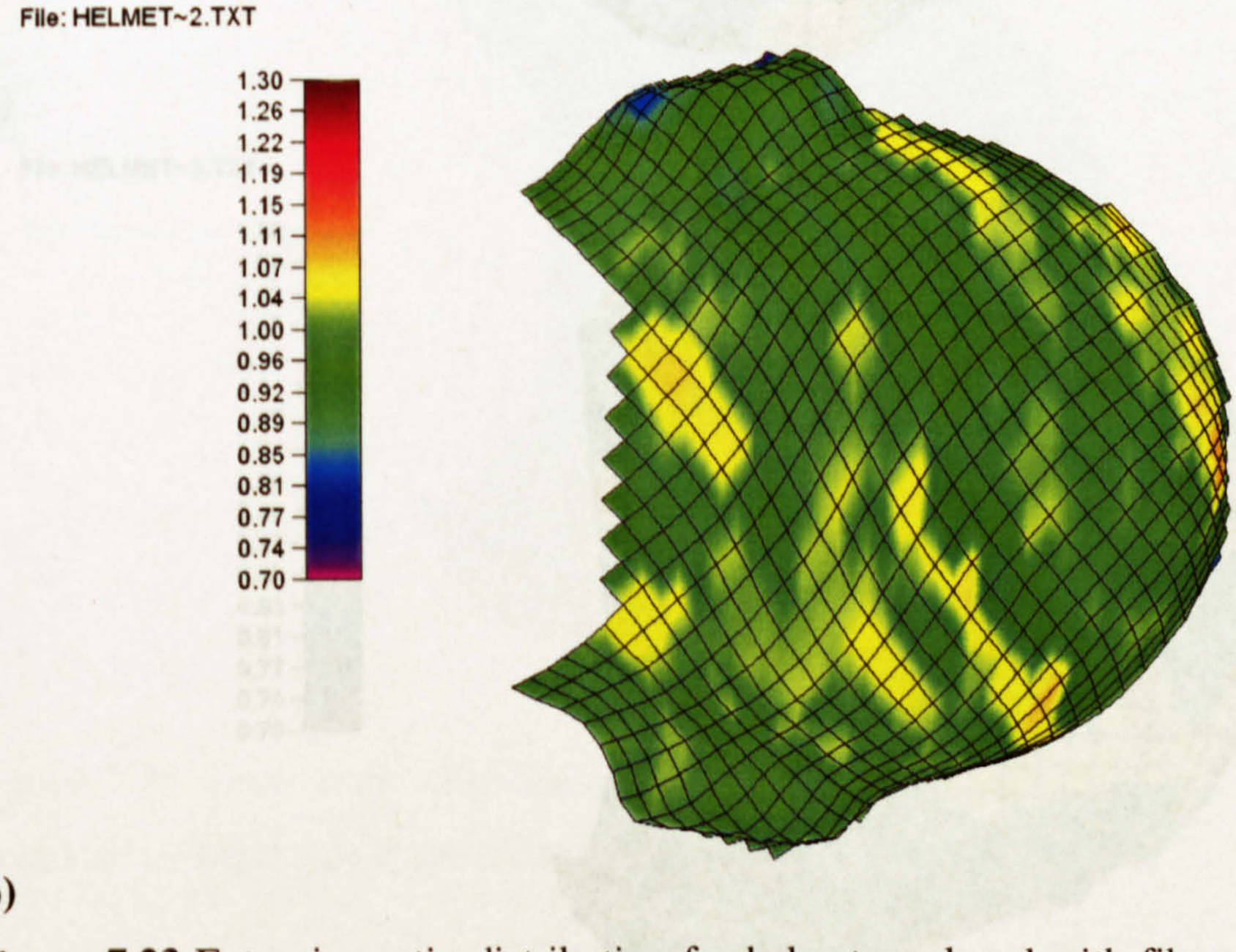

b)

Figure 7.23 Extension ratio distribution for helmet produced with fibres at ±60° to the axis of symmetry **a)** direction x **b)** direction y.

Finally Figure 7.24 shows the measured extension ratio in both grid directions for a helmet produced with fibre at 0/90° orientation. Extension ratios were in the range

0.79-1.16. A general view of the three helmets shows that most of the geometry is subjected to small changes in grid spacing and only localised regions of significant changes are observed due to either the manual lay-up producing stretching of the material in the direction of lay-up or wrinkling.

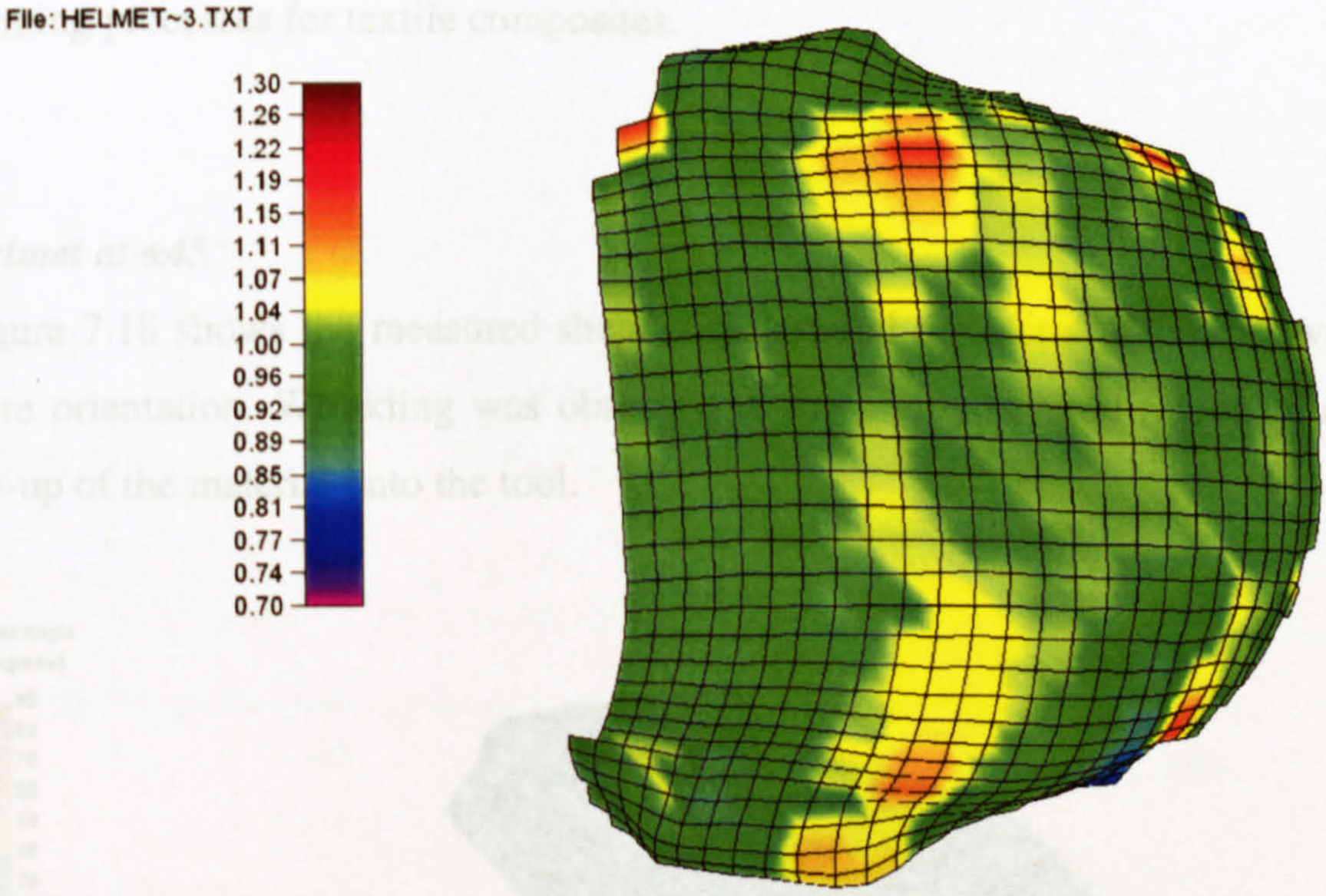

a)

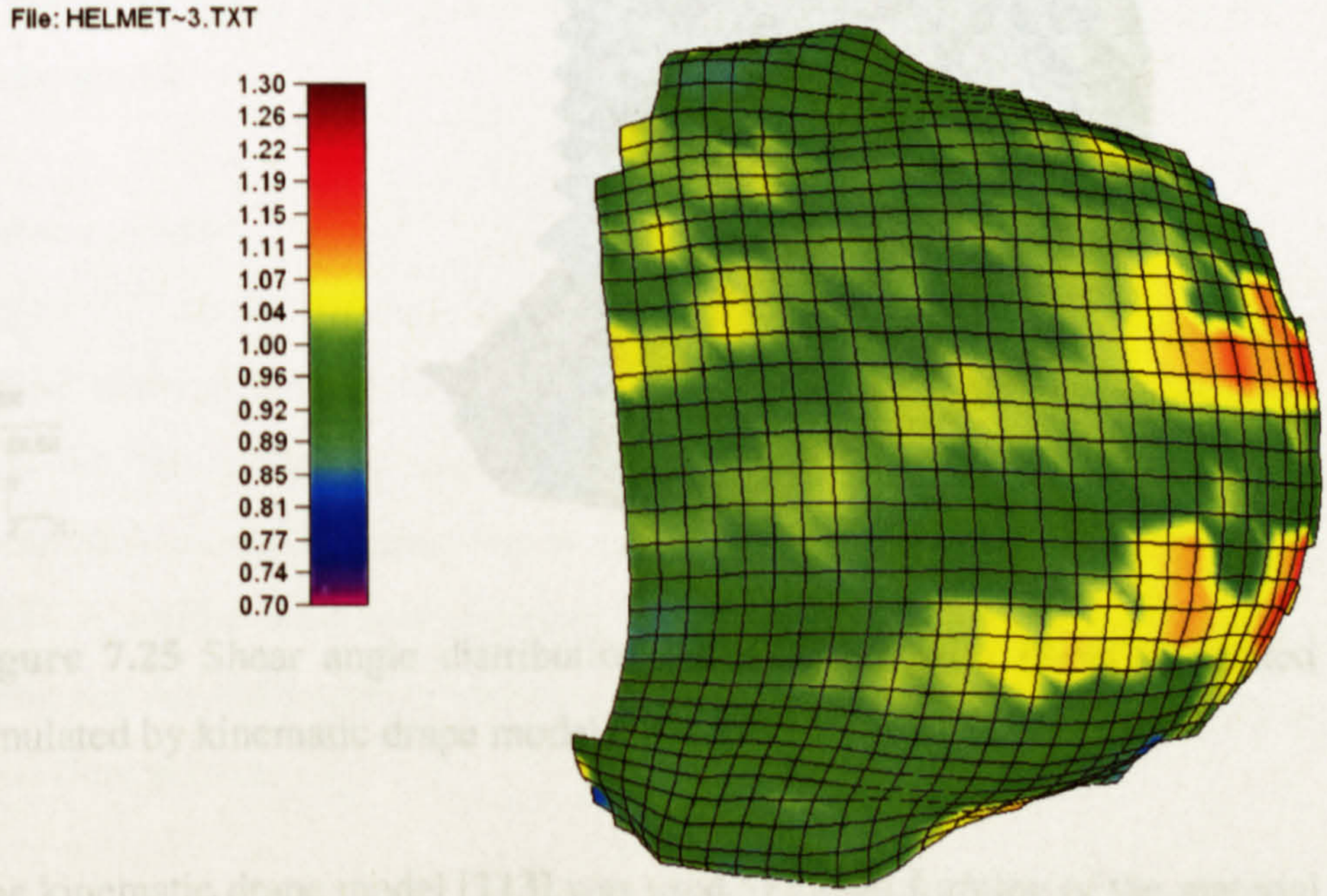

b)

Figure 7.24 Extension ratio distribution for helmet produced with fibres at 0/90° to the axis of symmetry **a)** direction x **b)** direction y.

7.4.3 Comparison between ASAME and Kinematic Drape Model

As in the case of hemispherical components this section is concerned with validation of software packages, specifically the kinematic drape model, capable of modelling forming processes for textile composites.

Helmet at ±45°

Figure 7.18 shows the measured shear angle around a material D helmet with ±45° fibre orientation. Wrinkling was observed in the highly sheared regions due to the lay-up of the material onto the tool.

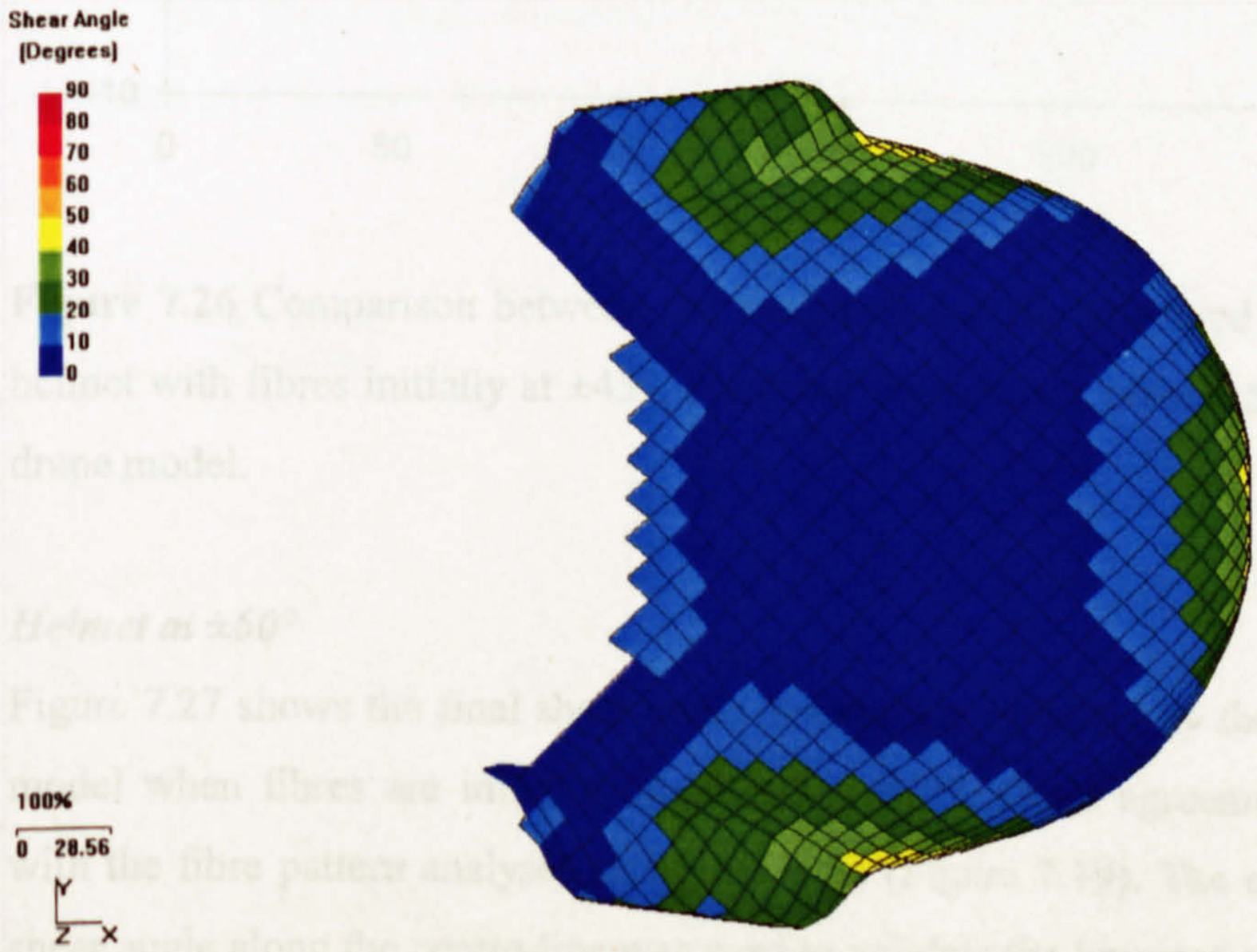

Figure 7.25 Shear angle distribution for a helmet with fibres orientated at ±45° simulated by kinematic drape model.

The kinematic drape model **[113]** was used to model forming of the material onto the component. Figure 7.25 shows the output display for the simulation. At first sight, both ASAME and the drape model appear to show similar fibre patterns. However, to validate this result Figure 7.26 shows a comparison between the measured and the predicted shear angle along the centre-line of the helmet. The initial deformation of

the fabric near the topmost point of the component induced an a constant difference of around 10°, which was not considered in the simulation.

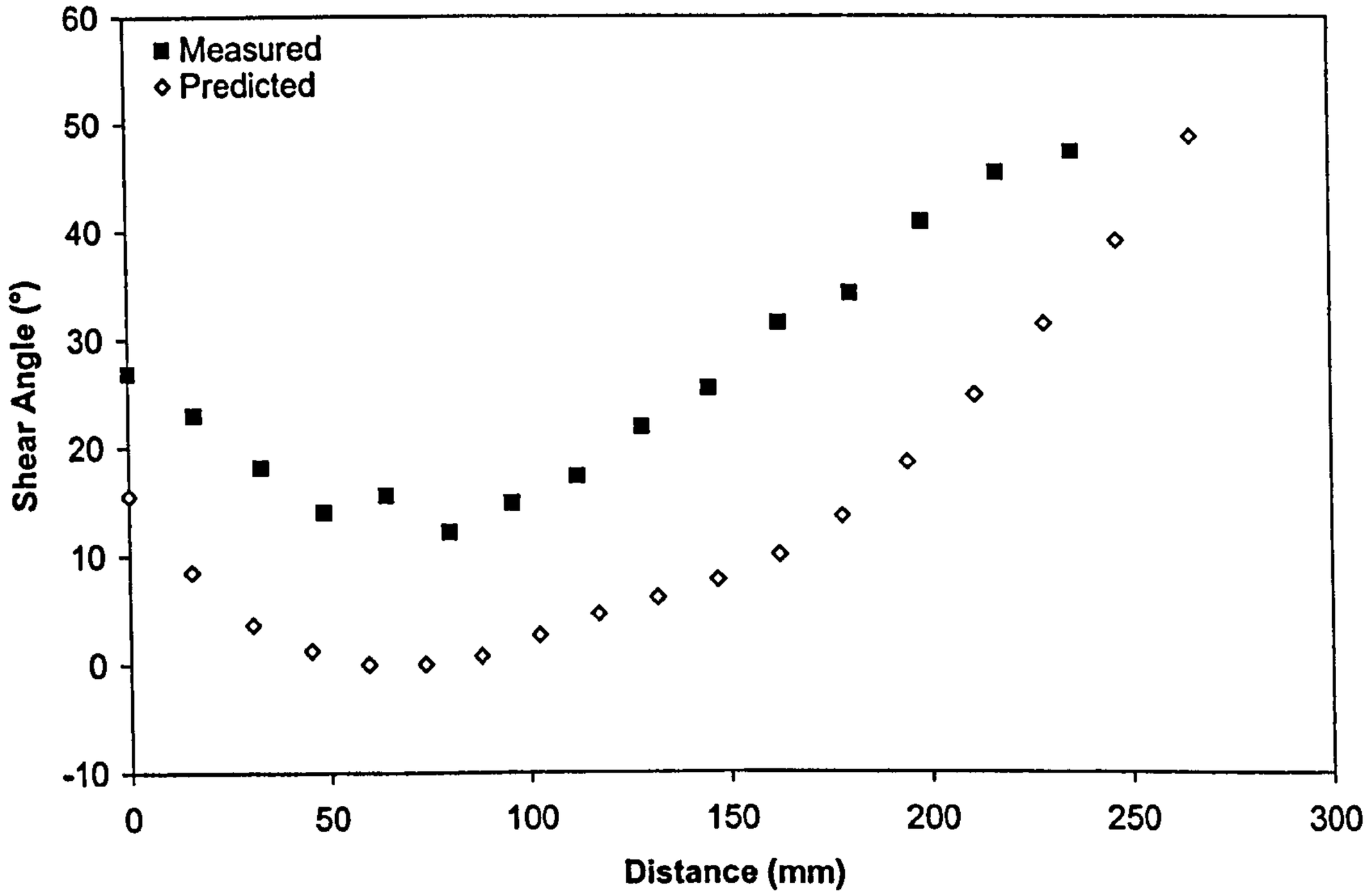

Figure 7.26 Comparison between the measured and the predicted shear angle for a helmet with fibres initially at ±45°. Predicted values were obtained by the kinematic drape model.

Helmet at ±60°

Figure 7.27 shows the final shear angle distribution obtained by the kinematic drape model when fibres are initially orientated at ±60°. Good agreement was observed with the fibre pattern analysed using ASAME (Figure 7.19). The comparison of the shear angle along the centre-line was used to validate the kinematic approach (Figure 7.28). A similar trend was observed. However, slightly higher values were measured using the ASAME system showing once again the effect of material lay-up on the final fibre pattern.

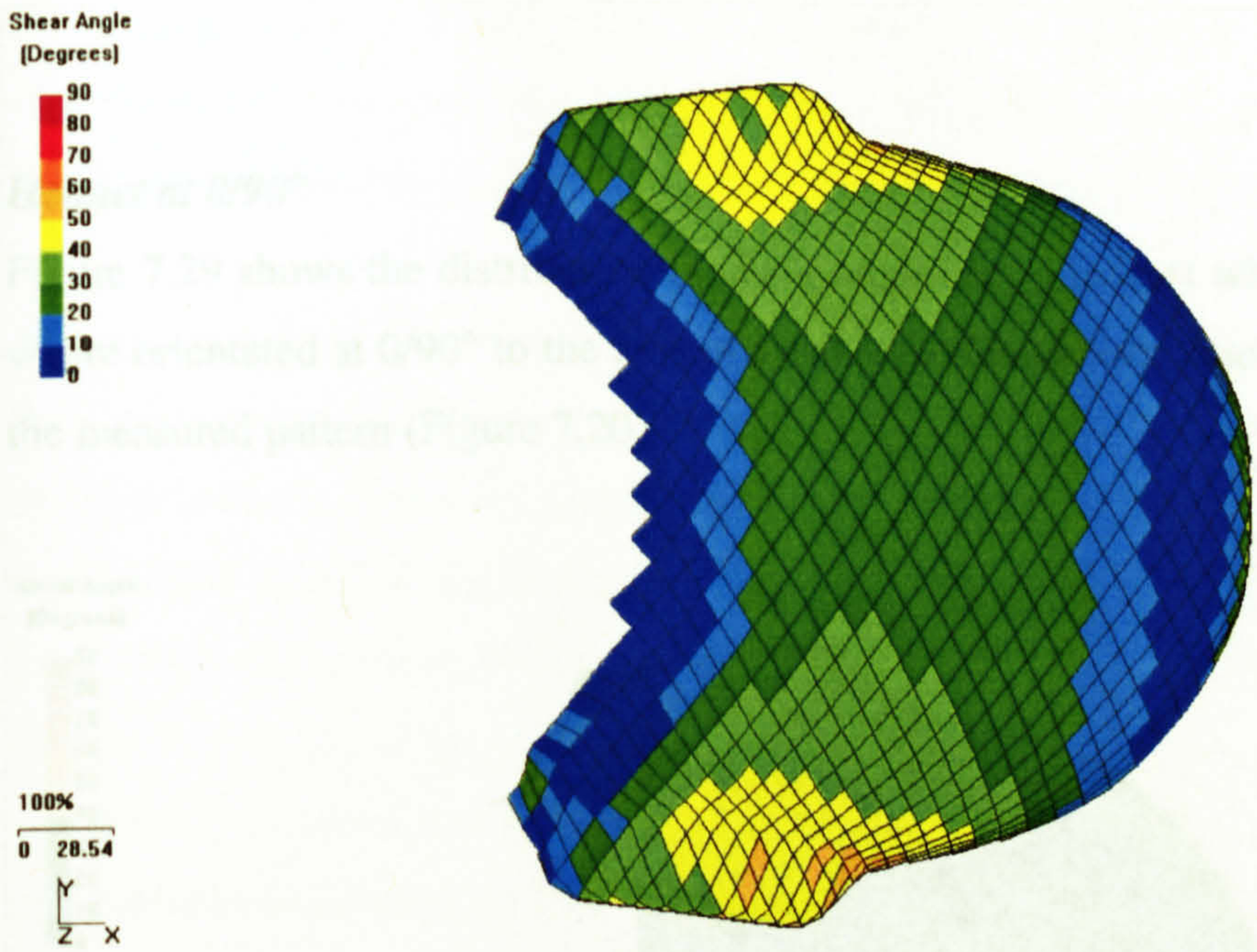

Figure 7.27 Shear angle distribution for a helmet with fibres orientated at ±60° simulated by kinematic drape model.

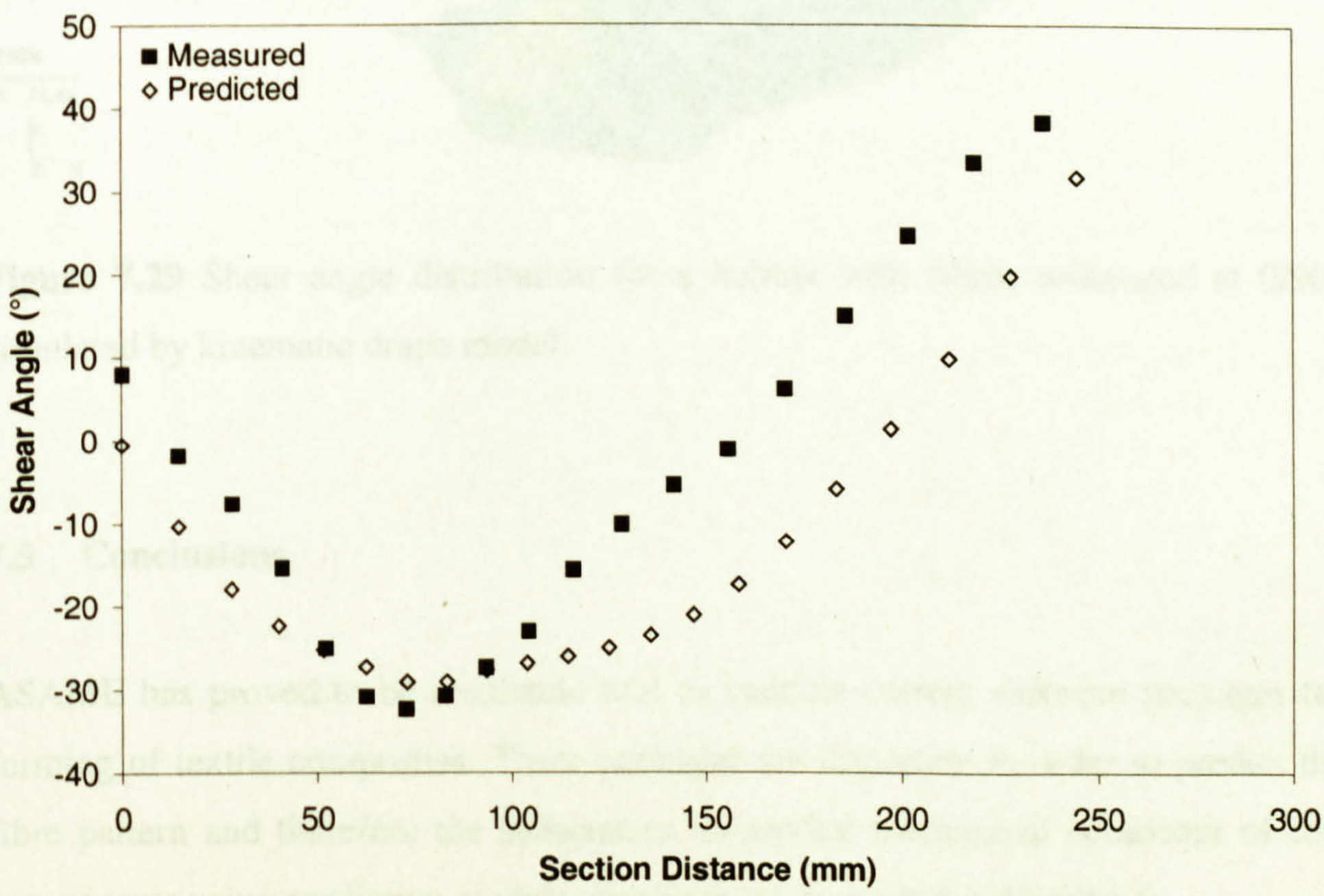

Figure 7.28 Comparison between the measured and the predicted shear angle for a helmet with fibres initially at ±60°. Predicted values were obtained by the kinematic drape model.

Helmet at 0/90°

Figure 7.29 shows the distribution of shear angles for a helmet where initially fibres where orientated at 0/90° to the axis of symmetry. Good correlation is observed with the measured pattern (Figure 7.20).

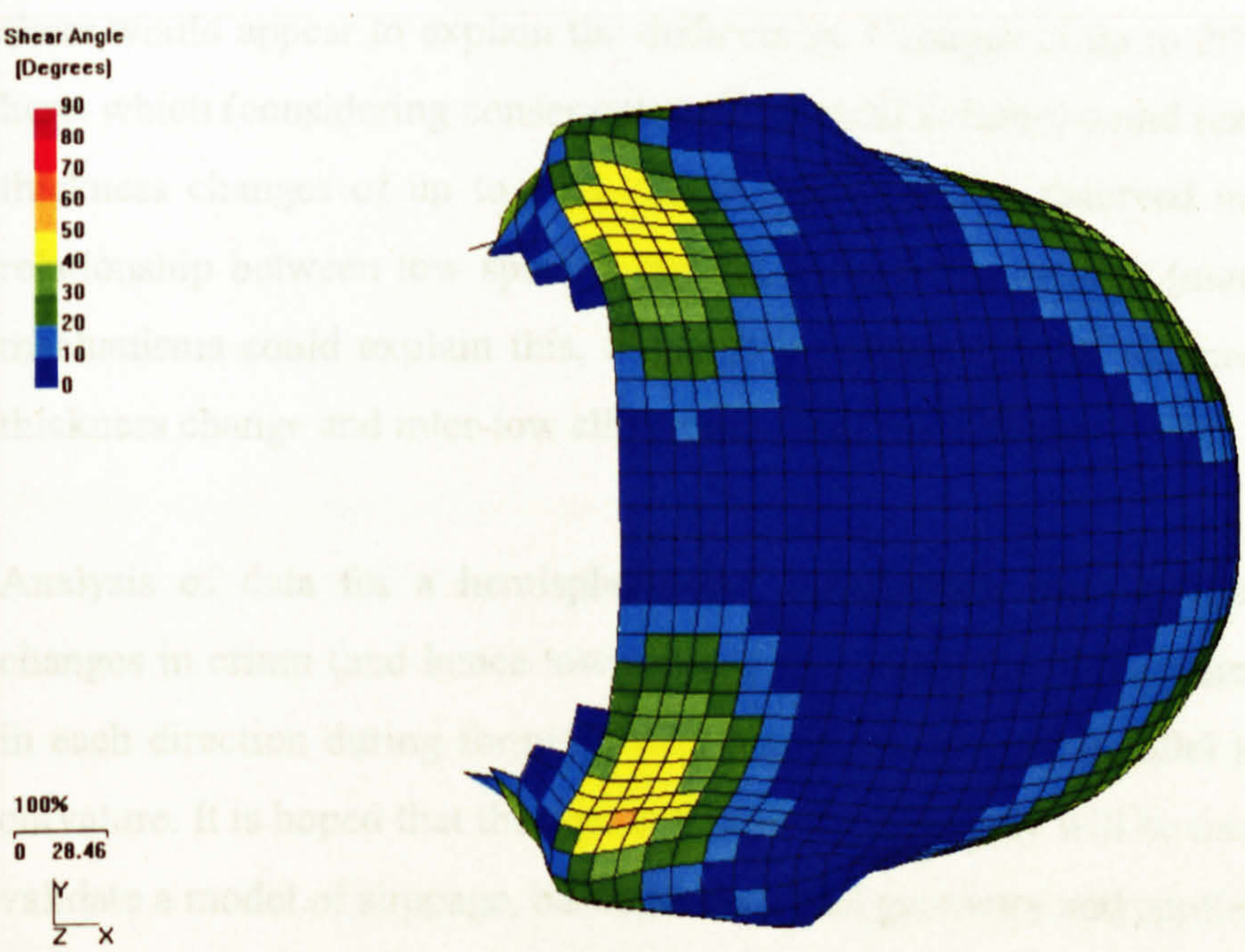

Figure 7.29 Shear angle distribution for a helmet with fibres orientated at 0/90° simulated by kinematic drape model.

7.5 Conclusions

ASAME has proved to be a suitable tool to validate current software packages for forming of textile composites. These packages are important in order to predict the fibre pattern and therefore the subsequent in–service mechanical behaviour of real components using predictive models such as those presented in Chapter 6.

Fibre patterns have been analysed and simulations have been tested for two geometries: a hemisphere and a helicopter pilot helmet. Reasonable agreement was observed between the measured and the predicted fibre pattern for materials B, C and

D on the geometries. Void content measurements for a material B hemisphere were also measured, however levels of void content differed from the predicted values due to the use of a flexible vacuum bag that varied the applied pressure.

A large amount of fibre architecture data has been obtained in this study. It is clear that the material used has an influence on the deformed fibre pattern, even for a symmetric component such as a flanged hemisphere. Changes in tow spacing during shear would appear to explain the differences. Changes of up to 20% were observed here, which (considering conservation of material volume) could result in component thickness changes of up to 36%. Some evidence was observed indicating a direct relationship between tow spacing and shear angle for prepreg (material C). Several mechanisms could explain this, although a combination of reduced spacing due to thickness change and inter-tow slip would seem most likely.

Analysis of data for a hemisphere and a helicopter pilot helmet suggested that changes in crimp (and hence tow spacing) are likely due to the force applied locally in each direction during forming, with higher forces used parallel to lines of higher curvature. It is hoped that the data collected for this study will be used to develop and validate a model of slippage, based on both tool geometry and applied forces.

8 Discussion and Conclusions

8.1 Introduction

This chapter discusses the work included within the main body of this thesis, with reference to the overall theme described in Chapter 1. The contents of each chapter are summarised and assessed to evaluate their implications in the forming and consolidation of textile composites. Several recommendations for further work are made, and the overall conclusions are presented.

8.2 General discussion

This thesis is concerned mainly with the study of defects that may appear during forming and consolidation of textile composites, and their prediction. The overall objective of this research was to identify the effects of such defects and textile deformation on consolidation and formability and subsequent mechanical properties.

The vacuum forming process presented in Chapter 3 is a suitable process to study the effects of processing parameters and deformation on mechanical properties of textile composite structures. Experimental data is presented in Chapter 4, where the measured quality and deformation of flat plaques was correlated with mechanical properties. It was observed that void contents over 10% reduced flexural and tensile strength by 50% independently of the material. A similar effect was observed on the mechanical behaviour of sheared flat plaques, where high levels of void content decreased the measured tensile properties. During testing of sheared flat plaques, fibres reoriented with the loading direction leading to a change in the elastic behaviour of the samples.

A consolidation model for commingled materials that predicts void content as a function of processing parameters was presented in Chapter 5. This model was controlled by two parameters: an empirical value that controls the yarn permeability and the number of agglomerations, where an agglomeration is a forming of fibres

within a yarn surrounding a single void. An isothermal vacuum process was modelled initially due to the facility to control time at pressure, which provided a range of flat plaques with void contents ranging from 16% to less than 1%. The analysis of void distribution was a difficult task. This analysis demonstrated that a large amount of voids were located in the inter-tow region. This observation led to separate the consolidation model into two problems: evolution of inter-tow voids and encroachment of the matrix into the fibre bundles. Scatter between predicted and experimental void content was caused by the observed disappearance of inter-tow voids. However, a simple geometrical model accounted for such an effect. Industrial compression moulding processes were also modelled and non-isothermal vacuum forming was studied by introducing the predicted temperature profile characteristic of each experiment. Temperature gradient across the thickness showed no effect on the consolidation of the laminates used in this research. However, thicker laminates would require to include the temperature profile across the thickness. Finally, an analysis of the effect of deformation on consolidation was presented and contrasted with experimental results. As expected from the experiments in-plane shear did not affect the final void content of the sheared flat plaques studied in this research.

In Chapter 6 two stress concentration models that predicted the effect of circular voidage on mechanical properties were presented. The criteria resulted in a two-parameter model that was capable of predicting void content with reasonable accuracy. However, the point stress criterion produced marginally better results. A model that predicts the elastic and failure behaviour of sheared flat plaques was also presented in Chapter 6. This model is based on the assumption that textile composites are composed of two unidirectional laminae. Elastic constants were predicted using simple micromechanical models and classical laminate theory, and failure was predicted using the maximum stress criterion. Initial damage during testing is difficult to measure and the shape of the strain – stress curves did not show a clear point of failure; therefore ultimate tensile properties were measured and compared to predicted initial tensile properties. The effect of waviness on the mechanical properties was also studied, but no significant effect on the mechanical properties was predicted. A simple model based on in-plane shear of the fibre bundles, which related strain and realignment of the fibres, was presented. However

its implication in the prediction of the mechanical properties was not considered, being a possible subject for further study.

Chapter 7 includes a thorough analysis of deformation during forming of complex components using textile composites. The components used were a flanged hemisphere and a helicopter pilot helmet; both were laid up by hand and consolidated under vacuum. For the latter a number of ply orientations were used to determine the effect on both the modes and levels of deformation. A photogrammetry system was used to determine the positions of grid lines marked on the material prior to deformation. From this information, distributions of fabric thickness, fabric shear angle and level of inter-tow movement were determined. Measurements of void content for a hemisphere component were compared with consolidation model predictions. In addition to provide a comprehensive set of validation data for modelling studies, the data generated here demonstrated the modes of deformation exhibited when forming a three-dimensional component. In particular, significant levels of inter-tow slip were evident. A kinematic model was used to predict the final fibre pattern of the components. Although reasonable correlation was observed between measured and predicted fibre patterns, the results indicated the importance of accurate material properties and boundary conditions on the prediction of fibre patterns.

8.3 Recommendation for further work

In light of the work performed some important improvements/studies that could be undertaken are:

- The fact that void content affects the mechanical properties has been widely studied and explained. However, depending on the process used to form and consolidate the textile composite the spatial distribution of voids within the laminate remains unknown. This could also have an important effect on the mechanical properties. For example voids have a key importance in a laminate loaded to flexure, where voids close to the surface could lead to a concentration of stresses leading to premature failure. Further work is recommended to

determine the distribution of voids depending on the consolidation process and to predict the effect that different void distributions have on mechanical properties.

- A consolidation model for thin commingled glass/polypropylene textile composite laminates has been presented. However further development would be focused on the effect of temperature on the consolidation of thick laminates and on the consolidation of thermoset prepregs.
- In Chapter 6, compressive or shear behaviour were not considered in prediction of failure stresses for sheared flat plaques. These areas require further work to developed biaxial failure envelopes that could be implemented into software packages.
- Software packages for structural analysis of composites should consider the effect of realignment of the fibres during loading on the mechanical properties. Little study has been made in this field and further study has to be done.

8.4 Major conclusions

This section includes a summary of the major conclusions arising from the work described in this thesis.

- Sensitivity studies revealed that at least 80% of the cross sectional area of coupons had to be analysed to obtain an accurate measurement of the void content of the laminate.
- Measurements from consolidated laminates revealed that a void content of less than 2% could be achieved with suitable vacuum forming process parameters applying a pressure of 950 mbar. This value is comparable to that expected for applying a pressure of 30 bar in compression moulding.
- Image analysis and mechanical testing revealed that low void content does not significantly affect mechanical properties, as would be expected. However for void levels of over 10%, a reduction in strength of approximately 50% was observed.
- An existing model based on Darcy's law flow front progression was modified to account for the effect of shear thinning, capillary effects and compaction of

the reinforcement. Sensitivity studies revealed the effect of the number of agglomerations on the predicted void content. Disagreement with the predicted void content was explained by the presence of the voids in the inter-tow region as shown in micrographs.

- Simple stress fracture criteria were proposed to predict the effect of voids on the strength of composite laminates. These criteria assumed that fracture occurs when the stress at some characteristic distance away from the discontinuity reaches the strength of a fully consolidated laminate. Excellent correlation between measured and predicted strengths was obtained.
- A series of existing models have been combined to predict failure stress for laminates based on sheared textile composites. Classical laminate theory was used to determine the stresses within the material, with biaxial fabric assumed to consist of two unidirectional layers with no crimp. The maximum stress failure criterion was used to predict first ply failure, and this provided reasonable correlation for commingled glass/PP woven laminates.
- The material used to form hemisphere and helicopter pilot helmet components has a clear influence on the deformed fibre pattern, even for the same symmetric component. Changes in tow spacing during shear appeared to explain the differences.

REFERENCES

[1] Partridge I.K., ed., "Advanced composites", Elsevier Applied Science, London, 1989.

[2] Wakeman M.D., "Non-isothermal compression moulding of glass fibre reinforced polypropylene composites", Ph.D. Thesis, University of Nottingham, 1997.

[3] Ye L. and Friedrich K., "Processing of thermoplastic composites from powder/sheath- fibre bundles", Journal of Materials Processing Technology, Vol. 48, 1995, pp. 317-324.

[4] Osten S., John C.S., Guillon D., and Renault T., "Compression moulding of twintex and random fibre thermoplastic moulding materials", Society of Plastics Engineers, Proceeding of the 55th Annual Technical Conference – ANTEC 97, 1997, Vol.2, pp. 2432-2436.

[5] Akovali G., ed., "Handbook of composite fabrication", Shawbury, Rapra Technology, 2001.

[6] Okine R.K., "Analysis of forming parts from advanced thermoplastic composite sheet materials", Journal of Thermoplastic Composite Materials, Vol. 2, No.,1989, pp. 50-76.

[7] Svensson N. and Shishoo R., "Manufacturing of thermoplastic composites form commingled yarns - A review", Journal of Thermoplastic Composite Materials, Vol. 11, 1998, pp. 22-56.

[8] Kurek K. and Bledzki A.K.., "The effect of micropores on mechanical properties of laminates", Polimery , Vol. 4, 2000, pp. 271-281.

[9] Kang M.K., Lee W.I. and Hahn H.T., "Formation of microvoids during resin-transfer molding process", Composites Science and Technology, Vol. 60, 2000, pp. 2427-2434 .

[10] Bernhardsson J. and Shishoo R., "Effect of processing parameters on consolidation quality of GF/PP commingled yarn based composites", Journal of Thermoplastic Composite Materials, Vol 13, 2000, pp. 292-313.

[11] Santulli C., Brooks R., Long A.C. and Rudd C.D., "Influence of micro-structural voids on the mechanical and impact properties in commingled E-

glass/polypropylene thermoplastic composites", Journal of Materials: Design and Applications Part L 216, 2002, pp. 85-100.

[12] Perov Y.Y. and Kruzhkova E.Y., "Express determination of polymer composite porosity", Mechanics of Composite Materials, Vol. 31, 1995, pp. 585-587.

[13] Salvado C., Wai M.., and Hunter A., "Simultaneous determination of matrix and porosity content by non-destructive method", Society of Plastics Engineers, Proceedings of the 47th Annual Technical Conference and Exhibits, 1989, pp.1048-1050.

[14] Gros X.E., "Current and future trends in non-destructive testing of composite materials", Annales de Chimie, Science des Materiaux, Vol. 35, 2000, pp. 539-544.

[15] Jeong H., "Effects of voids on the mechanical strength and ultrasonic attenuation of laminated composites", Journal of Composite Materials, Vol. 31, 1997, pp. 276-292.

[16] Mouritz A.P., "Ultrasonic and interlaminar properties of highly porous composites", Journal of Composite Materials, Vol. 34, 2000, pp. 218-239.

[17] Clayden N.J., "Non Destructive testing of thermoplastic composites by NMR imaging", The Institution of Electrical Engineers, IEE Colloquium (Digest), No.33, 1994, pp. 3/1-3/2.

[18] Guild F.J. and Summerscales J., "Microstructural image analysis applied to fibre composite materials - A review", Composites, Vol. 24, No. 5, 1993, pp. 383-393.

[19] Anon, "Textile glass reinforced plastics – determination of void content – loss on ignition, mechanical disintegration and statistical counting methods", International Organisation for Standardisation, ISO 7822: 1990 (E).

[20] Frost J.D., Kuo C.Y., "Automated determination of the distribution of local void ratio from digital images", Geotechnical Testing Journal, Vol. 19, 1996, pp. 107-117.

[21] Ghiorse S.R., "A comparison of void measurement methods for carbon/epoxy composites", Materials Laboratory, US Army Laboratory Command, 91-00671, 1991.

[22] Gao F., Patrick J.W. and Walker A., "The characterisation of cracks and voids in 2D carbon/carbon composites", Carbon, Vol. 31, 1993, pp. 103-108.

[23] Marr D.W.M., Wartenberg M., Schwartz K.B., Agamalian M.M. and Wignall G.D., "Void morphology in polyethylene carbon black composites", Macromolecules, Vol. 30, 1997, pp. 2120-2124.

[24] Matzinos P. D., Patrick J. W. and Walker A., "The efficiency and mechanism of densification of 2-D C/C composites by coal-tar pitch impregnation", Carbon, Vol. 38, No.8, 2000, pp. 1123-1128.

[25] Pearce N.R.L., Guild F.J. and Summerscales J., "The use of automated image analysis for the investigation of fabric architecture on the processing and properties of fibre-reinforced composites produced by RTM", Composites Part A, Vol. 29, No. 7, 1998, pp. 829-837.

[26] Summerscales J., Guild F.J., Pearce N.R.L. and Russell P.M., "Voronoi cells, fractal dimensions and fibre composites", Journal of Microscopy, Oxford, Vol. 201, No. 2, 2001, pp. 153-162.

[27] Gutowski T.G., Morigaki T. and Cai Z., "The Consolidation of Laminate Composites", Journal of Composite Materials, Vol. 21, 1987, pp. 172-188.

[28] Gutowski T.G., Cai Z., Bauer S., Boucher D., Kintyre J. and Wineman S., "Consolidation experiments for laminate composites", Journal of Composite Materials, Vol. 21, 1987, pp. 650-669.

[29] Gutowski T.G., ed., "Advanced composites manufacturing", New York, John Wiley & Sons, 1997.

[30] Gibson A.G. and Manson J.E., "Impregnation technology for thermoplastic composites", Journal of Composites Manufacturing, Vol. 3, No. 4, 1992, pp. 223-233.

[31] Ye L., Friedrich K., Cutolo D. and Savadori A., "Manufacturing of CF/PEEK composites from powder/sheath fibre preforms", Composites Manufacturing, Vol. 5, No. 1, 1994 , pp. 41-50.

[32] Yun E.J., Kim T.W. and Lee W.J., "Resin impregnation and autohesion in carbon/PEEK composites", Development of Carbon Fibres and Their Application, Vol. 22, No. 6, 1990, pp. 655-661.

[33] Van West B.P., Pipes R.B. and Advani S.G., "The consolidation of commingled thermoplastic fabrics", Polymer Composites, Vol. 12, No. 6, 1991, pp. 417-427.

[34] Van West B.P., Pipes R.B. and Advani S.G., "The draping and consolidation of commingled fabrics", Composites Manufacturing, Vol. 2, No. 1, 1991, pp. 10-22.

[35] Kim D., Lee W.I. and Friedrich K., "A model for a thermoplastic pultrusion process using commingled yarns", Composites Science and Technology, Vol. 61, No.8, 2001, pp. 1065-1077.

[36] Amico S. and Lekakou C., "An experimental study of the permeability and capillary pressure in resin-transfer moulding", Composites Science and Technology, Vol. 61, No. 13, 2001, pp. 1945-1959.

[37] Connor M., Toll S., Månson J.A.E. and Gibson A.G., "A model for the consolidation of aligned thermoplastic powder impregnated composites", Journal of Thermoplastic Manufacturing, Vol. 8, No. 2, 1995, pp. 138–162.

[38] Lee W.I., Springer G.S. and Smith F.N., "Pultrusion of thermoplastics – A model", Journal of Composite Materials, Vol. 25, No. 12, 1991, pp. 1632-1652.

[39] Pipes R.B., Hearle J.W.S., Beaussart A.J. and Sastry A.M., "A constitutive relation for the viscous flow of an oriented fibre assembly", Journal of Composite Materials, Vol. 25, No. 9, 1991, pp. 1205-1217.

[40] Gebart B.R., "Permeability of unidirectional reinforcements for RTM", Journal of Composite Materials, Vol. 26, No. 8, 1992, pp. 1100-1133.

[41] Hou T.H., "A resin Flow Model for Composite Prepreg Lamination Process", Society of Plastics Engineers, Proceedings of the 44th Annual Technical Conference, ANTEC 86, Boston, 1986, pp. 1300-1305.

[42] Cain T., Wakeman M.D., Brooks R. and Long A.C., Rudd C.D., "Towards an integrated processing model for a co-mingled thermoplastic composite", Proceeding of the 11th International Conference on Composite Materials, Gold Coast, Australia, Vol. 5, 1997, pp. 366-376.

[43] Cain T., Wakeman M.D., Brooks R. and Long A.C., Rudd C.D., "Structural automotive components using thermoplastic composites - Final report", University of Nottingham, 1998.

[44] Bernet N., Michauld V., Bourban P.E. and Manson J.A.E., "An impregnation model for the consolidation of thermoplastic composites made from commingled yarns", Journal of Composite Materials, Vol. 33, No. 8, 1991.

[45] Bernet N., Michaud V., Bourban P.-E., and Manson J.-A.E., "Commingled yarn composites for rapid processing of complex shapes", Composites Part A, Vol. 32, No. 11, 2001, pp. 1613-1626.

[46] Lee W.I. and Springer G.S., "A model of the manufacturing process of thermoplastic matrix composites", Journal of Composite Materials, Vol. 21, 1987, pp. 1017-1055.

[47] Seo J.W. and Lee W.I., "A model of the resin impregnation in thermoplastic composites", Journal of Composite Materials, Vol. 25, 1991, pp. 1127-1142.

[48] Klinkmuller V., Kastel R., Ye L. and Friedrich K., "On impregnation quality and resulting mechanical properties of compression moulded commingled yarn based thermoplastic composites", IUTAM (International Union of Theoretical and Applied Mechanics) Symposium on Microstructure-Property Interactions in Composite Materials, 1995, pp. 189-201.

[49] Klinkmuller V., Um M., Steffens M., Friedrich K. and Kim B., "A new model for impregnation mechanisms in different GF/PP commingled yarn composites", Applied Composite Materials, Vol. 1, 1995, pp. 351-371.

[50] Ye L., Friedrich K. and Kastel J., "Consolidation of GF/PP commingled yarn composites", Applied Composite Materials, Vol. 1, 1995, pp. 415-429.

[51] Ye L., Friedrich K., Kastel J. and Mai Y., "Consolidation of unidirectional CF/PEEK composites from commingled yarn prepreg", Composites Science and Technology, Vol. 54, 1995, pp. 349-358.

[52] Wilks C.E., "Processing technologies for woven glass/polypropylene composites", PhD Thesis, University of Nottingham, 1999.

[53] Leterrier Y. and G'Sell C., "Formation and elimination of voids during the processing of thermoplastic matrix composites", Polymer Composites, Vol. 15, No. 2, 1994, pp.101-105.

[54] Cunningham J.E., Monaghan P.F., Brogan M.T., and Cassidy S.F., "Modelling of pre-heating of flat panels prior to press forming", Composites Part A, Vol. 28, No. 1, 1997, pp. 17-24.

[55] Tavman I.H. and Akinci H., "Transverse thermal conductivity of fiber reinforced polymer composites", International Communications in Heat and Mass Transfer, Vol. 27, No. 2, 2000, pp. 253-261.

[56] Almeida S.F.M.d. and Neto Z.d.S.N., "Effect of void content on the strength of composite laminates", Composite Structures, Vol. 28, 1994, pp. 139-148.

[57] Costa M.L., Almeida S.F.M.d., and Rezende M.C., "The influence of porosity on the interlaminar shear strength of carbon/epoxy and carbon/bismaleimide fabric laminates", Composites Science and Technology, Vol. 61, No. 14, 2001, pp. 2101-2108.

[58] Wakeman M.D., Cain T.A., Rudd C.D., Brooks R. and Long A.C., "Compression moulding of glass and polypropylene composites for optimised macro- and micro- mechanical properties II. GMT", Composites Science and Technology, Vol. 59, 1999, pp. 709-726.

[59] Nilsson G., Fernberg S.P. and Berglund L.A., "Strain field inhomogeneities and stiffness changes in GMT containing voids", Composites Part A, Vol. 33, 2002, pp. 75-85.

[60] Lee D.-J. and Shin I.-J., "Effects of vacuum, mould temperature and cooling rate on mechanical properties of press consolidated glass fibre/PET composite", Composites Part A, Vol. 33, No. 8, 2002, pp. 1107-1114.

[61] Henninger F., Hoffmann J., and Friedrich K., "Thermoplastic filament winding with online-impregnation. Part B. Experimental study of processing parameters", Composites Part A, Vol. 33, No. 12, 2002, pp. 1684-1695.

[62] Awerbuch J. and Madhuckar M.S., "Notched strength of composite laminates: predictions and experiments - A review", Journal of Reinforced Plastics and Composites, Vol. 4, 1985, pp. 3-139.

[63] Ng S.-P., Lau K.J. and Tse P.C., "3D finite element analysis of tensile notched strength of 2/2 twill weave fabric composites with drilled circular hole", Composites Part B, Vol. 31, No. 2, 2000, pp. 113-132.

[64] Whitney J.M. and Nuismer R.J., "Stress fracture criteria for laminated composites containing stress concentrations", Journal of Composite Materials, Vol. 8, 1974, pp. 253-265.

[65] Waddoups M.E., J.R. Eisenmann J.R. and Kaminski B.E., "Macroscopic fracture mechanics of advanced composite materials", Journal of Composite Materials, Vol. 5, pp. 446-454, 1971.

[66] Mar J.W. and Lin K.Y., "Fracture correlation for tensile failure of filamentary composites with holes", Journal of Aircarft, Vol. 14, No. 7, 1977, pp. 703-704.

[67] Soriano E.d.A. and Almeida S.F.M.d., "Notch sensitivity of carbon/epoxy fabric laminates", Composites Science and Technology, Vol. 59, No. 8, 1999, pp. 1143-1151.

[68] Karlak R.F., "Hole effects in a related series of symmetrical laminates", Proc. Failure Modes in Composites IV, Chicago, 1977, pp. 105-117.

[69] Pipes R.B., Wetherhold R.C. and Gillespie J.W., "Notched strength of composite materials", Journal of Composite Materials, Vol. 13, 1979, pp. 148-160.

[70] Srivastava V.K., "Notched strength prediction of laminated composite under tensile loading", Materials Science and Engineering A, Vol. 328, 2002, pp. 302-309.

[71] Chen P., Shen Z., and Wang J.Y., "Prediction of the strength of notched fibre-dominated composite laminates", Composites Science and Technology, Vol. 61, No. 9, 2001, pp. 1311-1321.

[72] Krenchel, H. "Fibre reinforcement - theoretical and practical investigations of the elasticity and strength of fibre reinforced materials", Academisk Forlag, Copenhagen, 1964.

[73] Smith P., Rudd C.D. and Long A.C. "The effect of shear deformation on the processing and mechanical properties of aligned reinforcements", Composites Science and Technology, Vol. 57, 1997, pp 327-344.

[74] Turner M.R., "Tow placement studies for liquid composite moulding", Ph.D. Thesis, University of Nottingham, 1998.

[75] Tsai S.W. and Hahn H.T. "Introduction to composite materials", Technomic Publishing co. Inc, Lancaster, PA, USA, 1984.

[76] Morley J.G., "High performance fibre composites", London, Academic Press, 1987.

[77] Jones, R.M., "Mechanics of composite materials", New York, Hemisphere, 1975.

[78] Hofstee J., de Boer H., and van Keulen F., "Elastic stiffness analysis of a thermo-formed plain-weave fabric composite; Part I: geometry", Composites Science and Technology, Vol. 60, No. 7, 2000, pp. 1041-1053.

[79] Hofstee J. and van Keulen F., "Elastic stiffness analysis of a thermo-formed plain-weave fabric composite Part II: analytical models", Composites Science and Technology, Vol. 60, No. 8, 2000, pp. 1249-1261.

[80] Hofstee J., de Boer H. and van Keulen F., "Elastic stiffness analysis of a thermo-formed plain-weave fabric composite--part III: experimental verification", Composites Science and Technology, Vol. 62, No. 3, 2002, pp. 401-418.

[81] Crookston J.J., Long A.C., and Jones I.A., "Modelling effects of reinforcement deformation during manufacture on elastic properties of textile composites", Plastics, Rubber and Composites, Vol. 31, No. 2, 2002, pp. 58-65.

[82] Crookston J.J., Long A.C. and Jones I.A., "The effects of deformation during manufacture on the mechanical performance of textile reinforced polymer composites", Proceeding of 10th European Conference on Composite Materials, Bruges, June 2002.

[83] Highsmith A.L., Davis J.J. and Helms K.L.E. "The influence of fibre waviness on the compressive behaviour of unidirectional continuous fibre composites", Proceedings of the 10th Conference on Composite Materials, ASTM, San Francisco, USA, No. 1120, April 1990, pp. 20-36.

[84] Piggot M.R., "The effect of fibre waviness on the mechanical properties of unidirectional fibre composites: A review", Composites Science and Technology, Vol. 53, 1995, pp. 201-205.

[85] Bolotin V.V., "Theory of a reinforced layered medium with random initial irregularities", Polymer Mechanics, Vol. 2, 1966, pp. 7-11.

[86] Mrse A.M. and Piggot M.R., "Compressive properties of unidirectional carbon fibre laminates: II. The effects of unintentional and intentional fibre misalignments", Composites Science and Technology, Vol. 46, 1993, pp 219-227.

[87] Bogetti T.A., Gillespie J.W. and Lamontia M.A., "Influence of ply waviness on the stiffness and strength reduction on composite laminates", Journal of Thermoplastic Composite Materials, Vol. 5, October 1992, pp. 344-369.

[88] Ishikawa T., Chou T.W., "Stiffness and strength behaviour of woven fabric composites", Journal of Materials Science, Vol. 17, 1982, pp. 3211-3220.

[89] Chan W.S. and Chou C.J., "Effects of delamination and ply fibre waviness on effective axial and bending stiffness in composite laminates", Composite Structures, Vol. 30, 1995, pp. 299-306.

[90] Rai H.G., Rogers C.W. and Crane, D.A., "Mechanics of curved fibre composites", Proceedings of the 47th Annual Forum of the American Helicopter Society, Phoenix, Arizona, USA, May 1991, pp. 297-304.

[91] Hsaio H.M. and Daniel I.M., "Effect of fibre waviness on stiffness and strength reduction of unidirectional composites under compressive loading", Composites Science and Technology, Vol. 56, 1996, pp. 581-593.

[92] Hsiao H.M. and Daniel I.M., "Elastic properties of composites with fibre waviness", Composites Part A, 1996, Vol. 27, No. 10, pp. 931-941.

[93] Hatta H., Takei T., Taya M., "Effects of dispersed microvoids on thermal expansion behaviour of composite materials", Materials Science & Engineering A285, 2000, pp.99-110.

[94] Vogel J.H. and Lee D., "The automated measurement of strains from three-dimensional deformed surfaces", Journal of Metals, Vol. 42, 1990, pp. 8-13. 1990.

[95] "ASAME. The automated strain analysis and measurement environment. Reference manual", CamSys Inc., 2000.

[96] Montmitonnet P., "Simulation physique de la mise en forme: mesure de la déformation", Techniques de l'Ingénieur.

[97] Vetrotex International, "Le moulage sous vide", 2001.

[98] Mei Z. and Chung D.D.L., "Kinetics of autohesion of thermoplastic carbon fibre prepregs", International Journal of Adhesion and Adhesives, Vol. 20, 2000, pp. 173-175.

[99] Phillips R., Akyuz D.A. and Manson J.E., "Prediction of the consolidation of woven fibre-reinforced thermoplastic composites. Part I. Isothermal case", Composites Part A, Vol. 29, 1998, pp. 395-402.

[100] Long A.C., Wilks C.E. and Rudd C.D., "Experimental characterisation of a consolidation glass/polypropylene composite", Composite, Science and Technology, Vol. 61, pp.1591-1603, 2001.

[101] Roberts R.W. and Jones R.S., "Rheological characterization of continuous fibre composites in oscillatory shear flow", Composites Manufacturing, Vol. 6, No. 3-4, 1995, pp. 161-167.

[102] McGuinness G.B. and Bradaigh C.M.O., "Characterisation of thermoplastic composite melts in rhombus-shear: the picture-frame experiment", Composites Part A, Vol. 29, No. 1-2, 1998, pp. 115-132.

[103]Gutowski T.G., Morigaki T., and Cai Z., "The consolidation of laminate composites", Journal of Composite Materials, Vol. 21, 1987, pp. 172-188.

[104] Farina A., Cocito P., and Boretto G., "Flow in deformable porous media: modelling and simulations of compression moulding processes", Mathematical and Computer Modelling, Vol. 26, No.11, 1997, pp. 1-15.

[105] Palmers J., "Surface modification using low-pressure plasma technology", Medical Device & Diagnostic Industry Magazine, January 2000, pp. 96.

[106] Harrison P., Garcia Gil R., Clifford M.J., Long A.C., and Rudd C.D., "Draping of engineered prepregs and reinforced thermoplastics - Progress Report 8", University of Nottingham, 2001.

[107] Chhabra R.P. and Richardson J.J., "Non-Newtonian flow in the process industries", Butterworth Heinemann, 1999.

[108] Hull D. and Clyne T.W., "An introduction to composite materials", 2nd Edition, Cambridge University Press, Cambridge, 1996.

[109] Halpin J. C., "Primer on composite materials analysis", Technomic Publishing Company Inc, Lancaster, PA, USA, 1992.

[110] Composite, Science and Technology, Vol. 58, No. 7, 1998, pp. 999-1254.

[111] Composite, Science and Technology, Vol. 62, No. 12-13, 2002, pp. 1479-1797.

[112] Long A.C., "Preform design for liquid moulding processes", Ph.D. Thesis, University of Nottingham, 1994.

[113] Souter, B, "Effects of fibre architecture on formability of textile preforms", Ph.D. Thesis, University of Nottingham, 2001.

[114] Long A.C., Rudd C.D., Blagdon M., and Smith P., "Characterizing the processing and performance of aligned reinforcements during preform manufacture", Composites Part A, Vol. 27, 1996, pp. 247-253.

[115] Clifford M.J., Long A.C. and Rudd C.D., "Draping of engineered prepregs and reinforced thermoplastics - Progress Report 3", University of Nottingham, 2000.

[116] Clifford M.J., Long A.C. and Rudd C.D., "Draping of engineered prepregs and reinforced thermoplastics - Progress Report 2", University of Nottingham, 2000.

Appendix 1.1
Project Publications

Gil R.G., Long A.C. & Clifford M.J., "Vacuum consolidation of glass / PP commingled fabrics", Proc. 4th Congreso Nacional de Materiales Compuestos (MATERIALES COMPUESTOS '01), Spanish Association of Composite Materials, Gijon, Spain, November 2001, pp. 773-780.

Gil R.G., Long A.C., Harrison P. & Clifford M.J., "Consolidation modelling for textile composites", Proc. 9th International Conference on Fibre Reinforced Composites (FRC 2002), Newcastle upon Tyne, March 2002, pp.362-369.

Long A.C., Gil R.G., Harrison P., Clifford M.J., Sharma S.B. & Sutcliffe M.P.F., "Experimental analysis of fabric deformation during forming of textile composites", Proc. 5th International European Scientific Association for Material Forming (ESAFORM) Conference, Krakow, Poland, April 2002, pp. 279-282.

Sutcliffe M.P.F., Sharma S.B., Long A.C., Gil R.G., Harrison P., Clifford M.J. & Rudd C.D., "A comparison of simulation approaches for forming of textile composites", Proc. 5th International European Scientific Association for Material Forming (ESAFORM) Conference, Krakow, Poland, April 2002, pp. 311-314.

Long A.C., Crookston J.J., Gil R.G., Jones I.A. & Clifford M.J., "Effects of intra-ply shear during forming on tensile properties of textile composites", Proc. 6th International Conference on Textile Composites (TexComp 6), Philadelphia, USA, September 2002, Paper 5-08.

Harrison P., Long A.C., Clifford M.J., Gil R.G., Ward I.M. & Hine P.J., "An investigation into the thermoformability of hot-compacted polypropylene sheet", Automotive Composites and Plastics Conference (ACP 2002), Institude of Materials, Basildon, December 2002.

Santulli C., Gil R.G., Long A.C. & M. J. Clifford, "Void content measurements in commingled E-glass polypropylene composites using image analysis from optical micrographs", Science and Engineering of Composite Materials, Vol. 10, No. 2, 2002, pp. 77-90.

Gil R.G., Long A.C., Clifford M.J. & Harrison P., "Modelling of isothermal consolidation in glass / polypropylene commingled composites", Plastic, Rubber and Composites, Vol. 32, No. 2, 2003, pp. 47-56.

Gil R.G., Long A.C. & Clifford M.J., "Non-isothermal consolidation modelling and mechanical properties prediction for Glass/Polypropylene commingled fabrics", The 14th International Conference on Composite Materials, San Diego, July 2003.

Appendix 3.1

Steps to calculate percentage of void content using Aphelion

1. Switch on microscope.
2. Enter password.
3. Run Aphelion.
4. Click on Camera Definition.
5. Click on DT3155 > Edit Cameras…
6. Select the CCIR 512x512.
7. Adjust the size of the micrograph suitable for the specimen to analyse.
8. Click on Operator Selection icon > Image Acquisition > Grab/Snap > Image Grab (see Figure A1).
9. Image Grab window comes up. Select camera (DT 3155).
10. Click on Run Operator icon.
11. Select a magnification on the microscope.
12. Focus the image (voids have to be clear).
13. Click on Stop icon.
14. Click on image with right button.
15. Click on View > Pixel = Point (see Figure A2)
16. Draw a profile line along a void using the Profile Line icon (see Figure A2). A graph where the grey level along the profile line is displayed comes up.
17. Write down the grey level of the points along the profile line, which correspond to the void.
18. Steps 12 and 13 can be repeated on other voids.
19. Click on Operator Selection icon > Segmentation > Threshold> ImgThreshold.
20. Click on the Input box and select the image.
21. Set the Low and High grey levels of the voids. As a first approximation, the values obtained from steps 12, 13 and 14 can be used.
22. Click on Run Operator icon.
23. Click on Operator Selection icon > Analysis > Global > ImgArea.
24. Click on Input box and select the binary image.
25. Write down the number of pixels that correspond to voids.
26. The void content of the micrograph is the result of the equation:

$$\%VoidContent = \frac{Number\ of\ \ pixels\ that\ correspond\ to\ voids}{Total\ number\ of\ \ pixels\ of\ the\ window.} x100$$

27. Repeat the process for a representative number of micrographs.

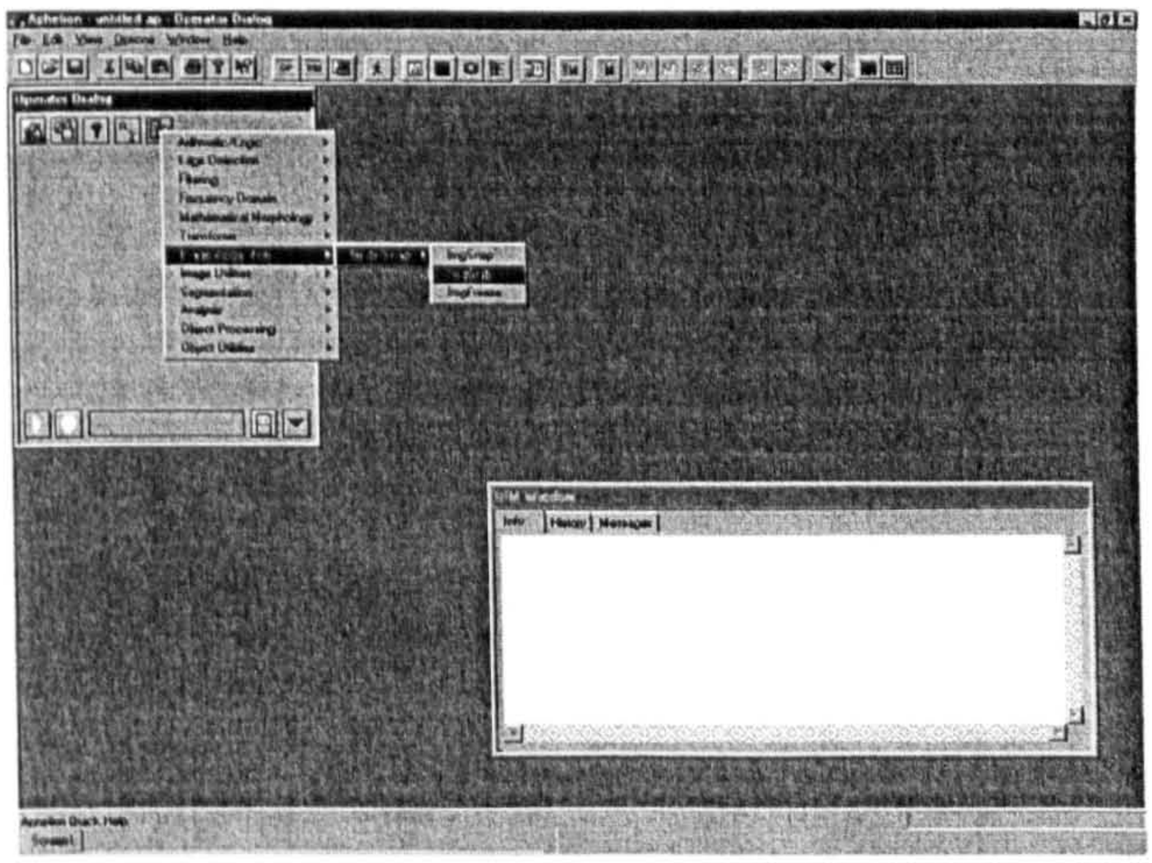

Figure A1 Acquisition of a micrograph.

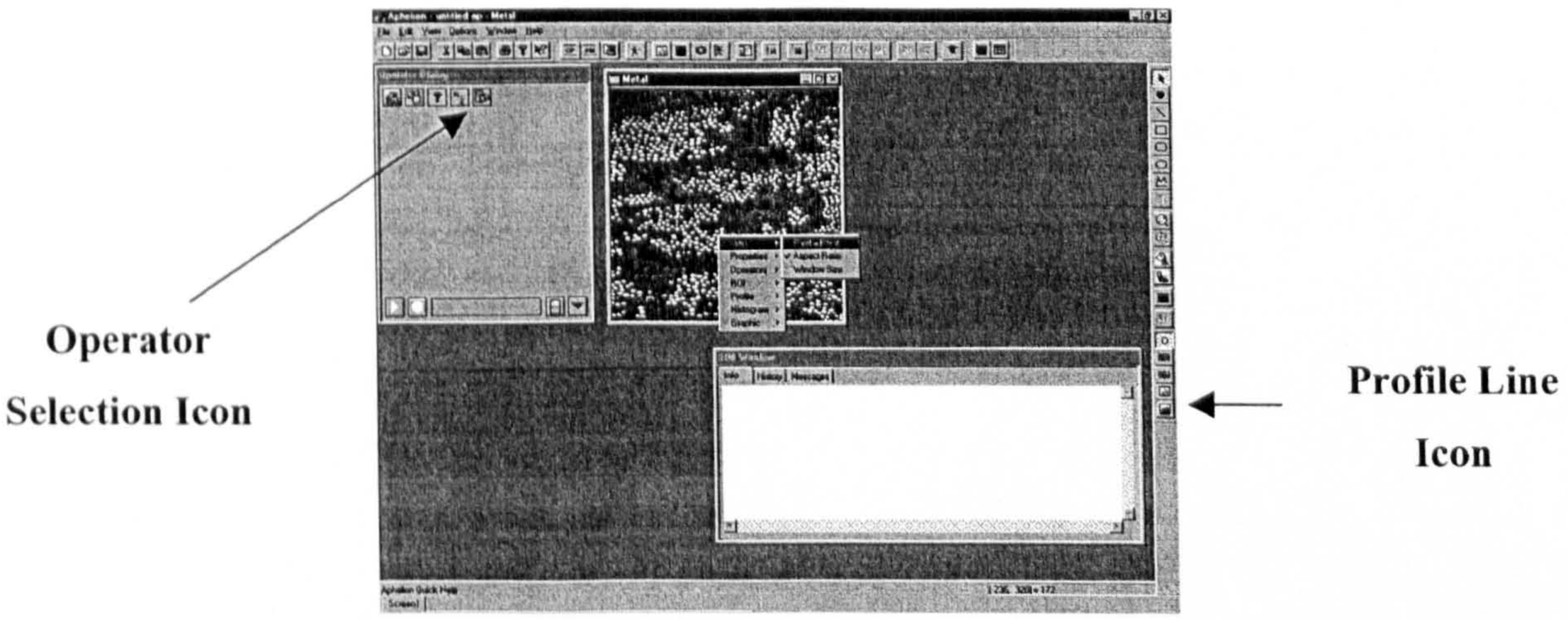

Figure A2 Position of Operator Selection icon and Profile Line icon.